Targeting zinc signalling to prevent cell division in cancer

A thesis submitted in accordance with the conditions governing candidates for the degree

of

Philosophiae Doctor in Cardiff University

By

Olivia Ogle

February 2020

Cardiff School of Pharmacy and Pharmaceutical Sciences
Cardiff University

Summary

Zinc is the second most abundant trace element in the human body and several disease states have been attributed to zinc dysregulation. Recent evidence has shown that zinc is a second messenger with roles in a diverse range of cellular signalling pathways. Of particular interest, is the discovery that cells require zinc to enter mitosis (cell division) and that several zinc transporter proteins have increased expression in cancer, a disease of uncontrolled cell division. Furthermore, post-translational modification has been shown to play a role in ZIP transporter activity. Understanding ZIP transporter regulation in cell division is key to revealing the mechanisms of zinc signalling in cancer. A combination of molecular and cell biological techniques have been used in this project to understand the role of ZIP transporter post-translational modification in cell division and to characterise novel anti-ZIP antibodies for their potential to stop tumour growth.

This project highlighted that ZIP10 undergoes ectodomain shedding in mitosis and in response to zinc availability; an important mechanism for maintaining cellular zinc homeostasis. Analysis of potential ZIP10 phospho-sites revealed the potential phosphorylation of ZIP10 on several residues in the loop between TMD3 and TMD4. Furthermore, the interaction of ZIP10 with cell cycle-regulated kinases including CDK1 and PLK1 in mitosis was demonstrated. In addition, novel antibodies against ZIP transporters ZIP6 and ZIP10, both of which have been implicated in several cancers, were developed and the work presented here demonstrated their ability to prevent cell division in breast cancer, prostate cancer and melanoma cell lines *in vitro*, and slow breast tumour growth *in vivo*. This project also provided the first indication that ZIP6- and ZIP10-mediated cell division is important for non-cancerous cells, supporting the evidence that zinc signalling mechanisms are vital to human health; a finding that is relevant to the wider field of cellular biology.

Acknowledgments

I would like to thank my supervisor, Dr Kathryn Taylor, for the opportunity to undertake this project, guiding me through each milestone of my PhD and providing invaluable feedback. I am also deeply grateful to my second supervisor, Dr Julia Gee, and my advisor, Dr Emma Lane, for the interesting discussions we had and for providing helpful advice. I would like to acknowledge Dr Gillian Seaton for her support with the *in vivo* work in this project.

I am particularly grateful to my fiancé, John, for his unwavering support and encouragement, and to our beagle, Berry, for her constant companionship. I am thankful to my family, especially my dad and grandad, for their love and for giving me the opportunities that led me to embark on this PhD. A special thanks to Silvia, for not only being a wonderful, supportive colleague but a great friend. An extended thanks to members of the breast cancer molecular pharmacology group, past and present, for sharing their knowledge and creating a wonderful working environment. To Sam, Mike, Richard, Laura and Sara, for making me feel so welcome in Cardiff that it has now become my permanent home.

Finally, this project would not have been possible without the funding provided by the Life Science Research Network Wales and the Cardiff University School of Pharmacy and Pharmaceutical Sciences. Their funding also enabled me to attend many conferences to share my work with experts in the field of zinc biology; in particular, the International Society of Zinc Biology in Japan which was an unforgettable experience.

Dedicated to Catherine Ogle, forever in my heart.

Table of Contents

List of figures

List of tables

Abbreviations

Ab	antibody
ADAM	a disintegrin and metalloproteinase
ADC	antibody-drug complex
ADP	adenosine diphosphate
AKT	protein kinase B
ANoVA	analysis of variance
APC	anaphase promoting complex
ATP	adenosine triphosphate
AU	arbitrary unit
BPH	benign prostate hyperplasia
BSA	bovine serum albumin
CaM	calmodulin
CD	cluster of differentiation
CDK	cyclin dependent kinase
CENPO	centromere protein O
CK2	casein kinase 2
CTS	cathepsin
CRISPR	clustered regularly interspaced short palindromic repeats
DAPI	4',6'-diamidino-2-phenylindole
DAPT	N-[N-(3,5-difluorophenacetyl)-L-alanyl]-S-phenylglycine t-butyl ester
DMAT	2-Dimethylamino-4,5,6,7-tetrabromo-1H-benzimidazole,4,5,6,7-Tetrabromo-N, N-dimethyl-1H-benzimidazol-2-amine, 4,5,6,7-Tetrabromo-N,N-dimethyl-1H-benzo[d]imidazol-2-amine
DMEM	Dulbecco's Modified Eagle Medium
DNA	deoxyribonucleic acid
DTT	dithiothreitol
EDTA	ethylenediaminetetraacetic acid
EGF	epidermal growth factor
EGFR	epidermal growth factor receptor
ELISA	enzyme-linked immunosorbent assay
EMT	epithelial to mesenchymal transition
EPO	erythropoietin
ER	endoplasmic reticulum
ERK	extracellular signal-regulated kinase
FACS	fluorescence activated cell sorting
FCS	foetal calf serum
GSK3	glycogen synthase kinase 3
HER2	human epidermal growth factor receptor 2
HRP	horseradish peroxidase
ICL	intracellular loop
kDa	kilodaltons
KO	knock-out
KRH	Krebs-Ringer-HEPES
KRT16	keratin 16
IF	immunofluorescence
IgE	immunoglobulin E

IgG	immunoglobulin G
IGFR	insulin-like growth factor receptor
INSR	insulin receptor
IP	immunoprecipitation
LRRK	leucine-rich repeat kinase
LB	lysogeny broth
MAP	mitogen activated protein
MAPK	mitogen-activated protein kinase
MCF	Michigan Cancer Foundation
MDA-MB	M.D. Anderson-metastatic breast cancer
MMAE	monomethyl auristatin E
MMP	matrix metalloproteinase
MRE	metal response element
MTF	metal transcription factor
mRNA	messenger ribonucleic acid
MS	mass spectrometry
mTOR	mechanistic target of rapamycin
NLS	nuclear localization signal
nMuMG	normal murine mammary gland
PBS	phosphate buffered saline
PD	pharmacodynamic
PEST	proline, glutamic acid, serine, threonine
PI3K	phosphoinositide 3 kinase
PK	pharmacokinetic
PKA	protein kinase A
PKG	protein kinase G
PLA	proximity ligation assay
PLK	polo-like kinase
PNGaseF	peptide-N-glycosidase F
Rf	retention factor
PR	progesterone receptor
PrP	prion protein
PSA	prostate specific antigen
RNA	ribonucleic acid
RPMI	Roswell Park Memorial Institute
RSK	ribosomal s6 kinase
S1P	site 1 protease
S2P	site 2 protease
SAC	spindle assembly checkpoint
SDS-PAGE	sodium dodecyl sulfate polyacrylamide gel electrophoresis
siRNA	silencing RNA
SLC	solute carrier
SOC	super optimal broth
STAT	signal transducer and activator or transcription 3
TBS	tris buffered saline
TBS-T	tris buffered saline with tween
TGF-β	transforming growth factor beta
TMD	transmembrane domain
TNF-α	tumour necrosis factor alpha

TPA	12-O-tetradecanoylphorbol-13-acetate
TPEN	N,N,N′,N′-tetrakis(2-pyridinylmethyl)-1,2-ethanediamine
UV	ultraviolet
WB	western blot
WT	wild-type
ZIP	Zrt-, Irt-like proteins
ZnT	zinc transporter protein

Chapter 1. General introduction

Zinc is a transition metal essential to life and is the 2nd most abundant trace element in the human body (McCall, Huang and Fierke, 2000) after iron. Zinc binds to 10% of all proteins in the mammalian proteome (Andreini *et al.*, 2006; Passerini *et al.*, 2007) and is a cofactor for over 300 enzymes across all enzyme classes (Vallee and Galdes, 1984) implicating a role for zinc in a large number of cellular processes.

The role of zinc in human health was first discovered as early as the 1960's when zinc deficiency was shown to lead to hypogonadism and dwarfism (Halsted and Prasad, 1961; Brown *et al.*, 2002). Zinc deficiency has since been linked to immune disorders (reviewed by Haase & Rink 2009), metabolic syndrome (reviewed by Miao et al. 2013) and acrodermatitis enteropathica, a genetic disease affecting the uptake of zinc in the gut (Moynahan, 1974). On the other hand, zinc excess causes cellular toxicity through altered calcium signalling (Brewer *et al.*, 1979) and inhibition of RNA and/or protein synthesis (Walther, Schulze and Forth, 1998). Zinc excess has also been linked to altered copper metabolism (Bremner, Young and Mills, 1976), neurodegeneration (reviewed by Sensi et al. 2009) and cancer (Taylor et al. 2008; Santoliquido and Southwick et al. 1976). The growing evidence that both zinc excess and zinc deficiency are detrimental to health, highlights the need for a tightly regulated mechanism to maintain its homeostatic balance.

1.1. Zinc is a second messenger

The total concentration of zinc in eukaryotic cells has been measured between 200–300 μM (Colvin *et al.*, 2010) and the concentration of free zinc is in the picomolar to very low nanomolar range (Krężel, Hao and Maret, 2007). The excess intracellular zinc is bound to metal binding proteins such as metallothionein and glutathione in a "muffler" (figure 1.1A) (Maret and Vallee, 1998; Colvin *et al.*, 2008) before being deposited in intracellular stores such as the endoplasmic reticulum (ER). Zinc is not available for use until it is released from the ER in response to a specific stimulus e.g. stimulation of the high affinity IgE (immunoglobulin E) receptor, FcεRI in mast cells (Yamasaki et al. 2007).

Figure 1.1. Intracellular zinc handling

A.

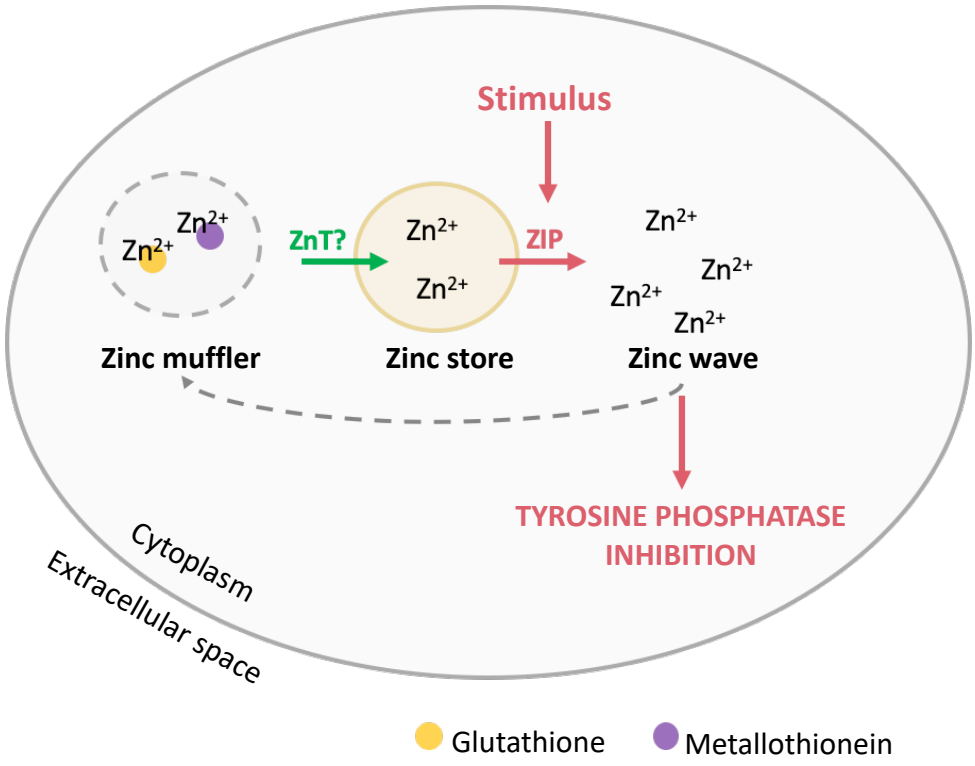

B.

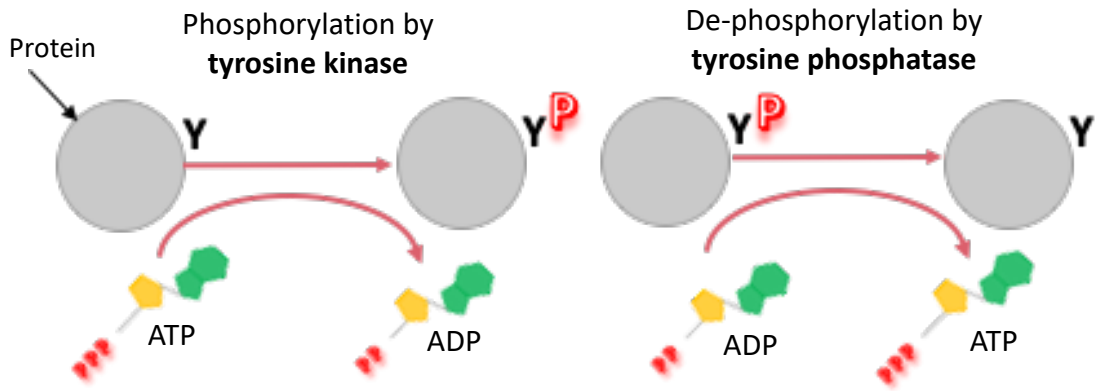

***A**. Zinc is buffered by glutathione and metallothionein in a zinc "muffler" and deposited into stores, likely via a ZnT transporter. A stimulus causes the release of zinc from stores via a ZIP transporter in the form of a zinc wave. The zinc wave causes widespread tyrosine phosphatase inhibition. Excess zinc is re-shuttled into stores via the muffler. **B**. Tyrosine (Y) phosphorylation by a tyrosine kinase is the transfer of a phosphoryl group from ATP to the tyrosine residue of a protein and is catalysed by tyrosine kinases. The reverse reaction involves the removal of the phosphoryl group from a tyrosine residue by a tyrosine phosphatase. The zinc released by the zinc wave causes tyrosine phosphatase inhibition and therefore prolongs the effects of tyrosine kinases. ATP, adenosine triphosphate.*

The release of zinc from stores in response to a specific stimulus is known as a "zinc wave" (figure 1.1A) and occurs on a timescale of minutes (Yamasaki et al. 2007). Zinc is released via a ZIP (Zrt-, Irt-like proteins) transporter (see section 1.2) and is dependent on calcium influx and MAP (mitogen-activated protein) kinase activation (Yamasaki *et al.*, 2007), although the exact mechanism is still unknown. The zinc released in the zinc wave causes widespread tyrosine phosphatase inhibition (figure 1.1B) (Haase and Maret, 2003), prolonging the activation of tyrosine kinases, which themselves require de-phosphorylation by phosphatases for their deactivation. Tyrosine phosphatase inhibition is particularly important in cancers, as many are driven by tyrosine kinase activation (Motiwala and Jacob, 2006). The increase of intracellular zinc in response to an extracellular stimulus to modulate a physiological response demonstrates that zinc is a second messenger and highlights the importance of maintaining intracellular zinc homeostasis.

1.2. Zinc transporters

Zinc cannot pass through membranes passively, and therefore its homeostasis is dependent upon zinc transporters. Two families of zinc transporter exist; the ZnT (zinc transporter protein; SLC30A) family, which transport zinc out of the cytoplasm, and the ZIP (SLC39A) family which transport zinc into the cytoplasm (figure 1.2A). The ZnT family consists of 10 members, all with 6 transmembrane domains (TMDs), and intracellular N- and C-termini. ZnT1 resides on the plasma membrane, while all other members are present on intracellular membranes (Palmiter and Findley, 1995). ZnT transporters work as Zn^{2+}/H^{+} exchangers (Ohana *et al.*, 2009).

Many of the ZIP transporters reside on the plasma membrane and bring zinc in from the extracellular surroundings (figure 1.2B). A few however, have been shown to reside on membranes of the endoplasmic reticulum (ZIP7), the Golgi apparatus (ZIP7, ZIP9 and ZIP13), or intracellular storage vesicles (ZIP8, ZIP13 and ZIP14) and release zinc from their intracellular compartments (Takagishi, Hara and Fukada, 2017).

The ZIP family of zinc transporters consists of 14 members which are divided into 4 groups; Subfamily I (ZIP9), Subfamily II: (ZIP1, ZIP2 and ZIP3), gufA subfamily (ZIP11), and the LIV-1 subfamily: (ZIP4, ZIP5, ZIP6, ZIP7, ZIP8, ZIP10, ZIP12, ZIP13 and ZIP14). Evolutionary relationships between the groups is depicted in the phylogenetic tree in figure 1.3A.

Figure 1.2. Zinc homeostasis regulation by the ZnT and ZIP transporters

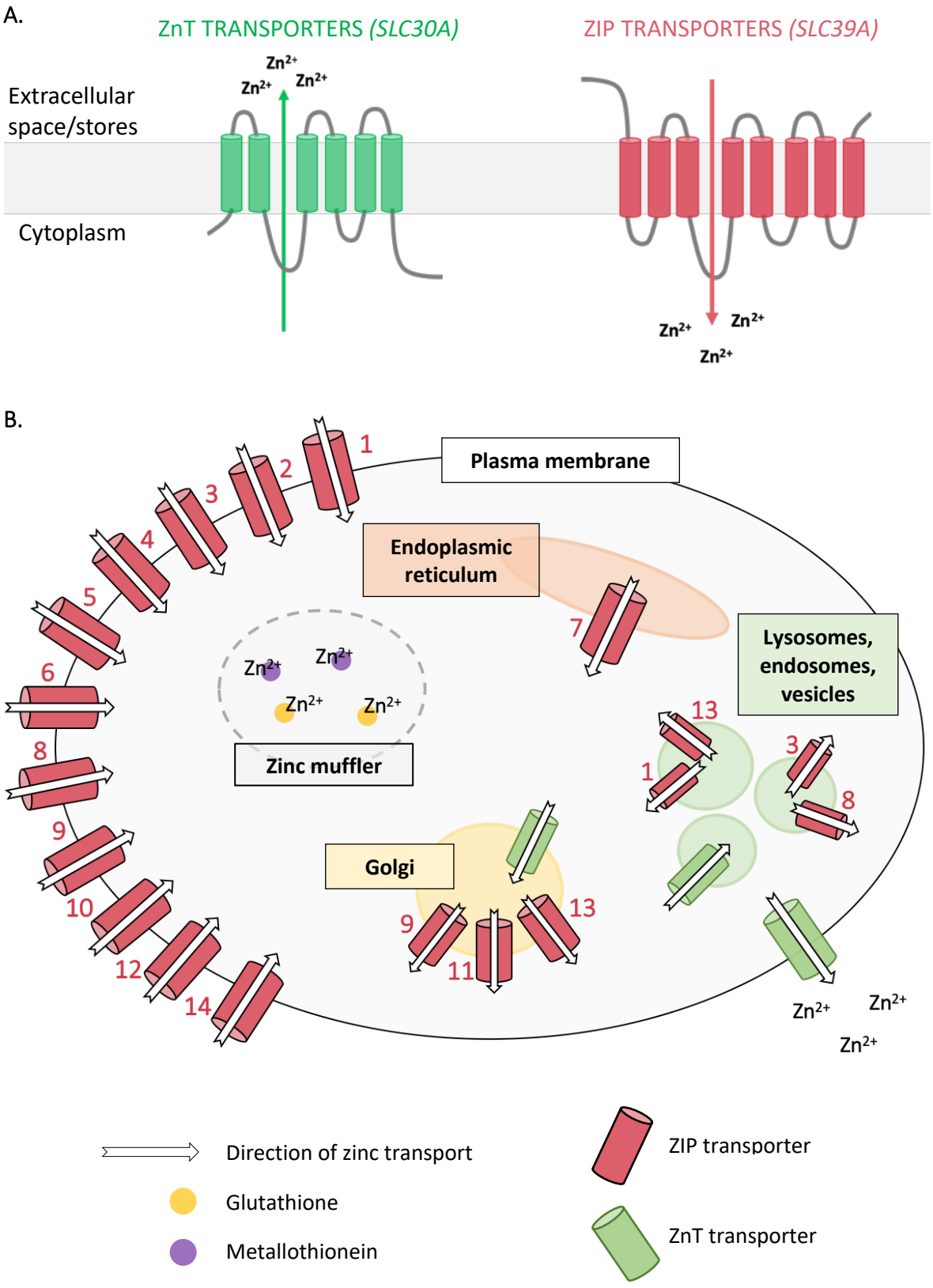

***A**. ZnT transporters (green) consist of 6 transmembrane domains and transport zinc out of the cytoplasm. ZIP transporters (pink) transport zinc into the cytoplasm. **B**. Known roles and locations of ZnT and ZIP transporters.*

Members of the LIV-1 family of ZIP transporters have 8 TMDs, a long extracellular N-terminus, and a short extracellular C-terminus (figure 1.3B). Across the protein there are multiple histidine rich regions, and it is believed that these regions are involved in zinc transport due to the ability of histidine to bind zinc (Guerinot, 2000).

The LIV-1 subfamily sequences contain a highly conserved *HEXPHE* (H, histidine; E, glutamic acid; X, any amino acid; P, proline) motif in TMD5 (Taylor *et al.*, 2007) (figure 1.4). This motif matches the catalytic zinc binding site of two members of the zinc metalloprotease superfamily; defined by their *HEXXH* motif as a signature zinc-binding sequence (Hooper, 1994; Dardel *et al.*, 1998).

A further conserved motif of the LIV-1 subfamily is the *CPALLY* (C, cysteine; P, proline; A, alanine; L, leucine; Y, tyrosine) motif located in the N-terminus (Taylor *et al.*, 2007) (figure 1.4). The whole motif contains 3 conserved cysteines which typically form disulphide bonds with other cysteine residues. There is an additional cysteine residue immediately upstream of the *HEXPHE* motif in TMD5 (figure 1.4), prompting the hypothesis that a tertiary structure is formed by the binding of the spare cysteine in the *CPALLY* motif with the cysteine in TMD5. In this case, the N-terminus would sit over the top of the transmembrane domains, potentially regulating zinc transport. There are two members of the LIV-1 family that do not possess the *CPALLY* motif, nor the cysteine residue in TMD5; ZIP7 and ZIP13. Interestingly, neither of these transporters have been shown to reside on the plasma membrane, implicating a potential relationship between these motifs and the localisation of ZIP transporters within the cell or regulation of zinc entry into the cell.

Figure 1.3. The LIV-1 family of ZIP transporters

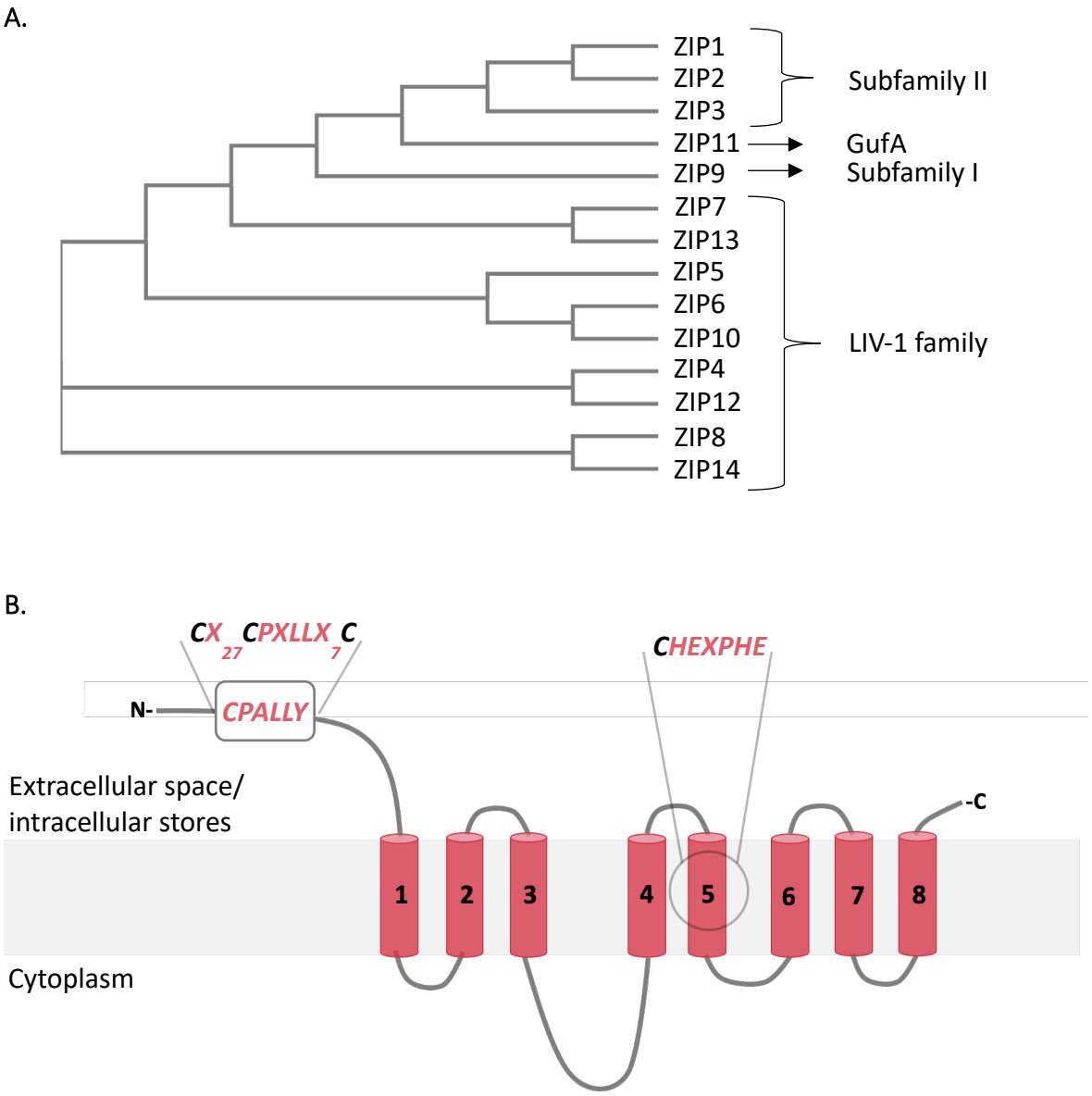

***A**. Phylogenetic tree of the human ZIP family of zinc transporters, divided into 4 groups, generated from Clustal Omega* (Goujon *et al.*, 2010). ***B**. Members of the LIV-1 family contain 8 transmembrane domains, a long extracellular N-terminus and a short C-terminus.*

Figure 1.4. Alignment of the 9 human members of the LIV-1 family of ZIP transporters

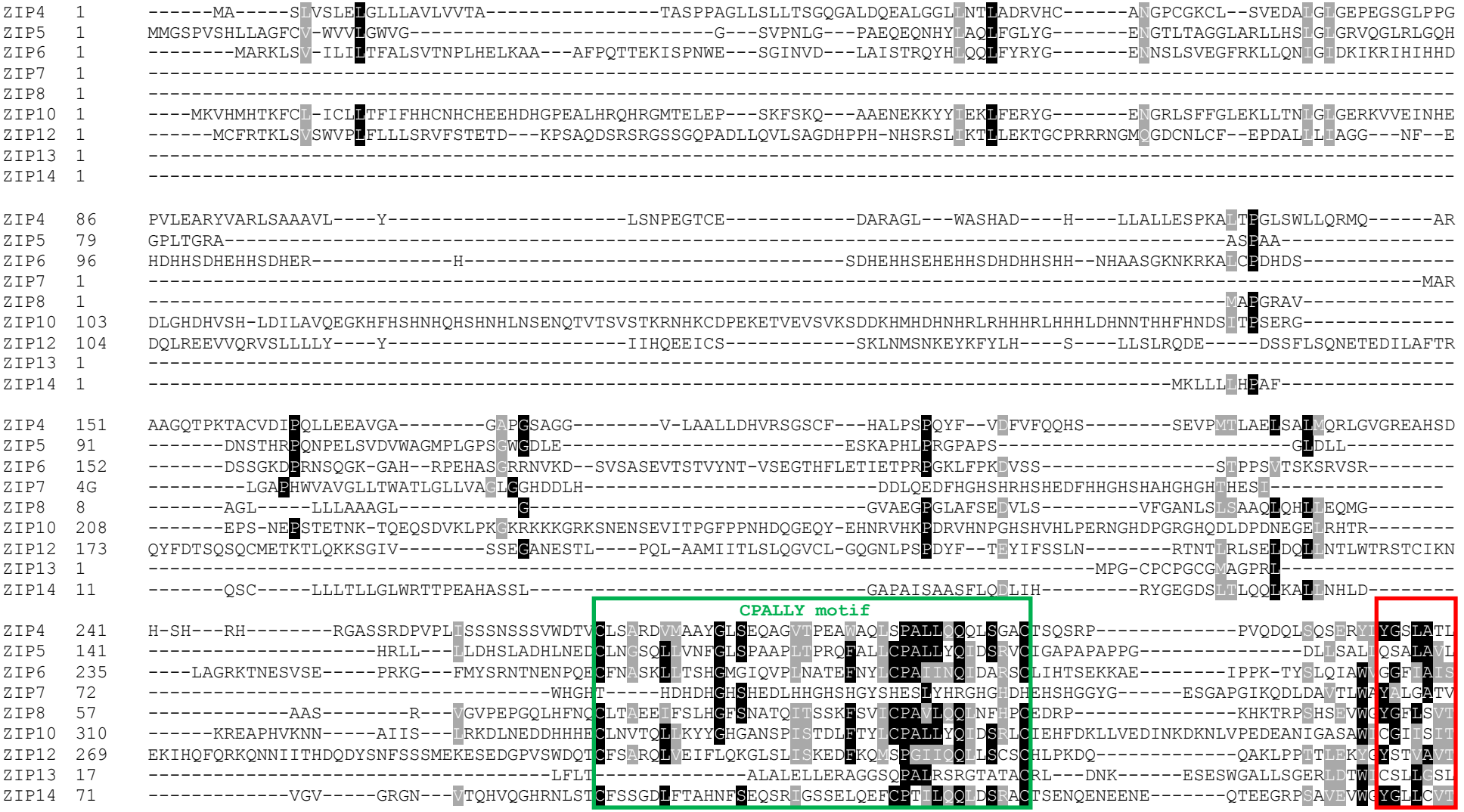

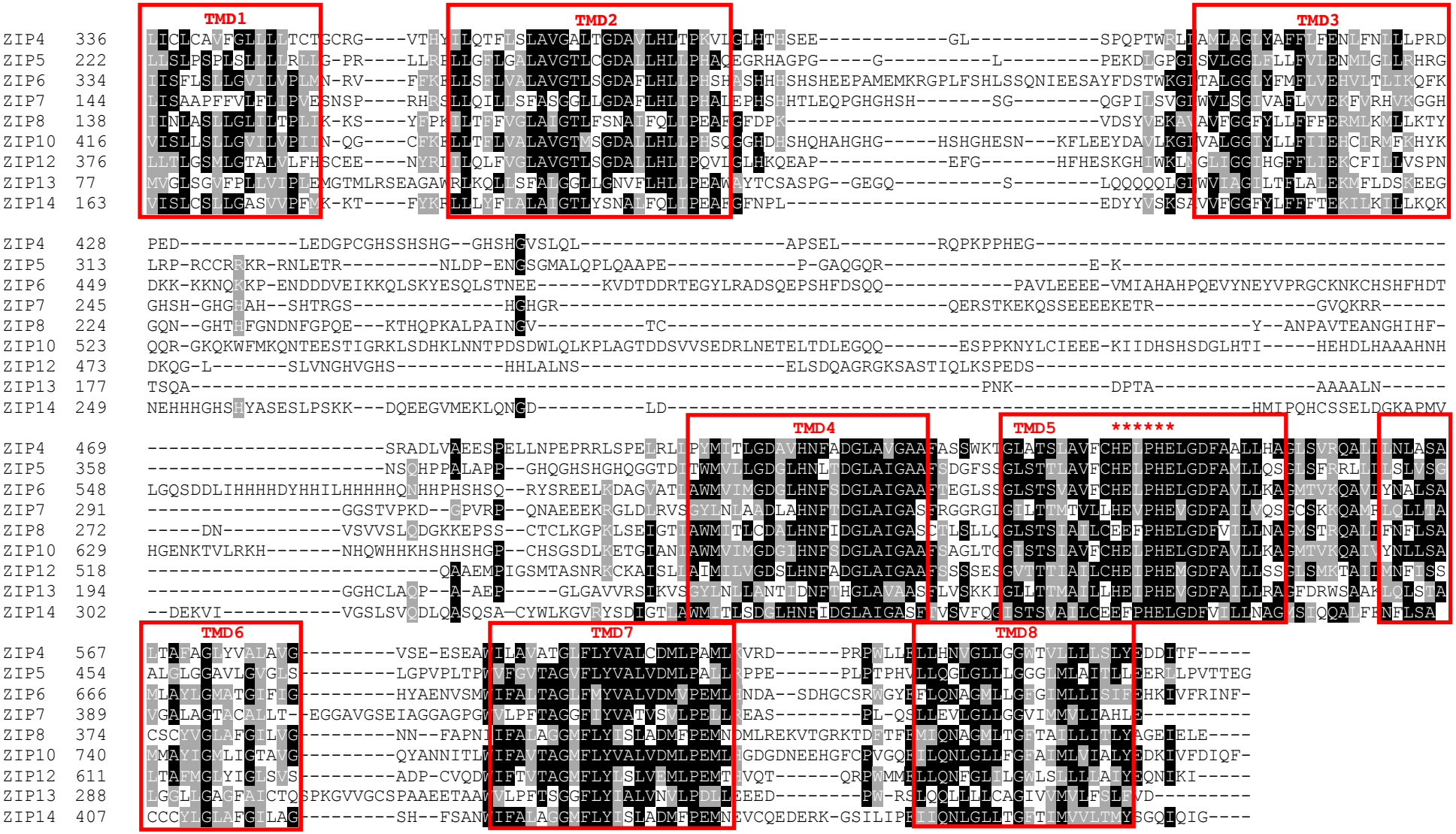

The CPALLY motif and transmembrane domains are highlighted with green and red boxes respectively. The starred region in TMD5 is the conserved HEXPHE motif. ZIP7 and ZIP13 do not contain the conserved C residue immediately before this motif. Alignment generated from Kalign (Li *et al.*, 2015)

1.3. Zinc and cell cycle regulation

Zinc is required for cells to move through the cell cycle; a tightly regulated series of events which allows cells to grow and divide. The cycle is split into distinct stages (figure 1.5A), each of which requires machinery specific to the events in that stage. In G1 (Gap 1), cells amplify their synthetic machinery ready for S (Synthesis) phase, where cells replicate their DNA (Rusan *et al.*, 2001). In G2 (Gap 2) cells reorganise their chromatin into chromosomes, and M (Mitosis) is the process by which normal cells divide. It is a tightly regulated process, and errors in mitotic signals can lead to uncontrolled cell division, or cancer. The whole process between the end of mitosis and the start of the next mitosis is also known as interphase. Intracellular zinc fluctuations have been measured throughout the cell cycle (Li and Maret, 2009), and there is a specific requirement for zinc at the transition between G1 and S phase (Li and Maret, 2009), G2 and M (Chesters, Petrie and Vint, 1989; Chesters and Petrie, 1999) and in G1 (Li and Maret, 2009). These timepoints are highlighted in figure 1.5A.

The finding that zinc is required for cells to enter mitosis (cell division) has led to speculation that it may be involved in the development of cancer, which is a disease of uncontrolled cell division (Asghar *et al.*, 2015). Mitosis itself is split into 5 stages, lasting approximately 1 hour in a 24-hour cell cycle (figure 1.5B). During prophase, the chromosomes tightly condense, becoming visible under a light microscope, while the microtubule spindle forms at the co-ordinating centre called the centrioles. In metaphase, the nuclear membrane disappears, and the condensed chromosomes line up in the middle of the cell (the metaphase plate). The microtubule spindles arrange their negatively charged ends at the centriole, and the positive end at the kinetochores (a protein complex associated with the centromere) (McDonald *et al.*, 1992). A checkpoint at metaphase ensures that the kinetochores are properly attached to the mitotic spindle so there is equal distribution of chromosomes at the end of mitosis (Foley and Kapoor, 2013). The tubules shorten, pulling the sister chromatids to opposite poles of the cell in anaphase. A nuclear membrane then begins to form around each group of chromatids, which begin to de-condense, and the spindle begins to break down (telophase). A pinch begins to form in the nuclear membrane, which develops further in cytokinesis, finally dividing the cell into two.

Figure 1.5. The cell cycle

A.

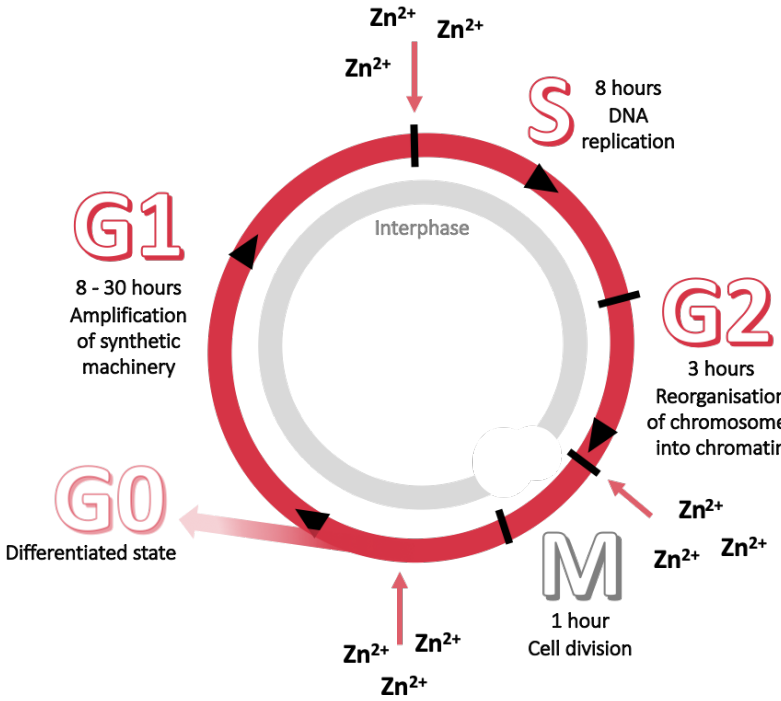

B.

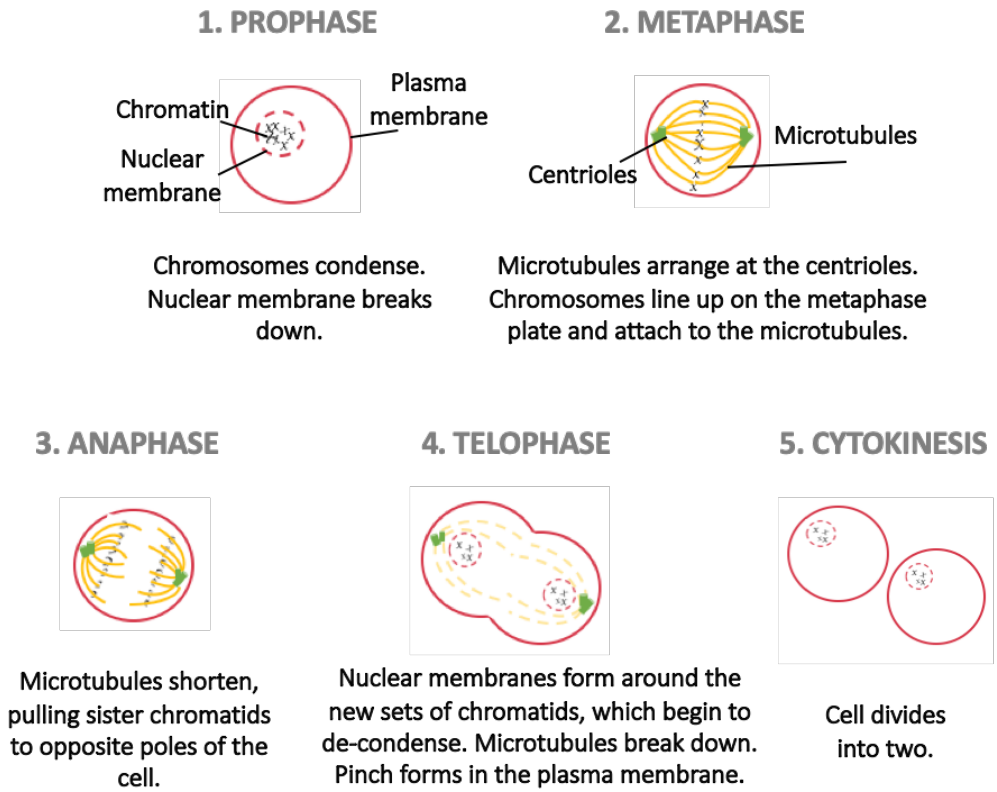

***A**. The cell cycle is divided into distinct stages. Timings shown are approximate for mammalian cells. After mitosis, cells can enter G0, also known as a 'resting' or differentiated state. **B**. Mitosis is further divided into 5 stages.*

1.4. Zinc and cancer

So far, zinc has been discussed in relation to its roles in inhibiting tyrosine phosphatases and passage of cells through the cell cycle. Both of these processes are important aspects of cancer; a large proportion of known oncogenes (genes with the potential to cause cancer) are known to be tyrosine kinases (Motiwala and Jacob, 2006) and cancer is a disease of uncontrolled cell division. It is therefore unsurprising that zinc has been implicated in cancer development and progression.

In addition, zinc has an established role in the proper functioning of matrix metalloproteases (MMPs). These are proteins which degrade the tissue matrix that surrounds cells, enabling cells to invade surrounding tissue, the first step required for cancers to develop in sites secondary to the original cancer (metastasis). Cancers that have spread have a poorer prognosis than those which remain in situ (Welch and Hurst, 2019). The catalytic domain of MMPs is a zinc binding motif, hence the need for zinc in order to function (Nagase and Woessner, 1999). This evidence suggests that zinc also has a role in the development of aggressive phenotypes in cancer.

In the following sections, the relationship with zinc and three specific cancers will be discussed in further detail.

1.4.1. Zinc and breast cancer

The breasts, also known as mammary glands, are comprised of glandular lobules which produce milk, and a system of ducts that transport milk to the nipple (figure 1.6). Breast cancer can occur in several cells of the breast, though a common site for breast cancer to develop is the epithelial lining of the ducts or lobules and are so-called ductal or lobular breast cancers.

Breast cancers are classified by their receptor status. Receptors are protein structures on the outside of all cells, which respond to chemical messengers from their environment. Breast cancer cells have three main cell surface receptors: oestrogen receptor, progesterone receptor (PR), and human epidermal growth factor receptor 2 (HER2) (reviewed by Akram et al. 2017). Oestrogen receptor-positive breast cancers depend on oestrogen for their growth and can therefore be treated with anti-oestrogens such as tamoxifen which prevents cell proliferation or aromatase inhibitors which prevent

oestrogen production in the body (Rozeboom, Dey and De, 2019). Patients with oestrogen receptor-positive breast cancers tend to have a good prognosis (Nasrazadani *et al.*, 2018). HER2 positive breast cancers respond to HER2-targeted agents such as the antibody trastuzumab, however these cancers tend to be more aggressive than the oestrogen receptor-positive cancers (Figueroa-Magalhães *et al.*, 2014). Triple negative breast cancers do not express any of these receptor types and there is therefore a lack of targeted therapies towards this type of breast cancer (Nasrazadani *et al.*, 2018).

Several studies have measured an increase in zinc in human breast tumour tissue compared with healthy breast tissue (Mulay *et al.*, 1971; Santoliquido PM, Southwick HW, 1976; Margalioth *et al.*, 1983; Jin *et al.*, 1999; Gumulec *et al.*, 2014) and this has also been replicated in mouse breast tumour tissue (Tupper, Watts and Wormall, 1955). In addition, one study showed that zinc was significantly increased in oestrogen receptor-positive areas of tumour, compared with oestrogen receptor-negative areas of invasive ductal cancers (Farquharson *et al.*, 2009), suggesting that zinc could be linked to oestrogen regulation in the breast tissue. X-ray fluorescence imaging of breast tumour tissues revealed zinc hyper-accumulation at the margins of oestrogen and progesterone receptor-positive breast tumours, and zinc was more evenly distributed within triple negative tumours (Chandler *et al.*, 2016). Increased zinc in benign breast tissue is associated with an increased risk of breast cancer development (Cui *et al.*, 2007) implicating the potential for the use of zinc as a biomarker of breast cancer risk.

Anti-hormone resistant breast cancer cells have double the amount of intracellular zinc when compared to wild-type (WT) breast cancer cells (Taylor M et al. 2008), suggesting a further increase in zinc in the more aggressive form of the disease. This hypothesis is supported by the data that show overexpression of the metal binding protein metallothionein in both breast cancer cells in culture and breast tumour tissue, and this is also associated with more invasive tumour types (Goulding *et al.*, 1995; Jin *et al.*, 1999; Yap *et al.*, 2009; Kim *et al.*, 2011). Metallothionein-bound zinc is thought to be the predominant form of zinc *in vivo* and its expression is induced by zinc itself.

Figure 1.6. Anatomy of the breast

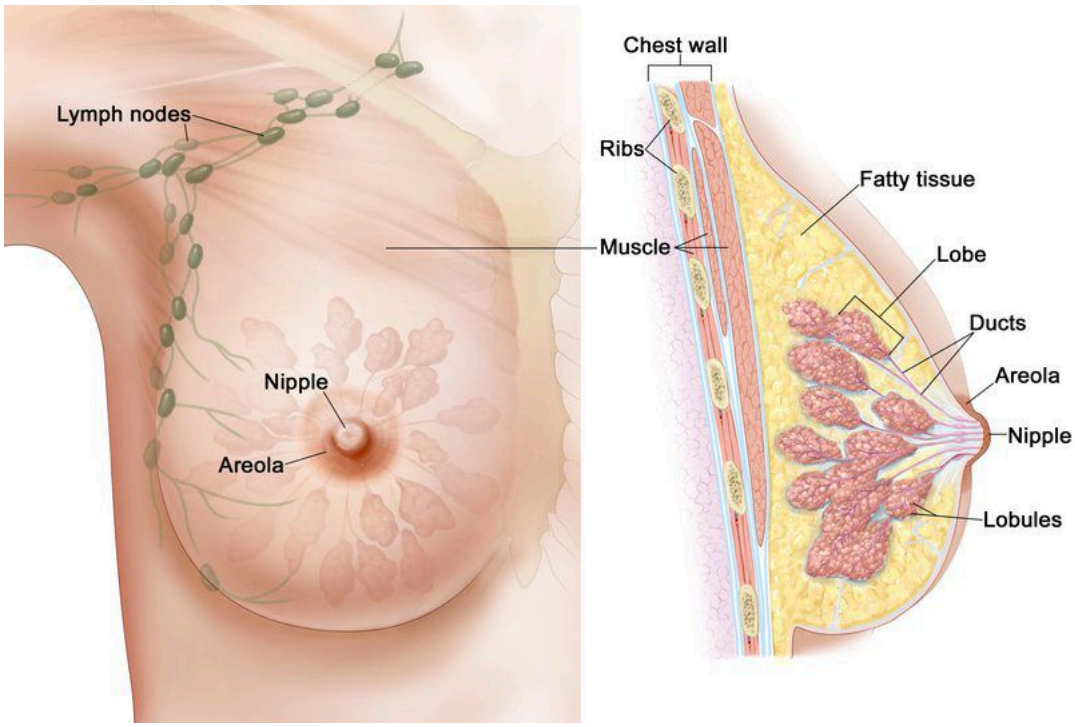

The glandular lobules produce milk which is transported to the nipple via a system of ducts. Cancers arising from the epithelial cells of the ducts or lobules are called ductal or lobular carcinomas respectively. Adapted from the National Breast Cancer Foundation.

The finding that zinc is increased in breast tumour tissue has led scientists to investigate other, less invasive, methods of measuring zinc in breast cancer patients. Serum zinc was shown to be decreased in patients with breast cancer compared with healthy controls (Gupta *et al.*, 1991; Gumulec *et al.*, 2014) however two other studies found no difference in the level of serum zinc in the two groups (Arinola and Charles-Davies, 2008; Wu, Tang and Xie, 2015). These data are somewhat conflicting and it should be noted here that zinc is known to bind albumin in the blood (Stewart *et al.*, 2003; Lu *et al.*, 2008), raising questions about the methods used to measure zinc. Further studies have measured zinc in the hair (Wu, Tang and Xie, 2015) finding a decrease in zinc compared to healthy patients, but no significant change in the serum of the same patients. Toenail clippings (Garland *et al.*, 1996) have also been studied in relation to zinc content and breast cancer risk, finding no association. The evidence suggests that measuring zinc directly in the breast tumour tissue is more reliable method to determine zinc content.

These data indicate that distinct subtypes of zinc dysregulation may exist, and these underlie phenotypic characteristics of breast cancers. It has even been suggested that zinc could be a reliable biomarker for grading breast cancers, as the concentration found in the tumour tissue correlates to the histological malignancy grade (Riesop *et al.*, 2015).

The increased zinc in breast tumour tissue implicates a role for zinc in breast cancer. Although its exact role remains to be determined, there is potential for zinc signalling pathways to be the target of new therapies in this cancer.

1.4.2. Zinc and prostate cancer

The prostate is a glandular organ of the male reproductive system with the primary function of secreting an alkaline fluid, which aids the motility and nourishment of sperm (Dunn, 2011). The gland has one of the highest concentrations of zinc in the body (Zaichick, Sviridova and Zaichick, 1997) due to its accumulation in the peripheral zone (figure 1.7), which is approximately 70% of the gland itself (Costello et al., 2004). Here, zinc has a well-established role in male fertility, sperm release and motility (Yoshida et al., 2008). Benign prostate hyperplasia (BPH) is the enlargement of the prostate gland and occurs commonly in older men. In BPH, the concentration of zinc in the central gland (about 25% of the prostate) is dramatically increased, often exceeding the normal concentration in the peripheral zone (Györkey *et al.,* 1967; Dhar *et al.,* 1973; Habib *et al.,* 1979; Franklin *et al.,*

2005). In contrast, in prostate cancer, there is a significant decrease in the concentration of zinc across the prostate (Györkey *et al.*, 1967; Dhar *et al.*, 1973; Habib *et al.*, 1979; Ogunlewe and Osegbe, 1989; Franklin *et al.*, 2005). This suggests that at the point of transformation to cancer cells, prostate cells lose their ability to accumulate zinc.

It is well-established that zinc has a chemo-protective role in the prostate. Zinc in this gland spares citrate from the citric acid cycle by inhibiting m-aconitase, allowing high amounts of citrate into prostate fluid (Costello *et al.,* 2005) (figure 1.7). This inhibitory effect protects against oxidative phosphorylation (Costello, Liu and Franklin, 1995; Costello *et al.*, 2005), which is supported by the data that show zinc deficient prostate cells have increased DNA damage (Yan *et al.*, 2008). Zinc also promotes a pro-apoptotic environment in the prostate (Feng *et al.*, 2002) by directly inducing Bax-mediated mitochondrial cytochrome c release, activating the caspase cascade which leads to apoptosis.

Currently, a widely used method to diagnose prostate cancer is the detection of prostate specific antigen (PSA) in the blood (Dunn, 2011). PSA is a serine protease released by the prostate however high PSA does not necessarily mean cancer is present because it is also released in BPH, infection, and trauma. Researchers are now seeking more specific ways to detect prostate disease, and the concentration of circulating zinc is one approach.

Two studies have shown an increase in serum zinc in patients with both benign and malignant prostate disease (Ogunlewe and Osegbe, 1989; Zhao *et al.,* 2016), while another showed an increase in benign prostate disease but a decrease in malignant disease (Goel 2006). The inconsistency highlights that measurements of zinc in the tissue directly are a more reliable indication of prostate disease than measurements in the circulation, as has also been shown in breast cancer.

Owing to the requirement of zinc in the protection of the prostate, it has been suggested that zinc supplementation could prevent prostate cancer development and indeed, in mice dietary zinc deficiency promoted prostate cancer growth (Prasad *et al.*, 2010; Fong *et al.*, 2018) while a study of over 35,000 men determined the risk of developing advanced prostate cancer decreased with an average intake of > 15 mg/day over a 10-year period (Gonzalez *et al.*, 2009).

Figure 1.7. Anatomy of the prostate

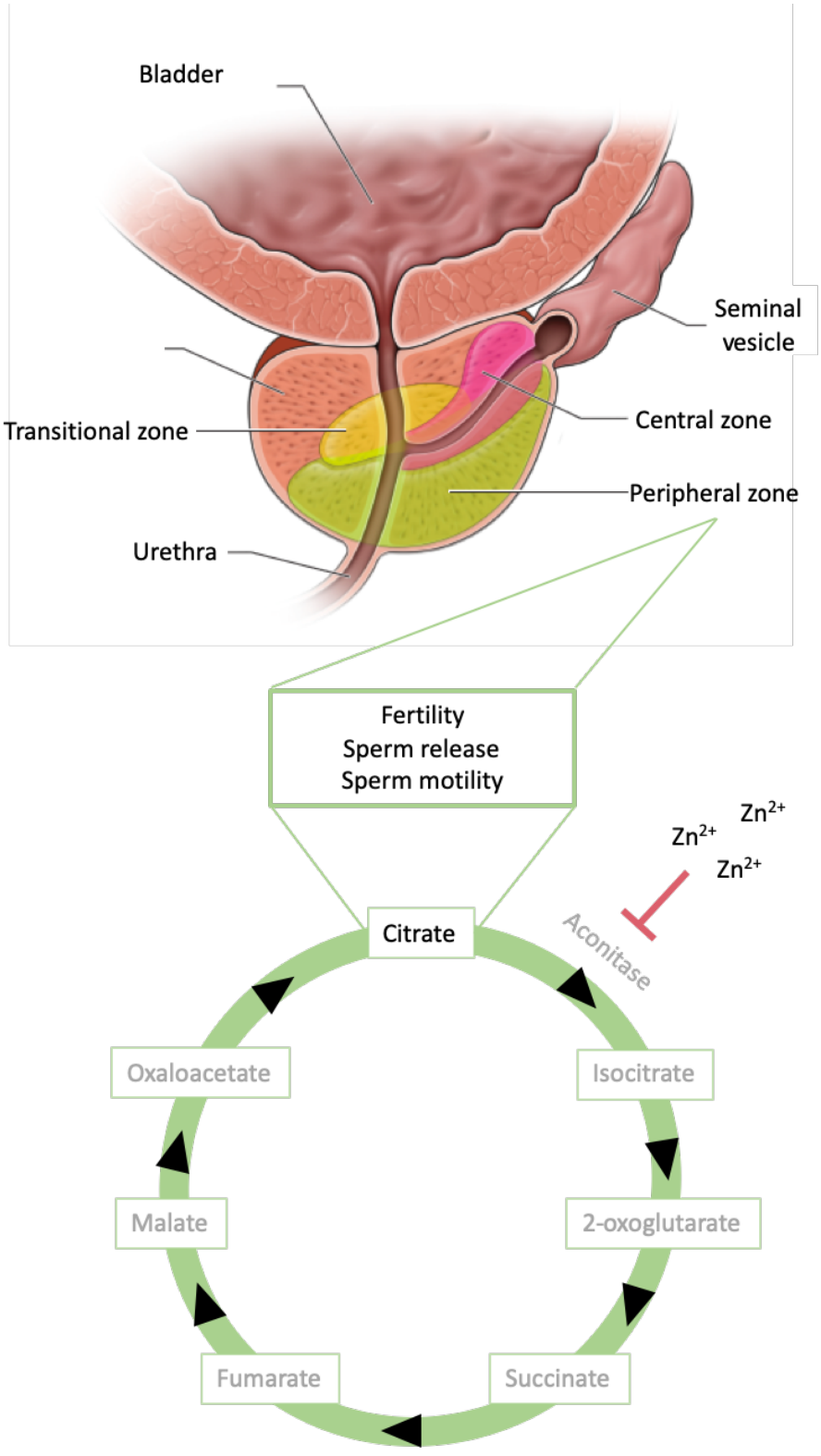

Zinc accumulates in the peripheral zone of the prostate gland. In the peripheral zone of the prostate, zinc inhibits m-aconitase in the citric acid cycle, preventing the production of isocitrate, and sparing citrate which plays a role in fertility, sperm release, and sperm motility.

In contrast, increased prostate cancer growth was seen in mice fed on high zinc diets (Prasad *et al.*, 2010) and in men taking zinc supplements for over ten years the risk of prostate cancer development was doubled (Kolonel, Yoshizawa and Hankin, 1988; Leitzmann *et al.*, 2003; Zhang *et al.*, 2009). One study showed that a daily dose of over 100 mg (almost 10 times the daily recommended dose for men) for 10 years doubled the risk of developing the disease (Leitzmann *et al.*, 2003). However, another study showed that increased zinc consumption had no effect on the risk of prostate cancer (Chang *et al.*, 2004). These results suggest there is an 'optimal' zinc concentration in the diet that could protect against prostate cancer. The evidence suggests that decreased dietary zinc increases the risk of prostate cancer though the beneficial effects of increasing dietary zinc are still under investigation.

1.4.3. Zinc and melanoma

The skin plays a role in several body functions including regulating body temperature, wound healing, UV (ultraviolet) protection and sensation. It is formed of two distinct layers; the epidermis and the dermis (figure 1.8). The outermost layer, the epidermis, provides a protective barrier to environmental toxins and pathogens, and contains the highest concentration of zinc out of all skin layers (Michaelsson G, Ljunghall K, 1980). The base of the epidermis is also home to melanocytes, the primary role of which is the production of melanin to protect against UV radiation (de Gruijl, 2017). Cancer originating in the melanocytes is called melanoma. The dermis is made mainly of collagen, elastin and connective tissue which give skin its strength and flexibility (Kolarsick, Kolarsick and Goodwin, 2006). It also contains immune cells such as mast cells which play a role in wound healing, a process in which zinc is involved, which helps to explain the high concentration of zinc in mast cells (Danscher G, Obel J, 1980).

Evidence suggests that zinc regulation is impaired in melanoma. A significant increase in serum zinc was measured in over 80% of melanoma patients in one study (Sánchez-Pedreño P, 1998). *In vitro*, exposure of melanocytes to extracellular zinc leads to a significant increase of intracellular zinc and is associated with overexpression of protein kinase B (also known as AKT), a known oncogene, and increased proliferation of melanocytes (Rudolf and Rudolf, 2017).

Figure 1.8. Anatomy of the skin

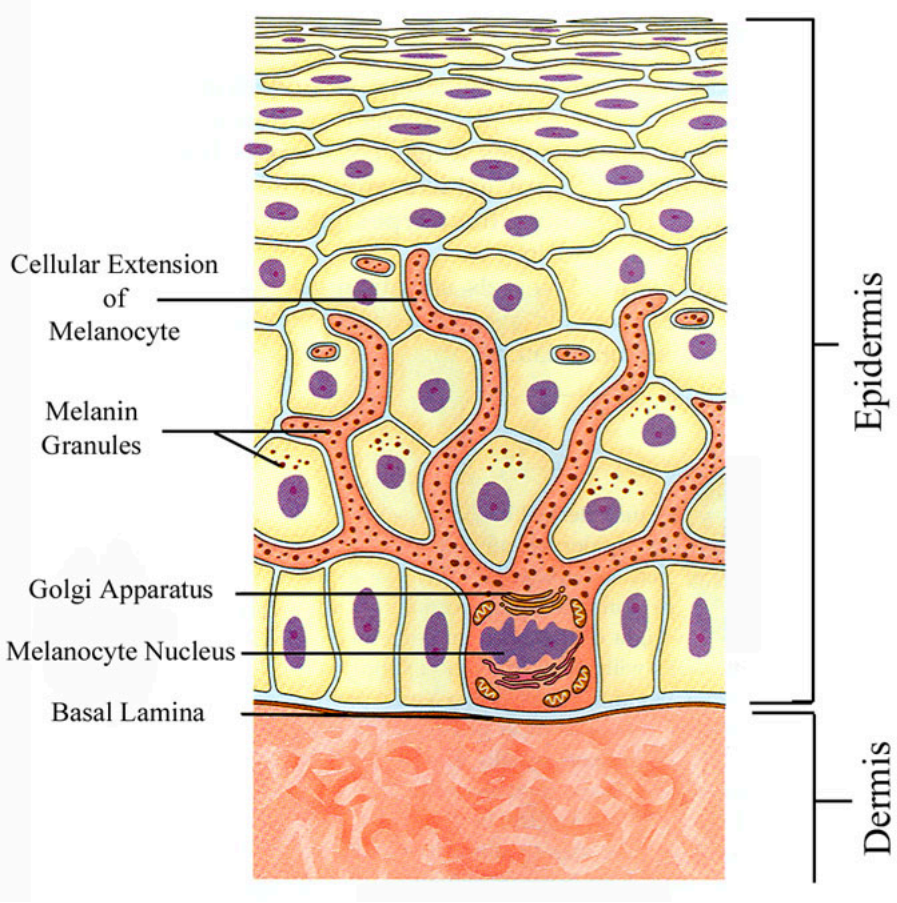

The skin is made of two main layers; the outermost epidermis and the dermis. Melanocytes produce melanin and reside in the base of the epidermis. Cancers arising from melanocytes are known as melanomas.

In addition to zinc, multiple studies have highlighted a positive correlation between metallothionein expression and melanoma progression (Weinlich *et al.*, 2003; Zamirska *et al.*, 2012; Emri *et al.*, 2013) and therefore its potential as a biomarker for detecting melanoma. Furthermore, Zamirska *et al.* (2012) demonstrated that metallothionein expression correlated with the proliferation marker Ki67 in squamous cell carcinoma, the second most common type of skin cancer. These data implicate overexpression of metallothionein and therefore zinc in the proliferation of melanoma and other skin cancers.

The potential role of zinc in cancers is not limited to those cancers presented here. Further studies have implicated its involvement in colorectal cancer (Kucharzewski *et al.*, 2003), renal cell carcinoma (Margalioth *et al.*, 1983) and liver cancer (Kew and Mallett, 1974). The exact role of zinc in cancer cell proliferation has not yet been determined, though a better understanding of the signalling pathways involved could offer new clinical biomarkers for cancer detection and/or therapies for cancer treatment.

1.5. ZIP transporters and cancer

The evidence presented in the previous section suggests a role for zinc in different cancers. However, some of the data regarding zinc concentrations in different tissues are contradictory and could be due to the tendency for zinc to be protein bound, and not freely available to study. More recently, researchers have begun studying zinc transporters and their downstream signalling pathways as a method to overcome the difficulties in studying zinc itself. There is growing evidence to suggest a role for the LIV-1 family of ZIP transporters in different types of cancer.

1.5.1. ZIP transporter ZIP7 and cancer

ZIP7 is within the top 10% of genes which are over expressed in clinical breast cancer with poor prognostic states (Taylor *et al.*, 2007), and it is also overexpressed in breast cancer cell lines which have developed resistance to tamoxifen (Taylor *et al.,* 2008). Acquired resistance to tamoxifen is a major clinical problem, with approximately 30% of women developing recurrent tumours within 10 years of treatment, and many of those will be metastatic (Haque and Desai, 2019). Increased ZIP7 in *in vitro* tamoxifen-resistant cells implicates ZIP7 in driving a more aggressive phenotype in breast cancer. Furthermore, protein expression of activated ZIP7 is significantly increased in both tamoxifen-resistant cells and human breast cancer tissue (Ziliotto *et al.*, 2019) suggesting the need for increased intracellular zinc

in these cells. This reflects the higher concentration of zinc measured in breast cancer tissue described earlier. Indeed, these cells have been shown to have an increased concentration of free intracellular zinc (Taylor et al. 2008). In addition, ZIP7 has been positively correlated with the proliferation marker Ki67 in breast cancer samples that demonstrated lymph node involvement (Taylor *et al.*, 2007). ZIP7 mRNA expression in breast cancer tissue is associated with a shorter relapse-free survival (Ziliotto *et al.*, 2019) highlighting the potential importance of ZIP7 as a prognostic indicator clinically.

It is not surprising the number of zinc signalling pathways being investigated as potential targets in cancer treatment, given the growing evidence of a role for zinc and ZIP transporters in cancer (Grattan and Freake, 2012). Activation of ZIP7 by CK2 (casein kinase 2) phosphorylation causes zinc release from intracellular stores (Taylor *et al.*, 2012) and widespread inhibition of tyrosine phosphatases. Tamoxifen resistant breast cancer cell lines as well as human tamoxifen resistant breast tumour tissue have increased zinc and increased protein expression of ZIP7 (Taylor *et al.*, 2007; K M Taylor *et al.*, 2008; Ziliotto *et al.*, 2019). Zinc treatment causes ZIP7-mediatied zinc release, and activation of pathways such as EGFR (epidermal growth factor receptor), IGF-R, MAPK (mitogen activated protein kinase), AKT, or Src, leading to activation of tyrosine kinases and a more aggressive phenotype (Taylor et al. 2008). The effect is abolished using ZIP7-targeted siRNA (silencing RNA). Phosphorylated ZIP7 is therefore not only a potential biomarker for aggressive phenotypes in breast cancer, but could realistically be a target for therapy. In addition, CK2 inhibitors have potential in preventing the activation of ZIP7 by phosphorylation, and have already shown potential as cancer therapies in leukaemia (Martins *et al.*, 2014), and glioblastoma (Zheng *et al.*, 2013). It has been shown that the CK2 inhibitor DMAT (2-Dimethylamino-4,5,6,7-tetrabromo-1H-benzimidazole,4,5,6,7-Tetrabromo-N,N-dimethyl-1H-benzimidazol-2-amine,4,5,6,7,Tetra-bromo-N,N-dimethyl-1H-benzo[d]imidazol-2-amine) causes tamoxifen-resistant breast cancer cell lines to die by apoptosis (Yde *et al.*, 2007).

1.5.2. ZIP transporter ZIP6 and cancer

ZIP6 is associated with oestrogen receptor-positive breast cancer (Manning *et al.*, 1993; Dressman *et al.*, 2001) and its expression is increased in those cancers which have spread to the lymph nodes (Manning *et al.*, 1994). Clinically, it is one of the genes used to distinguish luminal A breast cancer (Perou *et al.*, 2000; Tozlu *et al.*, 2006). ZIP6 has been linked to an acquired aggressive phenotype in pancreatic cancer tissue and pancreatic cells *in vitro* (Unno

et al., 2009; Sussman *et al.*, 2014), and is highly expressed in melanoma tissue (Sussman *et al.*, 2014), highlighting the potential for ZIP6 to be a useful biomarker in a number of cancers.

ZIP6 is a downstream target of STAT3 (signal transducer and activator of transcription 3), an oncogenic transcription factor that is elevated in many cancers (Avalle *et al.*, 2017) and constitutively active in breast cancer cells following oncogenic transformation (Garcia et al. 1997). ZIP6 is expressed as a pro-protein in the endoplasmic reticulum, and requires cleavage in the N-terminus before relocation to the plasma membrane (Hogstrand *et al.*, 2013) (figure 1.9). Zinc influx through ZIP6 causes inhibition of GSK3β (glycogen synthase kinase 3 beta; both directly and indirectly through activation of AKT), leading to the nuclear retention of Snail. Snail is a transcription factor that represses the expression of adhesion molecule E-cadherin (figure 9) (Hogstrand *et al.*, 2013). Cells then undergo a process called epithelial to mesenchymal transition (EMT), in which they gain invasive and migratory properties enabling them to become metastatic.

ZIP6 is associated with induction of EMT in both breast cancer cells (Hogstrand *et al.*, 2013) and pancreatic cancer cells (Unno *et al.*, 2009) through reduced E-cadherin expression and in prostate cancer cells (Lue *et al.*, 2011) through activation of MMP2 and MMP9 causing promotion of heparin binding EGF (epidermal growth factor) like growth factor activation and downstream EGFR signalling pathways. Furthermore, in pancreatic cancer tissue the level of ZIP6 expression is related to the tumour size and extent of infiltration into the lymphatic system (Unno *et al.*, 2009). A positive correlation between STAT3 and ZIP6 expression has also been demonstrated in clinical breast cancer samples (Taylor *et al.*, 2007), further implicating a role for ZIP6 expression and cancer development and progression.

Figure 1.9. The role of ZIP6 and STAT3 in epithelial to mesenchymal transition (EMT)

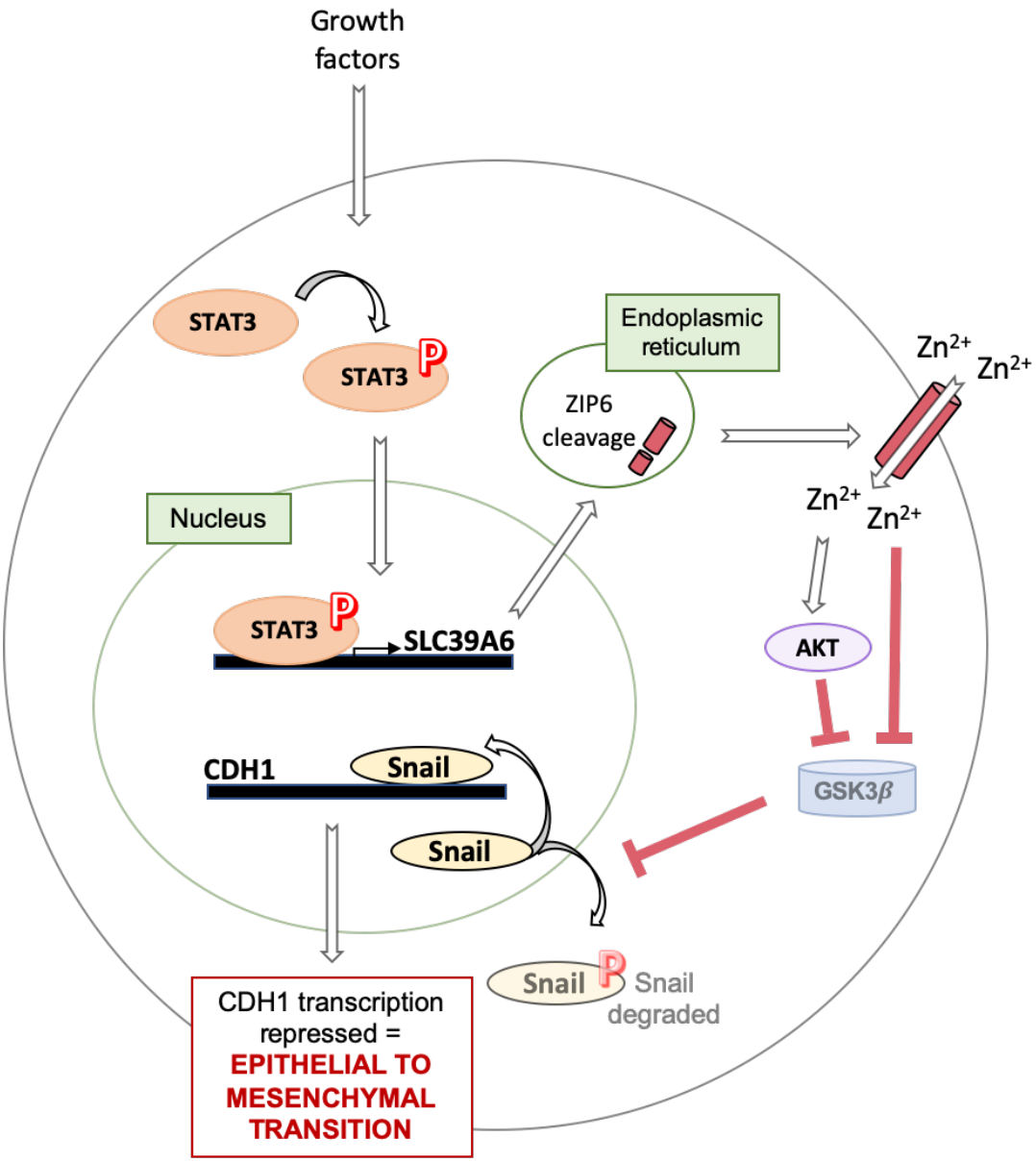

Transcriptional activation of ZIP6 by STAT3 causes zinc-dependent activation of AKT and inhibition of GSK3β. This prevents phosphorylation and degradation of Snail, and its nuclear retention represses transcription of CDH1, leading to cell detachment and EMT. Activation is shown in grey arrows and inhibition by pink lines.

1.5.3. ZIP transporter ZIP10 and cancer

ZIP10 has the closest sequence similarity with ZIP6 according to the phylogenetic tree in figure 1.3A. Clinically, there is a positive correlation of ZIP10 protein expression with oestrogen receptor expression (Taylor *et al.*, 2007) and metastasis of breast cancer to the lymph nodes (Kagara *et al.*, 2007). Increased ZIP10 mRNA expression has been shown in invasive breast cancer cell lines when compared to those that have less invasive properties (Kagara *et al.*, 2007). Significantly higher protein expression of ZIP10 is observed in high grade (grades 3–4) renal cell carcinoma as compared with lower grades (1–2) (Pal *et al.*, 2014).

Recent evidence suggests that ZIP10, like ZIP6, stimulates cell migration and proliferation in mammalian breast cancer cells (Taylor *et al.*, 2016). This is through the same mechanism as ZIP6 by inhibition of GSK3β and downregulation of E-cadherin expression. Increased ZIP10 mRNA in B-cell lymphoma promotes cell survival through inhibition of caspases and increased ZIP10 mRNA in this pathway is linked to STAT signalling (Miyai *et al.*, 2014), providing further evidence of a link between the oncogenic properties of STAT signalling pathways and ZIP transporters.

ZIP10 binds to ZIP6, forming a heteromer, and knockdown of either one of these transporters inhibits EMT (Yamashita *et al.*, 2004; Taylor *et al.*, 2016), which highlights the importance of both transporters in this process. ZIP6 and ZIP10 are both up to 10-fold more highly expressed in human oocytes than other ZIP transporters, and are essential for zinc accumulation in meiotic maturation (Kim *et al.*, 2010), implicating their co-expression and functional similarities in several cell types. ZIP6- and ZIP10-mediated zinc signalling has been linked to breast cancer cell motility when stimulated with glucose (Takatani-Nakase *et al.*, 2014), an important finding due to the increased risk of death in hyperglycaemic breast cancer patients compared to those who have healthy glucose levels.

1.5.4. Other ZIP transporters and cancer

There is growing evidence to suggest a role for a number of ZIP transporters in many types of cancer. ZIP1 has been shown to be downregulated in prostate cancer (Franklin *et al.*, 2005) and might explain the decrease in zinc associated with prostate cancer which was described in section 1.4.2. A similar effect has been suggested for ZIP4 (Chen *et al.*, 2012) and ZIP14 in prostate cancer (Xu *et al.*, 2016). ZIP14 downregulation has been detected in

liver cancer biopsies (Liu *et al.*, 2007) supporting a finding that these cancers also have less zinc (Al-Ebraheem, Farquharson and Ryan, 2009).

In contrast, upregulation of ZIP4 has been associated with pancreatic cancer (Li *et al.*, 2009). Increased expression of ZIP8 has been associated with oestrogen receptor-positive breast cancers of increasing grades (Chandler *et al.*, 2016). ZIP5 knock-out inhibits proliferation, migration and invasion of oesophageal cancer cells (Jin *et al.*, 2015) implicating a role for ZIP5 in oesophageal cancer development.

1.6. Targeting ZIP transporters to inhibit cell division in cancer

The evidence presented in this chapter highlights the involvement of both ZIP6 and ZIP10 in EMT; key components of this process are the loss of cell-cell adhesion molecules (Le Bras, Taubenslag and Andl, 2012) and the cell becoming more rounded, both of which are properties of cells entering mitosis (Pugacheva, Roegiers and Golemis, 2006; Hosseini *et al.*, 2019). Furthermore, zinc is required for cells to enter mitosis (Chesters, Petrie and Vint, 1989; Chesters and Petrie, 1999). Both transporters have been implicated as downstream targets of STAT3 which, itself has been linked to oncogenesis and malignancy in breast cancer (Vultur et al., 2004), squamous cell carcinoma of the head and neck (Steinman et al., 2003), prostate and ovarian cancers (Roy Garcia et al., 1997; Gao et al., 2001), colorectal cancer (Kusaba et al., 2006) and oral cancer (Gkouveris et al., 2014). Finally, cancer is a disease of uncontrolled cell division, highlighting the potential for ZIP6 and ZIP10 to be targeted to prevent cell division. To investigate how ZIP6 and ZIP10 could be targeted in more detail, it is important to first understand how both proteins are regulated at a post-translational level.

1.7. Post-translational modifications of ZIP transporters

Despite the growing evidence that ZIP transporters are associated with several cancers, relatively little is known about their regulation. A greater understanding of this might enable the generation of novel targeted cancer therapies. Two post-translational modifications (the enzymatic modification of proteins) have been shown to have a role in ZIP transporter regulation; phosphorylation and proteolytic cleavage (Kambe and Andrews, 2009; Taylor *et al.*, 2012).

1.7.1. ZIP transporter phosphorylation

Phosphorylation is an important modification which can activate or deactivate proteins across a large number of cellular processes. It is estimated that over 90% of proteins encoded by the human genome undergo phosphorylation (Ardito et al., 2017). The addition of a phosphate group to a specific amino acid changes the residue from hydrophobic to hydrophilic and a conformational change in the protein follows. The high reactivity of phosphate means that a phosphorylated protein can interact with many other proteins (Hunter, 2012), significantly increasing its signaling capacity. Phosphorylation is carried out by enzymes called kinases and can be quickly reverse by enzymes called phosphatases. The process of tyrosine phosphorylation and dephosphorylation is outlined in figure 1.1B, however tyrosine phosphorylation represents only a small fraction of phosphorylated residues across the cell; phospho-serine and phospho-threonine residues occur in a much greater abundance (Ardito et al., 2017).

ZIP7, which resides on the membrane of the endoplasmic reticulum, is activated by phosphorylation on two adjacent serine residues in the intracellular loop between TMD3 and TMD4 (Taylor *et al.*, 2012). Phosphorylation is by protein kinase CK2 (CK2) and the subsequent zinc release leads to the phosphorylation of multiple kinases associated with carcinogenesis including MAPK, PI3K-AKT (phosphoinositide 3 kinase-AKT) and MTOR (mechanistic target of rapamycin) (Nimmanon *et al.*, 2017). The involvement of ZIP7 in these pathways places ZIP7 and CK2 at the centre of intracellular zinc release and cancer progression and highlights the importance of phosphorylation as a post-translational modification.

The discovery that ZIP7 is activated by phosphorylation suggests that other ZIP transporters could be regulated in a similar way. Potential sites of phosphorylation have been identified in all other members of the LIV-1 family of ZIP transporters (Nimmanon and Taylor, 2019), however, much more experimental work needs to be carried out in order to examine the role of this modification in zinc transporter regulation.

1.7.2. ZIP transporter proteolytic cleavage

Proteolytic cleavage is an important regulator of many proteins. ZIP4, a member of the LIV-1 family of ZIP transporters, undergoes proteolytic cleavage immediately upstream of TMD1 (Kambe and Andrews, 2009). This cleavage is known as ectodomain shedding, because it

involves the removal of the N-terminal ectodomain, while the transmembrane regions in the protein remain in the plasma membrane. In periods of prolonged dietary zinc deficiency, only the transmembrane-spanning regions of ZIP4 are detected on the plasma membrane, indicating that ectodomain shedding occurs in response to zinc availability (Kambe and Andrews, 2009). In addition, cleavage is inhibited by mutations in ZIP4 that cause acrodermatitis enteropathica (which decreases zinc transport in the gut), suggesting that ectodomain shedding of ZIP4 activates zinc transport. Replenishment of zinc does not alter the levels of ZIP4 mRNA (Weaver *et al.*, 2007) confirming that the regulation is post-translational. Other ZIP transporters are also regulated by proteolytic cleavage; ZIP10 undergoes N-terminal ectodomain shedding, in response to zinc starvation in mouse neuroblastoma cells (Ehsani *et al.*, 2012) and N-terminal cleavage of ZIP6 occurs in the endoplasmic reticulum before localisation at the plasma membrane (Hogstrand *et al.*, 2013). These data indicate proteolytic cleavage is an important regulator of ZIP transporter activation and given the link with ZIP transporters and cancer it would be valuable to identify the proteases responsible for cleavage in order to understand further the mechanisms of cancer development and progression.

1.8. Hypothesis

The finding that expression of ZIP transporters ZIP6, ZIP7 and ZIP10 is significantly increased in breast cancer (Manning *et al.*, 1993; Dressman *et al.*, 2001; Kagara *et al.*, 2007; Taylor *et al.*, 2007), and the known involvement of zinc in cell cycle regulation (Chesters, Petrie and Vint, 1989; Chesters and Petrie, 1999; Li and Maret, 2009) has led our research group to investigate the underlying mechanisms of ZIP transporter regulation, and to explore novel ways of targeting zinc signalling pathways involved in cell division.

This project tested the hypotheses that:

1. ZIP10, like ZIP6 and ZIP7, is regulated by post-translational modification including proteolytic cleavage and phosphorylation;
2. The ZIP6/ZIP10 heteromer can be targeted to prevent cell division in multiple cancers.

1.9. Aims and objectives

The aims for this project are:

1. To investigate how ZIP10 is post-translationally modified

   Objectives for aim 1

   a. To analyse of the ZIP10 protein sequence and identify potentially important residues for post-translational modification;
   b. To investigate potential proteases involved in ZIP10 cleavage;
   c. To identify specific residues for ZIP10 phosphorylation and investigate phosphorylation by specific kinases.

2. To investigate the role of ZIP10 in cell division

   Objectives for aim 2

   a. To investigate post-translational modifications identified in aim (1) specifically during cell division;
   b. To identify mitotic proteins with which ZIP10 interacts, and investigate this interaction during mitosis;
   c. To investigate ZIP10 regulation throughout the cell cycle, and in response to zinc starvation.

3. To investigate the potential for targeting ZIP6 and ZIP10 to inhibit cell division

   Objectives for aim 3

   a. To evaluate specificity of novel anti-ZIP6 and -ZIP10 antibodies towards ZIP6 and ZIP10;
   b. To determine the appropriate concentration of the antibodies to inhibit cell division effectively in breast cancer, prostate cancer and melanoma cells;
   c. To evaluate the extent to which anti-ZIP6 and -ZIP10 antibodies inhibit cell division in normal (non-cancerous) cells;
   d. To identify the effect of targeting ZIP6 and ZIP10 on downstream cellular signalling pathways.

Chapter 2. Materials and methods

2.1. Software analysis of ZIP transporter sequences

A thorough search of bioinformatic databases was conducted to find out information about ZIP transporter protein sequences. Unless stated otherwise, the data refer to the human sequence of ZIP10 and was generated using FASTA format from the UniProt Knowledgebase (Consortium, 2018). Predicted sites of proteolytic processing were determined using the epestfind tool within the European Molecular Biology Open Software Suite (EMBOSS), and ELM (Eukaryotic Linear Motif) (Dinkel et al., 2016). Potential N-linked glycosylation of human ZIP10 was predicted using the NetNGlyc 1.0 server (Gupta, Jung and Brunak, 2004). Phosphorylation sites and their corresponding predicted kinases were determined using PhosphositePlus® (Hornbeck et al., 2004), PhosphoNET, PHOSIDA (Gnad et al., 2007), NetPhos (Blom et al., 2004), NetPhorest (Miller et al., 2008). The molecular mass of each predicted fragment was obtained from the Compute pI/Mw tool (Bjellqvist et al., 1993). Protein-protein interactions were determined through ELM and the Biological General Repository for Interaction Datasets (BioGRID) (Oughtred et al., 2019). Nuclear localisation signals (NLS) were identified using cNLS Mapper (Kosugi et al., 2009).

2.2. Cell culture

MCF7 (human breast adenocarcinoma) cells were cultured in RPMI 1640 (Roswell Park Memorial Institute) (Life Technologies; 21875-034) medium containing 5% foetal calf serum (FCS) (v/v) (Sigma; F2442). DU145 (human prostate carcinoma) cells were cultured in DMEM (Dulbecco's Modified Eagle Medium) (Gibco™; 11960-044) containing 10% FCS (v/v) and 200 mM L-glutamine, and SK-MEL-29 (human melanoma) cells were cultured in DMEM formulated with low glucose (Gibco™; 31885-023, 10% FCS (v/v), and 0.5 μg/mL insulin (Sigma; I0516). NMuMG (normal murine mammary gland) and NMuMG ZIP6 knockout (KO) cells were cultured in DMEM containing 10% FCS (v/v) and 200 mM L-glutamine (ThermoFisher; 25030024). All cells were supplemented with antibiotics (10 IU/mL penicillin, 10 μg/mL streptomycin) (Life Technologies; 15140-148) and an anti-fungal (2.5 μg/mL amphotericin B) (Life Technologies; 15290-018). The details of these growth media can be found in table 2.1. Cells were grown at 37 °C, in a humid environment with 5% CO_2. Growth medium was replaced every 3-4 days.

Cells were passaged by incubation in 5 mL trypsin/EDTA (ethylenediaminetetraacetic acid; Life Technologies; 15400-054) for 3-5 minutes at 37 °C. Cells were collected into a 30 mL

universal tube and the trypsin was neutralised with 5 mL fresh growth medium. The cells were spun at 168 x g for 5 minutes, the supernatant discarded, and the pellet resuspended in 5 mL fresh growth medium. 0.5 mL resuspended cells were grown in a new T25 flask for 6–7 days.

Cells were counted in a single cell suspension using an automated cell counter (Beckman Coulter™). Where cells were required for western blot or immunofluorescence, 1 x 10^5 cells were seeded onto 35 mm dishes with or without 22 x 22 mm 0.17 mm thick glass coverslips. For immunoprecipitation (IP), 3 x 10^5 cells were seeded onto 60 mm dishes. For PLA (proximity ligation assay) or anti-ZIP6/-ZIP10 antibody treatment, 1.5 x 10^4 cells were seeded into each well of an 8-well chamber slide (ThermoFisher; 171080).

2.3. Cell treatments

Cells were grown to 70–80% confluency before treatment for experiments. All treatments were made in fresh growth medium and carried out at 37 °C, in a humid environment with 5% CO_2.

a. **Mitotic synchronisation:** to synchronise cells in mitosis, they were treated with 150 nM nocodazole (Sigma; M1404) for up to 20 hours. In order for the cells to recover from nocodazole, the treatment was removed and replaced with normal growth medium for up to 6 hours.
b. **Zinc starvation:** to remove zinc from the culture medium, cells were treated with either 5 μM TPEN (N,N,N′,N′-tetrakis(2-pyridinylmethyl)-1,2-ethanediamine; Sigma; P4413) or serum-free growth medium (table 2.1) for 30 minutes.
c. **Zinc treatment:** to replenish zinc in the growth medium, cells were treated with 20 μM zinc (Sigma) and 10 μM sodium pyrithione (Sigma) in phenol-red-free RPMI medium (Life Technologies; 32404-014), with no FCS, antibiotics or antifungals added, for 10 minutes.
d. **Inhibition of ZIP10 proteolytic cleavage:** cells were treated for 10 minutes with protease inhibitors DAPT (N-[N-(3,5-difluorophenacetyl)-L-alanyl]-S-phenylglycine t-butyl ester; Sigma; D5942) or nelfinavir mesylate hydrate (Sigma; PZ0013) were used at 10 μM and 30 μM concentrations respectively.
e. **Antibody inhibition of mitosis:** nocodazole-induced mitosis was inhibited by incubation with 150 nM nocodazole with or without anti-ZIP6 (Y3) and -ZIP10 (N1)

antibodies for 18 hours (table 2.2). Antibodies were used at a range of concentrations from 0.4–28 μg/mL. Normal mouse/rabbit IgG (immunoglobulin G) antibodies (Santa Cruz; 2025 and 2027) were used as control antibodies at the same concentration as the anti-ZIP6 and -ZIP10 antibodies.

f. **Zinc assay:** to measure the intracellular free zinc content, cells were incubated in 5 μM FluoZin™-3 (ThermoFisher; F24195) for 30 minutes followed by centrifugation at 168 x g for 5 minutes. Cells were incubated in growth medium with 5% serum (v/v) for a further 30 minutes. All steps throughout the zinc assay were carried out in the dark.

Table 2.1. Cell lines used in this project and their respective growth medium

Cell line	Growth medium	FCS (v/v)	Antibiotics and anti-fungals	Other supplements
MCF7	RPMI 1640	5%	Penicillin, Streptomycin, amphotericin B	-
DU145	DMEM (4.5 g/L glucose)	10%	Penicillin, Streptomycin, amphotericin B	200 mM L-glutamine
SK-MEL-29	DMEM (1 g/L glucose)	10%	Penicillin, Streptomycin, amphotericin B	0.5 μg/mL insulin
NMuMG and NMuMG ZIP6 KO	DMEM (4.5 g/L glucose)	10%	Penicillin, Streptomycin, amphotericin B	200 mM L-glutamine
MDA-MB-231	DMEM (4.5 g/L glucose)	10%	-	-

Growth medium was supplemented with foetal calf serum (FCS), antibiotics and antifungals, L-glutamine and/or insulin.

Table 2.2. Anti-ZIP antibodies used in this project

Antibody	Supplier ID	Source	Epitope	Dilution used		
				WB	IF	OTHER
LIV-1 (E-20)	Santa Cruz; sc-84875	Rb	ICL TMD3–4; residues 500–550	-	1:100	PLA (1:100)
ZIP5	Abcam; ab76191	Rb	N-terminus; residues 38–87	1:1000	-	-
ZIP6 Y3	In-house	Ms	N-terminus; residues 238–254	1:1000	1:100	-
ZIP10 N1	In-house	Rb	N-terminus; residues 46–59	1:1000	1:100	-
ZIP10 N2	In-house	Ms	N-terminus; residues 46–59	1:500	1:100	-
ZIP10 N3	Sigma; HPA036513	Rb	N-terminus; residues 156–252	1:1000	1:100	-
ZIP10 L4	Abcam; ab33947	Rb	ICL TMD3–4; residues 514–530	1:1000	1:100	PLA (1:100)
ZIP10 L5	Sigma; SAB1401780	Ms	ICL TMD3–4; residues 514–621	1:1000	1:100	PLA (1:100)

The table indicates the supplies, species, and dilution at which the antibody was used in this project. The ZIP10 N1 antibody is polyclonal and the ZIP10 N2 antibody is monoclonal. IF, immunofluorescence; LIV-1, anti-ZIP6 antibody; WB, western blot; PLA, proximity ligation assay; FACS, fluorescence-activated cell sorting; ICL, intracellular loop; TMD, transmembrane domain; Rb, rabbit; Ms, mouse.

Table 2.3. Primary antibodies used in this project

Antibody	Supplier ID	Source	Dilution used		
			WB	IF	OTHER
CDK1	Cell Signaling technology; 9116	Ms	1:1:000	-	PLA (1:100)
pY^{15}CDK1	Cell Signaling technology; 4359	Rb	-	-	PLA (1:100)
Normal mouse IgG	Santa Cruz; sc-2025	Ms	-	-	Cell treatment (4 μg/mL)
Normal rabbit IgG	Santa Cruz; sc-2027	Rb	-	-	Cell treatment (10 μg/mL)
Pim-1	Cell Signaling Technology; 54523	Rb	1:1000	-	-
Pim-3	Cell Signaling Technology; 4165	Rb	1:1000	-	-
PKA	Cell Signaling Technology; 4782	Rb	1:1000	-	-
PLK1	Abcam; ab17056	Ms	1:100	-	PLA (1:100)
pT^{210}PLK1	Cell Signaling Technology; 5472	Rb	1:100	-	PLA (1:100)
pS^{10}Histone H3	Cell Signaling Technology; 9706	Ms	1:1000	1:200	FACS (1:100)
pS^{10}Histone H3	Cell Signaling Technology; 3377	Rb	1:1000	1:200	FACS (1:100)
pS^{727}STAT3	Cell Signaling Technology; 9136	Ms	1:1000	-	FACS (1:50); PLA (1:50)
pS^{727}STAT3	Santa Cruz; sc-8001	Rb	1:1000	1:50	FACS (1:50); PLA (1:50)
pSerine	Abcam; ab9332	Rb	1:1000	-	-
pThreonine	Cell Signaling Technology; 9386	Ms	1:1000	-	-
pTyrosine	Cell Signaling Technology; 8954	Rb	-	-	FACS (1:100)
V5	Invitrogen; R960-25	Ms	1:1000	1:1000	FACS (1:100)
V5	Abcam; ab15828	Rb	-	-	FACS (1:100)

The table indicates the supplies, species, and dilution at which the antibody was used in this project. WB, western blot; IF, immunofluorescence; PLA, proximity ligation assay; FACS, fluorescence-activated cell sorting; Rb, rabbit; Ms, mouse.

Table 2.4. Secondary antibodies used in this project

Antibody	Supplier ID	Source	Dilution used		
			WB	IF	OTHER
Anti-mouse Alexa Fluor® 488	Life Technologies; A10684	Gt	-	1:1000	FACS (1:1000)
Anti-mouse Alexa Fluor® 594	Life Technologies; A11032	Gt	-	1:1000	-
Anti-rabbit Alexa Fluor® 488	Life Technologies; A11034	Gt	-	1:1000	FACS (1:1000)
Anti-rabbit Alexa Fluor® 594	Life Technologies; A11072	Gt	-	1:1000	-
Anti-Rabbit Alexa Fluor® 647	Life Technologies; A21245	Gt	-	-	FACS (1:1000)
Anti-mouse HRP conjugated	Cell Signaling Technology; 7076	Hs	1:10,000	-	-
Anti-rabbit HRP conjugated	Cell Signaling Technology; 7074	Gt	1:10,000	-	-
β-actin HRP conjugated	Cell Signaling Technology; 5125	Rb	1:50,000	-	-
GAPDH HRP conjugated	Sigma; G9295	Rb	1:50,000	-	-

The table indicates the supplies, species, and dilution at which the antibody was used in this project. WB, western blot; IF, immunofluorescence; PLA, proximity ligation assay; FACS, fluorescence-activated cell sorting; Gt, goat; Hs, horse; Rb, rabbit.

2.4. Development of in-house antibodies

Anti-ZIP6 and -ZIP10 antibodies were generated by Biogenes GmBH, against human peptides *VSEPRKGFMYSRNTNEN* and *LEPSKFSKQAAENE* respectively. Epitopes are in the N-terminal ectodomain of each protein (figure 2.1).

2.5. Enzyme-linked immunosorbent assay (ELISA)

The concentration of in-house mouse antibodies was measured using the Mouse IgG total Ready-SET-Go!® ELISA assay (Affymetrix eBioscience; 88-50400), according to the manufacturer's protocol. For details of the buffers used, see appendix 1. In brief, each well of a 96-well plate was coated in 100 μL coating buffer and incubated overnight at 4 °C. Wells were washed twice in wash buffer and blocked with blocking buffer for 2 hours at 23 °C. The standard mouse IgG was measured in two-fold dilutions, with a starting concentration of 100 ng/mL. Unknown samples were pre-diluted 500-fold before 2-fold serial dilutions were made. 10 μL of the sample at each dilution was added to 90 μL assay buffer A and put into each well in duplicate, with 50 μL detection antibody. The plate was covered and incubated for 3 hours at 23 °C. The plate was then washed in wash buffer A four times, and 100 μL substrate solution added per well. This was left to develop at 23 °C for 15 minutes and 100 μL stop solution added to stop the reaction. The 96-well plate was measured at 450 nm and the concentration of antibodies derived from the standard curve using Microsoft® Excel for Mac.

2.6. Easy-Titer™ IgG assay

The concentration of the in-house rabbit antibodies was measured using the Easy-Titer Rabbit IgG Assay Kit (ThermoFisher; 23305) according to the manufacturer's protocol. In short, the rabbit IgG isotype control antibody (ThermoFisher Scientific; 31235) was diluted to 100 μg/mL in PBS (phosphate buffered saline), from which 2-fold dilutions were prepared in dilution buffer. Starting dilutions of the sample antibody were prepared in the dilution buffer ranging from 1:50 to 1:5000. Only samples which fit on the standard curve were used in the final calculation. 20 μL of pre-mixed Anti-IgG Sensitized Beads were added to each well of a 96-well plate, with 20 μL of standards or samples. The plate was mixed continuously for 5 minutes. 100 μL blocking buffer was added per well and the plate mixed for a further 5 minutes. The plate was measured at 405 nm and the concentration of antibodies derived from the standard curve using Microsoft® Excel for Mac.

Figure 2.1. Epitopes of in house anti-ZIP6 and -ZIP10 antibodies used to inhibit mitosis

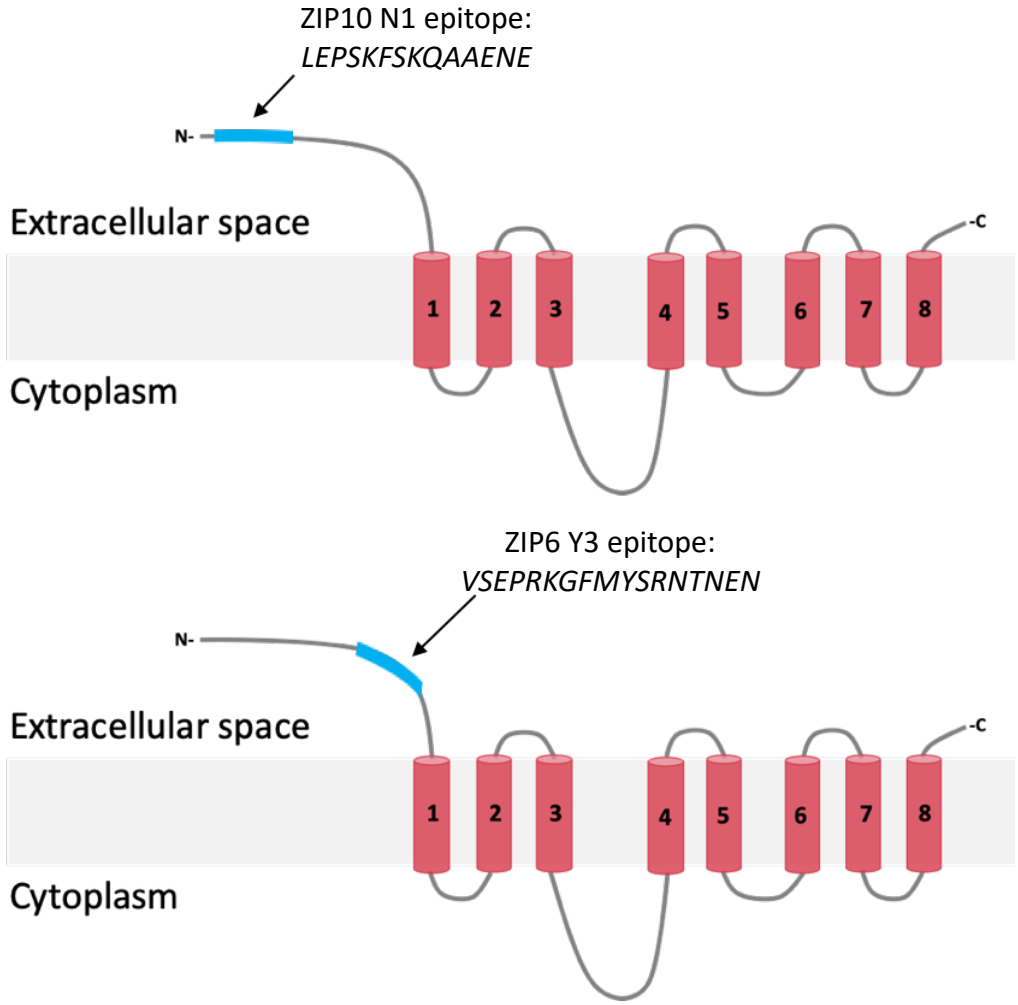

The epitopes of our in-house ZIP10 N1 (top) and ZIP6 Y3 (bottom) antibodies produced by Biogenes GmBH. The epitope of the anti-ZIP10 antibody is residues 46–59 (LEPSKFSKQAAENE) and the anti-ZIP6 antibody is 244–260 (VSEPRKGFMYSRNTNEN). Both antibodies are directed to the human ZIP10/ZIP6 sequences.

2.7. Antibody inhibition of cell growth

For long term growth experiments, 4 x 10^6 cells were seeded into each well of a 46-well plate (day 0). Anti-ZIP10 (N1) or normal rabbit IgG control antibodies (tables 2.2–2.3) were added on day 1 and cells were counted every day up to and including day 10. The concentrations of the antibodies used were 2.8 μg/mL and 5 μg/mL, made up in fresh growth medium. To count, cells were detached using 1 mL trypsin for 3–5 minutes at 37 °C. 3 mL isoton (Beckman Coulter; 8448011) was added to the trypsin and mixed gently. The cell suspension was drawn into a syringe via a 23 G needle to create a single cell suspension and the cells counted using a Beckman Coulter™.

2.8. Absorption of antibody peptide

ZIP10 antibody N1 was diluted 1:1000 in blocking buffer (5% non-fat dried milk [w/v] [Marvel] in TBS-T [tris buffered saline with tween] [appendix 2]) and separated between two tubes. The peptide which corresponds to the epitope of this antibody (*LEPSKFSKQAAENE*) was added to one tube at a 1 μg/mL concentration. Both tubes were incubated on a roller at 23 °C for 30 minutes. Western blot analysis was then carried out comparing the blocked antibody to the un-blocked antibody.

2.9. Generation of recombinant ZIP10 constructs

Site-directed mutagenesis to create phospho-ablative ZIP10 mutant constructs was performed by Mutagenex Inc in a wild-type ZIP10 construct in an ampicillin-resistant pcDNA3.1/V5-His-TOPO plasmid vector (Invitrogen; K4800-01) (figure 2.2). Individual residues of interest were mutated to alanine due to its lack of side-chain chemistry and lack of direct involvement in protein function. The mutations were confirmed by DNA sequencing. Mutant constructs which were made for this project are listed in table 2.5. Wild-type (WT) and mutant constructs were transformed into MAX Efficiency™ DH5α competent cells (Invitrogen; 18258-012) by heat shock at 42 °C for 45 seconds, followed by resting on ice for 2 minutes. Transformed bacteria were incubated in S.O.C medium and shaken vigorously at 37 °C for 60 minutes. The reactions were diluted 1:100 with S.O.C medium and 100 μL streaked onto LB (lysogeny broth) agar (Sigma; L2897) containing 100 μg/mL ampicillin (Sigma; A9518) and grown overnight at 37 °C.

Figure 2.2. The structure of the cDNA™3.1/V5-His-TOPO® plasmid vector

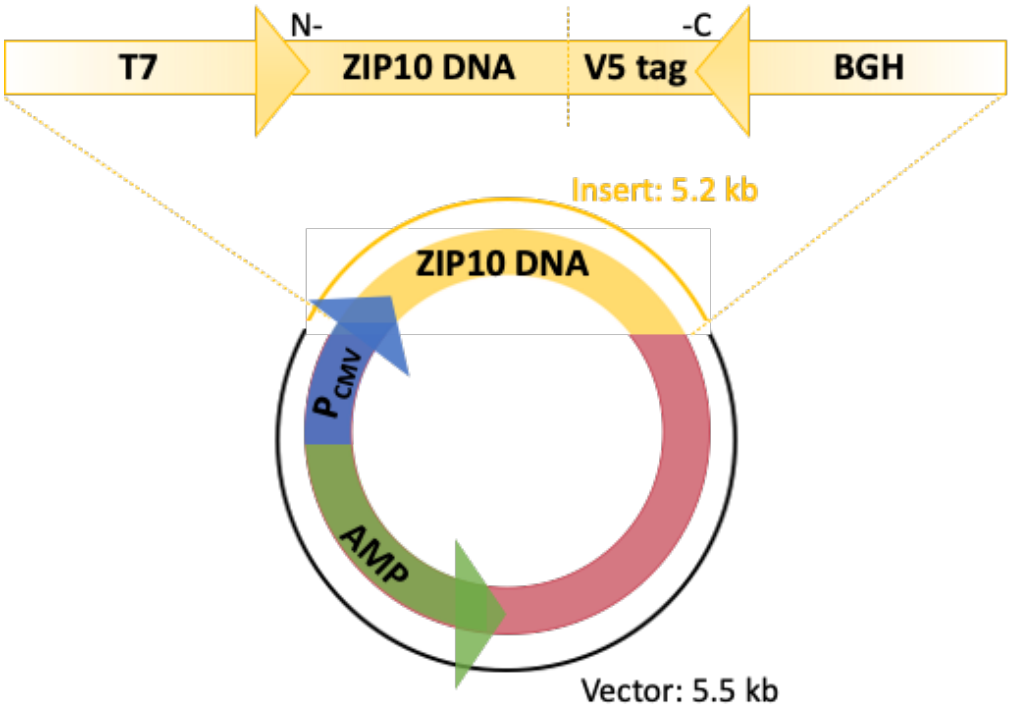

The construct contains an ampicillin resistance gene (AMP), P_{CMV} promotor, a T7 forward priming site, and a BGH reverse priming site. Human ZIP10 DNA with the stop codon removed and a C-terminal V5 tag was inserted by TOPO-TA cloning. kb, kilobases.

Table 2.5. Recombinant ZIP10 constructs used in this project

Wild-type residue(s)	Domain	New residue(s)	Name of construct
Arginine 309 (R309) Lysine 310 (K310) Arginine 311 (R311)	N-terminus	Alanine	Cleavage mutant 1
Lysine 390 (K390) Lysine 392 (K392)	N-terminus	Alanine	Cleavage mutant 2
Tyrosine 521 (Y521)	TMD3-4 ICL	Alanine	STAT3 binding mutant
Serine 539 (S539)	TMD3-4 ICL	Alanine	S359A
Threonine 540 (T540)	TMD3-4 ICL	Alanine	T540A
Serine 539 (S539) Threonine 540 (T540)	TMD3-4 ICL	Alanine	S539A/T540A
Serine 564 (S546)	TMD3-4 ICL	Alanine	S546A
Serine 570 (S570)	TMD3-4 ICL	Alanine	S570A
Serine 573 (S573)	TMD3-4 ICL	Alanine	S573A
Serine 591 (S591)	TMD3-4 ICL	Alanine	S591A

Constructs are named according to the residue which was mutated. The amino acid preceding the residue number is the original one and the one immediately after is the new one. R, arginine; K, lysine; Y, tyrosine; T, threonine; S, serine; A, alanine; ICL, intracellular loop; TMD, transmembrane domain. / indicates multiple residues in the same construct were mutated.

Plasmid DNA was extracted using the EndoFree Plasmid Kit (Qiagen; 12362) according to the manufacturer's protocol. For details of the buffers used, see appendix 3. In brief, one isolated colony was transferred to 5 mL LB broth (Sigma; L3022) containing 100 μg/mL ampicillin and grown for 8 hours with vigorous shaking at 37 °C. The starter culture was diluted 1:500 and grown overnight in 250 mL LB broth with vigorous shaking at 37 °C. Bacterial cells were harvested by centrifugation at 6000 x g for 15 minutes at 4 °C and the cell pellet resuspended in 10 mL buffer P1. The cells were lysed by the addition of 10 mL buffer P2, inversion of the tube 4–6 times and incubation at 23 °C for 5 minutes. To precipitate the cell material, 10 mL buffer P3 was added to the lysate, mixed vigorously, transferred to a QIAfilter cartridge and left at 23 °C for 10 minutes before filtering through the cartridge. 2.5 mL of buffer ER was added to the filtered lysate and incubated on ice for 30 minutes. The lysate was then washed twice in 30 mL buffer QC before genomic material was eluted with 15 mL buffer QN. DNA was precipitated by adding 10.5 mL isopropanol and spun at 15,000 x g at 4 °C for 30 minutes. The DNA pellets were washed in 5 mL 70% ethanol (v/v) and spun again at 15,000 x g at 4 °C for 10 minutes. The pellet was air-dried before resuspending in endotoxin-free buffer TE.

UV spectrophotometry was performed to determine the concentration of the plasmid DNA measuring absorbance at 260 nm (OD260) and the purity of the DNA was calculated by measuring the ratio of the absorbance at 260 nm to the absorbance at 280 nm (OD260/OD280). Agarose gel electrophoresis was carried out to determine the size of the plasmid against Quick-Load® 1 kb DNA ladder (New England Biolabs; N0468) and visualised on a UV transilluminator.

2.10. Transfection of recombinant ZIP10 constructs

4 μg recombinant DNA was added to 188 μL serum-free phenol-red-free growth medium (Life Technologies; 32404-014) and 7.5 μL of Lipofectamine™ 3000 Transfection Reagent and 7.5 μL enhancer (ThermoFisher Scientific; L3000015) was added to 188 μL serum-free phenol-red-free growth medium and thoroughly mixed. Within 5 minutes of adding DNA and lipofectamine to medium, the two mixtures were added together and incubated for 20 minutes at 23 °C. The DNA/Lipofectamine™ mixture was then added to phenol-red-free growth medium with 5% FCS (v/v) but no antibiotics or anti-fungal added. Transfection efficiency was enhanced with the addition of 3 mM sodium butyrate (Sigma; B5887) and

was performed with or without 150 nM nocodazole. Cells were incubated for 18 hours at 37 °C in a humid environment with 5% CO_2.

2.11. Immunofluorescence

Cells on 22 x 22 mm 0.17 mm thick glass coverslips were fixed in 3.7% formaldehyde (v/v) in PBS for 15 minutes, followed by 2 x 5-minute washes in PBS. Cells were permeabilised by submersion in 1% BSA (w/v; bovine serum albumin; Sigma; A7030) containing 0.4% saponin (w/v; Sigma; S7900) in PBS for 15 minutes and blocked in 10% normal goat serum (v/v; DAKO; X0907) in the 1% BSA/0.4% saponin buffer for 15 minutes. Primary antibodies were diluted in 1% BSA/0.4% saponin buffer according to the concentrations in table 2.3 and 100 µL was added to each coverslip, in a moisture chamber for 60 minutes. Excess antibody was removed by washing the coverslips three times in buffer, before the addition of 100 µL secondary antibody according to the dilutions in table 2.4 or phalloidin Alexa Fluor®488 (Life Technologies; A12379) at a 1:1000 dilution. Coverslips were incubated in secondary antibody for 30 minutes in a moisture chamber, protected from light. Vectorshield mounting medium with DAPI (4',6'-diamidino-2-phenylindole; Vector Laboratories) was used to mount coverslips onto glass slides. All processes were carried out at 23 °C. Cells were imaged using a Leica DMIRE2 epi-fluorescent microscope with a 63 x oil immersion lens. Photos were taken with OpenLab imaging software for Mac and processed minimally using ImageJ software. For inhibition of mitosis assays, images were taken of 6 fields of view for each treatment.

2.12. Proximity Ligation Assay

MCF7 cells grown on 8-well chamber slides were fixed in 3.7% formaldehyde (v/v) for 15 minutes, followed by two 5-minute washes in PBS. Proximity Ligation Assay was carried out using Duolink® In Situ PLA® Probe anti-mouse MINUS (Sigma; 92004) and anti-rabbit PLUS (Sigma; 92002) reagents, and Duolink® PLA Detection Reagents (Sigma; DUO92007 and DUO92008) according to the manufacturer's protocol. All incubations were carried out in a pre-heated humidity chamber at 37 °C unless stated otherwise. In brief, cells were blocked in Duolink® Blocking solution for 60 minutes. Primary antibodies (table 2.3) were diluted in Duolink® Antibody diluent, added to the cells, and incubated for 60 minutes at 23 °C. PLUS and MINUS PLA probes were diluted 1:5 in Duolink® Antibody Diluent, primary antibody washed from the cells and probes added for 60 minutes. 5 x Duolink® Ligation buffer was

diluted 1:5 in high purity water, and ligase added at a 1:40 dilution. The cells were washed, ligation mixture added and incubated for 30 minutes. 5 x Amplification buffer was diluted 1:5 in high purity water, and polymerase was added at a 1:80 dilution. Ligation solution was removed, and cells washed. Amplification solution was applied and incubated for 100 minutes. The cells were washed a final time and mounted onto a coverslip using Duolink® In Situ Mounting Media with DAPI (Sigma; DUO82040), away from light. Cells were imaged using a Leica DMIRE2 epi-fluorescent microscope with a 63 x oil immersion lens. Twenty-five images were taken 0.3 μm apart using the Openlab imaging software for Mac and processed minimally using ImageJ software. The number of dots was determined using ImageJ. The PLA procedure is outlined in figure 2.3.

Figure 2.3. Schematic demonstrating the proximity ligation assay (PLA) procedure

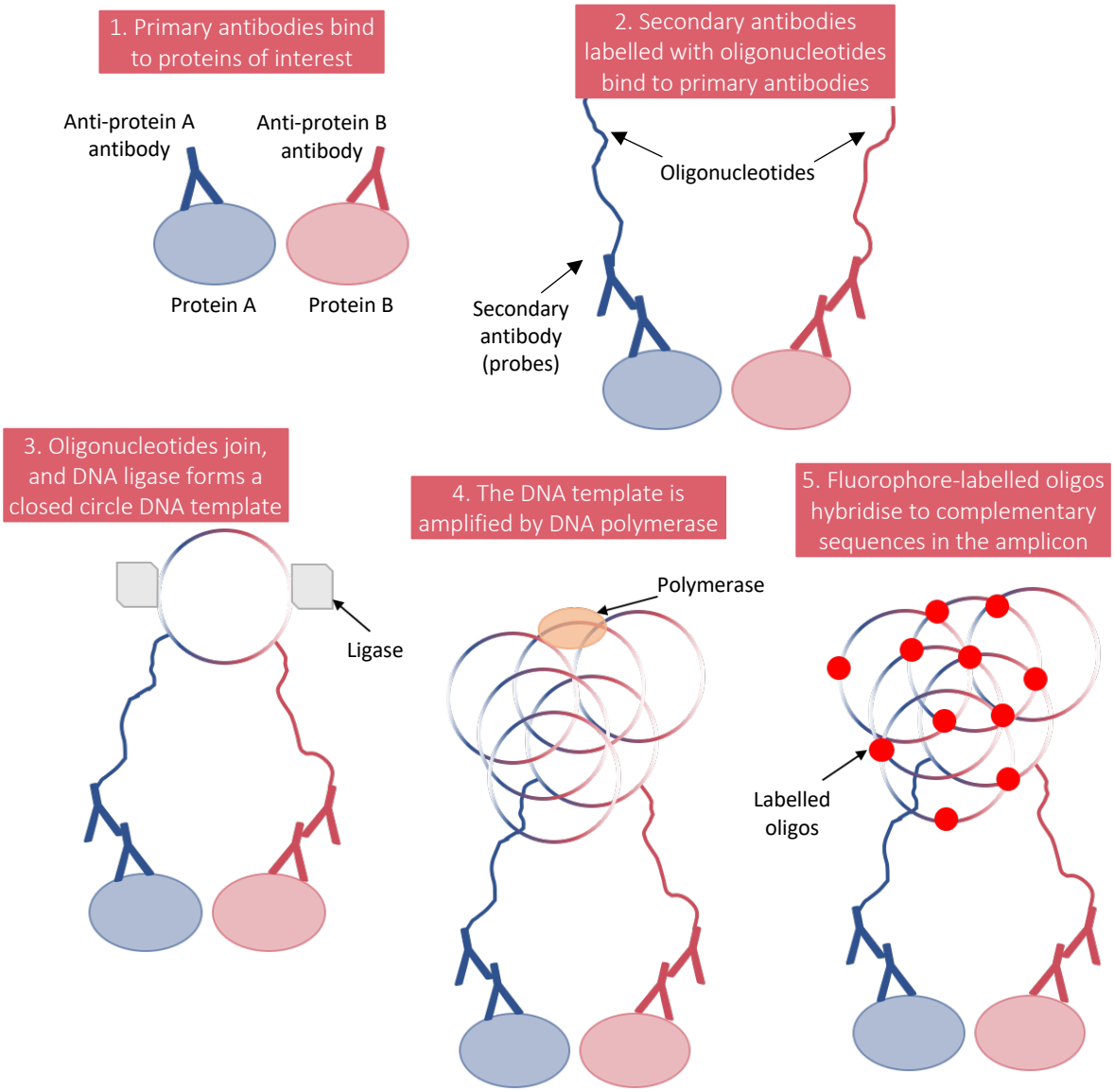

The sample population is incubated with two antibodies against the proteins of interest, raised in different species. Secondary antibodies labelled with oligonucleotide probes bind the primary antibodies. The oligonucleotides are joined by a ligase and the DNA is amplified if the proteins are within 40 nm of each other.

2.13. Cell surface protein isolation

MCF7 cells were seeded in 4 x T75 flasks per treatment arm and grown until 70% confluency. Cell-surface protein isolation was carried out using the Pierce™ Cell Surface Protein Isolation Kit (ThermoFisher Scientific; 89881) according to the manufacturer's protocol. In short, the medium was removed, and cells washed in ice-cold PBS twice. 10 mL Sulfo-NHS-SS-Biotin dissolved in PBS was added to each flask. The cells were incubated on a rocking platform for 30 minutes at 4 °C. 500 μL quenching solution was added to each flask to stop the reaction. Cells were scraped into solution and collected into a single tube per treatment arm. 4 flasks were rinsed with a single 10 mL volume of TBS (TRIS buffered saline) which was then added to the tube. Cells were spun at 500 x g for 3 minutes and the supernatant discarded. The cell-surface protein isolation procedure is outlined in figure 2.4.

Cells were resuspended in 500 μL lysis buffer, containing 2 mM sodium orthovanadate, (Sigma; S6508), 25 mM sodium fluoride (Sigma; 919), and 10 % protease inhibitor cocktail (v/v; Sigma; P8340), and incubated on ice for 30 minutes with brief vortexing at 5-minute intervals. Lysates were spun at 10,000 x g for 2 minutes at 4 °C and the supernatant transferred to a clean tube. 500 μL NeutrAvidin™ Agarose slurry was added to a spin column and spun at 1000 x g for 1 minute. 500 μL wash buffer was spun through the column at 1000 x g for 1 minute, twice. The clarified cell lysate was added to the column and incubated with end-over-end rotation for 60 minutes at 23 °C. The column was spun at 1000 x g for 1 minute and 500 μL wash buffer with protease inhibitors (see above) added and spun three times. 400 μL 50 mM DTT (dithiothreitol) in sample buffer was added to the column which was heated for 5 minutes at 100 °C. The column was spun at 1000 x g for 2 minutes to elute the protein and a trace of bromophenol blue added. Samples were analysed by SDS-PAGE (sodium dodecyl sulfate polyacrylamide gel electrophoresis) and western blot.

Figure 2.4. Schematic demonstrating the cell surface protein isolation procedure

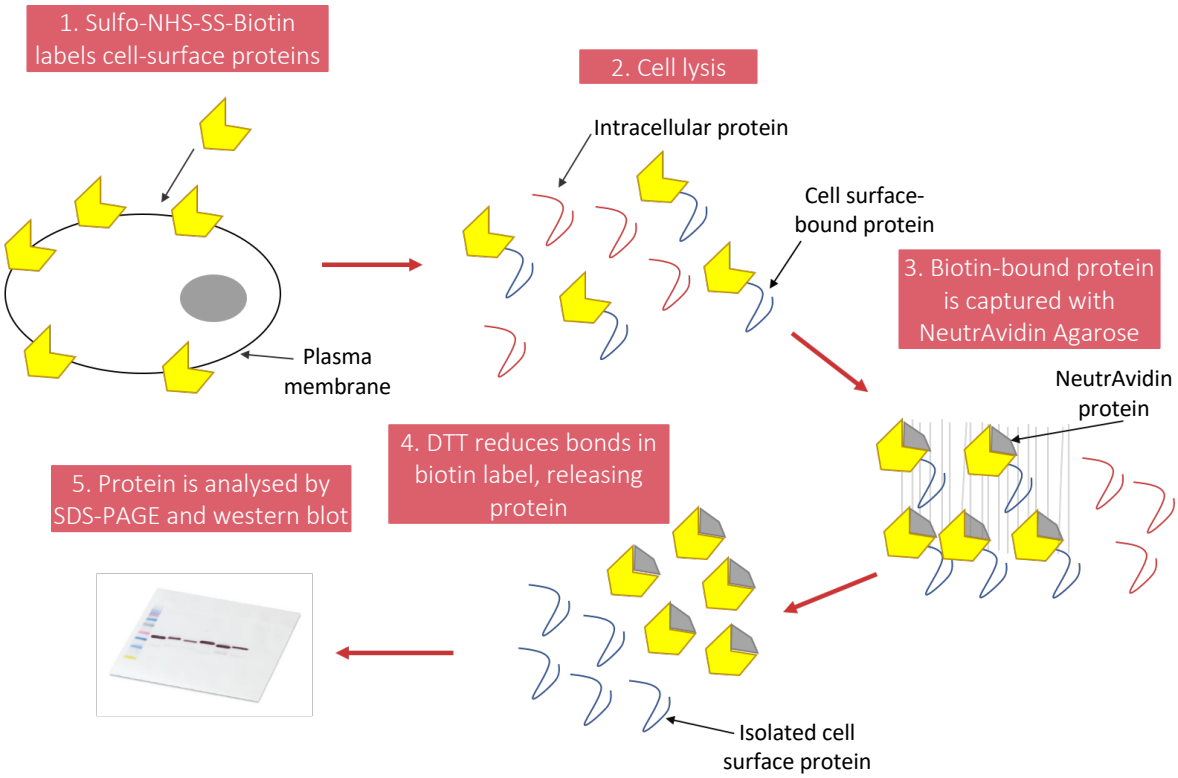

The sample population is incubated with Sulfo-NHS-SS-Biotin which binds extracellular regions of plasma membrane-bound proteins. The cells are lysed, and the biotin-labelled proteins separated from intracellular proteins using NeutrAvidin Agarose Resin. The isolated proteins are eluted and analysed using SDS-PAGE and western blot.

2.14. Cell lysis and determination of protein concentration

Cell growth medium was removed, and cells washed three times in ice-cold PBS. To collect floating cells, the growth medium was spun at 168 x g for 5 minutes, the cell pellets were washed in ice-cold PBS and lysed in 100 μL lysis buffer (appendix 4) containing 2 mM sodium orthovanadate, 25 mM sodium fluoride, and 10% protease inhibitor cocktail (v/v; Sigma; P8340). The adherent cells were washed three times in ice-cold PBS and lysed in 100 μL lysis buffer containing inhibitors. A cell scraper and pipette were used to collect the lysate into an Eppendorf tube. Cells which were analysed for pS^{10}Histone H3 protein expression were lysed in 2 x Laemmli buffer (appendix 5) and DNA was sheared by passing the sample through a 23 G needle 8 times, following transfer to the Eppendorf tube. The adherent and floating cell lysates were pooled into the same tube. Lysates were incubated on ice for 60 minutes, before centrifugation at 13,684 x g for 12 minutes, at 4 °C. The supernatant was then transferred to a clean Eppendorf tube.

The protein concentration of the lysates was determined using the BioRad microassay procedure based on the Bradford protein assay. In brief, the lysate was diluted 1:400 in 399 μL deionised water in duplicate. 100 μL protein assay dye reagent (Bio-Rad; 500-0006) was added to each tube and the mixture vortexed gently. 150 μL of the diluted lysate/dye solution was added to a 96-well plate and the absorbance measured at 595 nm. The protein concentration of the lysate was determined against a standard curve of BSA (Sigma; A7030) concentration of between 5 and 25 μg/mL.

2.15. Removal of N-linked glycans

To investigate glycosylation, cell lysate fractions expressing recombinant ZIP10 were incubated with 1000 units of PNGase F (peptide-N-glycosidase F; New England BioLabs; P0705S) for 24 hours at 37 °C before SDS-PAGE and western blot analysis.

2.16. Immunoprecipitation

500 μg of cell lysate was mixed with 1 μg of antibody against protein to be precipitated (table 2.3) in a total volume of 1 mL with lysis buffer containing 2 mM sodium orthovanadate, 25 mM sodium fluoride, and 10% protease inhibitor cocktail (v/v), vortexed briefly and incubated on a rotator for 2 hours at 4 °C to allow antigen/antibody complexes to form. The lysate/antibody mix was added to 30 μL of pre-washed EZ view protein A (for precipitation

with a rabbit antibody) or protein G (for precipitation with a mouse antibody) agarose beads (Sigma; E3403 and P6486) and incubated on a rotator for 3 hours at 4 °C. The antigen/antibody/bead complex was pelleted by centrifugation at 8500 x g for 30 seconds at 4 °C. The pellet was washed three times in 250 μL lysis buffer by incubation on a rotator for 5 minutes at 4 °C. After the final wash, the supernatant was discarded and 25 μL of lysis buffer and 25 μL of 2 x laemmli buffer added. The antigen/antibody/bead complex was denatured by boiling for 5 minutes and spun at 8500 x g to pellet the beads. The supernatant containing the immunoprecipitated protein was transferred to a clean Eppendorf tube before analysis by SDS-PAGE and western blot.

2.17. SDS-PAGE and western blot

Cell lysates were prepared for western blot by the addition of laemmli buffer (appendix 5) with 0.2 M DTT (Roche; 10708984001) and bromophenol blue (Merck; 108122) at a 1 μg/μL concentration. Proteins were denatured by boiling for 5 minutes and spun for ~20 seconds at 13,684 x g.

The concentration of SDS gels was determined based on the range of molecular mass of the proteins of interest. The composition of the resolving and stacking gels used in this project is shown in appendix 6.

Up to 50 μg of each sample and 3 μL Precision Plus Protein™ Standard (Bio-Rad; 161-0373) were loaded into the wells of an SDS gel, and the cassette filled with running buffer (appendix 7). Gel electrophoresis was run at 120 V for 90 minutes. The protein was transferred to an Amersham™ Protran™ 0.45 μM nitrocellulose membrane (GE Life Science; 10600002) in transfer buffer (appendix 8), at 100 V for 60 minutes, with an ice pack in the cassette to prevent overheating. The protein was stained with 0.1% (w/v) Ponceau S (Sigma; P-3504) in 5% acetic acid to confirm the consistent transfer of protein across the membrane. Membranes were blocked for 1 hour at 23 °C in 5% (w/v) non-fat dried milk (Marvel) in TBS-T (appendix 2), followed by a 30-minute wash in TBS-T on a rocking platform. The primary antibody solution was made using TBS-T with 5% Western Blocking Reagent (v/v; Roche; 11921673001) and 1 mM sodium azide (NaN_3) and the primary antibody at the concentration in table 2.3. Membranes were incubated in 5 mL primary antibody solution overnight at 4 °C. Membranes were washed for 15 minutes in TBS-T, followed by incubation

in HRP-conjugated (horseradish peroxidase-conjugated) secondary antibody, made up in TBS-T containing 1% Marvel (w/v; table 2.4) for 1 hour at 23 °C.

For loading control proteins, HRP-conjugated β-actin or GAPDH was used at a 1:50,000 dilution made up in TBS-T containing 5% Western Blocking Reagent (v/v) and incubated with membranes for 1 hour followed by a 30-minute wash in TBS-T on a rocking platform.

The protein was detected by mixing two reagents from either Pierce® ECL Western Blotting Substrate (Thermo Scientific; 32209), Clarity™ Western ECL Substrate (BioRad; 102030516), or SuperSignal® West Femto Maximum Sensitivity Substrate (ThermoFisher Scientific; 34095) at a 1:1 ratio. 200 μL of the mixed reagent was added to each membrane in a cassette which was exposed to X-ray film (Photon Imaging Systems; FM024) in a dark room. The density of the bands was measured using ImageJ and the results analysed using Microsoft® Excel for Mac.

2.18. Determination of protein molecular mass from western blot

To determine the molecular mass of proteins in a sample, the distance travelled by molecular mass markers and the protein of interest had migrated through a gel was measured (figure 2.5A). *Rf* (retention factor) values for the markers and the protein of interest were determined using the following equation:

$$Rf\ value\ of\ protein = \frac{Migration\ distance\ of\ marker\ (mm)}{Migration\ distance\ of\ dye\ front\ (mm)}$$

The *Rf* value for each molecular mass marker was then plotted into a graph against the known molecular mass (figure 2.5B) and the molecular mass of the protein of interest determined from the line graph.

Figure 2.5. Method to determine protein Rf value of unknown protein

A.

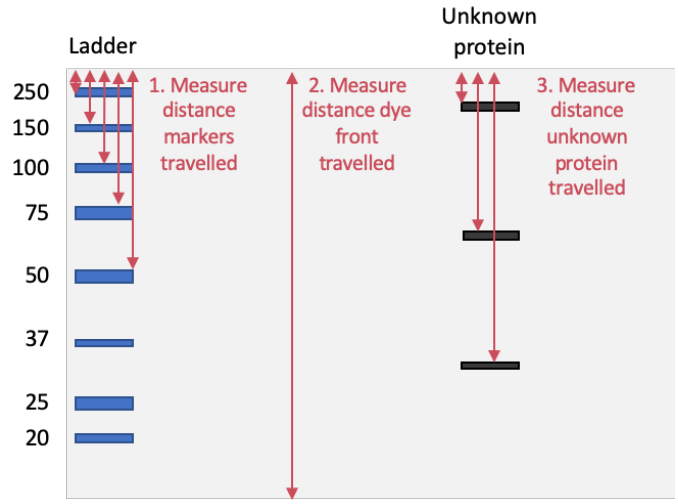

B.

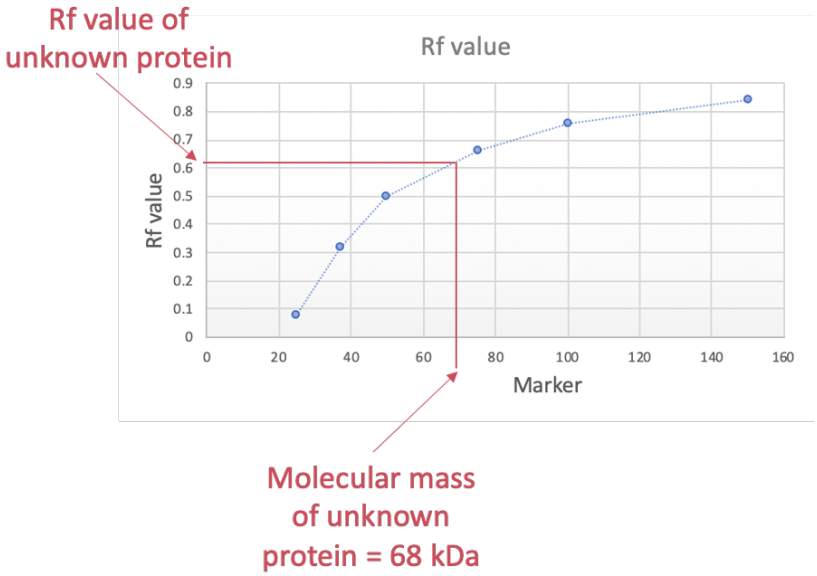

A*. The distance each protein in the molecular mass marker, and each protein of interest travelled is measured, with the distance the dye front travelled.* ***B****. Rf values of molecular mass markers are plotted into a line graph and the molecular mass of the protein interest can then be extracted from the graph.*

2.19. Protease array

Cells were analysed using the Proteome Profiler Human Protease Array Kit (R&D Systems; ARY021B) to determine protease activation throughout mitosis, according to the manufacturer's protocol. In brief, cells were lysed in Lysis Buffer 17 (R&D Systems; 895943) with 10 μg/mL aprotinin (Sigma; A6279), 10 μg/mL leupeptin (Tocris; 1167), and 10 μg/mL pepstatin (Tocris; 1190).

Membranes were blocked in array buffer 6 at 23 °C for 60 minutes. 200 μg of lysate was incubated with detection cocktail antibody at 23 °C for 60 minutes, and the lysate/antibody mix then incubated with membrane overnight at 4 °C. The membranes were washed and incubated with Streptavidin-HRP (1:20,000) in blocking buffer at 23 °C for 30 minutes.

Chemi reagent mix was added to the membrane and the light reaction detected over a 10-minute period. The density of the dots was measured using ImageJ and the results analysed using Microsoft® Excel for Mac. Heat maps were generated using GENE-E matrix visualisation and analysis platform (The Broad Institute).

2.20. Fluorescence-activated cell sorting (FACS) analysis

Cell growth medium was collected, and adherent cells detached from surfaces using 1 mL trypsin at 37 °C for 3–5 minutes. The adherent cells were collected using a cell scraper and pipette and added to the growth medium containing floating cells. The pooled cells were spun at 168 x g for 5 minutes. The supernatant was discarded, and cell pellets were washed in fresh growth medium and the centrifugation was repeated. Cell pellets were resuspended in 50 μL primary antibody solution (table 2.3) made in Krebs-Ringer-HEPES (KRH) buffer (appendix 9) and incubated on ice for 60 minutes. Cells were spun at 0.1 x g for 10 minutes at 4 °C, and pellets washed in 500 μL ice-cold PBS. Pellets were resuspended in 50 μL secondary antibody (table 2.4) made in KRH buffer and incubated for 30 minutes, protected from light. Cells underwent a final centrifugation step and were resuspended in 500 μL PBS and transferred to FACS tubes. The cell suspension was measured with a BD FACSVerse Flow Cytometer and analysis was performed with BD FACSuite software and FlowJo.

2.21. Animal study

MDA-MB-231 cells were grown in DMEM medium supplemented with 10% FCS (v/v) (table 2.1) and maintained at 37 °C with 5% CO_2 and 5% O_2. Approximately 160,000 cells, mixed with Corning® Matrigel® Growth Factor Reduced Basement Membrane Matrix (Appleton Woods) and PBS at a 1:1 ratio were injected subcutaneously into both dorsal flanks of 10 Athymic Nude female mice. All animal xenograft procedures were performed in accordance with the Animals (Scientific Procedures) Act 1986 and approved by the UK Home Office (PPL 30/3433). Of the 10 xenograft mouse models, 2 mice did not develop tumours and 1 mouse developed tumours at a date later than the others and therefore a total of 7 mice were used for the study.

Mice began treatment with the N-terminal targeted anti-ZIP6 antibody when tumours were a minimum of 4 mm^3 in volume. The antibody was used at 1 mg/kg. The mice received treatment via intraperitoneal injection every 4 days and tumours were measured by calipers in 2 directions to calculate the volume. Mice were harvested by schedule 1 cervical dislocation 24 hours after the last dose. Lung, liver, and kidney tissue was fixed in 4% formalin and stored at 4 °C. Half of the tumour tissue was formalin-fixed and the remainder frozen in RNAlater (Sigma; R0901).

2.22. Data presentation and statistical analysis

N numbers (n = x) refer to the number of biological replicates. Results are displayed as mean ± standard error of the mean from three biological replicates. In the text, the standard error of the mean is reported immediately after the mean value as *'(s = X)'* where *s* is the standard error.

Statistical analysis was carried out using t-test or analysis of variance (ANoVA) with Dunnett's or Bonferroni post-hoc or Student t-test analysis. Statistical significance was considered when the p value was less than 0.05 ($p < 0.05$). The analysis was performed using GraphPad (Prism) and IBM software.

Chapter 3. Characterisation of ZIP10 regulation in mitosis

3.1. Introduction

The finding that zinc is required for cells to enter mitosis (Chesters, Petrie and Vint, 1989; Chesters and Petrie, 1999) and that two zinc transporters, ZIP6 and ZIP10 are required for epithelial to mesenchymal transition (Hogstrand *et al.*, 2013; Taylor *et al.*, 2016), the first stage of which, cell rounding, is also the first stage of mitosis (Pugacheva, Roegiers and Golemis, 2006; Hosseini *et al.*, 2019) suggests that both transporters may also play a role in mitosis. Furthermore, they have each been associated with several cancers (Pan *et al.*, 2017), a disease of uncontrolled mitosis.

ZIP6 is activated by N-terminal cleavage in the endoplasmic reticulum, before movement to the plasma membrane (Hogstrand *et al.*, 2013). This cleavage occurs at a PEST site, a region of protein that is rich in proline (P), aspartic acid (E), serine (S) or threonine (T) residues, and characteristic of proteins with a short half-life (Zhuang, Northup and Ray, 2012). ZIP10 and other ZIP transporters are also regulated by proteolytic cleavage (Kambe and Andrews, 2009; Ehsani *et al.*, 2012) but this modification has not been studied specifically in relation to mitosis.

ZIP6 binds to the serine 727 phosphorylated form of the known oncogene STAT3 during mitosis (Nimmanon *et al.,* 2020). The STAT3 binding site in ZIP6 is tyrosine (Y) 473, located in the intracellular loop between TMD3 and TMD4. ZIP10 also has a predicted STAT3 binding site, with the consensus *YXXQ* motif, suggesting that pS^{727}STAT3 may also bind ZIP10 in mitosis. Both ZIP6 and ZIP10 are involved in epithelial to mesenchymal transition and cell migration through STAT3-dependent pathways (Unno *et al.*, 2009; Hogstrand *et al.*, 2013; Taylor *et al.*, 2016). STAT3 is upregulated in several cancers (Garcia et al. 1997) and there is growing evidence that ZIP6 and ZIP10 have a strong relationship with STAT3 therefore their own role in cancer development and progression could be more prominent than is currently understood.

To understand the role that the ZIP6/ZIP10 heteromer plays in mitosis, it is important to understand the regulation of each protein individually. Since ZIP6 regulation by cleavage and protein-protein interaction with pS^{727}STAT3 has been identified, this chapter investigates the regulation of ZIP10 in mitosis by both proteolytic cleavage and protein-protein interactions.

3.2. Aims and objectives

The aims of this chapter are to investigate the proteolytic cleavage of ZIP10 in mitosis and to explore binding of ZIP10 to other proteins in mitosis

The objectives of this chapter are:

a. To identify potentially important sites of post-translational modification in ZIP10 using computer software

b. To characterise post-translational modification sites in ZIP10 using different ZIP10 targeted antibodies

c. To investigate ZIP10 glycosylation status

d. To determine whether ZIP10 undergoes proteolytic cleavage in mitosis

e. To investigate the interaction of ZIP10 with other mitotic proteins.

3.3. Methods

3.3.1. Software analysis of the ZIP10 sequence for cleavage and glycosylation sites

To identify potential sites of ZIP10 proteolytic cleavage, the human protein sequence in FASTA format was analysed using software including ePESTfind (EMBOSS) (Gouw et al., 2017) and ELM (Dinkel *et al.*, 2016). The Compute pI/Mw (Bjellqvist *et al.*, 1993) software was used to determine approximate sites of proteolytic cleavage based on the band sizes detected on a western blot with anti-ZIP10 antibodies. For full details of the antibodies used refer to table 2.4. Cleavage was then assessed in MCF7 breast cancer cells in the presence of nocodazole to assess ZIP10 processing in mitosis. Peptide-N-glycosidase F (PNGase F) was used to detect the presence of N-linked glycosylation side-chains in ZIP10.

3.3.2. Isolation of ZIP10 from the plasma membrane

To investigate ZIP10 ectodomain shedding in mitosis, a cell-surface protein isolation experiment was carried out, in which cells were incubated in Sulfo-NHS-SS-Biotin (biotin) to label exposed lysine residues on extracellular regions of cell surface proteins. Cell surface proteins were separated from intracellular proteins with agarose bound NeutrAvidin protein. The cell surface proteins were eluted and analysed by SDS-PAGE and western blotting, using both N-terminal and intracellular anti-ZIP10 antibodies.

3.3.3. Investigation of ZIP10 cleavage in recombinant ZIP10

To further investigate ZIP10 proteolytic cleavage, two mutant ZIP10 constructs were made by site-directed mutagenesis, performed by Mutagenex Inc. Residues of interest were mutated to alanine due to its lack of side-chain chemistry. The wild-type (WT) human ZIP10 sequence in a pcDNA3.1/V5-His TOPO vector was used as template for mutagenesis (figure 2.2). The mutant constructs that were made for the study of ZIP10 cleavage are shown in figure 3.1A. Successful mutagenesis was confirmed by DNA sequencing (figure 3.1B). The WT and mutant ZIP10 constructs were transfected into MCF7 cells in the presence of nocodazole, to synchronise cells in mitosis. The ZIP10 band sizes were assessed using SDS-PAGE and western blotting. An anti-V5 antibody was used to ensure only recombinant ZIP10 was detected, because the MCF7 cell line also expresses endogenous ZIP10.

Further analysis of ZIP10 cleavage in response to zinc availability was carried out by treating MCF7 cells with either serum-free medium or 5 μM TPEN for 30 minutes. ZIP10 was analysed using SDS-PAGE and western blotting, followed by immunofluorescence.

3.3.4. Investigation of proteases active in mitosis

Investigation of proteases responsible for the cleavage of ZIP10 was carried out using the Proteome Profiler Human Protease Array Kit, membrane-bound antibodies targeted to several proteases were incubated with MCF7 cell lysates. Signals from the antibodies were detected using chemiluminescence, and those proteases that were increased in mitosis were deemed possible proteases for the cleavage of ZIP10 in mitosis. These proteases were further investigated by treatment of MCF7 cells with protease inhibitors DAPT, a presenilin inhibitor, and nelfinavir, an S2P (site 2 protease) inhibitor at 10 μM and 30 μM respectively, for 10 minutes. The presence of ZIP10 cleavage products was then assessed using SDS-PAGE and western blotting.

3.3.5. Investigation of ZIP10 interaction with pS^{727}STAT3

ZIP10 localisation in mitotic MCF7 cells was assessed using immunofluorescence, and the binding of ZIP10 to pS^{727}STAT3 was assessed using proximity ligation assay (PLA). The Duolink® In Situ Detection Kit – Orange was used to detect the proximity of the proteins and was imaged using a Leica DMIRE2 epi-fluorescence microscope. The dots were quantified using ImageJ software. Further investigation of ZIP10 binding to pS^{727}STAT3 in mitosis was carried out by producing a recombinant ZIP10 mutant construct, in which Y521 was mutated to alanine (Y521A) using site-directed mutagenesis, carried out by Mutagenex Inc. The DNA sequence that was mutated is shown in figure 3.1 and successful mutagenesis was confirmed by DNA sequencing (figure 3.1B). WT ZIP10 and the Y521A construct were transfected into MCF7 cells. The recombinant protein was separated from the endogenous protein by immunoprecipitation with an anti-V5 antibody and assessed for the presence of pS^{727}STAT3 using SDS-PAGE and western blotting.

Figure 3.1. Mutant ZIP10 constructs made for use in this chapter

A.

Construct	WT DNA sequence	Mutant DNA sequence
ZIP10 cleavage mutant 1	ACTAGAAAGAGAGAA	ACTgcAgcGgcAGAA
ZIP10 cleavage mutant 2	AATAAGGATAAAAAC	AATgcGGATcgAAAC
ZIP10 STAT3 binding mutant (Y521A)	CACTACAAA	CACgcCAAA

B.

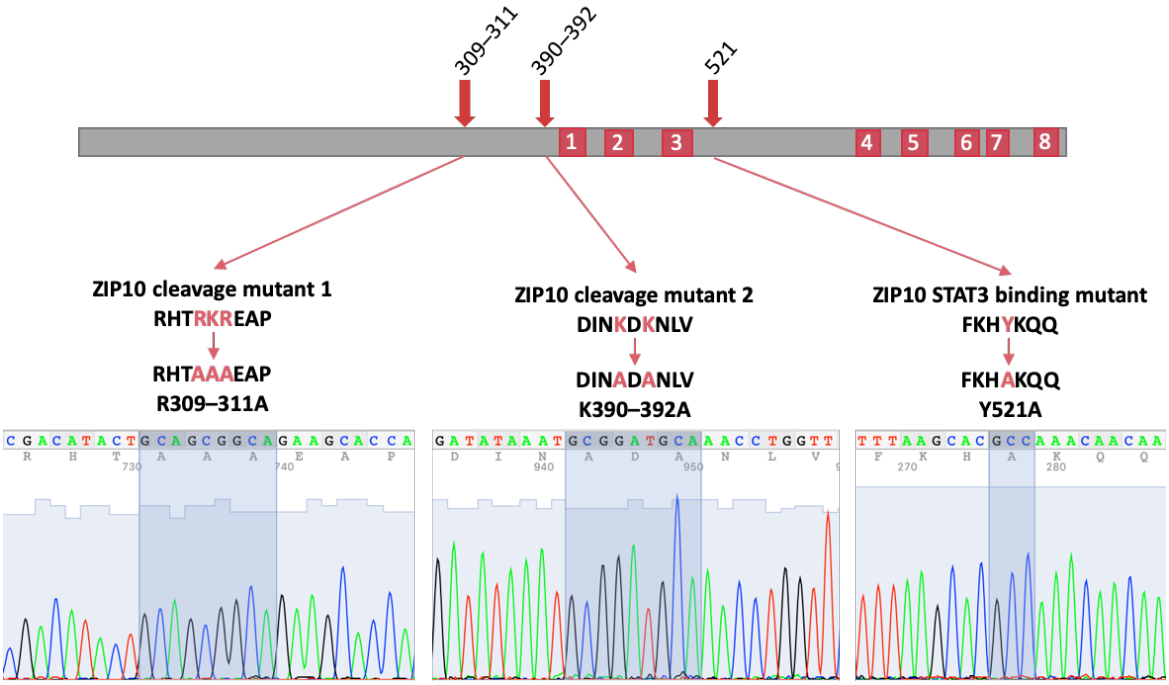

A*. The human DNA sequences of the ZIP10 mutant constructs that were made by site-directed mutagenesis for use in this chapter. Cleavage mutant 1 and cleavage mutant 2 were used in the study of ZIP10 proteolytic cleavage and the ZIP10 STAT3 binding mutant was used to investigate ZIP10 interaction with STAT3. Mutated codons are underlined and individual nucleotides that were altered are lower-case.* ***B****. Successful site-directed mutagenesis was confirmed by DNA sequencing, and the corresponding chromatograms are presented. R, arginine; K, lysine; Y, tyrosine; A, alanine.*

3.4. Results

3.4.1. Potential ZIP10 proteolytic cleavage sites

To identify potential cleavage sites of ZIP10, a thorough software analysis was carried out using the ePESTfind (Gouw et al., 2017) and ELM (Dinkel *et al.*, 2016) software. Predicted cleavage sites in ZIP10 are shown in table 3.1. Two potential PEST sequences were identified, the first in the N-terminus (residues R206-K219), upstream of the *CPALLY* motif, and a second one in the intracellular loop between TMD3 and TMD4 (residues R576–K594). Several other cleavage sites were predicted using the ELM software (table 3.1). It is interesting to note that the majority of the predictions of proteolytic cleavage of ZIP10 occur in either the N-terminus or cytoplasmic loop between TMD3 and TMD4. These may be the most important regions within the protein for post-translational modifications and therefore key to regulation of the protein. There is one cleavage site predicted in the C-terminus, though it is unclear what role a cleavage this close to the end of the protein would have on its regulation.

Prediction using the ELM software is based on short consensus sequences throughout the protein, the cellular compartment it is localised to, and the tertiary structure of the relevant region of the protein. However, many of the matches may be false positives and therefore the cleavage of ZIP10 was then investigated experimentally.

3.4.2. Investigation of endogenous ZIP10 cleavage

To investigate the cleavage of ZIP10 experimentally, basal MCF7 cell lysates were analysed by SDS-PAGE and western blot, using several anti-ZIP10 antibodies. Three antibodies targeting the N-terminus of ZIP10 were used (figure 3.2A); N1, N2 and N3. Both N1 and N2 had the same epitope (residues 46–59), however, N1 was a polyclonal and N2 a monoclonal antibody. The epitope for antibody N3 was further downstream, at residues 156–252. Each antibody was used to detect ZIP10 in the MCF7 cell lysates and *Rf* values were calculated to determine the exact size of protein detected with each antibody (figure 3.2B).

Table 3.1. Predicted cleavage sites in the ZIP10 protein

Domain	Position	Sequence	Potential Cleavage Protein
N-terminus	25–26	NHC–HE	Signal Peptidase Complex
	41–45	RGMTE	Proprotein convertase SKI1
	84–88	KLLTN	Proprotein convertase SKI1
	93–95	ERK	N-Arginine Dibasic Convertase
	148–150	KRN	Proprotein convertase 1/2
	206–219	RGEPSNEPSTETNK	PEST
	232–234	KRK	NEC1/NEC2 cleavage site
	232–234	KRK	N-Arginine Dibasic Convertase
	237–239	GRK	N-Arginine Dibasic Convertase
	306–312	RHTRKRE	Proprotein convertase 7
	308–310	TRK	N-Arginine Dibasic Convertase
	310–312	KRE	Proprotein convertase 1/2
	324–326	LRK	N-Arginine Dibasic Convertase
TMD3–4 ICL	516–520	RMFKH	Proprotein convertase SKI1
	542–544	GRK	N-Arginine Dibasic Convertase
	576–594	RLNETELTDLEGQQESPPK	PEST
	608–612	SHSDG	Caspase-3/7
	633–637	KTVLR	Proprotein convertase SKI1
	636–638	LRK	N-Arginine Dibasic Convertase
C-terminus	824–828	KIVFD	Proprotein convertase SKI1

Sites were predicted using ePESTfind (EMBOSS) (Gouw *et al.*, 2017) *and ELM* (Dinkel *et al.*, 2016) *with the human sequence of ZIP10 in FASTA format. ICL, intracellular loop. – indicates the exact site of signal peptide cleavage.*

Using the Compute pI/Mw (Bjellqvist *et al.*, 1993) software it was possible to determine the approximate site of cleavage in the ZIP10 protein based on the band sizes detected by western blot. When using this tool, residues 1–25 were removed as this is a signal peptide sequence that is removed before translocation of the protein the plasma membrane. This ensured greater accuracy when determining the approximate site of cleavage as only the mature protein was accounted for.

Each of the N-terminal antibodies detected a band of 105 kDa (figure 3.2B). This is likely to be the whole ZIP10 protein as it is the largest that was detected, and it was seen with each of the three antibodies. The full ZIP10 protein is predicted by software to be 94 kDa. With removal of the signal peptide however the bare amino acid sequence is 91 kDa, indicating some post-translational modification occurs, increasing the total molecular mass to 105 kDa and decreasing the mobility of the protein through the gel.

Although antibodies N1 and N2 have the same epitope, additional bands were detected by antibody N1. These were measured at 70 kDa, 55 kDa, and 45 kDa (figure 3.2B). It is probable these additional bands are non-specific, as the antibody is polyclonal and binds different regions within the epitope. Monoclonal antibody N2 detected only the full size ZIP10 protein at 105 kDa.

To determine whether any of the additional bands detected with antibody N1 were non-specific, an immunising peptide blocking experiment was performed (figure 3.2C). Prior to probing the nitrocellulose membrane, the antibody was incubated with excess peptide that corresponded to the epitope the antibody recognises. The antibody is then no longer able to bind to epitope on the membrane, and therefore specific ZIP10 bands detected with the blocked antibody appear less dense than those detected with the control (unblocked antibody).

The 105, 70, 55, and 45 kDa bands appear less dense in the blocked sample compared to the control, though the effect on the 70 kDa band was less obvious than the others. This could be an indication that the ZIP10 70 kDa band is non-specific, or perhaps the conditions at the time of cell lysis were not optimal for this cleavage.

Figure 3.2. Characterisation of N-terminal ZIP10 antibodies

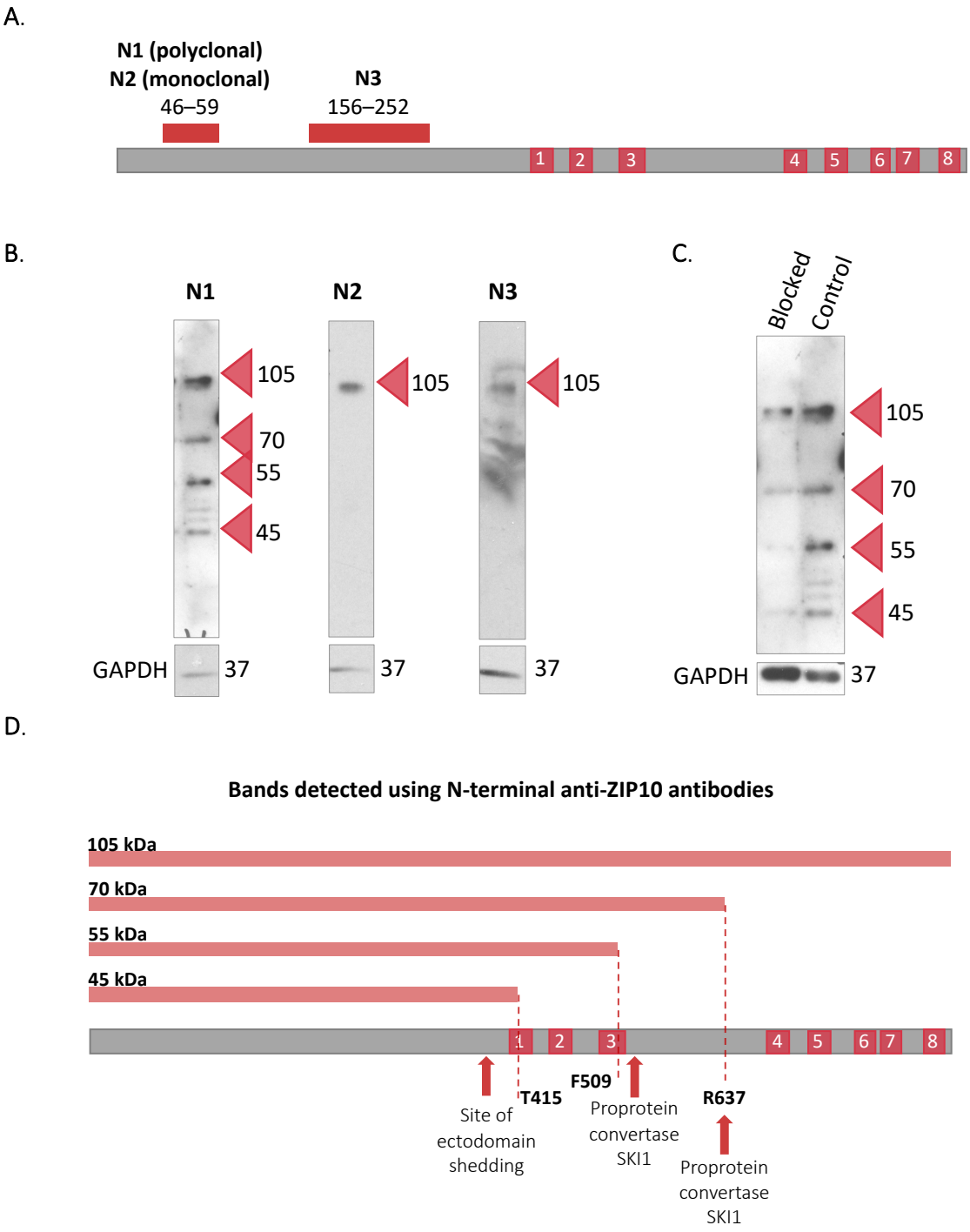

***A**. The epitopes of the N-terminal anti-ZIP10 antibodies are shown as a bar with the residue numbers of the epitopes. Further information about the antibodies is detailed in table 2.4. Boxes with numbers in represent the TMDs. **B**. SDS-PAGE and western blot analysis of basal MCF7 cells using the N-terminal ZIP10 antibodies. GAPDH was used as a loading control. Numbers represent the molecular mass of protein bands in kilodaltons (kDa). **C**. SDS-PAGE and western blot analysis of MCF7 cells using the N1 antibody blocked with the immunising peptide prior to incubation in the membrane, compared to the N1 antibody which was not blocked (control). **D**. Approximate residues of ZIP10 cleavage were calculated using the Compute pI/Mw (Bjellqvist et al., 1993) tool based on the molecular mass of the bands detected in B and C. Proteases predicted to cleave ZIP10 are indicated with pink arrows.*

The band of 70 kDa detected with antibody N1 could represent a fragment of ZIP10 following proteolytic cleavage at approximately residue R637 in the intracellular loop between TMD3 and TMD4 (figure 3.2D). The band detected at 55 kDa could represent cleavage at approximately residue F509 (figure 3.2D). Residue F509 is within TMD3 and there are no predicted cleavage sites in this region, though it is in close proximity to residue R516 in the intracellular loop, which is predicted to be cleaved (table 3.1) and therefore cleavage at R516 may be responsible for the generation of the 55 kDa band. Both of these identified cleavage sites (R637 and R516) are predicted to be cleaved by proprotein convertase SKI1 (table 3.1) indicating the potential processing of ZIP10 by this enzyme. Further experimental work is required to determine the conditions in which either cleavage occurs.

The 45 kDa band detected with antibody N1 could correspond to cleavage at approximately residue T415 (figure 3.2D). This falls within TMD1 and there are no predictions of cleavage here, however this is in close proximity to the ectodomain shedding site previously described by Ehsani *et al.*, (2012) and a fragment of this size may be the result of additional processing e.g. glycosylation. For this reason, the 45 kDa band was not ruled out as the potential ectodomain shedding of ZIP10.

Antibodies L4 and L5 are targeted to epitopes in the ZIP10 intracellular loop between TMD3 and TMD4 (figure 3.3A). Antibody L4 detected a ZIP10 fragment of 44 kDa (figure 3.3B). The Compute pI/Mw software was used to determine which fragment of ZIP10 this band could represent (figure 3.3C). The band could represent a C-terminal fragment of ZIP10, the product of cleavage at approximately residue G434. This residue is in the intracellular loop between TMD1 and TMD2 and, owing to the lack of predicted cleavage in this region (table 3.1), it is not likely that cleavage occurs here. Alternatively, the fragment could represent a central region of the protein, following cleavage in the N-terminal at approximately residue G250, and in the intracellular loop at residue R637. The latter was identified as a potential cleavage site using the N-terminal antibodies in figure 3.2. Furthermore, residue G250 in the N-terminus is in close proximity to the predicted cleavage at G237-K239 by N-Arginine Dibasic Convertase (table 3.1).

Figure 3.3. Characterisation of intracellular ZIP10 antibodies

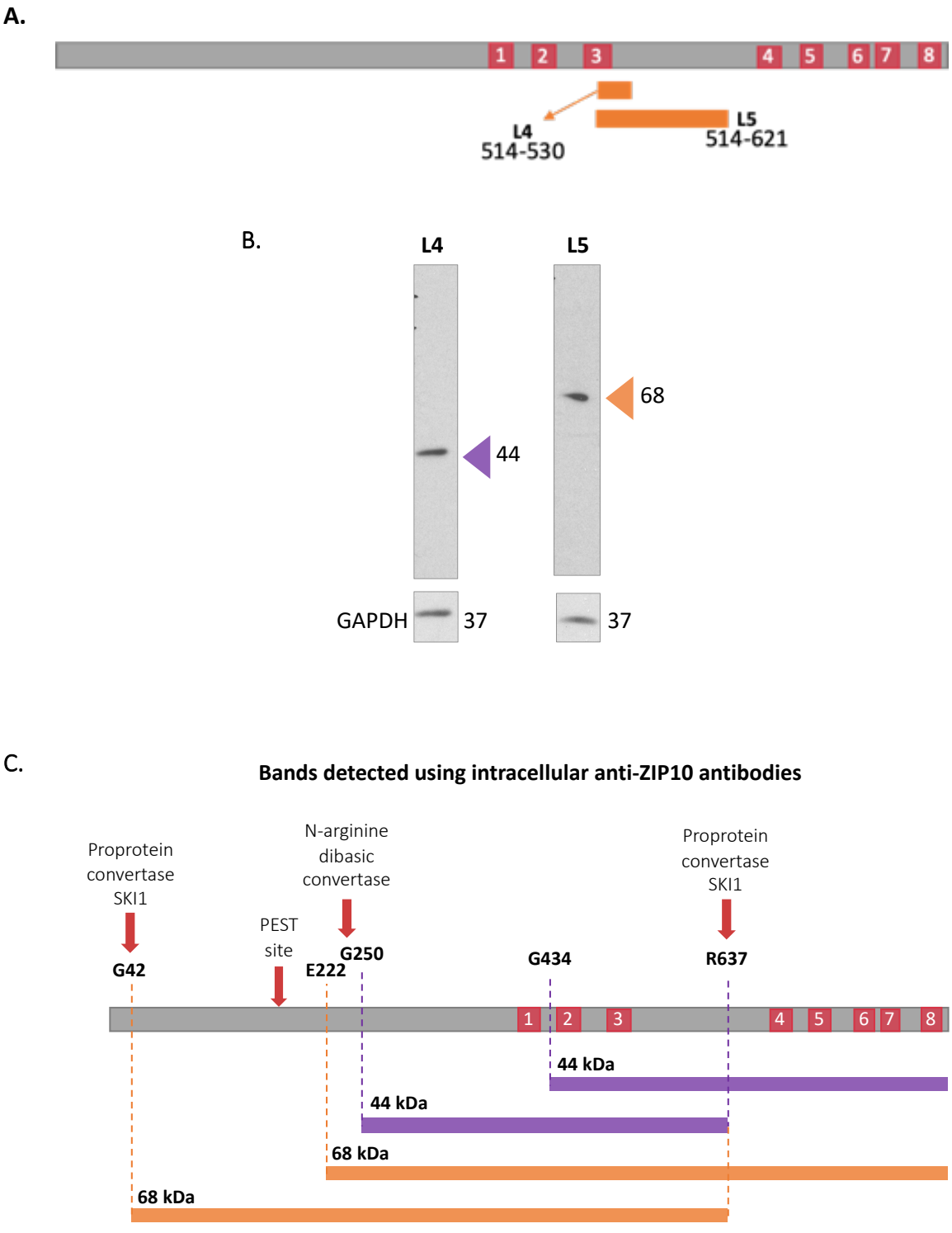

***A**. The epitopes of the intracellular anti-ZIP10 antibodies are shown as a bar with the residue numbers of the epitopes. Further information about the antibodies is detailed in table 2.4 in chapter 2. **B**. SDS-PAGE and western blot analysis of basal MCF7 cells using the intracellular anti-ZIP10 antibodies. GAPDH was used as a loading control. Numbers represent the molecular mass of protein bands in kDa. **C**. Approximate residues of ZIP10 cleavage were calculated using the Compute pI/Mw (Bjellqvist et al., 1993) tool based on the molecular mass of the bands detected in B. Proteases predicted to cleave ZIP10 are indicated with pink arrows.*

Antibody L5 detected a band of 68 kDa (figure 3.3B). Using the Compute pI/Mw software, it was determined that a C-terminal fragment of ZIP10 weighing 68 kDa would be the product of cleavage at approximately residue E222 (figure 3.3C). This residue is in close proximity to the predicted N-terminal PEST site, at 206–219 (table 3.1), suggesting that ZIP10 may undergo N-terminal PEST site cleavage, similarly to ZIP6. Alternatively, if the previously identified cleavage at R637 is correct, the 68 kDa band must be further towards the N-terminal of ZIP10. It may be generated following cleavage at residue G42 in the N-terminus and R637 in the intracellular loop. Each of these sites are predicted to be cleaved by proprotein convertase SKI1, further implicating a link between this enzyme and ZIP10 processing.

3.4.3. Investigation of recombinant ZIP10 cleavage

To characterise ZIP10 cleavage further, recombinant WT ZIP10 with a C-terminal V5 tag was transfected into MCF7 cells. The cells were lysed and analysed by western blot with an anti-V5 antibody (figure3.4A) that detected two distinct ZIP10 fragments with molecular masses of 110 kDa and 63 kDa (figure 3.4B). The fragments were confirmed to be recombinant ZIP10 as they were not detected in the un-transfected cells or those transfected with the empty lipid vector. The largest recombinant ZIP10 band (110 kDa) is 5 kDa bigger than the full-size endogenous protein detected with the N-terminal antibodies in figure 3.2, confirming the V5 tag alone weighs 5 kDa. The size of these bands can therefore be adjusted to 105 kDa and 58 kDa (figure 3.4C). A C-terminal fragment of ZIP10 weighing 58 kDa could be the result of cleavage around residue R309 (figure 3.4C), which is predicted in table 3.1, by N-Arginine Dibasic Convertase.

The anti-V5 antibody did not detect 44 kDa or 68 kDa bands corresponding to those detected by the intracellular ZIP10 antibodies in figure 3.3. This supports the hypothesis that the 44 and 68 kDa bands are not C-terminal fragments of ZIP10 and are regions from the central portion of the protein instead.

Figure 3.4. Characterisation of recombinant ZIP10 by western blot

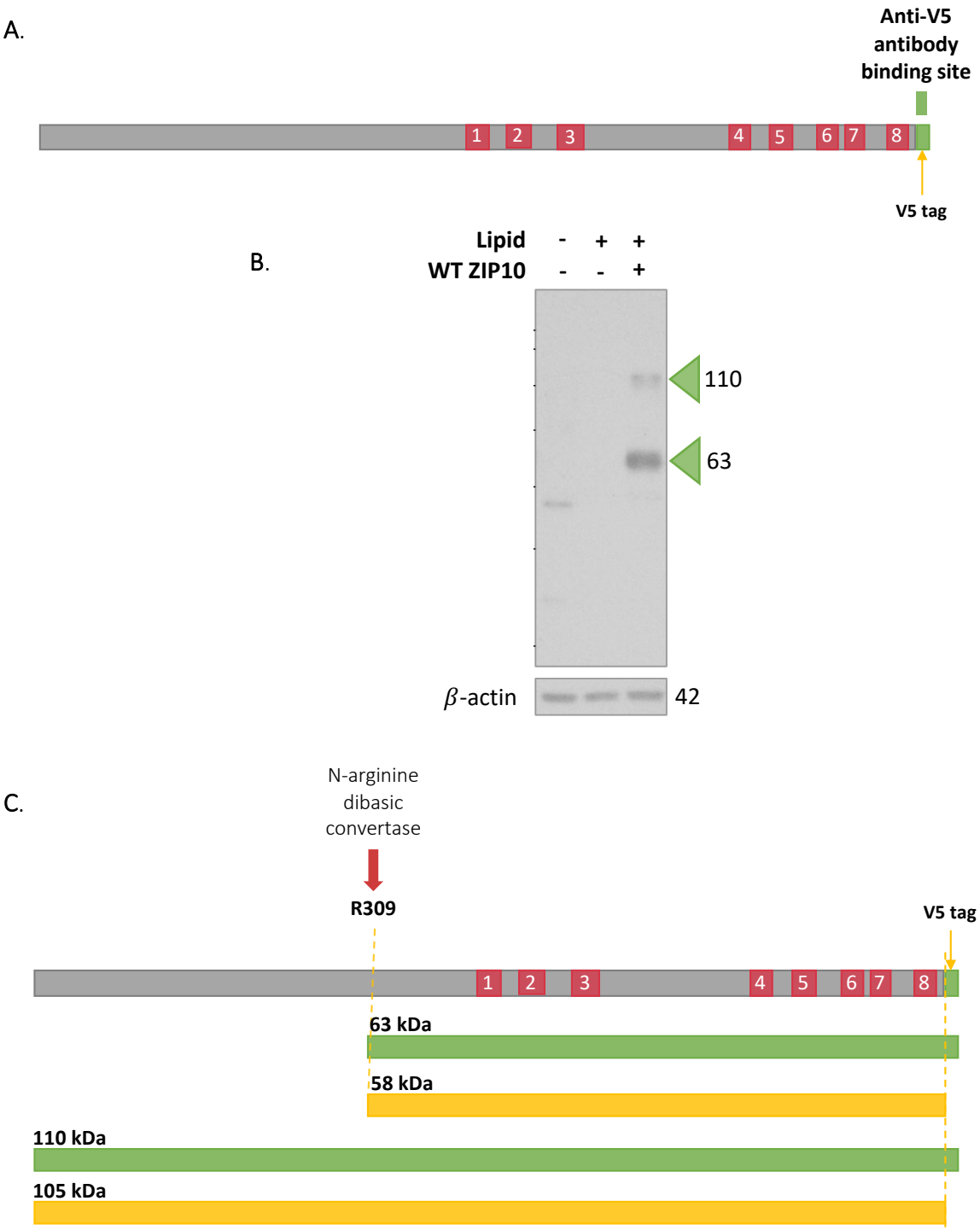

***A**. The location of the V5 tag at the C-terminal end of the ZIP10 protein and the location of the anti-V5 antibody binding. **B**. SDS-PAGE and western blot analysis of WT ZIP10-transfected MCF7 cells using the anti-V5 antibody. β-actin was used as a loading control. Numbers represent the molecular mass of protein bands in kDa. **C**. Approximate residues of ZIP10 cleavage were calculated using the Compute pI/Mw (Bjellqvist et al., 1993) tool based on the molecular mass of the bands detected in B. Proteases predicted to cleave ZIP10 are indicated with pink arrows.*

Taking into account all the western blot data collected so far, the remaining potential fragments of ZIP10 are outlined in figure 3.5 with the potential protease responsible for cleavage at each site. The approximate cleavage sites in ZIP10 based on the western blot analysis presented here do not align exactly to those cleavage sites predicted in table 3.1. One reason for this may be the post-translational modification of ZIP10 that is not taken into account when determining the molecular masses of protein fragments using the Compute pI/Mw (Bjellqvist et al., 1993) software. Glycosylation of ZIP10 was next examined to assess the impact of this modification on the ZIP10 band sizes seen with the various antibodies seen so far.

Figure 3.5. ZIP10 fragments and potential cleavage sites based on all antibodies

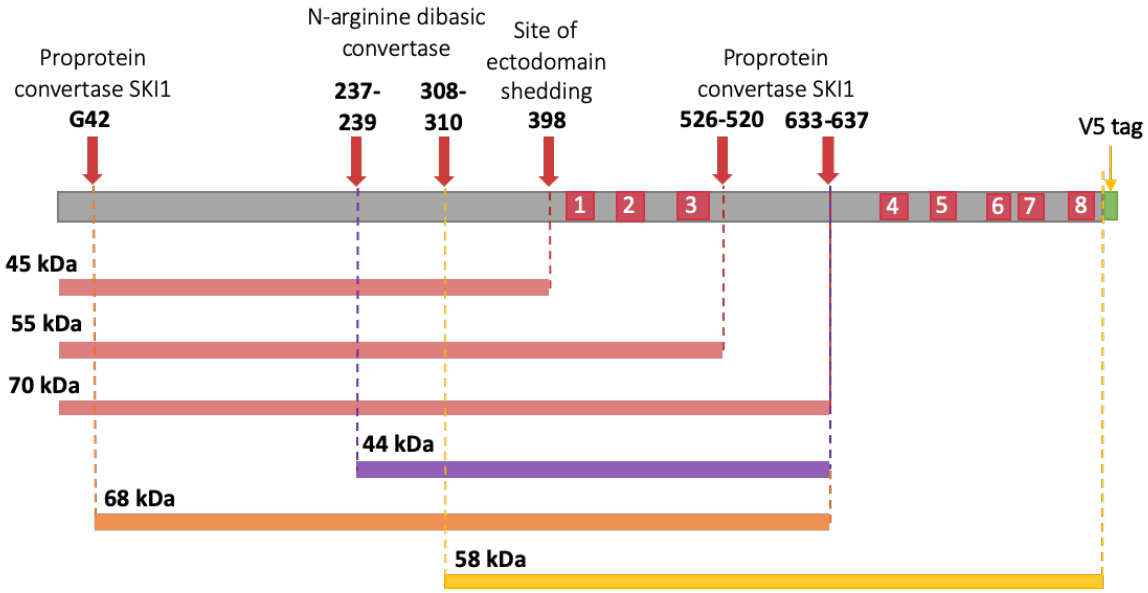

Potential ZIP10 cleavage sites and the proteases responsible for cleavage based on western blot data collected using multiple anti-ZIP10 antibodies (figure 3.2–3.3) and an anti-V5 antibody (figure 3.4).

3.4.4. ZIP10 glycosylation

ZIP10 is regulated by glycosylation, particularly in the N-terminus (Ehsani *et al.*, 2012). To investigate this further and determine how glycosylation affects the band sizes seen so far, the human protein sequence of ZIP10 was analysed for *NxT/S* acceptor sites where the *N* is the glycosylated residue and *X* is any amino acid.

There are 10 *NxT/S* sites in the human protein sequence of ZIP10 (figure 3.6A), however only regions destined to be extracellular undergo N-linked glycosylation, therefore the 3 sites in the intracellular loop between TMD3 and TMD4, and 1 site in TMD4 were disregarded. In the N terminus, 5 *NxT/S* sites were predicted to be glycosylated with strong potential. Three of the predictions in this region have been experimentally confirmed in mouse ZIP10 (Ehsani *et al.*, 2012). A further N-linked glycosylation site was predicted in the extracellular loop between TMD6 and TMD7 with moderate potential.

To investigate ZIP10 glycosylation experimentally, WT ZIP10-expressing MCF7 cell lysates were treated with PNGase F. This is an amidase that removes N-linked glycosylation side chains from proteins. The samples were analysed by SDS-PAGE and western blot and assessed for the difference in mobility of the V5 bands, compared with the untreated lysates. Both the full length ZIP10 and the C-terminal ZIP10 fragment demonstrated greater mobility during electrophoresis following digestion with PNGase F (figure 3.6B) compared with the untreated lysates. The full length ZIP10 band was reduced in size by 20 kDa suggesting up to 8 N-linked glycans had been removed. The smaller, C-terminal fragment of ZIP10 shifted 5 kDa suggesting two glycosylation sites are downstream of the cleavage site which generates this band (residues T308-K310). These data confirm that the predicted glycosylation sites identified in figure 3.6A may all be glycosylated in basal conditions.

The presence of glycosylation side chains on the ZIP10 protein highlights that the ZIP10 cleavage sites determined here using western blot are approximate and might explain why they do not match perfectly to the predicted ZIP10 cleavage sites in table 3.1. However, the work presented here has highlighted the complexity of ZIP10 processing and therefore the need to investigate specific ZIP10 cleavage sites in more detail.

Figure 3.6. N-linked glycosylation of ZIP10

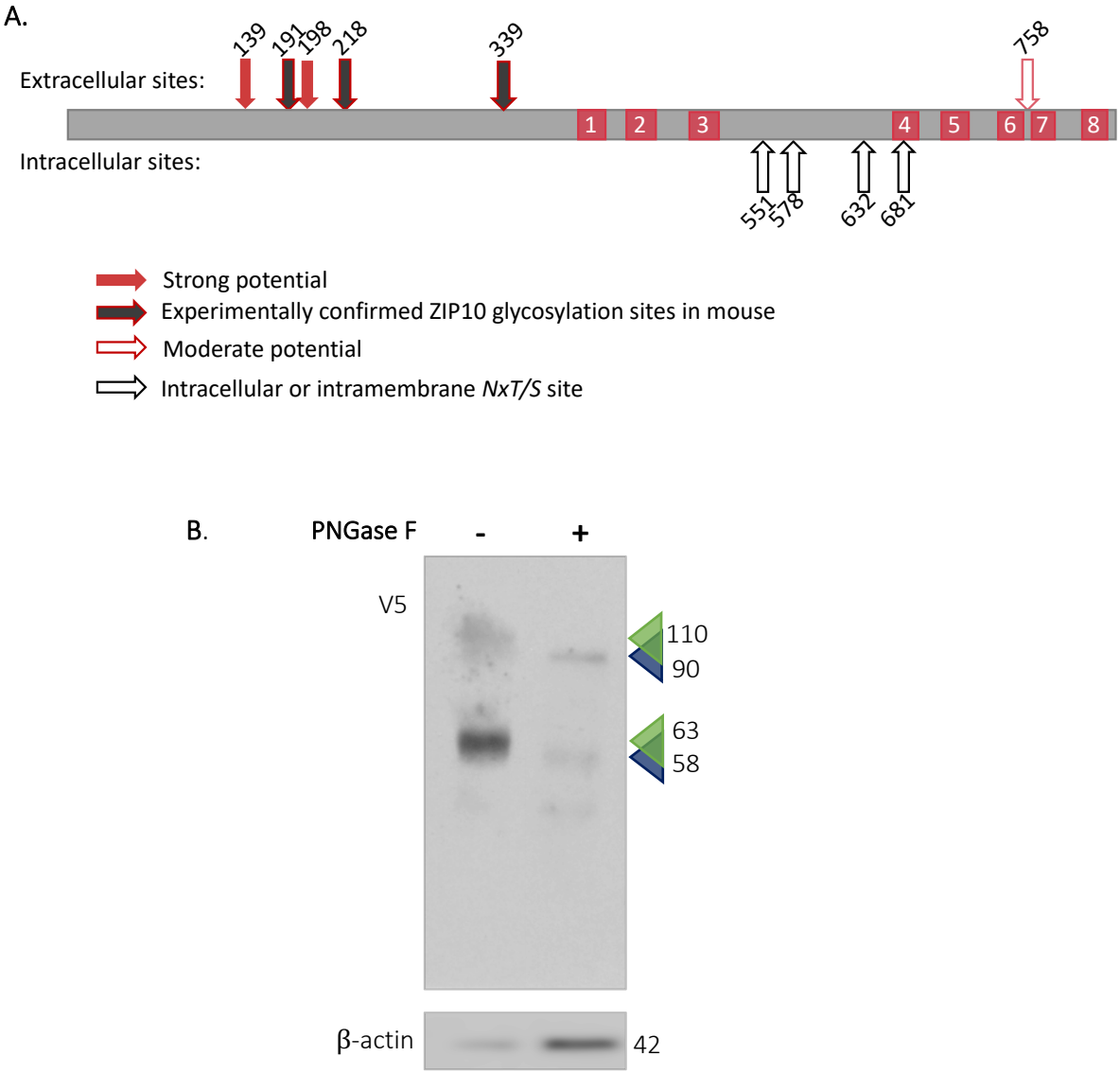

***A**. NxT/S sites present in the human ZIP10 protein sequence are predicted to be glycosylated. **B**. MCF7 cells in basal conditions were lysed and treated with PNGase F to digest glycosylation side chains. The products were analysed by SDS-PAGE and western blot, probing for V5 and β-actin. Green arrows are the bands of samples with no PNGase F treatment. Blue arrows are the bands following PNGase F treatment. Numbers represent the molecular mass of bands measured in kDa.*

3.4.5. Proteolytic processing of ZIP10 in mitosis

The western blot analysis presented in the previous sections suggests that ZIP10 undergoes proteolytic cleavage. Further work is required to determine the exact sites of cleavage and under which conditions they occur. As ZIP10 is known to undergo ectodomain shedding (Ehsani *et al.*, 2012) and the 45 kDa band detected with antibody N1 could reasonably represent the N-terminal ectodomain (figure 3.5), this cleavage was investigated in the context of mitosis.

MCF7 cells were synchronised in mitosis by treatment with 150 nM nocodazole, which prevents microtubule polymerisation, halting cells in prophase (the first stage in mitosis). The treatment was given for 20 hours and the cells were lysed and analysed by SDS-PAGE and western blot. Histone H3 is a DNA bound protein that becomes phosphorylated on serine residue 10 during mitosis (Hendzel *et al.*, 1997) and therefore it was used as an indicator of mitosis (figure 3.7A). The amount of pS^{10}Histone H3 present in the cells treated with nocodazole was significantly increased ($p < 0.001$) compared with the untreated cells (figure 3.7B), confirming successful mitotic synchronisation.

In the mitotic population, the 45 kDa ZIP10 fragment detected with antibody N1 was increased significantly ($p < 0.001$) and the full size 105 kDa fragment was reduced (figure 3.8A). These data suggest proteolytic cleavage of the N-terminal ectodomain of ZIP10 in prophase (the stage of mitosis where cells are halted in the presence of nocodazole). No differences were seen in the bands detected with the intracellular antibodies (targeted to epitopes within the ZIP10 protein that reside on the inside of the cell) between untreated cells and those treated with nocodazole (figure 3.8B-C) suggesting that, if they are ZIP10 fragments, their processing may not be related to mitosis.

Figure 3.7. pS[10]Histone H3 as a marker of mitosis

A.

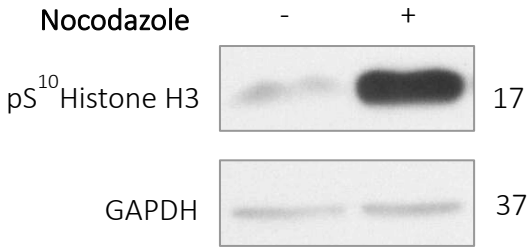

B.

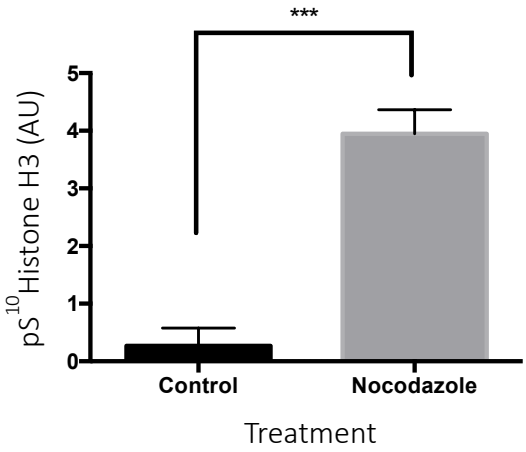

***A**. MCF7 cells treated with 150 nM nocodazole for 20 hours and analysed by western blot for pS[10]Histone H3. Numbers represent the molecular mass of protein bands in kDa. **B**. Protein expression was normalised to GAPDH expression and presented as mean ± standard error (n = 3). Statistical significance was measured using a paired t-test. *** p < 0.001. AU, arbitrary unit.*

Figure 3.8. ZIP10 N-terminal cleavage in mitosis

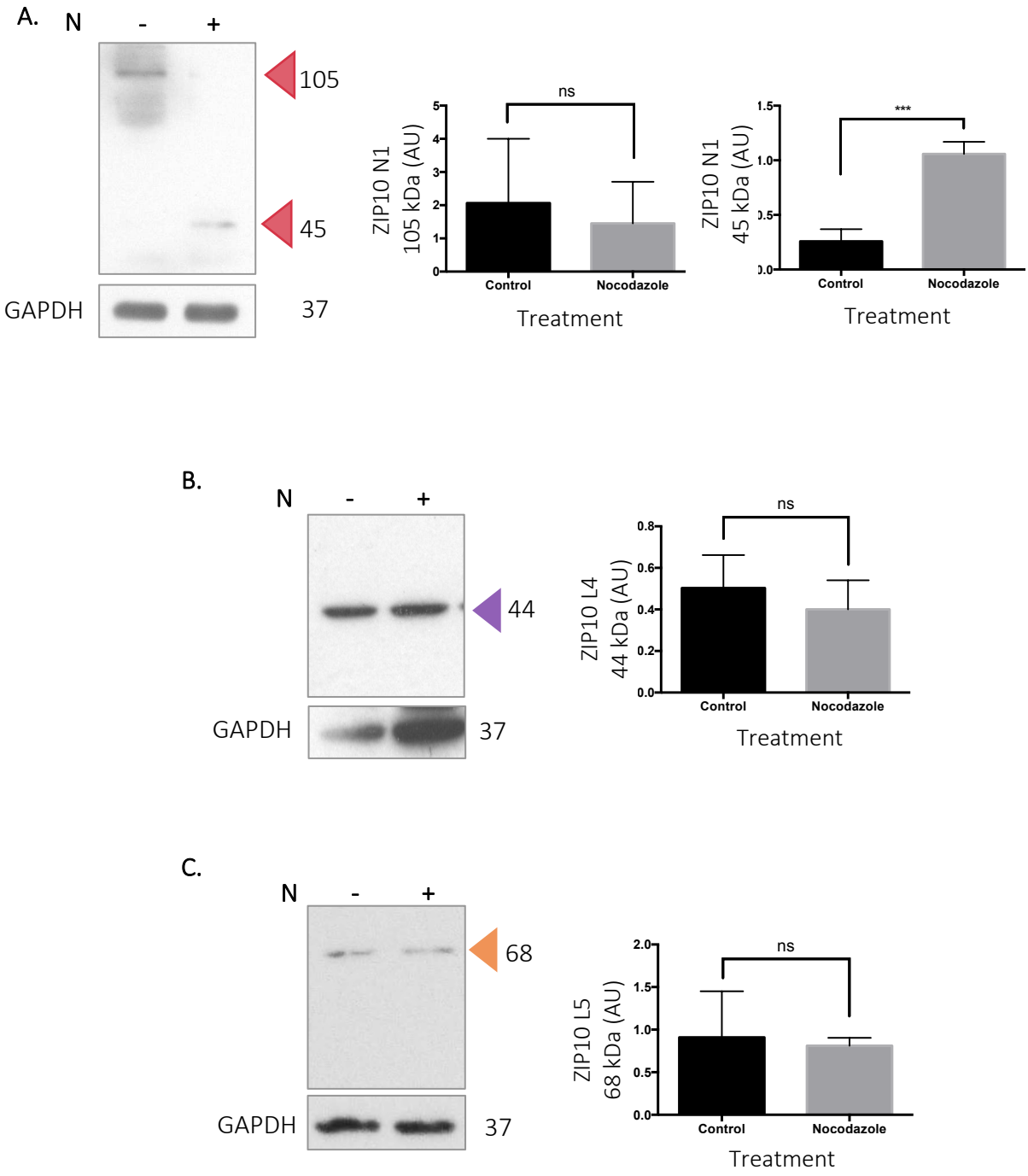

*MCF7 cells treated with 150 nM nocodazole for 20 hours and analysed by western blot for ZIP10 using three of the anti-ZIP10 antibodies; N1 (**A**), L4 (**B**), and L5 (**C**). Numbers represent the molecular mass of protein bands in kDa. Protein expression was normalised to GAPDH expression and presented as mean ± standard error (n = 3). Statistical significance was measured using a paired t-test. *** p < 0.001. N, nocodazole; ns, not significant; AU, arbitrary unit.*

3.4.6. Localisation of ZIP10 in mitosis

The western blot data presented here suggest that ZIP10 is regulated by cleavage in mitosis. To visualise the location of ZIP10 and its fragments during mitosis, MCF7 cells grown on coverslips were treated with nocodazole and fixed. Anti-ZIP10 antibodies were used to stain for ZIP10 and pS^{10}Histone H3 was used as a marker of mitotic cells. Using the N-terminal targeted ZIP10 N2 antibody, ZIP10 appears to be increased in the mitotic cells compared with the non-mitotic cells (figure 3.9A). The pattern of staining, however, is not suggestive of plasma membrane localisation and more so cytoplasmic localisation, alluding to the potential internalisation of the N-terminus following ectodomain shedding.

N-terminal antibody N3 displayed stronger fluorescence in mitotic cells compared to non-mitotic cells (figure 3.9B), and interestingly, it also demonstrated a fluorescent stain around the nucleus in a non-mitotic cell (figure 3.9B; white arrow), although there is no evidence in the literature to suggest that ZIP10 is present on the nuclear membrane. To understand whether the likelihood that this finding could be real ZIP10 staining, the epitope sequence for this antibody was analysed in BLAST. The search did not return a similarity to other proteins implicating localisation of this protein, or a fragment of it, to the nuclear membrane.

Neither the L4 nor the L5 antibodies appeared to detect specific ZIP10 staining on the plasma membrane of MCF7 cells (figure 3.9C-D). However, antibody L5 did show distinct punctate staining in the nucleus of non-mitotic cells (figure 3.9E). If this staining is specific, it is the first indication that ZIP10 (or a fragment of ZIP10) could locate to the nucleus during interphase. It should be noted here that the absence of ZIP10 staining on the plasma membrane with both of these antibodies may be because the epitopes for both antibodies overlap with TMD3 and are not fully accessible to the antibody. In addition, the binding of ZIP6 to ZIP10 in a heteromer (Taylor *et al.*, 2016) could block the binding sites for the antibodies.

To investigate the localisation of the ZIP10 N-terminus further, the staining with the N-terminal antibody was repeated in cells which were not permeabilised with saponin. Since the N-terminus of ZIP10 is outside the cell, entry of the antibody through the plasma membrane is not necessary to visualise ZIP10 using this antibody. It should be noted that the formaldehyde used in the fixing process partially permeabilises cells, as evidenced by

the presence of pS^{10}Histone H3 staining in some cells (figure 3.10); the primary and secondary antibodies could only enter the cells if there were sufficient gaps in the plasma membrane to get through.

Figure 3.9. Localisation of ZIP10 in non-mitotic and mitotic MCF7 cells

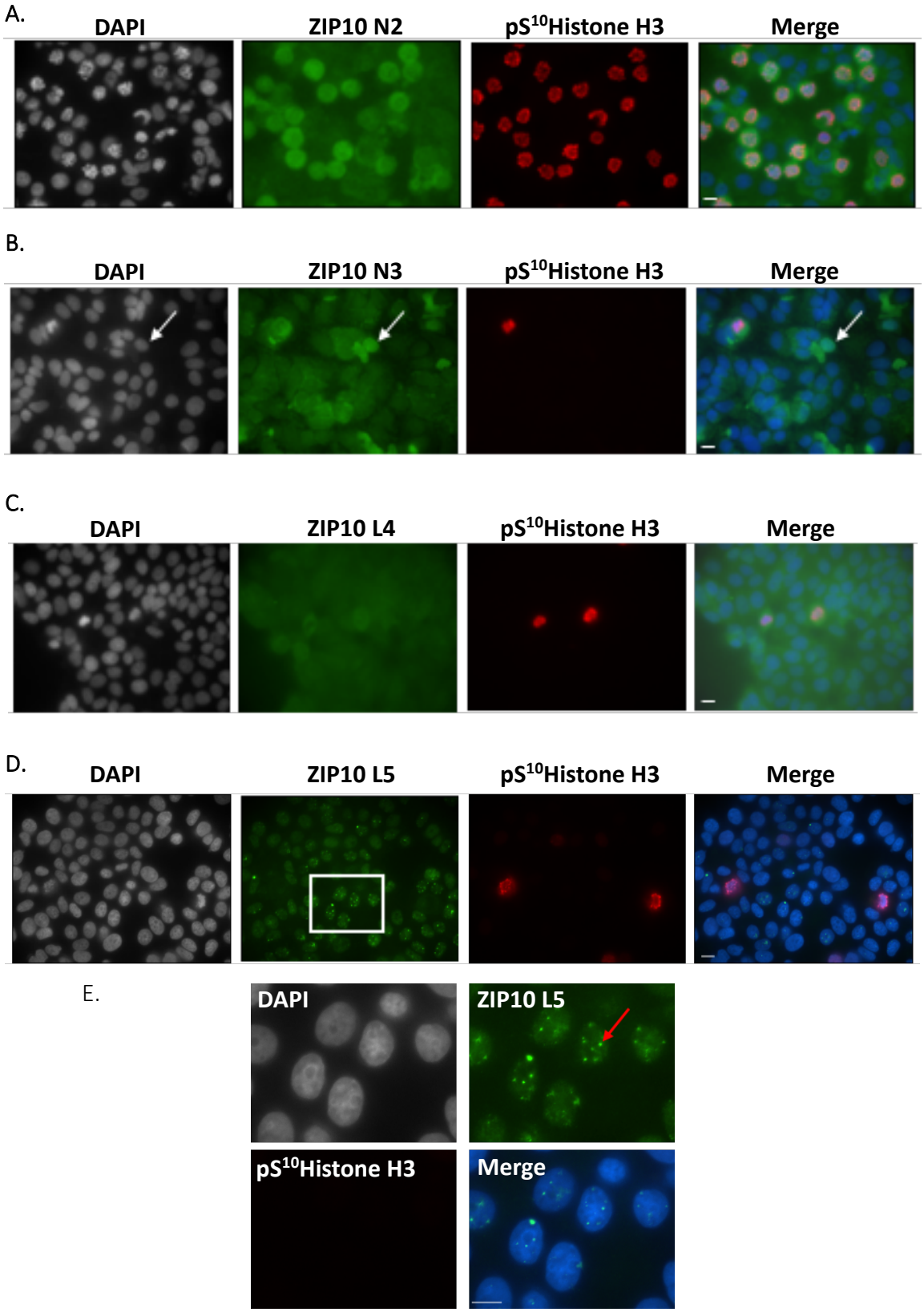

*MCF7 cells were fixed and stained for ZIP10 (green) using antibodies N2 (**A**), N3 (**B**), L4 (**C**), L5 (**D**) and pS[10]Histone H3 (red). Alexa Fluor®-fluorophore conjugated secondary antibodies were used for detection of proteins. The white arrow indicates the peri-nuclear ring seen with antibody N3 in a non-mitotic cell. The white box in D is magnified in **E** to highlight the nucleoli staining (red arrow) seen using the L5 antibody. Nuclei were stained with DAPI (blue). Scale bars: 10 μm.*

Figure 3.10. Localisation of ZIP10 in non-permeabilised mitotic MCF7 cells

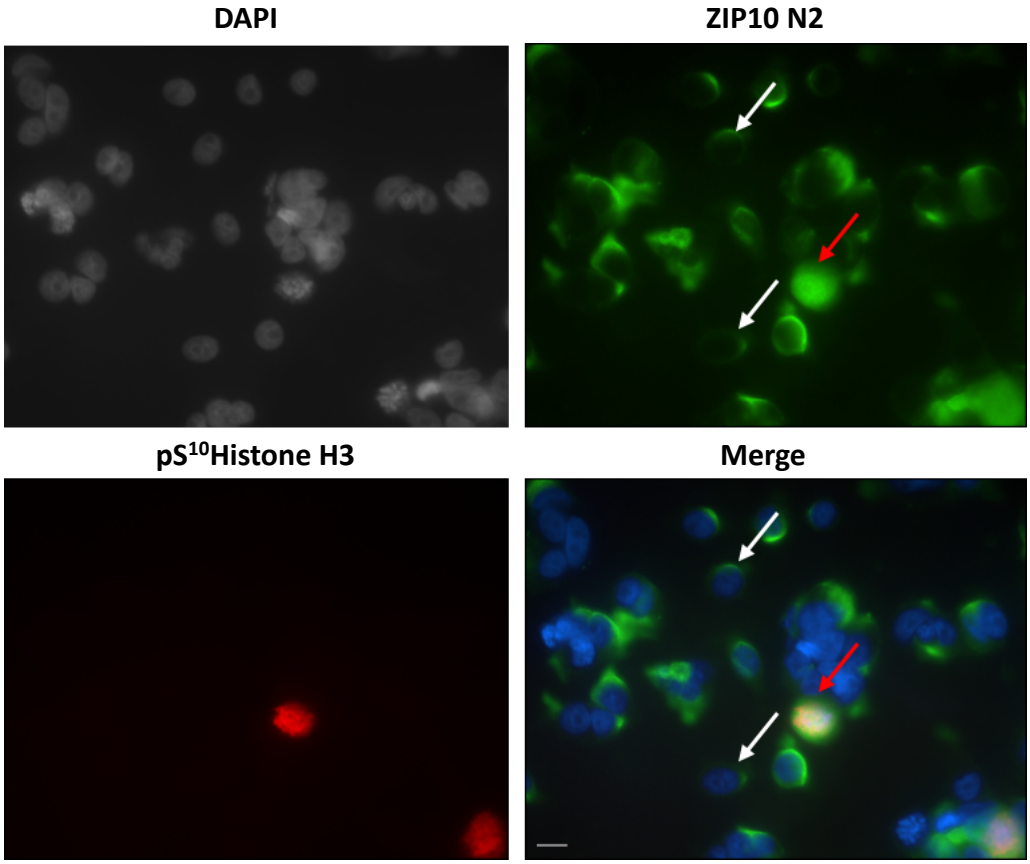

MCF7 cells were fixed and stained for ZIP10 (green) using antibody N2 and pS[10]Histone H3 (red). Alexa Fluor®-fluorophore conjugated secondary antibodies were used for detection of proteins. The staining process was carried out using buffer that contained no saponin. The white arrows indicate non-mitotic cells and red arrows indicate mitotic cells. Nuclei were stained with DAPI (blue). Scale bars: 10 μm.

Less background staining was seen with the anti-ZIP10 antibody in non-permeabilised conditions compared with permeabilised conditions, however, the mitotic cell (highlighted by the yellow arrow) still showed increased ZIP10 but not associated specifically with the plasma membrane. In contrast, some non-mitotic cells appeared to show ZIP10 staining in a ring surrounding the cell, suggestive of plasma membrane staining. These data suggest that ZIP10 may be localised to the plasma membrane preceding mitosis, and the N-terminal ectodomain is shed in prophase. At this point, it may become internalised.

The location of the C-terminal fragment of ZIP10 was then investigated in MCF7 cells transfected with WT ZIP10 and stained with an anti-V5 antibody. Recombinant ZIP10 was seen on the plasma membrane of both mitotic (figure 3.11A; yellow arrow) and non-mitotic cells (figure 3.11B; white arrows). This finding is evidence that at least the C-terminal region of ZIP10 is present on the plasma membrane at a time in the cell cycle other than mitosis and supports the hypothesis that the full length of ZIP10 is present on the plasma membrane preceding mitosis, before ectodomain shedding occurs during mitosis.

The data collected thus far indicate the cleavage of ZIP10 around residue K390 in the early stages of mitosis, and that the C-terminal end of ZIP10 remains on the plasma membrane during mitosis. To further assess the N-terminal ectodomain shedding of ZIP10 in mitosis, a cell surface protein isolation experiment was carried out. MCF7 cells treated with nocodazole were labelled with biotin which binds to exposed lysine residues on extracellular regions of plasma membrane-bound proteins. The cells were lysed, and biotin-bound membrane proteins separated from non-membrane proteins. Once separated, the biotin-bound proteins were eluted, and the isolated plasma membrane proteins analysed using SDS-PAGE and western blotting.

To confirm that biotin did not label proteins which are intracellular, both biotin-labelled and non-biotin-labelled samples were analysed for the presence of intracellular protein GAPDH (figure 3.12A). GAPDH was absent in the biotin-labelled samples but present in the non-labelled samples, confirming there was no contamination of intracellular proteins in the samples labelled with biotin.

Figure 3.11. Localisation of recombinant WT ZIP10

A.

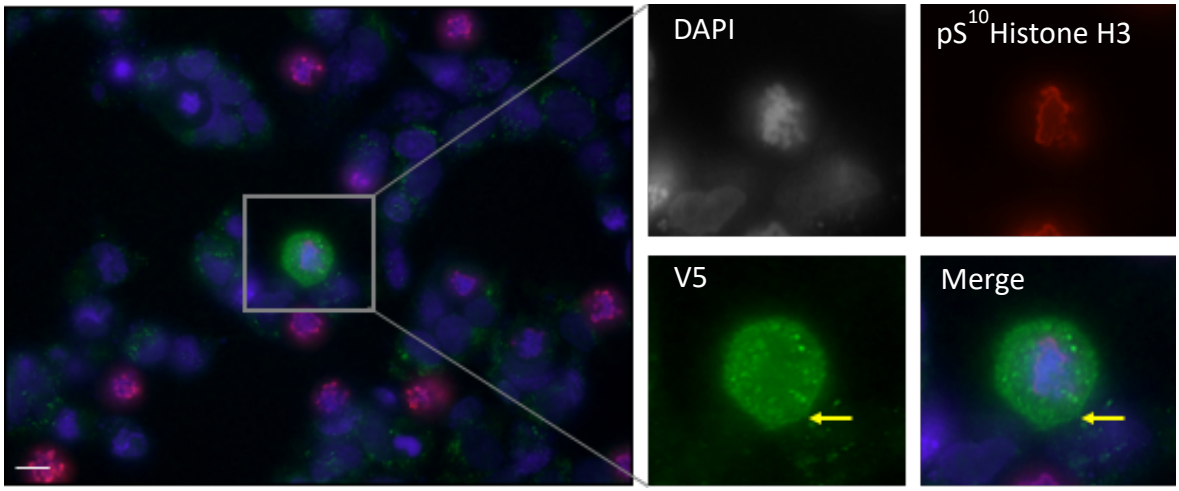

B.

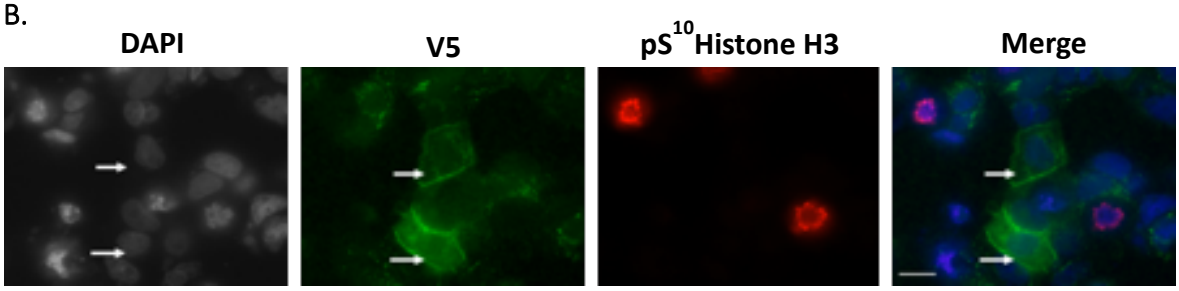

MCF7 cells were transfected with recombinant WT ZIP10 in the presence of nocodazole for 18 hours. Cells were fixed and stained using anti-mouse pS[10]Histone H3, and anti-rabbit V5 antibodies. Anti-mouse Alexa Fluor® 594 (red) and anti-rabbit 488 (green) secondary antibodies were used to detect the proteins. DAPI was used to stain the cell nuclei (blue). Scale bars: 10 μm. Images were taken from several fields of view on the coverslip and two representative images are shown. ***A****. white arrows indicate non-mitotic cells.* ***B****. yellow arrow indicates area where plasma membrane staining of a mitotic cell, with the anti-V5 antibody is apparent.*

In the mitotic population, the presence of full-size ZIP10 on the plasma membrane, as detected by the N-terminal antibody N1, was decreased compared with the untreated cells (figure 3.12B). This supports the hypothesis that the N-terminal ectodomain is cleaved off in mitosis. The membrane was then probed with an intracellular ZIP10 antibody (L4) to investigate whether the intracellular region of ZIP10 was still associated with the plasma membrane following ectodomain shedding. The 44 kDa band detected with this antibody was increased in the presence of nocodazole compared to the untreated cells (figure 3.12C), suggesting that this fragment of ZIP10 is a product of ectodomain shedding.

The ZIP10 band sizes presented in figure 3.5 suggest that the 44 kDa band detected with intracellular antibody L4 is the product of cleavage at residues 237–239. However, ectodomain shedding is expected to occur at approximately residue D398. The cell-surface protein isolation experiment supports the hypothesis that the 44 kDa fragment is in fact the product of ectodomain shedding and a second cleavage immediately upstream of TMD8 (figure 3.13). This is in close proximity to the predicted C-terminal cleavage site predicted in table 3.1, at residues 824–828, and could be an indication that this cleavage is genuine. This would also explain why the anti-V5 antibody does not detect the same fragment; the V5 tag would be removed following cleavage at 824–828.

3.4.7. Investigation of specific proteolysis sites in ZIP10 in mitosis

To determine the exact site of ZIP10 ectodomain shedding in mitosis recombinant ZIP10 constructs with mutated cleavage sites were produced. Two potential cleavage sites of interest were selected for investigation; 309–311 (RKR) and 390–392 (KDK). 309–311 was chosen as it not only overlaps with predicted cleavage sites in table 3.1, but is also in close proximity to residue 300, shown by Ehsani *et al.* (2012) to be an approximate location for cleavage. 390–392 was chosen because cleavage at this site would generate an N-terminal fragment of ZIP10 of approximately 45 kDa, as shown in figure 3.13 and has been determined as the site for N-terminal ectodomain shedding in murine ZIP10 (Ehsani *et al.*, 2012). The sequences each contain 2 lysine residues (K) which are a common target of trypsin-like proteases (Olsen, Ong and Mann, 2004).

Figure 3.12. Isolation of ZIP10 from the plasma membrane

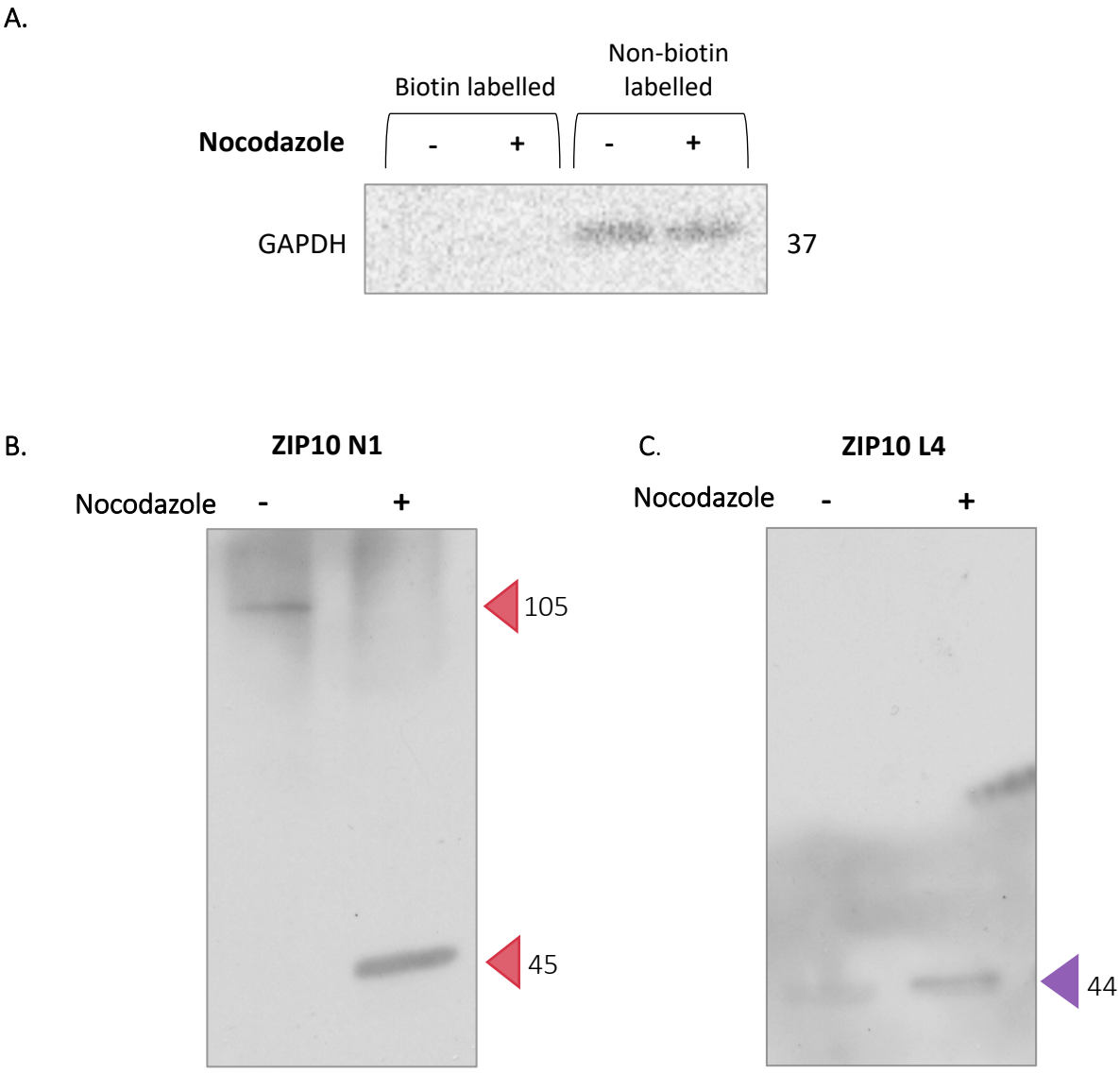

MCF7 cells were treated with nocodazole and cell surface proteins were labelled with biotin. The cells were lysed, and the biotin-labelled proteins separated from intracellular proteins using agarose bound NeutrAvidin protein. ***A****. The separated cell-surface proteins were compared to non-biotin labelled cell lysates and analysed using an anti-GAPDH antibody.* ***B-C****. The cell-surface proteins were analysed using N-terminal anti-ZIP10 N1 (B) and intracellular anti-ZIP10 L4 (C) antibodies. Numbers represent the molecular mass of protein bands in kDa.*

Figure 3.13. ZIP10 fragments and potential sites of cleavage in mitosis

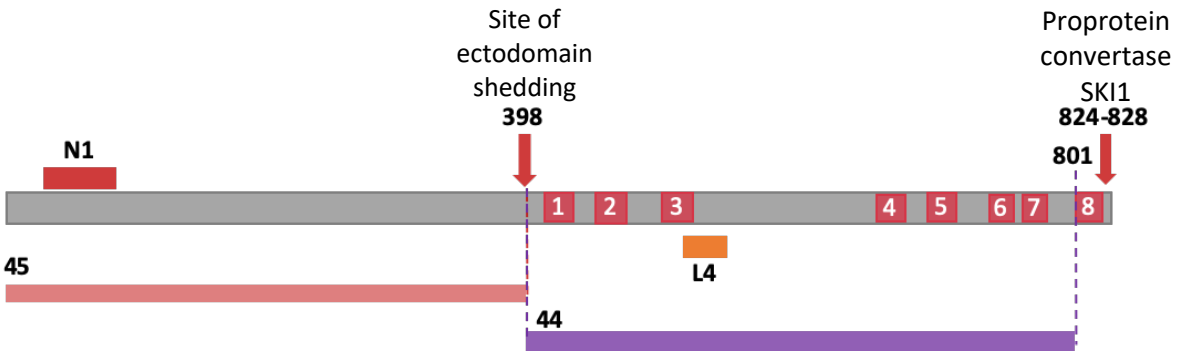

Potential sites of ZIP10 cleavage in mitosis and the ZIP10 band sizes detected on a western blot using the N-terminal ZIP10 antibody (N1) and the intracellular ZIP10 antibody (L4).

To investigate the potential cleavage at 309–311 and 390–392, the sequences were mutated by site-directed mutagenesis. The arginine and lysine residues were mutated to alanine residues due to its lack of side-chain chemistry and therefore protected from cleavage by a protease. The mutants were named cleavage mutant 1 and cleavage mutant 2 respectively.

Each mutant construct was expressed in MCF7 cells with or without nocodazole. The cells were lysed and analysed using SDS-PAGE and western blot, probing for C-terminal V5 (figure 3.14). The bands detected are confirmed to be recombinant ZIP10 as they are not present in the un-transfected cells or those transfected with the empty lipid vector. In the cells expressing cleavage mutant 1, the anti-V5 antibody detected a full size 110 kDa band and a smaller 63 kDa band, similarly to the cells expressing WT ZIP10 (figure 3.14). This suggests that residues 309–311 is not an important cleavage site in mitosis and is not the site for cleavage that generates the smaller 63 kDa V5 band. In contrast, in the cells expressing cleavage mutant 2, the anti-V5 antibody did not detect the smaller 63 kDa band (figure 3.14), indicating N-terminal cleavage occurs at residues 390–392, as the recombinant protein cannot undergo cleavage to generate this fragment. In addition, the amount of full-size protein present in these cells is greater than that in the cells expressing the WT protein, further indicating that cleavage has been prevented.

The full length 110 kDa band of ZIP10 is decreased in the nocodazole treated cells compared with those that were not treated with nocodazole, reflecting the western blot data in figure 3.8A that showed decreased full-length endogenous ZIP10 with the N-terminal antibody, following treatment with nocodazole. However, the smaller 63 kDa recombinant ZIP10 band is also decreased following treatment with nocodazole whereas the 45 kDa seen with the N-terminal antibody is increased in this scenario (figure 3.8). These data could suggest that the 63 kDa band is degraded soon after the cleavage that generates it, possibly owing to the C-terminal V5 tag rendering it misfolded or inactive.

3.4.8. Investigation of ZIP10-cleaving proteases in mitosis

The investigation into ZIP10 cleavage sites highlighted potential proteases that may be responsible for ZIP10 proteolytic cleavage. Since this chapter is focussed on ZIP10 processing in mitosis, a protease array assay was carried out to identify proteases with increased activity in mitosis. MCF7 cells were treated with nocodazole (N) and the treatment was removed for 1 (N + 1) or 2 (N + 2) hours, enabling the cells to move through mitosis. N samples were

enriched for cells in prophase, whereas N + 1 and N + 2 samples were enriched for cells in metaphase and anaphase/telophase respectively. The cell lysates were incubated on a membrane containing several antibodies targeted to different proteases. The grid showing the various antibodies on the membrane is shown in figure 3.15 and the list of proteases to which these antibodies bind is shown in table 3.2. A positive signal is detected when a particular protease is present in a given sample.

Figure 3.14. Site-directed mutagenesis of potential ZIP10 cleavage sites

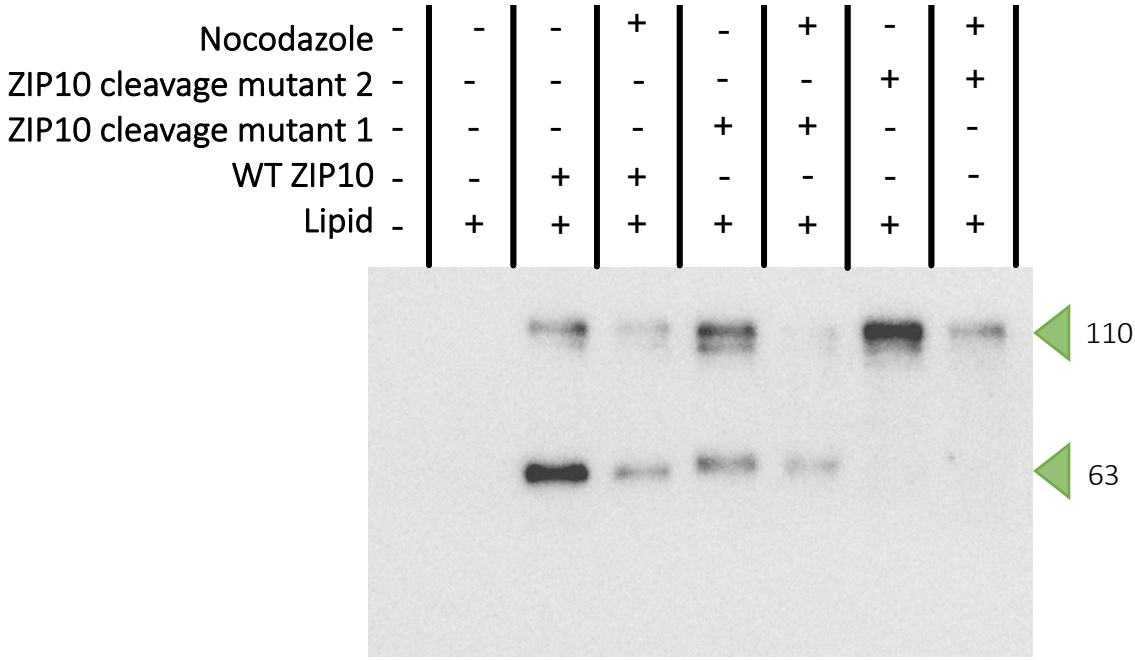

MCF7 cells were transfected with either WT ZIP10 or the ZIP10 cleavage mutants. Cells were lysed and analysed using SDS-PAGE and western blotting with an anti-V5 antibody (n = 1). Numbers represent the molecular mass of protein bands in kDa.

The profile of a protease responsible for cleaving ZIP10 in mitosis is likely to increase in the nocodazole-treated cells compared to the untreated cells. It may then decrease through metaphase and anaphase/telophase or remain activated through the later stages of mitosis if cleavage. The protease array for each of the 4 samples (untreated, nocodazole, nocodazole +1 and nocodazole +2) is shown in figure 3.16A. The signal from each protease is presented as a pair of dots and the proteases that gave a positive signal in each sample are indicated. The presence of ADAM9 (a disintigrin and metalloproteinase 9), MMP1, MMP7, presenilin and proprotein convertase appear increased in the nocodazole-treated cells compared with the untreated cells. In contrast, MMP8 is decreased in the nocodazole-treated cells compared with the untreated cells. CTS (cathepsin) A/B/C/V, MMP12 and MMP7 do not appear to change in the nocodazole-treated cells but decrease later in mitosis, and MMP1 and kallikrein 13 is increased only in the later stages of mitosis.

The relative intensities of the dots in each sample is shown in a heat map in figure 3.16B. Here, blue represents the lowest density of a protease across the four samples and red is the highest density. ADAM9 and presenilin are at their highest intensities in the later stages of mitosis, while MMP7 and proprotein convertase are increased in prophase, indicating their activation in the early stages of mitosis.

These data are reflected in the graph in figure 3.17, where the dots have been normalised to control dots on the membrane. Given the earlier data that suggested ZIP10 cleavage in mitosis, it is possible that either ADAM9, presenilin, MMP7 or proprotein convertase is the protease responsible. Interestingly, proprotein convertase is one of the proteases predicted to cleave ZIP10 in several places (residues 41–45, 84–88, 148–150, 306–312, 310–312, 516–520, 637–637 and 824–828). Together with the data from the protease array assay, this supports cleavage of ZIP10 by a proprotein convertase in mitosis.

3.4.9. Investigation into ZIP10 proteolysis in response to zinc starvation

The evidence presented in this chapter so far suggests that the full-size ZIP10 protein is present on the plasma membrane before mitosis starts. Zinc is required for cells to enter mitosis (Chesters, Petrie and Vint, 1989; Chesters and Petrie, 1999) and therefore it is hypothesized here that zinc entry into the cell via ZIP10 enables the cell to enter mitosis, and that ZIP10 ectodomain shedding is a “switch off” mechanism for ZIP10-mediated zinc entry.

Figure 3.15. Protease array assay coordinates

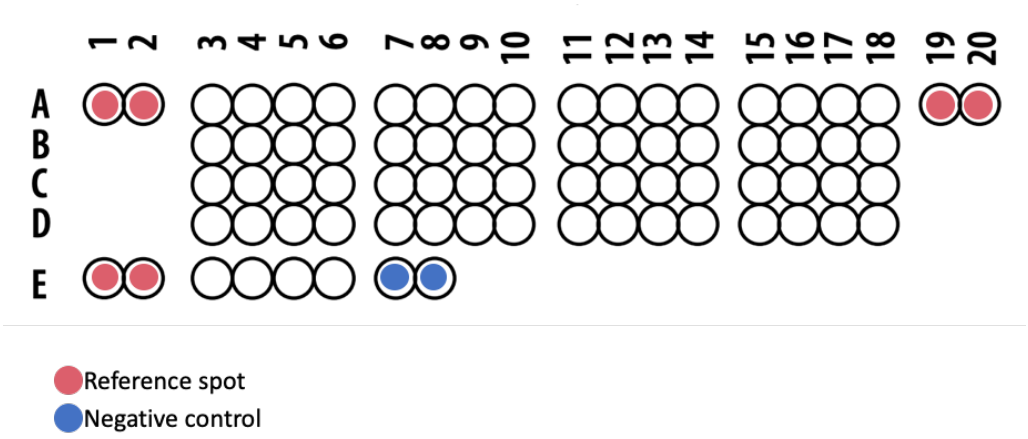

The coordinates show the layout of antibodies targeted at several proteases on a membrane used in the protease array assay. Reference spots were used as positive controls for quantifying proteases in test samples and negative controls were used to confirm there were no background signal from the antibodies.

Table 3.2. Location of specific protease antibodies on the protease array assay membrane

Coordinate	Analyte	Coordinate	Analyte
A3, A4	ADAM8	C5, C6	Kallikrein 7
A5, A6	ADAM9	C7, C8	Kallikrein 10
A7, A8	ADAMTS1	C9, C10	Kallikrein 11
A9, A10	ADAMTS13	C11, C12	Kallikrein 13
A11, A12	Cathepsin A	C13, C14	MMP 1
A13, A14	Cathepsin B	C15, C26	MMP 2
A15, A16	Cathepsin C	C17, C18	MMP 3
A17, A18	Cathepsin D	D3, D4	MMP 7
B3, B4	Cathepsin E	D5, D6	MMP 8
B5, B6	Cathepsin L	D7, D8	MMP 9
B7, B8	Cathepsin S	D9, D10	MMP 12
B9, B10	Cathepsin V	D11, D12	MMP 13
B11, B12	Cathepsin X/Z/P	D13, D14	Neprilysin/CD10
B13, B14	DPPIV/CD26	D15, D16	Presenilin 1
B15, B16	Kallikrein 3/PSA	D17, D18	Proprotein convertase 9
B17, B18	Kallikrein 5	E3, E4	Proteinase 3
C3, C4	Kallikrein 6	E5, E6	uPA/Urokinase

Coordinates refer to the spots on the membrane in figure 3.16.

Figure 3.16. Protease array assay in mitotic cells

A.

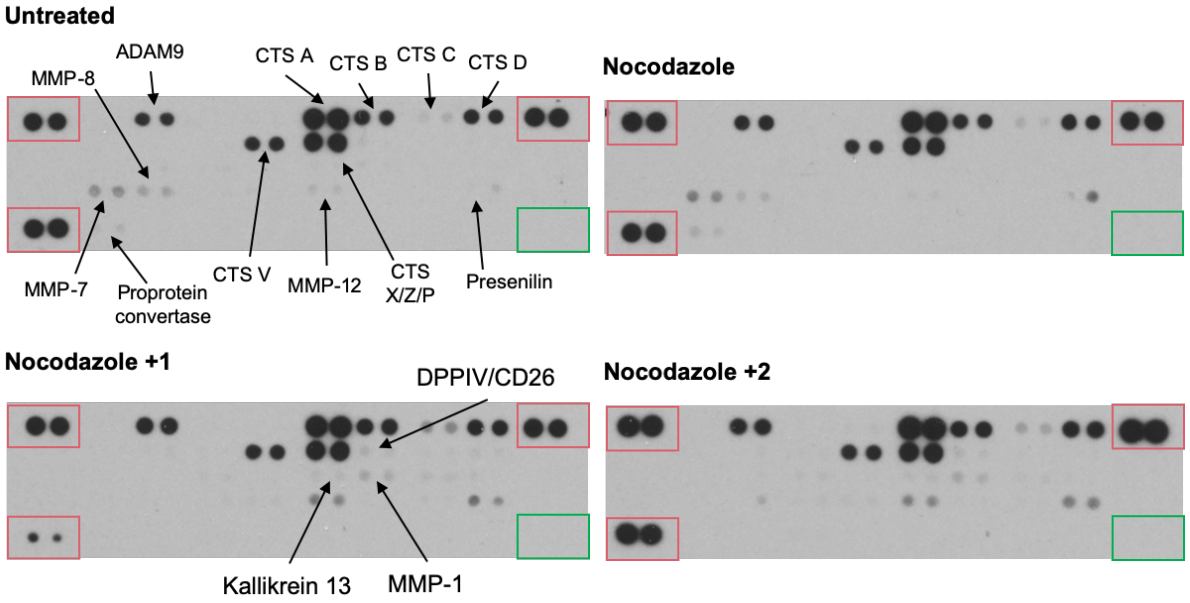

B.

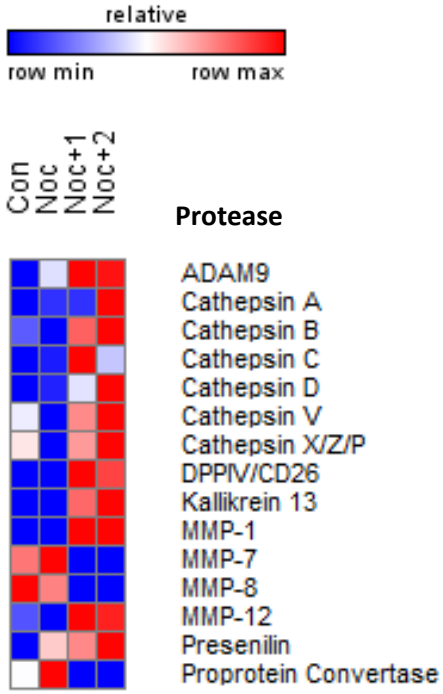

***A**. MCF7 cells treated with nocodazole with/without a 1 or 2 hour recovery period were lysed and analysed by protease array. The signal for each protease is presented as a pair of duplicate dots. For reference, there are positive control dots (pink boxes), and a negative control area of the membrane (green boxes). Arrows indicate those proteases which generated a signal with at least one treatment. **B**. Densitometry data from the protease array are presented as a spectrum of colour where blue represents the lowest value in the row and red the highest value in a row, irrespective of absolute signal intensities. The heat map was generated using GENE-E matrix visualisation and analysis platform (Broad Institute).*

Figure 3.17. Protease array assay densitometry data

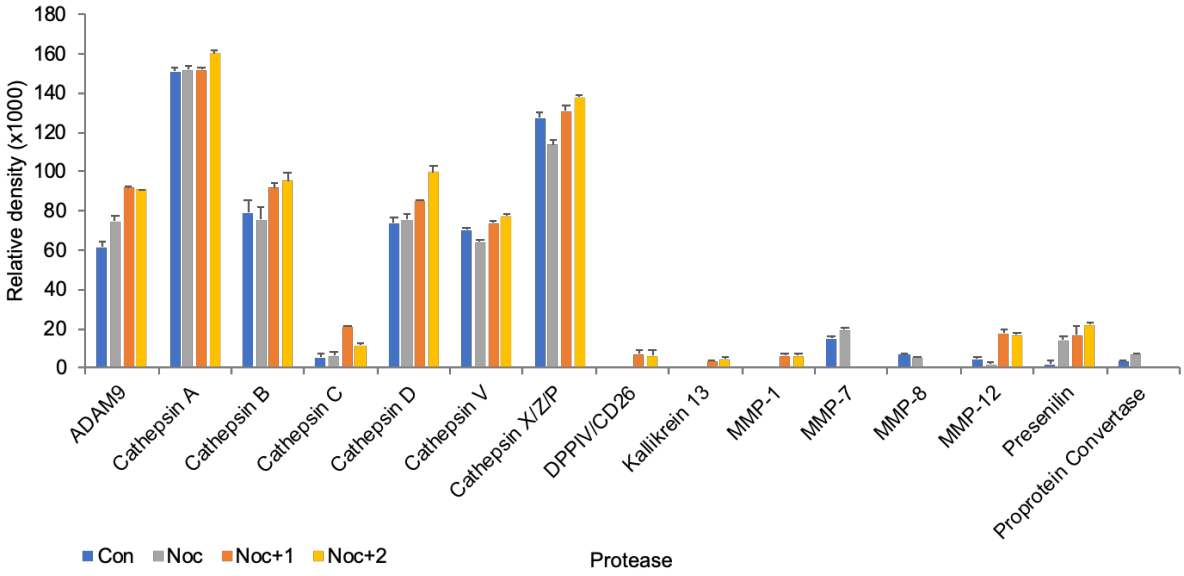

Densitometry data from the protease array in figure 4.17A are presented as mean of the duplicate dots ± standard error. No statistical analysis was performed owing to the sample size (n = 2).

To test the hypothesis that ZIP10 activity is regulated by the presence of zinc, MCF7 cells were deprived of non-protein bound zinc partially or completely, by serum starvation or TPEN treatment respectively. The cells were lysed and analysed by SDS-PAGE and western blot (figure 3.18A). In response to serum starvation, the amount of full-size ZIP10 increased (figure 3.18B) though this was not significant, and this could be due to the cells still being able to access intracellular zinc, as it had only been removed from the growth medium. In the presence of 5 μM TPEN the amount of full-size ZIP10 present increased significantly ($p < 0.01$) (figure 3.18B) suggesting that the full length of ZIP10 is increased at the plasma membrane to recover the lost zinc. TPEN is membrane permeable and chelates both extracellular and intracellular zinc, which explains the difference in ZIP10 increase following TPEN treatment compared with serum starvation.

To confirm the finding that ZIP10 was increased in low levels of zinc, MCF7 cells treated with TPEN were fixed and stained for using anti-ZIP10 and -F-actin antibodies. The staining demonstrated increased ZIP10 across the field of view in the TPEN-treated cells compared with the untreated population (figure 3.18C). These data support the hypothesis that the full length of ZIP10 is increased when cells are starved of zinc, and this could due to either decreased ectodomain shedding or increased ZIP10 production, or both.

An interesting finding from the protease array assay carried out earlier in this chapter was the potential cleavage of ZIP10 by presenilin or proprotein convertase. Presenilin is a component of the γ-secretase complex, which cleaves proteins in transmembrane domains (Lewis *et al.*, 2016). Proprotein convertase is a site-1 protease (S1P), cleavage by which is followed by a second cleavage by a site-2 protease (S2P), also in a transmembrane domain (Seidah *et al.*, 2013). Both proteases cleave proteins which have already undergone ectodomain shedding (Brown *et al.*, 2000; Beel and Sanders, 2008). Therefore, it was interesting to investigate whether ZIP10 may undergo TMD cleavage following ectodomain shedding.

MCF7 cells were treated with zinc because the assumption based on previous results in this chapter was that ZIP10 would undergo ectodomain shedding in the presence of zinc, and ectodomain shedding would need to have occurred before TMD cleavage. The cells were then treated with either a presenilin inhibitor, DAPT, or an S2P inhibitor, Nelfinavir. The cells were lysed and analysed by SDS-PAGE and western blot, using intracellular ZIP10 antibodies L4 and L5 (figure 3.19A).

Figure 3.18. ZIP10 protein expression in response to zinc starvation

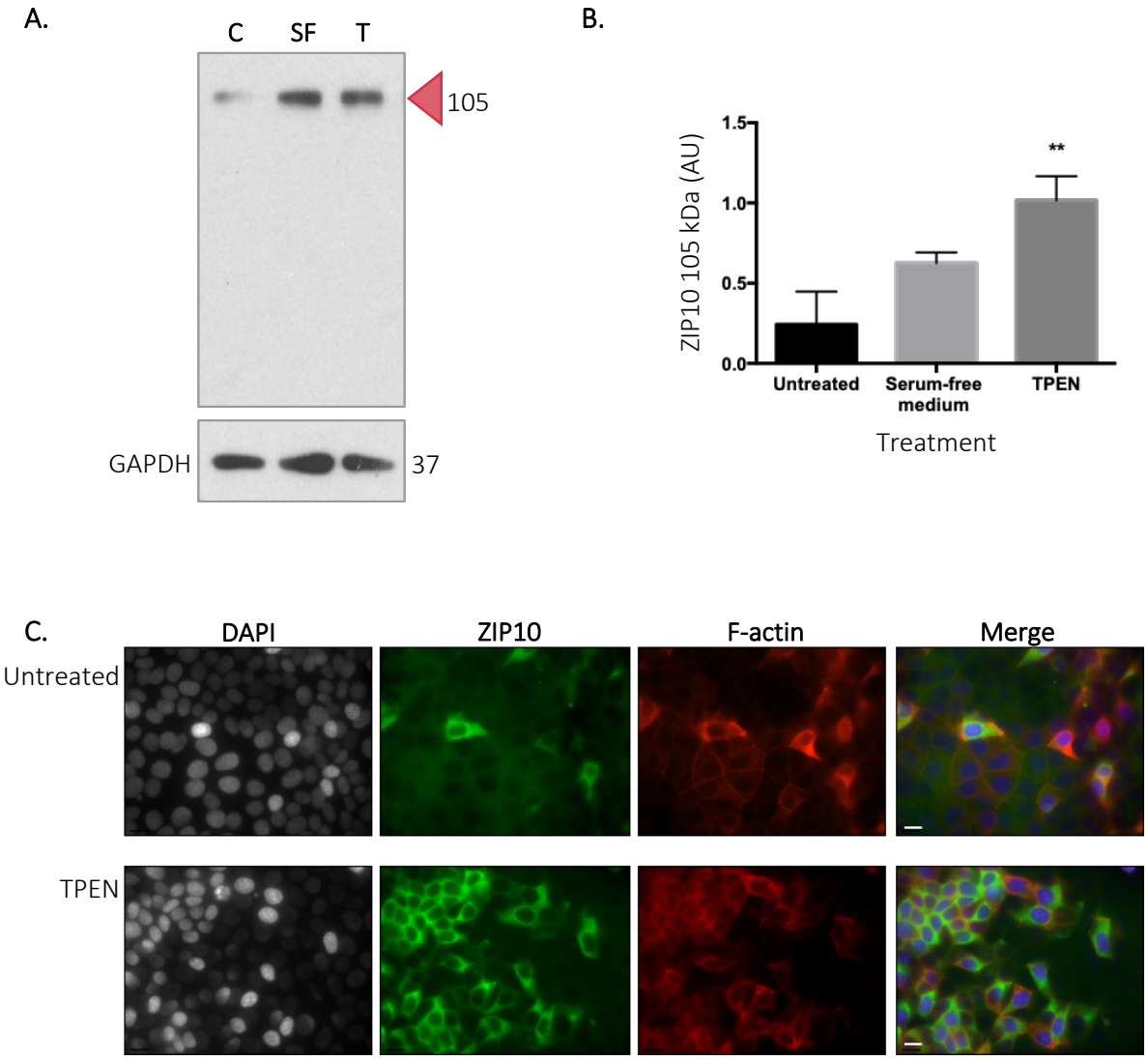

MCF7 cells were treated with serum-free (SF) medium or 5 μM TPEN (T) for 30 minutes. ***A****. The cells were lysed and analysed by SDS-PAGE and western blot, with an N-terminal anti-ZIP10 antibody (N1). Numbers represent the molecular mass of protein bands in kDa. C, control (untreated).* ***B****. Protein expression was normalised to GAPDH expression and presented as mean ± standard error (n = 3). Statistical significance was measured using ANoVA, compared to the untreated population. ** p < 0.01. AU, arbitrary unit.* ***C****. Cells treated with TPEN were fixed and stained using an anti-ZIP10 antibody (N2) (green) and F-actin (red). Alexa Fluor® fluorophore-conjugated secondary antibodies were used for detection of proteins. Cell nuclei were stained with DAPI (blue). Scale bars: 10 μm.*

Figure 3.19. Investigation of potential ZIP10 cleavage proteases

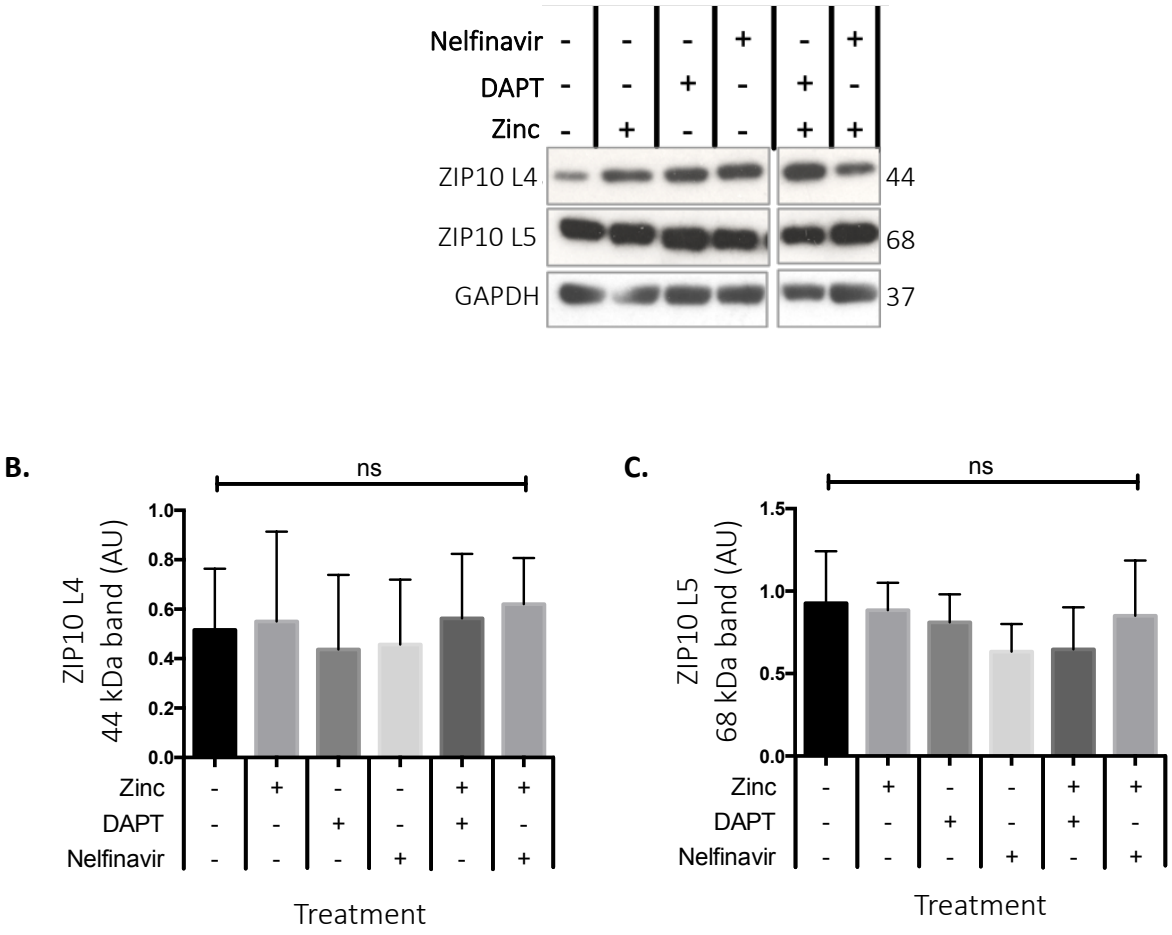

***A**. MCF7 cells were treated with protease inhibitors with/without zinc and the lysates analysed by western blot. All samples were run on the same gel at the same time but not in adjacent wells. Protein expression of the ZIP10 L4 band (**B**) and the ZIP10 L5 band (**C**) was normalised to GAPDH expression and presented as mean ± standard error (n = 3). Statistical significance was measured using ANoVA compared to the untreated population. ns, not significant; AU, arbitrary unit.*

The amount of the 44 kDa and 68 kDa ZIP10 bands detected with antibodies L4 and L5 respectively did not change in the presence of zinc with or without DAPT or Nelfinavir (figure 3.19B-C), suggesting that neither presenilin nor S2P cleave ZIP10, at least not under these conditions. It should not be ruled out, however, that a TMD cleavage of ZIP10 could occur following ectodomain shedding in mitosis, particularly owing to the fact that presenilin activity was increased in mitosis according to the protease array assay (figure 3.16).

3.4.10. ZIP10 interaction with other proteins in mitosis

So far, this chapter has focussed on processing of ZIP10 by glycosylation and proteolytic cleavage in mitosis. However, another factor which is important to consider in the regulation of ZIP10 is the binding of ZIP10 to other proteins. ZIP10 forms a heteromer with ZIP6 (Taylor *et al.*, 2016) and recent data from our group have determined that this heteromer also forms in mitosis (Nimmanon *et al*, 2020). ZIP6 binds pS^{727}STAT3 via a STAT3 binding site in the intracellular loop between TMD3 and TMD4 (Nimmanon *et al*., 2020). pS^{727}STAT3 is the dominant form of STAT3 in the cell in mitosis, and like ZIP6 and ZIP10, is increased in mitotic cells compared to non-mitotic cells (figure 3.20A). The human protein sequence of ZIP10 was analysed for the presence of a STAT3 binding site (*YXXQ*, where *X* means any amino acid) and it was discovered that ZIP10 contains a STAT3 binding site (521–524) in the same region as ZIP6, between TMD3 and TMD4 (figure 3.20B).

To investigate whether ZIP10 does bind pS^{727}STAT3 in mitosis, a proximity ligation assay was carried out on MCF7 cells treated with nocodazole using an anti-ZIP10 antibody (L4) and an anti-pS^{727}STAT3 antibody. Oligonucleotide-labelled secondary antibodies bind to the primary antibodies and are joined together by connecting oligonucleotides if the two proteins of interest are in close proximity. DNA ligase forms a closed circle of DNA and DNA polymerase amplifies the signal up to 1000-fold. If the two proteins of interest are in close proximity a red dot is seen when the cells are imaged by immunofluorescence (figure 3.21A). The dots are then quantified in mitotic cells and compared to non-mitotic cells.

Figure 3.20. STAT3 binding site on ZIP10

A.

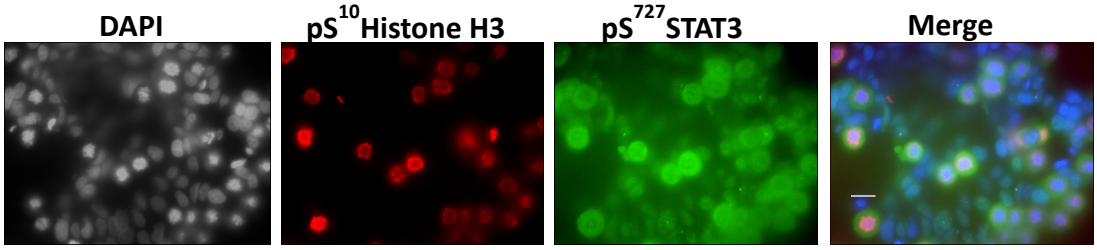

B.

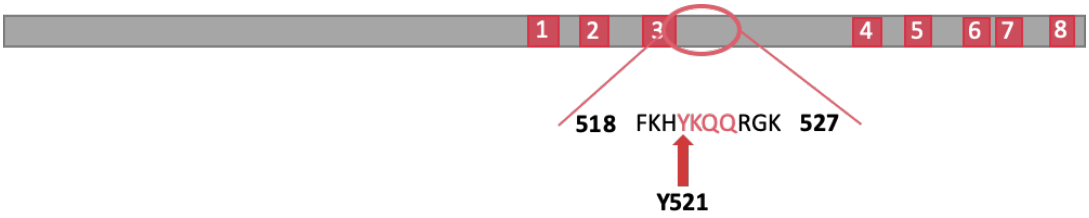

***A**. Immunofluorescent staining of MCF7 cells treated with nocodazole and stained for with anti-pS^{727}STAT3 and anti-pS^{10}HistoneH3 antibody. Nuclei are stained with DAPI (blue). Scale bar: 10 μm. **B**. STAT3 binding site in the intracellular loop between TMD3 and TMD4 of ZIP10.*

An average of 93 dots (s = 36 dots) was counted per mitotic cell compared with 18 dots (s = 12 dots) in non-mitotic cells ($p < 0.001$) (figure 3.21B), indicating that the two proteins are in close proximity during mitosis. Control experiments were carried out in which each antibody was used individually. The number of dots in mitotic and non-mitotic cells with only the ZIP10 antibody was 28 (s = 9 dots) and 10 respectively (s = 4 dots), and with the pS^{727}STAT3 antibody alone the number of dots was less than 3 in both mitotic and non-mitotic cells. These results suggest that pS^{727}STAT3 binds ZIP10 in mitosis, as well as ZIP6.

To investigate in further detail the binding together of ZIP10 and pS^{727}STAT3 in mitosis a mutant recombinant ZIP10 construct was made, in which Y521 was mutated to alanine. The mutant construct was named the ZIP10 STAT3 binding mutant (Y521A). MCF7 cells were transfected with WT ZIP10 or the mutant in the presence of nocodazole. The cells were lysed and the recombinant protein immunoprecipitated using an anti-V5 antibody. The immunoprecipitated proteins were analysed by SDS-PAGE and western blot with an anti-pS^{727}STAT3 antibody. Less pS^{727}STAT3 precipitated with WT ZIP10 in the presence of nocodazole compared with the untreated population (figure 3.21C) expressing WT ZIP10. This is contradictory to the proximity ligation assay, which showed increased ZIP10 binding to pS^{727}STAT3 in mitosis (figure 3.21A-B). There was no difference in the amount of pS^{727}STAT3 that precipitated with WT ZIP10 compared to the mutant, indicating that STAT3 may not bind ZIP10 via the STAT3 binding site, Y521, in the intracellular loop. However, the presence of pS^{727}STAT3 in the untransfected cells and those transfected only with the lipid vector indicates a problem with the negative controls; the anti-V5 antibody should not bind to anything in these samples and therefore no protein should be present. Therefore, the immunoprecipitation experiment cannot be fully relied upon and the binding of ZIP10 tyrosine residue 521 to pS^{727}STAT3 should not be ruled out.

To gain a deeper understanding of the signalling pathway in which ZIP10 may be involved in mitosis, a computer software search of proteins with which ZIP10 has been shown to interact was carried out. The identified proteins are listed in table 3.3 and are organised into their role in the cell in figure 3.22. Proteins were identified in a wide array of cellular processes including ciliogenesis, transcription, DNA repair, cytoskeleton regulation and protein-protein interactions, highlighting the wide-ranging cellular processes in which ZIP10 may be involved. In particular, 4 proteins were of interest due to their role in cell cycle regulation (highlighted in table 3.3); borealin (CDCA8), centromere protein O (CENPO), kinesin-like protein KIF18A (KIF18A), and condensin-2 complex subunit H2 (NCAPH). These

proteins are all involved in chromosome movement in mitosis, suggesting an intracellular role for ZIP10 (or a fragment of) in addition to zinc influx. It is possible that the N-terminal ectodomain has a role in chromosome movements if it is internalised following ectodomain shedding.

Figure 3.21. pS^{727}STAT3 and ZIP10 interaction in mitosis

A.

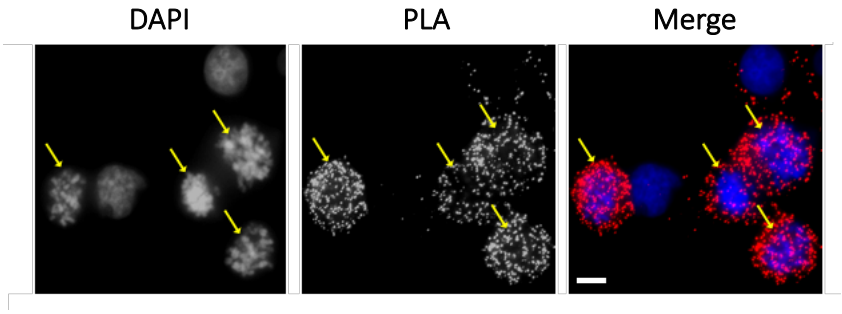

B.

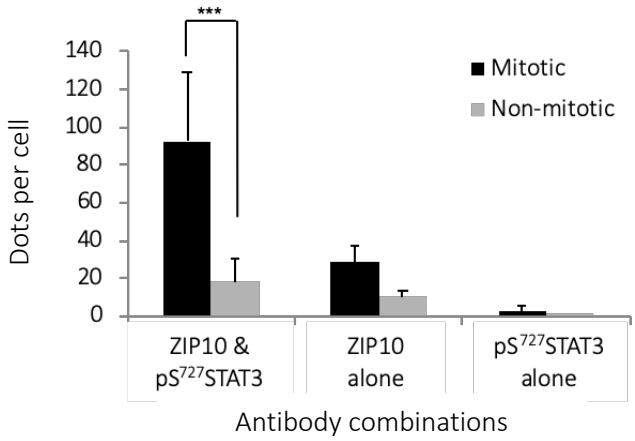

C.

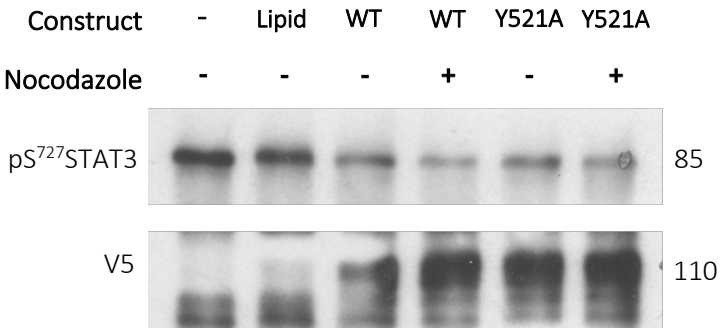

***A**. Proximity ligation assay (PLA) using anti-ZIP10 (L4) and anti-pS^{727}STAT3 antibodies in nocodazole-treated MCF7 cells. Yellow arrows indicate mitotic cells. Nuclei are stained with DAPI. Twenty-five images were taken at 3 μm apart and were merged for quantification of dots. Each cell population was imaged in three separate fields of view and a representative image is shown. Dots represent instances where the proteins of interest are within 40 nm of each other. Scale bar: 10 μm. **B**. The number of dots per cell was counted and averaged per mitotic/non-mitotic cell. The data are presented as mean ± standard error (n = 3). Statistical significance was measured using paired t-test compared to the non-mitotic population. **C**. Immunoprecipitation of MCF7 cell lysates, transfected with WT ZIP10 or the STAT3 binding mutant, with or without nocodazole. Recombinant ZIP10 was immunoprecipitated using an anti-V5 antibody and pS^{727}STAT3 was detected on the western blot (n = 1). An anti-V5 antibody was used to confirm successful immunoprecipitation of the recombinant protein. Numbers represent molecular mass of protein bands in kDa.*

Table 3.3. Experimentally confirmed protein interactions with ZIP10

Gene	Method	Description	Ref
AFF1	ACMS	Nuclear protein related to Fragile X E syndrome family of proteins.	1
BMPR1A	ACMS	Transmembrane serine/threonine kinase	1
BRCA1	ACMS	DNA repair protein	2
CCR6	ACMS	G-protein coupled receptor	3
CDCA8	ACMS	Component of the chromosomal passenger complex (CPC) in mitosis	1
CENPO	ACMS	Component of the CENPA-CAD complex, which is recruited to centromeres and is involved in assembly of kinetochore proteins, mitotic progression and chromosome segregation	1
CTDSPL	PLMS	Neuronal gene silencing in non-neuronal cells	4
CUL1	ACMS	Component of cullin-RING-based SCF ubiquitin-protein ligase complex	1
DCLRE1B	ACMS	DNA repair protein	1
EGLN3	ACMS	Catalyses hydroxylation of hypoxia-inducible factor-α	5
ELAVL1	ACRNA	RNA-binding protein, increases mRNA stability	6
GALNT6	ACMS	O-linked protein glycosylation in the Golgi apparatus	3
GTF3C2	ACMS	RNA polymerase III-mediated transcription	1
GYPB	ACMS	A minor sialoglycoprotein in erythrocyte membranes	3
HRAS	PLMS	GTPase in Ras/MAPK pathway	7
HTR2C	ACMS	G protein coupled receptor which responds to signalling by serotonin	3
K8.1	ACMS	Herpes virus glycoprotein	8
KIF18A	ACMS	Microtubule-depolymerising protein involved in suppressing chromosome movements in mitosis	1
KIF7	ACMS	Control of ciliary localisation	1
KRAS	PLMS	GTPase in Ras/MAPK pathway	7, 9
LPAR1	ACMS	Receptor for lysophosphatidic acid	3
LPCAT2	ACMS	Acetyltransferase	3
METTL9	ACMS	Methylation to mediate protein-protein interactions	3
MYC	ACMS	Transcription factor for growth-related genes	1
NCAPH	ACMS	Regulatory unit of condensin complex, a complex required for conversion of interphase chromatin into mitotic-like condensed chromosomes	1
NRAS	PLMS	GTPase in Ras/MAPK pathway	7, 9
NRN1L	ACMS	Secreted protein, enhances neuronal survival	3
PTPRG	PLMS	Tyrosine phosphatase	4

RNASEH2B	ACMS	Component of RNAse H2, involved in degradation of RNA: DNA hybrids	1
RNF4	ACMS	Ubiquitin E3 ligase	10
ROCK1	ACMS	Protein kinase, involved in regulation of actin cytoskeleton and cell polarity	1
SIGLECL1	ACMS	Adhesion molecule	3
SLC39A5	ACMS	Zinc transporter	3
SMAD3	ACMS	Signal transducer for receptors of TGF-β	1
SPINT2	ACMS	Tumour suppressor through inhibition of HGFA	3
TCF20	ACMS	Transcription factor for MMP-3	1
TCTN3	PLMS	Component of the tectonic-like complex, involved in ciliogenesis	11
TGOLN2	PLMS	Membrane-protein which may play a role in exocytic vesicle formation	12
TMEFF1	ACMS	Transmembrane protein, involved in neural patterning	3
TMEM17	PLMS	Component of the tectonic-like complex, involved in ciliogenesis	11
TMEM216	PLMS	Component of the tectonic-like complex, involved in ciliogenesis	11
TNKS	ACMS	ADP-ribosylltransferase in Wnt signalling pathway	1
TRIM25	ACMS	Ubiquitin E3 ligase	13
WBP1	ACMS	Mediates protein-protein interactions	3
XRCC1	ACMS	DNA repair protein	1

Proteins which have been confirmed experimentally to interact with ZIP10. Highlighted proteins are of particular interest owing to their known role in cell cycle regulation. ACMS, affinity-capture mass spectrometry; ADP, adenosine diphosphate; PLMS, proximity label mass spectrometry; ACRNA, affinity-capture RNA; Ref, references. (1) Hein et al., 2015; (2) Ertych et al., 2016; (3) Huttlin et al., 2017; (4) St-Denis et al., 2016; (5) Rodriguez et al., 2016; (6) Abdelmohsen et al., 2009; (7) Bigenzahn et al., 2018; (8) Kovalski et al., 2019; (9) Davis et al., 2015; (10) Kumar et al., 2017; (11) Gupta et al., 2015; (12) Liu et al., 2018; (13) Choudhury et al., 2017.

Figure 3.22. Predicted protein interactions with ZIP10

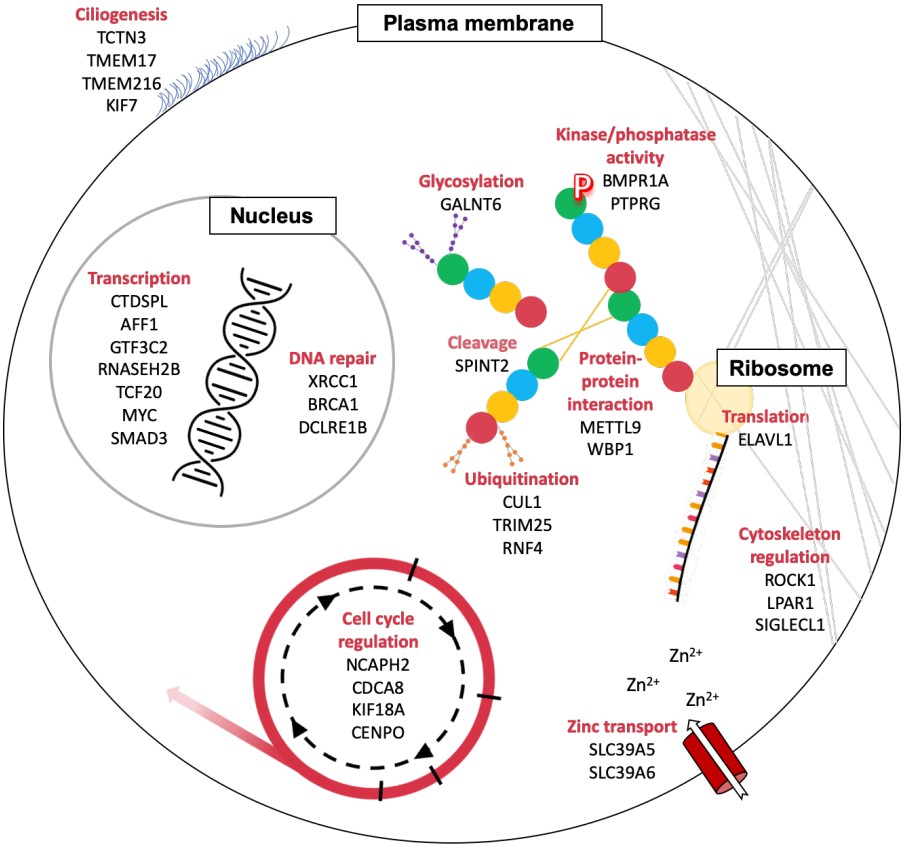

Gene names for human proteins with which ZIP10 has been shown experimentally to interact with, organised by cellular processes. Protein-protein interactions were determined through ELM and the Biological General Repository for Interaction Datasets (BIoGRID) (Oughtred et al., 2019).

3.5. Discussion

In this chapter, the regulation of ZIP10 by post-translational modification in mitosis has been explored. Western blot was used in the first instance to gain an understanding of ZIP10 cleavage, and both cleavage and glycosylation of ZIP10 were both found to contribute to the generation of several different band sizes. Glycosylation is a common post-translational modification of proteins, with not one specific role. The addition of glycan side-chains is used to monitor protein folding in the endoplasmic reticulum, they act as ligands for receptors and their size affects protein-protein interactions (Wormald *et al.*, 2002). This modification adds mass of approximately 2.5 kDa to proteins and therefore a common reason why protein band sizes may appear different on a western blot to the expected size of the protein alone. The data presented in this chapter indicated that up to 5 N-linked glycan chains may be present on the N-terminus of ZIP10, and this is supported by the work of Ehsani *et al*., (2012) which showed 3 N-linked glycosylation chains in the N-terminus of mouse ZIP10. Furthermore, these chains are added sequentially and ZIP10 can be cleaved prior to them all being filled, resulting in an immature ZIP10 fragment being shed (Ehsani *et al.*, 2012), which further complicates the analysis of ZIP10 fragment size.

Once ZIP10 cleavage and glycosylation had been confirmed, site-directed mutagenesis, protease array assays and proximity ligation assays were then used to ask more direct questions about ZIP10 modification and how this affects ZIP10 regulation in mitosis.

3.5.1. Ectodomain shedding of ZIP10

To investigate the site of ZIP10 ectodomain shedding in mitosis, two separate ZIP10 mutants were made, targeting two potential sites of cleavage. Residues 309–311 (RKR) were predicted to be a ZIP10 cleavage site, (table 3.1) which would correspond to the 63 kDa band seen with V5 staining on the western blot in figure 3.4B. The second site, residues 390–392 (KDK) was chosen because, although there was no predicted cleavage in this region, the C-terminal end of arginine (R) and lysine (K) residues are known to be the target of proteases such as trypsin (Olsen, Ong and Mann, 2004) and proprotein convertase enzymes, which cleave proteins according to the consensus sequence [R/K]-X_n-[R/K]↓ (where 'n' means any number and ↓ means the site of cleavage (Seidah and Chrétien, 1999). This sequence can be found in ZIP10 at residues K382-X_7-K390. Mutation of residues 390–392 abolished a smaller, recombinant C-terminal cleavage fragment of ZIP10 (detected with the anti-V5

antibody), suggesting the smaller 63 kDa band is the product of cleavage at residues 390–392. Residue 390 is a ubiquitin site according to PhosphoSitePlus® (Hornbeck *et al.*, 2004), which supports the hypothesis that ubiquitination of lysine 390 is the first step towards ZIP10 ectodomain shedding. This is further supported by the data from Ehsani *et al.* (2012) that shows mouse ZIP10 undergoes ectodomain shedding at approximately residue 400 (Ehsani *et al.*, 2012), which is equivalent to residue D398 in human ZIP10.

3.5.2. ADAM10 and presenilin

A particularly interesting finding regarding ZIP10 is its evolutionary link to the cellular prion protein (PrP^C) (Schmitt-Ulms *et al.*, 2009). PrP^C shares sequence similarity with the N-terminal sequence of ZIP10, ZIP6, and ZIP5 which are found on the same arm of the phylogenetic tree of the LIV-1 family of ZIP transporters (figure 1.3A). The role of PrP^C in a healthy individual is poorly understood, however a conformational change forms the disease-associated protein, PrP^{SC} which accumulates in the brain causing brain damage (Kovacs and Budka, 2008).

Proteolytic cleavage of the prion protein involves three separate cleavage events; alpha cleavage (Vincent *et al.*, 2001), beta cleavage (McMahon *et al.*, 2001) (mostly associated with the disease forming prion protein), and ectodomain shedding. The membrane-bound metalloprotease ADAM10 has been identified as the protease responsible for ectodomain shedding of the prion protein (Altmeppen *et al.*, 2012). In this chapter, ADAM9 was one of the proteases identified as being increased in MCF7 cells synchronised in mitosis (figure 3.16B) indicating a member of the ADAM family of metalloproteases could be responsible for the ectodomain shedding of ZIP10 as well. Increased expression of ADAM proteins is a hallmark of many cancers (Hartmann, Herrlich and Herrlich, 2013) further indicating its potential cleavage of ZIP10 at this stage.

Furthermore, the activity of both ADAM10 and ADAM9 is zinc-dependent (Kelwick *et al.*, 2015). The zinc transported into the cell by ZIP10 may be the trigger for ADAM9/10 activation to remove the ZIP10 N-terminus, as a “switch off” mechanism (figure 3.23). This is a simple but potentially very effective mechanism by which ZIP10 may interact with other proteins to regulate its own activity in a negative feedback loop. This hypothesis is supported by the data in this chapter that showed the full-length of ZIP10 is increased during zinc starvation. Many members of the LIV-1 family of ZIP transporters also possess histidine-rich

regions, which can bind zinc (reviewed by Taylor and Nicholson, 2003), further supporting the hypothesis that proteolytic cleavage of ZIP transporters could be dependent on the presence of zinc.

In addition to ectodomain shedding, the prion protein is known to undergo a novel gamma (γ) cleavage by the catalytic unit of the γ-secretase complex, presenilin (Lewis *et al.*, 2016). Abnormal presenilin function causes improper chromosome segregation providing evidence that this protease has an important role in the cell cycle, specifically mitosis (Boeras *et al.*, 2008). This is supported by the protease array data in this chapter that showed an increase in presenilin in mitosis and could link ZIP10 to an additional cleavage step by γ-secretase (figure 3.23).

Substrates for γ-secretase are generally derived from large precursor proteins that undergo prerequisite ectodomain shedding (Haapasalo and Kovacs, 2011). Shedding occurs in proximity to the plasma membrane and recognition by γ-secretase is generally enhanced if the residual ectodomain is shorter than 30 residues. If ZIP10 underwent cleavage at K390, the residual ectodomain would comprise 18 residues, so recognition by γ-secretase would be possible. Pre-shedding dimerisation has been reported by a number of γ-secretase substrates (Beel and Sanders, 2008). Dimerisation of ZIP transporters is not unknown and has been proven in ZIP4 (Zhang, Sui and Hu, 2016). Cleavage by γ-secretase tends to be at the C-terminal end of a transmembrane helix just inside the membrane-cytosolic interphase and mutations in valine (V) immediately adjacent to the cleavage site in ErbB4 (Vidal *et al.*, 2005) and Notch 1 receptor (Huppert *et al.*, 2000) abrogate this cleavage.

ZIP10 has similarly positioned valines at residues 425, 428 (TMD1), 720 (TMD5), 774 and 777 (TMD7). There are also valines at the C-terminal ends of TMD6 and TMD8, however these are positioned at the membrane-extracellular interface, so they do not fit the criteria for cleavage by γ-secretase. Further research into these residues would be useful to determine whether ZIP10 undergoes intramembrane cleavage by the γ-secretase complex.

3.5.3. Site-2 proteases and intramembrane cleavage

In addition to the potential cleavage of ZIP10 by ADAM9/10 and the γ-secretase complex, ZIP10 sequence analysis revealed several potential cleavage sites throughout the N-terminus, intracellular loop between TMD3 and TMD4, and the C-terminus. The prediction of proteases responsible for cleavage generated some interesting ideas. While caspases 3

and 7 have known roles in apoptosis (reviewed by McIlwain, Berger and Mak, 2013) and proprotein convertases 1 and 2 are only present in neuroendocrine cells (Muller and Lindberg, 1999), some of the predicted proteases could be linked to ZIP10 cleavage. N-arginine dibasic convertase is a metalloendopeptidase, containing the *HXXEH* zinc-binding motif, requiring zinc for function (Pierotti *et al.*, 1994), further suggesting that ZIP10 cleavage in the MCF7 breast cancer cells is zinc-dependent.

The database search also predicted cleavage of ZIP10 by proprotein convertase SKI1, which was also increased in mitotic cells in the protease array assay. Proprotein convertase SKI1 is a site 1 protease (S1P), substrates of which are known to undergo a second cleavage in a transmembrane domain by a site-2 protease (S2P), to release a cytosolic transcription factor that is then translocated to the nucleus (reviewed by Seidah *et al.*, 2013). Remarkably, it is common for ectodomain shedding to represent the rate-limiting step for further cleavage events in a transmembrane domain and this is known as regulated intermembrane proteolysis (Brown *et al.*, 2000). S2Ps are zinc-binding multi-transmembrane proteins containing conserved *HEXXH* motif, characteristic of zinc metalloproteases (Li *et al.*, 2013).

To conclude, the data presented here indicate that ZIP10 regulates its own activity via a zinc-dependent negative feedback loop. ZIP10 may undergo sequential processing, and in this case, the second cleavage could be in a transmembrane domain (figure 3.23). In addition, the presence of zinc binding motif *HEXXH* in both metalloproteases and ZIP transporters raises the question of whether ZIP transporters possess protease activity themselves, via their *HEXPHE* motif in TMD5 (see section 1.2). Whether or not the ZIP10 fragments have further roles in the cell or if they get degraded straight away remains to be determined.

Figure 3.23. Potential sequential processing of ZIP10

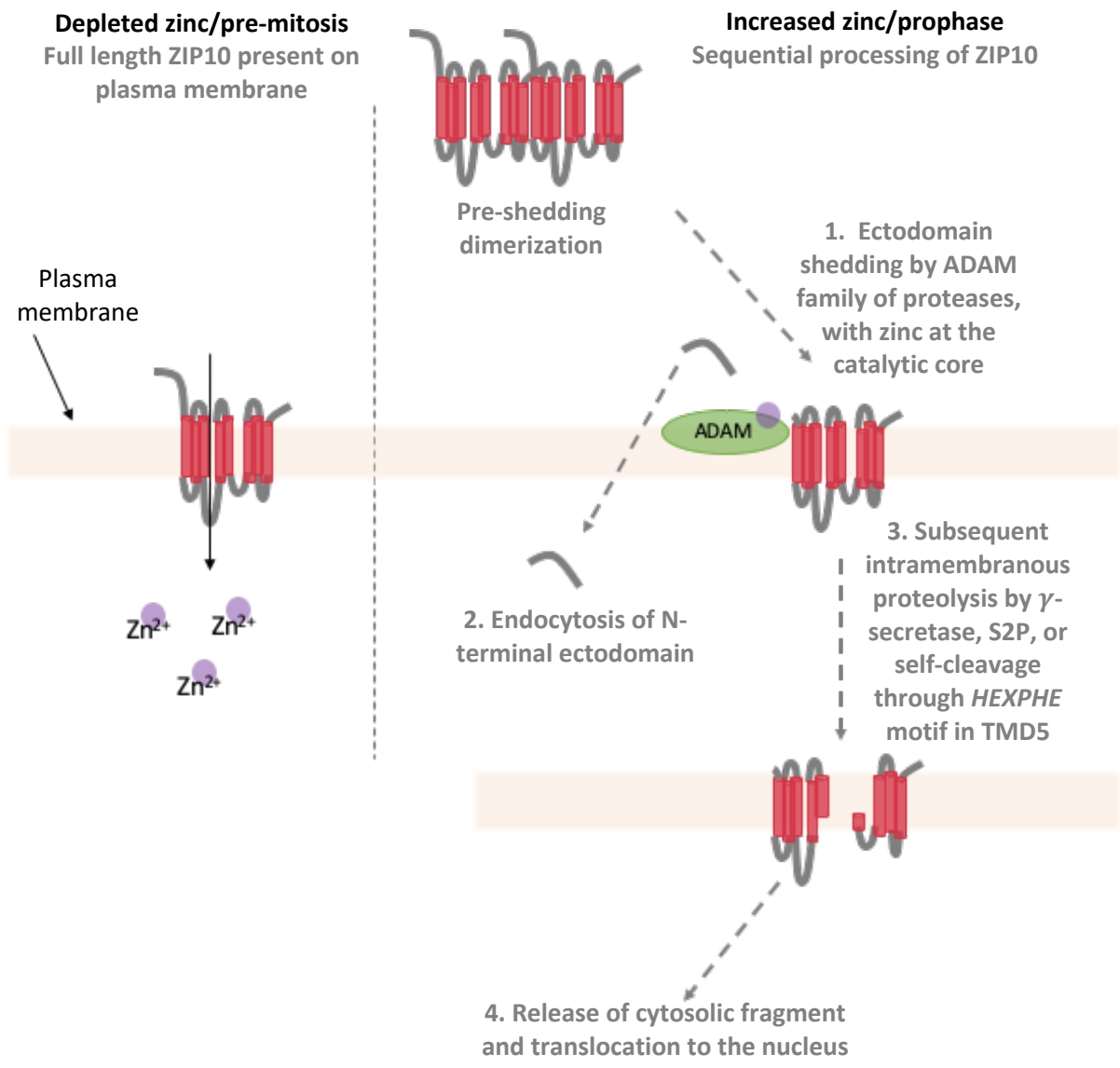

Proposed sequential processing of ZIP10 by proteolytic cleavage. ZIP10 undergoes ectodomain shedding by an ADAM metalloprotease in the presence of zinc. The remaining protein is a substrate for intramembrane cleavage by γ-secretase, a site-2 protease or ZIP10's own proteolytic activity via the HEXXH motif in TMD5.

3.5.4. ZIP10 cleavage products

The fact that the ZIP10 N-terminus was detectable by both western blot and immunofluorescence following ectodomain shedding suggests that it is not degraded outside the cell. Ectodomain shedding is not unique to ZIP10 within the LIV-1 family of ZIP transporters; ZIP4 is processed in the same way (Kambe and Andrews, 2009) and the N-terminus becomes a peripheral membrane protein following the catalytic cleavage, suggesting it may become internalised. This is indeed the case with the extracellular domain of Notch, which undergoes trans-endocytosis into the cell before endocytic degradation (Hansson *et al.*, 2010). It is possible therefore that the N-terminus of ZIP10 is also internalised.

The L5 anti-ZIP10 antibody showed punctate nuclear staining of non-mitotic cells by immunofluorescence (figure 3.9E), suggestive of nucleoli localization of a fragment of ZIP10 in interphase, following cleaving in mitosis. Fragments of ZIP transporters have never been shown to be transported to the nucleus, however it is not a new concept; the intracellular domain of Notch exerts functions in the nucleus following ectodomain cleavage and gamma secretase proteolysis (Hartmann, Herrlich and Herrlich, 2013), and the fibroblast growth factor receptor regulates tumour proliferation, invasion and progression through the cell cycle after translocation to the nucleus in pancreatic cells (Coleman *et al.*, 2014). However, the use of ZIP10 antibodies L4 and L5 is complicated by the location of their epitopes, which overlap the C-terminal end of TMD3. The full epitope therefore may be inaccessible and mean that the antibody cannot bind, and the staining seen with these antibodies is non-specific. In addition, the formation of the ZIP6/ZIP10 heteromer could mean that the long intracellular loop of each transporter is held in a structure which is also inaccessible for the antibodies to bind. Both antibodies can detect protein on a western blot because the protein has been denatured and therefore separated from the lipid bilayer and any other proteins in the complex.

3.5.5. ZIP10 responds to zinc in the environment

The analysis of ZIP10 cleavage has revealed the potential for ZIP10 to be regulated by the presence of zinc, in particular in mitosis. This is supported by the western blot data that showed an increase in the full-size ZIP10 protein in response to zinc starvation and implicates ZIP10 is an important protein in maintaining homeostatic zinc balance.

ZIP10 is also regulated at a transcriptional level in response to zinc availability in the cell. ZIP10 mRNA is increased in response to zinc starvation by TPEN treatment in both cardiomyocytes (Thokala *et al.*, 2019) and hepatocytes (Lichten *et al.*, 2011), and zinc re-supplementation in both cells reverses the effect. In hepatocytes, the increase in ZIP10 mRNA with zinc starvation was accompanied by an increase in the ZIP10 protein at the plasma membrane. *In vivo*, red blood cells of zinc-deficient mice have increased ZIP10 protein (Ryu *et al.*, 2008), and increased mRNA and protein in the brain and liver (Lichten, Liuzzi and Cousins, 2007; Lichten *et al.*, 2011) which is reversed by zinc repletion in the diet, suggesting that ZIP10 expression can also respond to zinc in the diet.

However, the ZIP10 protein has also been shown to undergo ectodomain shedding in response to zinc starvation in mouse neuroblastoma cells (Ehsani *et al.*, 2012). This contradicts the data presented here and implicates the differential processing and roles for ZIP10 across different tissues. In addition, ZIP10 mRNA and protein is increased in kidney epithelial cells in response to increased zinc (Kaler and Prasad, 2007). In fact, the promoter region of the ZIP10 gene (SLC39A10) contains a metal response element (MRE) (Wimmer *et al.*, 2005) that responds to metal transcription factor (MTF1). A further promoter region has since been identified, containing additional MRE clusters (Zheng *et al.*, 2008). The different MREs in the ZIP10 promoter regions can respond differently to MTF1 binding (figure 3.24). This explains ZIP10 downregulation in zebrafish gills and kidney in response to zinc excess and zinc deficiency respectively (Feeney *et al.*, 2005) and is further evidence of tissue specific responses to zinc availability via ZIP10.

MTF1 is activated by zinc binding (Radtke *et al.*, 1993) and subsequently binds the SLC39A10 promoter region (Wimmer et al. 2005; Lichten et al. 2011). Therefore, a negative feedback mechanism whereby zinc influx induces MTF1-mediated ZIP10 repression and inhibition of further zinc influx is suggested (figure 3.24). On the other hand, zinc-dependent binding to the second MRE in the ZIP10 gene causes ZIP10 upregulation and further zinc influx through a positive feedback loop (figure 3.24).

Figure 3.24. Differential transcription of ZIP10 following MTF1 activation

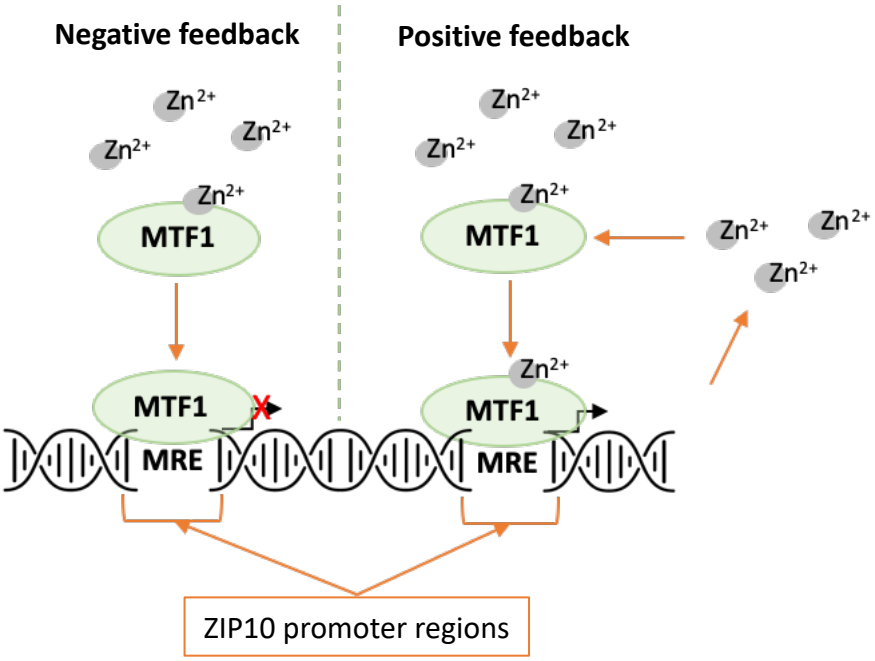

Metal transcription factor (MTF) responds to zinc in its environment and becomes activated to either repress (left) or activate (right) the transcription of the ZIP10 gene (SLC39A10). Transcription is dependent upon the metal response element (MRE) within the SLC39A10 promoter region to which MTF1 binds.

3.5.6. Interaction of ZIP10 with other proteins in mitosis

Proximity ligation assay data presented in this chapter demonstrated the close proximity of pS^{727}STAT3 and ZIP10 in mitosis. Although these data were contradicted by the immunoprecipitation experiment that was carried out, the negative controls in the latter experiment were not reliable owing to the presence of pS^{727}STAT3 and suggesting that the agarose beads used in the experiment may have bound non-specifically to proteins in the lysate, contaminating the sample. Therefore, the PLA experiment is more reliable in determining the binding together of ZIP10 and pS^{727}STAT3 in mitosis. PLA determines whether proteins are within 40 nm of each other (close proximity), but not necessarily bound together. Despite the STAT3 binding site in ZIP10, the two proteins may not be physically bound and the dots that were seen in the PLA could have been a result of both proteins being bound to ZIP6 (Nimmanon *et al.,* 2020). In this complex it is reasonable to predict that proteins are within 40 nm of each other (figure 3.25). Additional steps in the immunoprecipitation experiment such as blocking the beads before use may help to determine the physical interaction of ZIP10 and pS^{727}STAT3 in mitosis. An alternative option would be affinity chromatography in which a protein of interest i.e. ZIP10 is held in a matrix before a cell lysate is passed through and the retained proteins analysed.

Furthermore, the tyrosine residue of the STAT3 binding motif must be phosphorylated before recognition by STAT3 can occur (Shao *et al.*, 2004). ZIP10 Y521 has not been shown to be phosphorylated and is not predicted by any predictive software (see chapter 4) implicating it may not be a suitable STAT3 binding site. On the other hand, ZIP6 Y473 is phosphorylated (Wu *et al.*, 2010) which makes it a more appropriate site for STAT3 binding.

The first study to identify a non-transcriptional role for STAT3 also revealed its interaction with stathmin, a microtubule-destabilising protein with a known role in mitotic spindle assembly (Iancu *et al.*, 2001; Ng *et al.*, 2006). The interaction of pS^{38}stathmin with pS^{727}STAT3 was confirmed by proximity ligation assay (Nimmanon *et al*., 2020). Therefore, it is possible that ZIP6 and ZIP10 are part of a much larger mitotic complex at the start of mitosis.

In addition, ZIP10 has been shown to interact with several other mitotic proteins: borealin, kinesin-like protein KIF18A, CENPO, and NCAPH. According to table 3.3, each of these proteins have roles in either chromosome attachment to the spindles or chromosome

segregation both of which are expected to occur in metaphase and anaphase respectively, after ZIP10 ectodomain shedding in prophase. If the N-terminus is internalised after cleavage, it is possible that it plays a role in the formation of other mitotic structures before it is degraded.

It is important to note that the data in table 3.3 are from large scale interactome studies that often investigate lysates of entire cells and therefore do not take into consideration the different compartments that intracellular proteins would usually residue. Therefore, many of the proteins listed are likely to be false positives and experimental investigation of specific interactions based on these studies alone should be undertaken with caution. Furthermore, some of the interactions were determined using proximity label mass spectrometry which only identifies the close proximity of proteins instead of direct interactions; the close proximity of two proteins involved in separate signalling pathways could be completely coincidental.

Figure 3.25. Close proximity of pS^{727}STAT3 and ZIP10 in mitosis

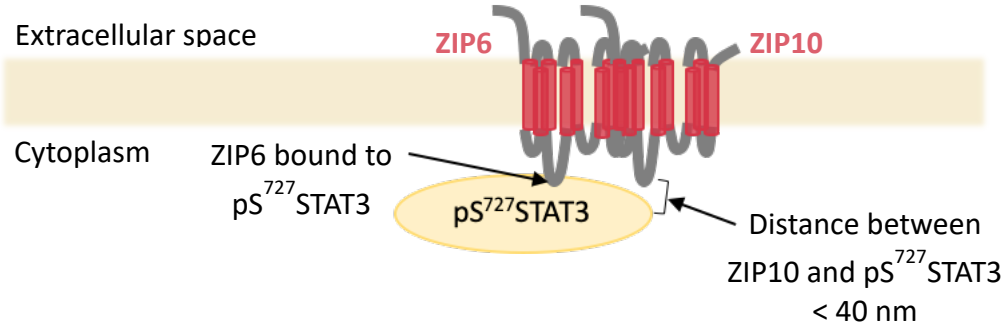

Binding of ZIP6 and pS^{727}STAT3 via the STAT3 binding site in the ZIP6 intracellular loop and binding of ZIP6 and ZIP10 in the heteromer leads to close proximity of ZIP10 and pS^{727}STAT3 during mitosis. Proximity ligation assay determines proteins within 40 nm of each other which is likely for ZIP10 and pS^{727}STAT3.

3.5.7. Chapter summary and conclusions

In this chapter, several molecular and cellular biology techniques have enabled the study of ZIP10 regulation in mitosis and for a number to conclusions to be made about the post-translational modification of ZIP10. Western blotting with anti-ZIP10 antibodies targeted to different epitopes detected many different fragments of ZIP10 and, together with the results from a database search of potential cleavage sites, the likely sites of ZIP10 cleavage were identified. Site-directed mutagenesis and expression of recombinant ZIP10 mutant constructs in breast cancer cells determined that K390-K392 is a likely site for ectodomain shedding. ZIP10 protein expression is increased in breast cancer cells during zinc starvation, presumably to maintain the homeostatic balance of intracellular zinc, and it is the full-length of ZIP10 present on the plasma membrane before mitosis begins. Biotin labelling of mitotic breast cancer cells revealed that ectodomain shedding of ZIP10 occurs in prophase, after mitosis has begun and this may be the first stage in sequential processing of ZIP10, though the proteases responsible for both cleavages remain unknown. Zinc dependent ADAM9 or ADAM10, proprotein convertase SKI and presenilin are all possible candidates. Furthermore, proximity ligation assay and immunoprecipitation data highlighted that, pS^{727}STAT3 associates with the ZIP6/ZIP10 heteromer in mitosis, though the binding is not to ZIP10 itself. pS^{727}STAT3 is bound to ZIP6. The N-terminal ectodomain of ZIP10 may be internalised and associated with additional mitotic proteins in metaphase and anaphase.

To build upon this understanding of ZIP10 regulation further, the next chapter will focus on ZIP10 regulation by phosphorylation; already known to be the activating modification in another ZIP transporter, ZIP7.

Chapter 4. Investigation of ZIP10 phosphorylation

4.1. Introduction

Phosphorylation is the most widely studied post-translational modification of proteins. The addition of a phosphate group to a specific amino acid changes the residue from hydrophobic to hydrophilic and a conformational change in the protein follows. The high reactivity of phosphate means that a phosphorylated protein can interact with many other proteins (Hunter, 2012), significantly increasing its signalling capacity. Over two thirds of proteins coded by the human genome undergo phosphorylation of at least one residue, though it is predicted that over 90% of proteins are phosphorylated (Ardito *et al.*, 2017). Phosphorylation is carried out by enzymes called kinases and can be quickly reversed by phosphatases (figure 1.1B). Many cancers have been attributed to the dysregulation of kinase signalling pathways (Hanahan and Weinberg, 2011), which highlights the importance of this modification in health and disease.

Phosphorylation of ZIP7 on two adjacent serine residues (S275 and S276) in the long cytoplasmic loop between TMD3 and TMD4 activates the transporter and causes the release of zinc from intracellular stores in the form of a 'zinc wave' (Taylor *et al.*, 2012). The released zinc drives cell growth and proliferation via widespread inhibition of tyrosine phosphatases, including those in the MAPK and mTOR signalling pathways (Nimmanon *et al.*, 2017). Phosphorylation of ZIP7 is carried out by protein kinase CK2 (Taylor *et al.*, 2012), a kinase associated with cell proliferation (Yde *et al.*, 2008; Zheng *et al.*, 2013), DNA repair (Loizou *et al.*, 2004), and cell death evasion (reviewed by Ahmad *et al.*, 2008), all of which are hallmarks of cancer.

ZIP7 activation by phosphorylation highlights not only the potential for other members of the LIV-1 family to be regulated by phosphorylation as well, but the potential mechanism for the link between ZIP transporters and cancer development. To understand whether phosphorylation is involved in the regulation of ZIP10, this chapter investigates specific residues predicted to be phosphorylated and the kinases with which ZIP10 may interact.

4.2. Aims and Objectives

The aim of this chapter is to investigate whether ZIP10 is regulated by phosphorylation in mitosis.

The specific objectives for this chapter are to:

a. To identify specific residues of phosphorylation in the ZIP10 protein

b. To determine how phosphorylation on these residues relates to the function of ZIP10 in cell division

c. To investigate which kinases may be responsible for the phosphorylation of ZIP10

d. To identify the signalling pathways in which ZIP10 may be involved based on the kinases with which it interacts.

4.3. Methods

4.3.1. Software analysis of the ZIP sequence for phospho-sites

To identify potential phosphorylation sites in ZIP10, the human protein sequence in FASTA format was analysed using a variety of software which predicts phosphorylation sites and responsible kinases. Software used included PhosphoSitePlus® (Hornbeck *et al.*, 2004), PhosphoNET, PHOSIDA (Gnad *et al.*, 2007), NetPhos (Blom et al., 2004), and NetPhorest (Miller et al., 2008). Residues of interest were chosen based on the number of references which confirm their phosphorylation by mass spectrometry experiments, and those which were located in the cytoplasmic loop between TMD3 and TMD4, owing to the known phosphorylation of ZIP7 in this region (Taylor *et al.*, 2012). Residues predicted to be phosphorylated specifically by cell cycle kinases were also chosen for further investigation.

4.3.2. Development and investigation of recombinant ZIP10 phospho-mutants

To investigate ZIP10 phosphorylation experimentally, phospho-ablative mutant ZIP10 constructs were made by site-directed mutagenesis, performed by Mutagenex Inc. Residues of interest (figure 4.1A) were mutated to alanine due to its lack of hydroxy group (-OH) which is needed for the addition of a phosphate group during phosphorylation. The WT human ZIP10 sequence in a pcDNA3.1/V5-His TOPO vector was used as a template for mutagenesis (figure 2.2). Primers were designed with the desired codon for the mutant residue (figure 4.1B) and DNA sequencing confirmed successful mutagenesis (figure 4.1C).

The WT and mutant ZIP10 constructs were transfected into MCF7 breast cancer cells in the presence of nocodazole to synchronise cells in mitosis. The level of phospho-serine in the cells expressing recombinant ZIP10 was assessed using SDS-PAGE and western blot.

Functional analysis of the ZIP10 constructs was carried out using fluorescence-activated cell sorting (FACS). Intracellular free zinc content of cells was assessed using the zinc-specific fluorescent dye, FluoZin™-3, and differences between cells expressing WT ZIP10 or mutant constructs was compared. Cells were also assessed for their ability to enter mitosis using an anti-pS^{727}STAT3 primary antibody and a secondary antibody conjugated to a fluorophore.

4.3.3. Investigation of ZIP10 interaction with cell cycle-specific kinases

The interaction of ZIP10 with specific kinases predicted to phosphorylate ZIP10 was assessed by proximity ligation assay (PLA) using intracellular ZIP10 (L4 and L5), total CDK1 (cyclin dependent kinase 1), total PLK1 (polo-like kinase 1), pY^{15}CDK1 and pT^{210}PLK1 antibodies. The L4 and L5 ZIP10 antibodies were used in these experiments because their epitopes are on a region of ZIP10 that is located inside the cell, and the proteins that were under investigation for ZIP10 interaction (CDK1 and PLK1) are also located inside the cell. The ligation reaction that occurs during the experiment (figure 2.3) is only possible if the antibodies bind to epitopes in the same cellular compartment. The Duolink® In Situ Detection Kit – Orange was used to detect the proximity of the proteins and was imaged using a Leica DMIRE2 epi-fluorescent microscope. The dots were quantified using ImageJ software.

MCF7 cells were transfected with WT and mutant ZIP10 and the recombinant protein was separated from the whole cell lysates by immunoprecipitation with an anti-V5 antibody. The protein was analysed for association with kinases by SDS-PAGE and western blot, using antibodies targeted to total PIM1, total PIM3, and total PKA.

Figure 4.1. Phospho-null ZIP10 mutants made for the study of ZIP10 phosphorylation

A.

Construct	WT DNA sequence	Mutant DNA sequence
S539A	GAATCAACT	GAAgCAACT
T540A	TCAACTATT	TCAgCgATT
S546A	CTTTCAGAT	CTTgCAGAT
S570A	GACTCGGTT	GACgCGGTT
S591A	GAATCCCCT	GAAgCCCCT
Y596A	AATTACCTT	AATgcCCTT

B.

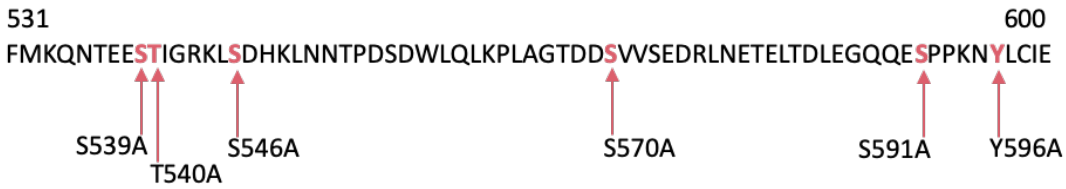

C.

***A**. A 70 amino acid stretch of the human ZIP10 protein sequence in the intracellular loop between TMD3 and TMD4, in which all the phosphorylated residues of interest lie. **B**. The human DNA sequences of the ZIP10 mutant constructs that were made by site-directed mutagenesis. Mutated codons are underlined and individual nucleotides that were altered are lower-case. **C**. Successful site-directed mutagenesis was confirmed by DNA sequencing, and the corresponding chromatograms are presented. S, serine; T, threonine; Y, tyrosine; A, alanine.*

4.4. Results

4.4.1. Prediction of potential ZIP10 phosphorylation sites

The PhosphoSitePlus® (Hornbeck *et al.*, 2004) software was used to determine specific residues of ZIP10 which are phosphorylated. The software collates data from published studies in which mass spectrometry has been used to identify phosphorylated residues. The search returned 15 phosphorylation sites in ZIP10; listed in table 4.1. The residues are located in either the N-terminal ectodomain (4) or the long intracellular loop between TMD3 and TMD4 (11), implicating these domains as functionally significant in the regulation of ZIP10. This reflects what was seen in the previous chapter, with the potential cleavage of ZIP10 in these domains.

In addition to identifying ZIP10 phosphorylation sites, many databases were used to identify potential kinases which may phosphorylate these residues. The databases predict potential kinases based on consensus binding sequences in the protein of interest. The kinases predicted to phosphorylate ZIP10 are listed in table 4.1 and further information about their roles in the cell is found in table 4.2.

Four of the predicted phosphorylation sites are located in the N-terminus of ZIP10, which is extracellular. Although extracellular phosphorylation can occur in proteins, given the low number of records citing these as phosphorylated residues by comparison to the intracellular residues, it is likely these modifications are either transient or are of less functional significance. Furthermore, the N-terminus undergoes cleavage in the early stages of mitosis so any phosphorylation side chains would be removed; it is likely therefore that ZIP10 N-terminal phosphorylation is not relevant in mitosis. On the other hand, it is possible that, if the N-terminus is internalised following ectodomain shedding (as was alluded to in the previous chapter), phosphorylation then occurs on the intracellular fragment which could then contribute to further signalling pathways which have not been explored here.

The remaining phosphorylation sites were located in the intracellular loop between TMD3 and TMD4, agreeing with ZIP7 phosphorylation and supporting data presented in the previous chapter that this region is an important ‘hub’ of ZIP transporter regulation.

Over 90% of the phosphorylated residues in ZIP10 are either serine or threonine. This is unsurprising as it is predicted that serine/threonine phosphorylation accounts for over 90%

of protein phosphorylation in a cell (Olsen *et al.*, 2006). Serine 591 (S591) is the residue with the highest number of records citing its phosphorylation (18 records) implicating that this residue is an important modification in the regulation of ZIP10. Three different databases predicted this residue to be phosphorylated by CDK1, a kinase with well-established roles in progression of the cell cycle from G2 to M (table 4.2). Furthermore, one reference which identified phosphorylation on this residue specifically mapped mitotic phosphorylation (Kettenbach *et al.*, 2011) which leads to an exciting hypothesis of ZIP10 phosphorylation by CDK1 on serine 591 in mitosis. This could be a key modification to activate ZIP10-mediated zinc influx in mitosis.

Another interesting observation was the phosphorylation of serine 539 (S539) and threonine 540 (T540) in the TMD3–4 intracellular loop. These residues are adjacent to each other and both predicted to be phosphorylated by PLK1. In particular, S539 was identified as phosphorylated by PLK1 through the use of a small molecule inhibitor of PLK1 prior to mass spectrometry (Kettenbach *et al.*, 2011). PLK1 has several known roles in mitosis (table 4.2) which implicates these residues as additional potentially important sites for ZIP10 modification in mitosis. Interestingly, serine 570 (S570) was also predicted to be phosphorylated by PLK1, further implicating this mitotic kinase as an important regulator of ZIP10 activity in mitosis.

Phosphorylation on adjacent residues echoes the phosphorylation of ZIP7 on S275 and S276 also in the intracellular loop between TMD3 and TMD4 (table 4.3). It is interesting that S275 and S276 in ZIP7 are also phosphorylated by the same kinase, but in this case CK2. Further investigation of the remaining members of the LIV-1 family of ZIP transporters (table 4.3) identified an additional double phosphorylation site in ZIP7 (S293 and T294) and one in ZIP6 also (S478 and T479). In ZIP6, both residues are predicted to be phosphorylated by the same kinase, CK2. The double phosphorylation of adjacent residues in the intracellular loop between TMD3 and TMD4 is a potentially important modification in the regulation of ZIP transporters.

Table 4.1. ZIP10 phosphorylation sites and predicted kinases

	Residue	Sequence	No. of records citing MS data	Predicted kinase			
				PhosphoNET	PHOSIDA	NetPhos	NetPhorest
N-terminus	T44	RGMTELE	1	MAPK/PKG/PIM1		(CDK1)	CK2
	S49	LEPSKFS	1	JNK1/JNK3		(CDK1)	GRK
	S52	SKFSKQA	1	MLKL/CK1		PKC	
	S323	AIISLRK	1	PIM1/PKC		PKC	PKC
TMD3–4 intracellular loop	T536	KQNTEES	5	ATR		(CaM-II)	ACTR
	S539	TEESTIG	7	PLK1-3/βARK1/PIM1		(GSK3)/(CDK1)	
	T540	EESTIGK	3	PLK1-3/LRRK2		(GSK3)	
	S546	RKLSDHK	6	PIM3/PIM1/PIM2	PKA	PKA/RSK/PKG	PKA
	T553	LNNTPDS	6	JNK1/JNK3/JNK2	NEK6	(p38MAPK)	P38/JNK
	S556	TPDSDWL	2	IKKb/CK2a1		(CK2)	CK2
	S570	TDDSVVS	2	PIM2/PIM1	PLK1	(CDK1)	
	S573	SVVSEDR	2	CK2a2/PIM2/PIM1	CK1	CK2/CK1	CK2
	T583	TELTDLE	1	CK2a2/CK2a1	CK2	CK2/CDK1	CK2
	S591	QQESPPK	18	CDK1/CDK2	CDK1/CDK2	(CDK5)	CDK1
	Y596	PKNYLCI	10	Syk		(INSR)	Src

ZIP10 phospho-sites were predicted using PhosphoSitePlus® (Hornbeck et al., 2004). Kinases were predicted using PhosphoNET, PHOSIDA (Gnad et al., 2007), NetPhos (Blom et al., 2004), and NetPhorest (Miller et al., 2008). Analysis was completed using the human ZIP10 protein sequence in FASTA format. Highlighted in red are residues that were chosen for further experimental research, for reasons described in the text. MS, mass spectrometry; S, serine; T, threonine. Y, tyrosine. Blank spaces indicate no kinase prediction. Kinases in brackets did not meet the threshold score in NetPhos of 0.5.

Table 4.2. Role of kinases predicted to phosphorylate ZIP10

Kinase	Site	Description	Reference
βARK1	S539	Major regulator of GPCR signalling pathways	Penela *et al.*, 2019
CaM-II	T540	Memory formation	Bayer and Schulman, 2019
CDK family	S539 S591	G2/M transition (CDK1) G1/S transition (CDK2) Increases expression of cyclins and other CDKs (CDK5)	Fung and Poon, 2005 Malumbres and Barbacid, 2009 Shupp, Casimiro and Pestell, 2017
GSK3	S539	Diverse roles in intracellular signalling pathways. Linked to Bipolar disorder and Alzheimer's disease	Grimes and Jope, 2001
INSR	Y596	Regulation of glucose homeostasis	Hubbard, 2013
LRRK2	T540	Modulates neuronal plasticity. Linked to Parkinson's disease	Zach, Felk and Gillardon, 2010
PIM family	S539 S546 S570	Phosphorylation of CdC25C at G2-M transition Regulation of PLK1 phosphorylation during mitosis	Bachmann *et al.*, 2006 Adam *et al.*, 2018
PKA	S546	cAMP-dependent kinase associated with lipid metabolism and cardiac function	Manni *et al.*, 2008
PKG	S546	cGMP-dependent kinase associated with smooth muscle relaxation	Francis *et al.*, 2010
PLK family	S539 T540 S570	Entry into mitosis, anaphase, spindle assembly and cytokinesis (PLK1) Centriole duplication (PLK2) DNA replication (PLK3)	Lee, Jang and Lee, 2014
RSK	S546	MAPK-activated family of protein kinases with roles in cell proliferation and survival	Roux and Blenis, 2004
Src	Y596	Promotion of cell survival, angiogenesis and cell invasion pathways	Frame and Roskoski, 2017
Syk	Y596	B- and T-cell receptor signalling	Mócsai, Ruland and Tybulewicz, 2010

Kinases predicted to be involved in ZIP10 phosphorylation of residues of interest (highlighted in red in table 4.1). Kinases were predicted using PhosphoNET, PHOSIDA (Gnad et al., 2007), NetPhos (Blom et al., 2004), and NetPhorest (Miller et al., 2008).

Table 4.3. Adjacent phosphorylation sites in members of LIV-1 family of ZIP transporters

ZIP	Residue	Sequence	No. of records citing MS data	Predicted kinase
6	S478 T479	SQLSTNE QLSTNEE	26 5	CK2 CK2/PKC
7	S275 S276	EKQSSEE KQSSEEE	24 24	CK2/ CK2/CK1
	S293 T294	RGGSTVP GGSTVPK	2 1	PKA/PKG PKC
10	S539 T540	TEESTIG EESTIGK	7 3	PLK1-3/βARK1/PIM1 PLK1-3/LRRK2

Adjacent phospho-sites in the LIV-1 family of ZIP transporters were predicted using PhosphoSitePlus® (Hornbeck et al., 2004). All residues are in the intracellular loop between TMD3 and TMD4. Kinases were predicted using PhosphoNET and NetPhos (Blom et al., 2004). Analysis was completed using the human ZIP protein sequences in FASTA format. MS, mass spectrometry; S, serine; T, threonine.

Table 4.4. Tyrosine phosphorylation sites in members of the LIV-1 family of ZIP transporters

ZIP	Region	Residue	Sequence	No. of records citing MS data
4	TMD1–2 ICL	Y359	VTHYILQ	1
6	N-terminus	Y192	STVYNTV	1
	TMD3–4 ICL	Y473	LSKYESQ	1
		Y493	TEGYLRA	11
		Y528	QEVYNEY	126
		Y531	YNEYVPR	65
10	TMD3–4 ICL	Y596	PKNYLCI	10
12	N-terminus	Y140	NKEYKFY	2
14	TMD3–4 ICL	Y258	HSHYASE	1

Tyrosine phospho-sites in the LIV-1 family of ZIP transporters were predicted using PhosphoSitePlus® (Hornbeck et al., 2004). ICL, intracellular loop; MS, mass spectrometry; Y, tyrosine.

Serine 546 (S546) was identified by 6 studies as a phosphorylated residue, one of which looked specifically at cells synchronised in mitosis (Olsen *et al.*, 2010), implicating another potentially important residue in mitosis. However, another database, PHOSIDA, predicted the phosphorylation of S546 specifically during both M and G1. These are the first data to indicate a role for ZIP10 at a different time point in the cell cycle.

Excitingly, a tyrosine (Y) residue in ZIP10 was predicted to be phosphorylated (Y596). Regulation of ZIP transporters by tyrosine phosphorylation has never been studied, although other members of the LIV-1 family of ZIP transporters do also have predicted tyrosine phosphorylation sites (table 4.4). However, given the known role of zinc in the inhibition of protein tyrosine phosphatases, it is an interesting idea that zinc release from intracellular stores could cause zinc influx from extracellular space through the prolonged activation of ZIP transporters on the plasma membrane. This is discussed in further detail later in this chapter.

Having completed a database search of the phosphorylation status of ZIP10, the residues highlighted in red in table 4.1 were chosen to be investigated further experimentally due to the reasons explained here in the text.

4.4.2. Serine 591 phosphorylation of ZIP10

Serine 591 phosphorylation of ZIP10 was investigated in this project due to the high number of papers citing its phosphorylation (18) and the known role of the kinase predicted to be responsible (CDK1), in mitosis. These predictions led to the hypothesis that phosphorylation of this residue activates ZIP10 in mitosis.

To investigate the phosphorylation of S591 experimentally, a phospho-ablative ZIP10 mutant construct was made using site-directed mutagenesis. The residue was mutated to alanine (S591A) and successful mutagenesis was confirmed by DNA sequencing (figure 4.1C). The WT ZIP10 and S591A constructs were transfected into MCF7 cells in the presence of nocodazole and the cells were lysed and analysed for phospho-serine by western blot (figure 4.2A). The anti-phospho-serine antibody detected several bands, due to the abundance of serine-phosphorylated proteins in cells. The band highlighted by the pink box has a molecular mass similar to that of the V5 band (110 kDa) and could represent serine phosphorylated recombinant ZIP10 protein.

Figure 4.2. Analysis of phospho-serine in cells expressing the S591A ZIP10 mutant

A.

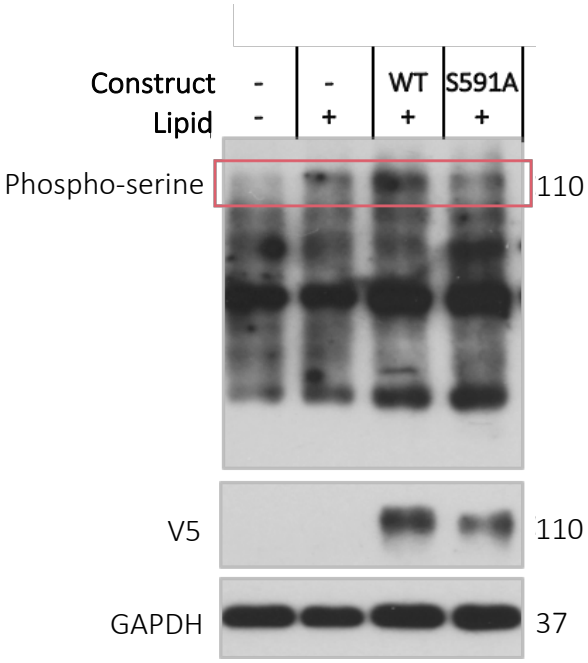

B.

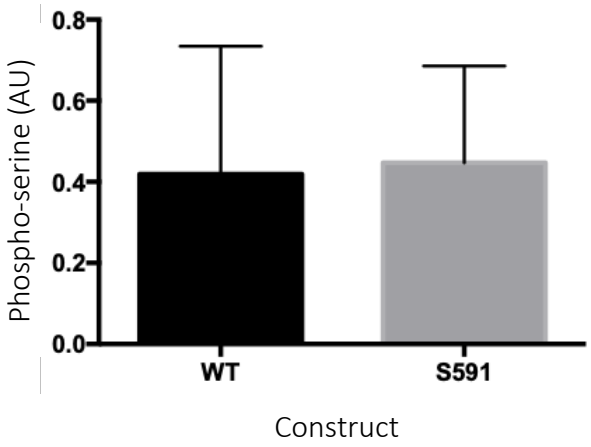

***A**. Western blot analysis of phospho-serine in MCF7 cells transfected with either WT ZIP10 or the S591A mutant construct in the presence of nocodazole. Numbers represent the molecular mass of protein bands in kilodaltons (kDa). **B**. Protein expression of phospho-serine was normalised to V5 and is presented in a bar graph as mean ± standard error (n = 3). Statistical significance was measured using a paired t-test, but no significance was found. AU, arbitrary unit.*

The amount of phospho-serine appears to be decreased in the cells expressing the S591A mutant compared with those cells expressing WT ZIP10, however upon normalisation to the V5 band, the amount of phospho-serine is not significantly different in the two populations (figure 4.2B). Furthermore, the phospho-serine band is present in the cells transfected with the lipid only indicating there may be other, endogenous proteins of 110 kDa which are also serine-phosphorylated, and these may interfere with the western blot analysis of the recombinant protein.

4.4.3. Effect of ZIP10 S591 phosphorylation on zinc influx

A more thorough experimental investigation into the S591 phosphorylation of ZIP10 was carried out using fluorescence-activated cell sorting (FACS). This flow cytometry technique separates individual cells based on their fluorescence characteristics and can therefore analyse only the populations of cells which express a particular protein.

Here, MCF7 cells were transfected with either WT ZIP10 or the S591A mutant, in the presence of nocodazole. An AlexaFluor® 647 conjugated anti-V5 antibody was used to detect the cells expressing the recombinant protein. Cells transfected with the lipid only were used as a negative control to determine the background signal from the antibody. The histogram in figure 4.3A shows the fluorescence intensity of V5 in the cells transfected only with the lipid, and the P1 population is V5-negative i.e. these cells do not express recombinant protein.

The P1 gate was applied to the V5 fluorescence intensity histograms for cells transfected with WT ZIP10 (figure 4.3B-C) and the S591A mutant (figure 4.3D-E). The P2 population is V5-positive (i.e. these cells express the recombinant protein). The percentage of cells expressing the recombinant protein is shown highlighted on the graph. The percentage of cells expressing recombinant WT ZIP10 increased in the presence of nocodazole (24.6% to 26.1%; figure 4.3B-C) reflecting the increased need for ZIP10 in mitosis. However, the increase is only marginal and is unlikely to be significant if statistical analysis were to be performed. For these experiments both adherent cells and those floating in the medium were collected which could explain the increase in ZIP10 following nocodazole treatment compared with the western blot in figure 3.14 (using only adherent cells) that showed decreased ZIP10 following nocodazole treatment. If expression of recombinant ZIP10 stimulates cells to detach from their surroundings (for either mitosis or EMT), it could result in less ZIP10 being detected when only the adherent cells are collected for experimentation.

Furthermore, the FACS experiment does not separate ZIP10 fragments as in the western blot so it is not possible to accurately determine which fragment of ZIP10 is being detected in each sample; it is likely to be a mixture, but the ratios remain unknown.

Interestingly, the percentage of cells expressing the S591A mutant is decreased in the presence of nocodazole (18.2% to 16.7%; figure 4.3D-E), which may reflect increased degradation of the non-functional protein at a time in the cell cycle (mitosis) when ZIP10 is required in abundance.

Figure 4.3. Fluorescence intensity of recombinant WT and S591A ZIP10 in MCF7 cells

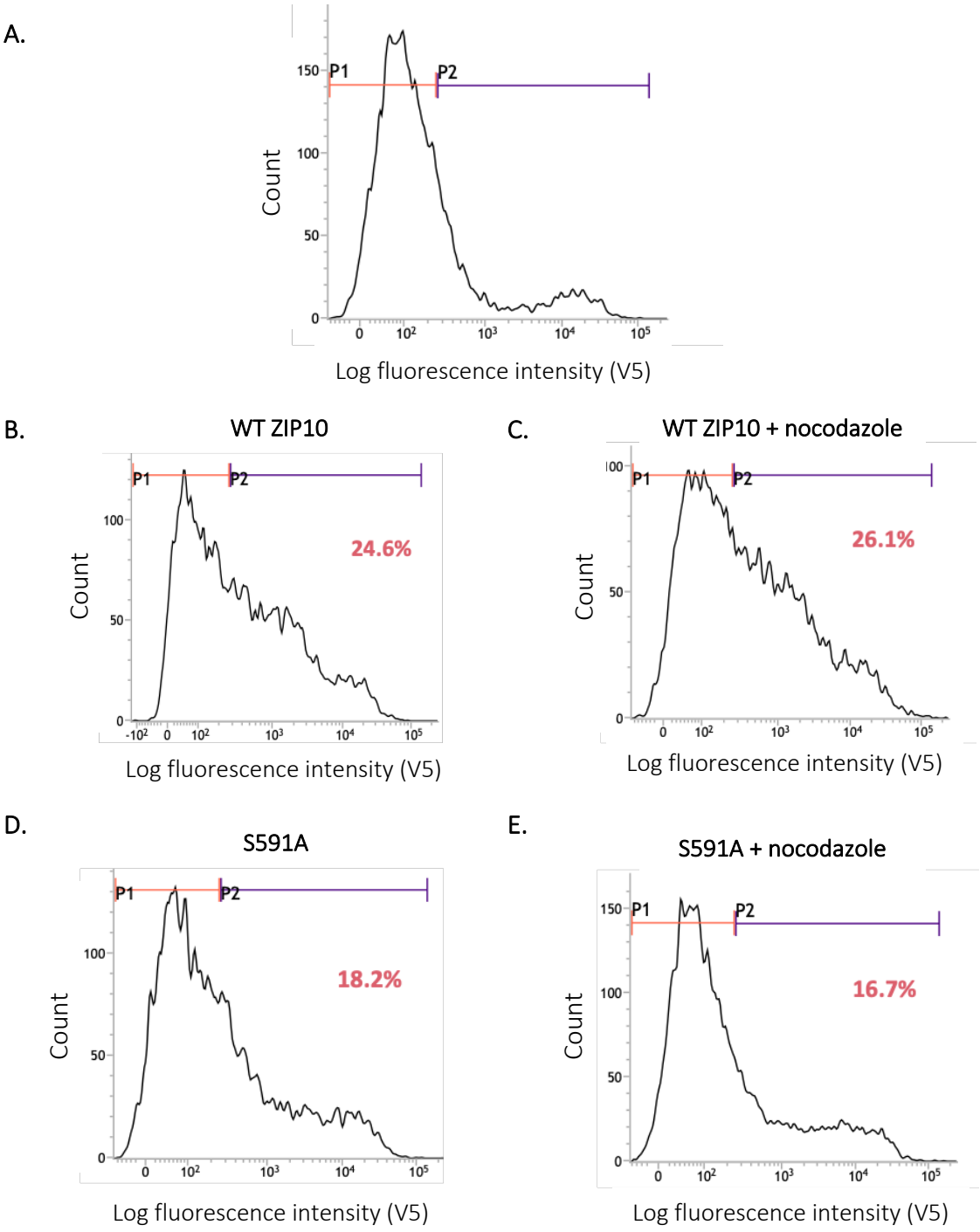

MCF7 cells were transfected with WT ZIP10 or the S591A mutant, with or without nocodazole and were analysed by FACS using a fluorophore conjugated anti-V5 antibody. ***A****. The V5-negative (P1) and V5-positive (P2) populations were determined using the log fluorescence intensity histogram of the fluorophore conjugated anti-V5 antibody in a sample transfected with the lipid only.* ***B-E****. The P1 and P2 population gates were applied to the V5 log fluorescence intensity histograms of each sample population. The numbers in pink represent the percentage of V5-positive cells (i.e. those cells expressing the recombinant protein) in each sample. No statistical analysis was performed owing to the sample size (n = 1).*

The P2 population (V5-positive) in each cell sample was analysed further for the presence of intracellular zinc. If S591 phosphorylation is an activating modification of ZIP10, the cells expressing the phospho-ablative mutant are expected to contain less intracellular zinc than those cells expressing WT ZIP10. FluoZin™-3 indicator is a small molecule sensor which displays a > 50-fold increase in fluorescence when bound to saturating levels of zinc (Gee *et al.*, 2002), and was used here to measure free zinc in the transfected cells. In the untreated sample, the V5-positive cells had lower fluorescence intensity of FluoZin™-3 when they were expressing the S591A mutant (figure 4.4A; pink line) compared with the cells expressing WT ZIP10 (figure 4.4A; black line). The left shift in fluorescence intensity of FluoZin™-3 in the mutant expressing cells demonstrates lower intracellular zinc in these cells compared with those cells expressing WT ZIP10. The fluorescence intensity of FluoZin™-3 was also decreased in the nocodazole-treated cells expressing the S591A mutant compared with those expressing WT ZIP10 (figure 4.4B). The mean fluorescence intensity in each population is presented as a bar graph in figure 4.4C, and shows reduced free zinc in the cells expressing the S591A mutant compared with WT ZIP10.

Interestingly, in the cells expressing WT ZIP10, there does not appear to be an increase in the intracellular free zinc following treatment with nocodazole (figure 4.4C). This may be due to the zinc which enters the cell at the start of mitosis becoming quickly bound to protein and therefore undetectable by FluoZin™-3 after 18 hours of mitotic synchronisation. Furthermore, approximately only 30% of cells are mitotic after nocodazole treatment so it is possible that a shift in FluoZin™-3 would be more apparent if there were more mitotic cells in the population.

4.4.4. Effect of ZIP10 S591 phosphorylation on mitotic entry

The data presented in this chapter so far suggest that phosphorylation of ZIP10 S591 is necessary for zinc entry into the cell. To investigate whether this modification is a prerequisite for mitotic entry, pS^{727}STAT3 was used as a mitotic marker in the presence of either WT ZIP10 or the S591A mutant in MCF7 cells treated with nocodazole. Not only is pS^{727}STAT3 present in mitosis and absent in interphase (figure 4.5), but S727 phosphorylation of STAT3 is directly related to the presence of zinc (Kitabayashi *et al.*, 2010), hence it was a good marker of ZIP10-mediated mitosis to use in this experiment.

Figure 4.4. Fluorescence intensity of FluoZin™-3 in cells expressing recombinant ZIP10

A.

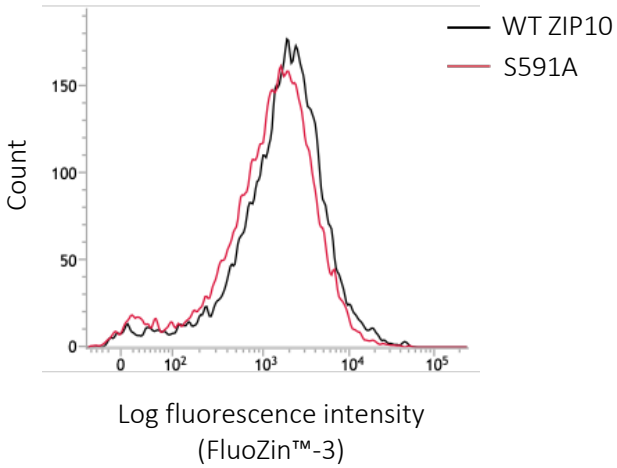

B.

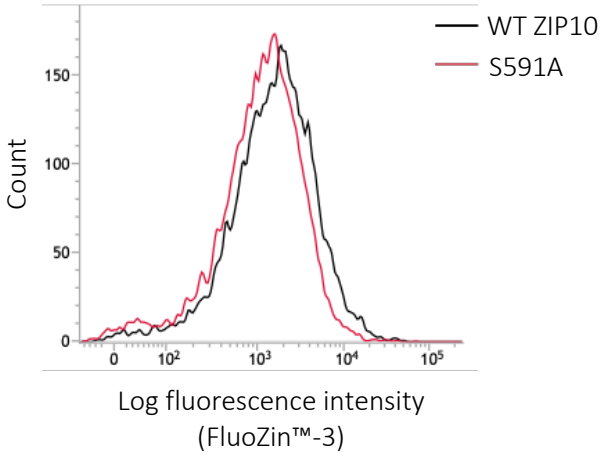

C.

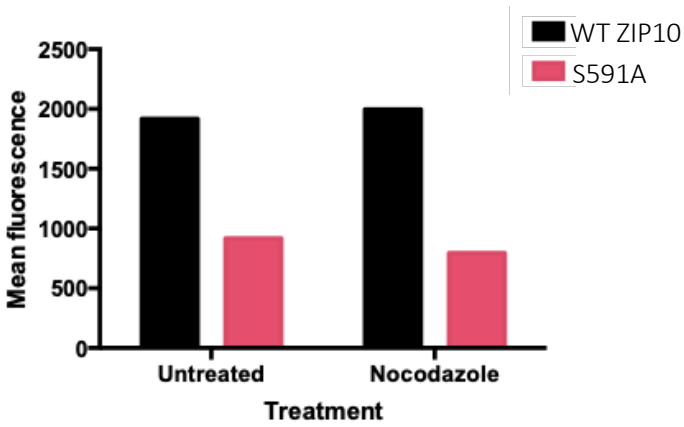

*The log fluorescence intensity histogram of FluoZin™-3 in MCF7 cells expressing WT ZIP10 (black lines) or the S591A mutant construct (pink lines) in the absence (**A**) or presence (**B**) of nocodazole. **C**. Fluorescence intensity of FluoZin™-3 is presented as geometric mean. No statistical analysis was performed owing to the sample size (n = 1).*

First, it was important to confirm that pS^{727}STAT3 in mitotic cells could be detected by FACS analysis. MCF7 cells treated with nocodazole were stained for pS^{727}STAT3 and pS^{10}Histone H3. There was increased fluorescence intensity for both pS^{10}Histone H3 (figure 4.6A) and pS^{727}STAT3 (figure 4.6B) in mitosis as shown by the right shift in the fluorescence intensity peak of each antibody, when the cells were treated with nocodazole (pink lines).

Dot plots were generated to directly compare the fluorescence of pS^{727}STAT3 and pS^{10}Histone H3 in each cell in untreated conditions (figure 4.6C) or following treatment with nocodazole (figure 4.6D). The quadrants split the cells into one of four categories; lower left quadrant (pS^{727}STAT3 negative and pS^{10}Histone H3 negative), lower right quadrant (pS^{727}STAT3 negative and pS^{10}Histone H3 positive), upper left quadrant (pS^{727}STAT3 positive and pS^{10}Histone H3 negative), upper right quadrant (pS^{727}STAT3 positive and pS^{10}Histone H3 positive). The position of the peaks in figure 4.6A-B were used to determine where the quadrants should be placed. The shift of many cells from the lower left quadrant in untreated conditions towards the upper right quadrant following nocodazole treatment indicates cells become positive for both pS^{727}STAT3 and pS^{10}Histone H3 in mitosis.

The percentage of cells positive for pS^{727}STAT3 in each sample (UL and UR quadrants combined) is shown in a bar graph in figure 4.6E. Following treatment with nocodazole, the percentage of cells positive for pS^{727}STAT3 increased to 47.28% from just 6.58% in the untreated population. This was accompanied by an increase in pS^{10}Histone H3 positive cells to 64.32% in the nocodazole-treated population from just 1.5% in the untreated population.

Interestingly, there was a population of cells positive for pS^{10}Histone H3 in the nocodazole-treated sample that was not positive for pS^{727}STAT3 (figure 4.6D). It is possible this represents a population of pre-mitotic cells, in which the pS^{10}Histone H3 demonstrates punctate staining in the nuclei (Hendzel *et al.*, 1997) but the chromosomes are not yet condensed. However, since zinc is required for S727 phosphorylation of STAT3 (Kitabayashi *et al.*, 2010), this would be expected to occur before condensation of the chromosomes and therefore S10 phosphorylation of histone H3. This result suggests that while a subset of cells may exist in a pre-mitotic state, zinc influx and S727 phosphorylation of STAT3 is still required as a switch to allow cells to fully enter mitosis.

Figure 4.5. pS^{727}STAT3 as a marker of mitosis

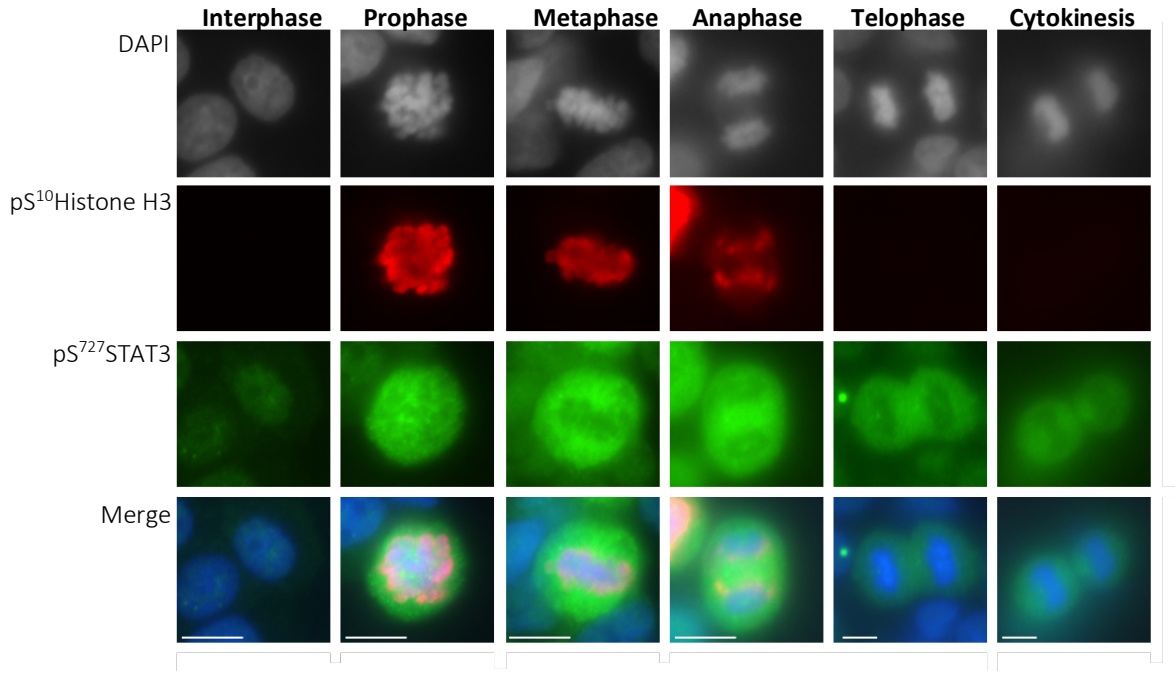

MCF7 cells were treated with nocodazole for 20 hours or the treatment was removed for up to 2 hours and replaced with normal growth medium to allow cells to move through mitosis. Cells were fixed and stained for pS^{10}Histone H3 (red) and pS^{727}STAT3 (green). Nuclei were stained with DAPI (blue). Images were taken from three different coverslips (nocodazole, nocodazole +1 or +2 hour recovery) to allow for individual cells to be imaged at different stages of mitosis. Scale bars: 10 μm.

Figure 4.6. Analysis of pS[10]Histone H3 and pS[727]STAT3 protein expression using FACS

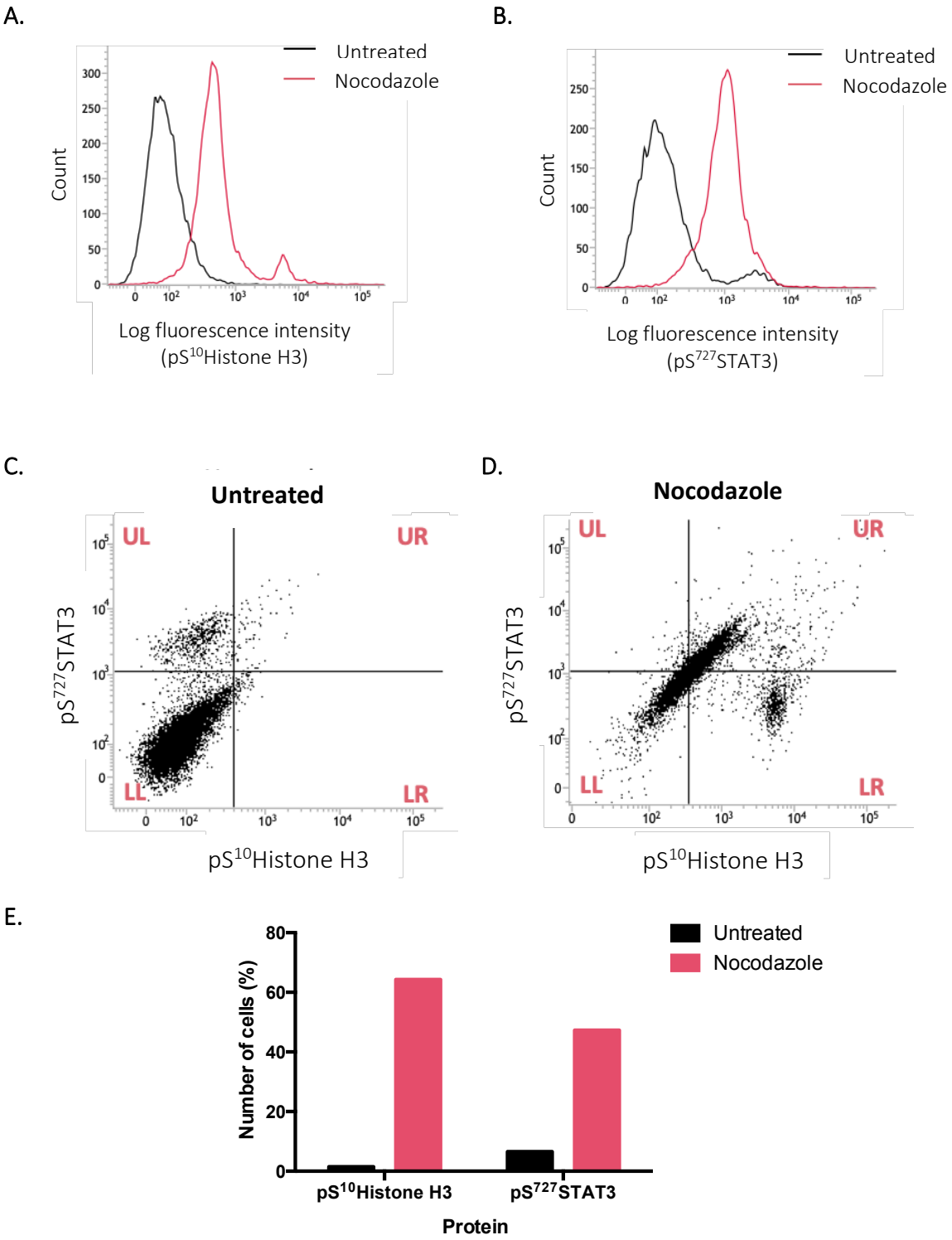

*The log fluorescence intensity histogram of pS[10]Histone H3 (**A**) and pS[727]STAT3 (**B**) in untreated (black lines) and nocodazole-treated (pink lines) MCF7 cells. Dot plots show the fluorescence intensity of both pS[10]Histone H3 (x axis) and pS[727]STAT3 (y axis) in individual cells untreated (**C**) and treated with nocodazole (**D**). Quadrants were drawn on the dot plots to separate cells negative for both proteins (LL, lower left), positive for pS[10]Histone H3 only (LR, lower right), positive for pS[727]STAT3 only (UL, upper left) or positive for both proteins (UR, upper right). **E**. The percentage of cells positive for pS[10]Histone H3 and pS[727]STAT3 in each sample (UL and UR quadrants combined) is presented in a bar graph. No statistical analysis was performed owing to the sample size (n = 1).*

The results demonstrate that pS^{727}STAT3 is a suitable marker for mitosis using FACS analysis of nocodazole-treated cells. Next, MCF7 cells were transfected with WT ZIP10 or the S591A mutant in the presence of nocodazole, and the anti-pS^{727}STAT3 antibody was used to determine whether the number of cells entering mitosis was decreased in cells expressing the S591A mutant, compared with WT ZIP10. An anti-V5 antibody was used as a marker of cells expressing recombinant ZIP10. Cells transfected with the lipid vector only were used as a negative control to determine the background signal from the antibodies (anti-V5 and anti-pS^{727}STAT3). The histogram shows the fluorescence intensity of V5 (figure 4.7A) and pS^{727}STAT3 (figure 4.7B) in the cells transfected only with the lipid. The P1 population is V5-negative i.e. these cells do not express recombinant protein and the P3 population is pS^{727}STAT3 negative. These gates were then applied to the corresponding histograms of cells transfected with WT ZIP10 or the S591A mutant with or without nocodazole and these were used to create dot plots to show the pS^{727}STAT3 fluorescence against V5 in individual cells (figure 4.8A-D). The quadrants split the cells into one of four categories; lower left quadrant (V5 negative and pS^{727}STAT3 negative), lower right quadrant (V5 positive and pS^{727}STAT3 negative), upper left quadrant (V5 negative and pS^{727}STAT3 positive), upper right quadrant (V5 positive and pS^{727}STAT3 positive). The percentage of cells positive for both V5 and pS^{727}STAT3 in each sample (UR quadrants only) is presented in a bar graph in figure 4.8E.

Almost 10% of cells expressing WT ZIP10 were positive for pS^{727}STAT3 when they were left untreated, compared with over 46% when treated with nocodazole (figure 4.8E), confirming that expression of recombinant WT ZIP10 does not alter pS^{727}STAT3 expression in mitosis, because the pS^{727}STAT3 expression is similar in the non-transfected cells in figure 4.6E (47%). However, untreated and nocodazole-treated cells expressing the S591A mutant had a reduced percentage of cells which were positive for pS^{727}STAT3 (6.55% and 11.57% respectively; figure 4.8E). In fact, 26.3% of cells expressing the S591A mutant were negative for pS^{727}STAT3 even in the presence of nocodazole (figure 4.8D), highlighting that these cells were unable to enter mitosis. These data suggest ZIP10 phosphorylation of serine 591 is crucial for mitotic entry.

Figure 4.7. Analysis of pS^{727}STAT3 and V5 protein expression in transfected cells using FACS

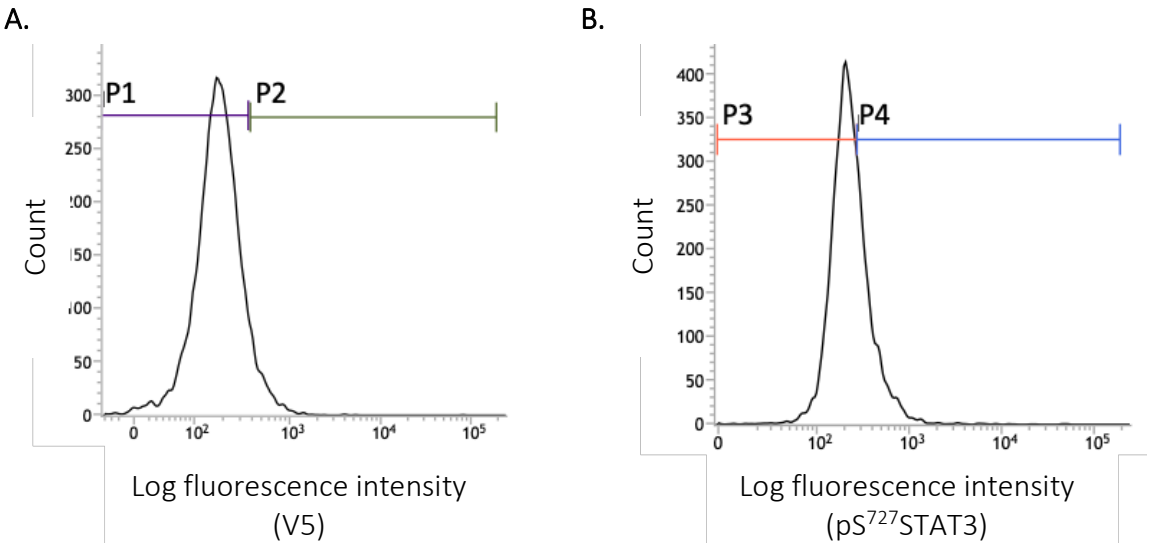

*The log fluorescence intensity histogram of V5 (**A**) and pS^{727}STAT3 in (**B**) in MCF7 cells transfected with a lipid vector (n = 1). Populations P1 and P3 are negative for V5 and pS^{727}STAT3 respectively while P2 and P4 are positive for V5 and pS^{727}STAT3 respectively. These gates were applied to the corresponding histograms for cells transfected with WT ZIP10 or the S591A mutant and used to generate the dots plots in figure 4.8.*

Figure 4.8. Effect of ZIP10 serine 591 phosphorylation on pS^{727}STAT3 protein expression

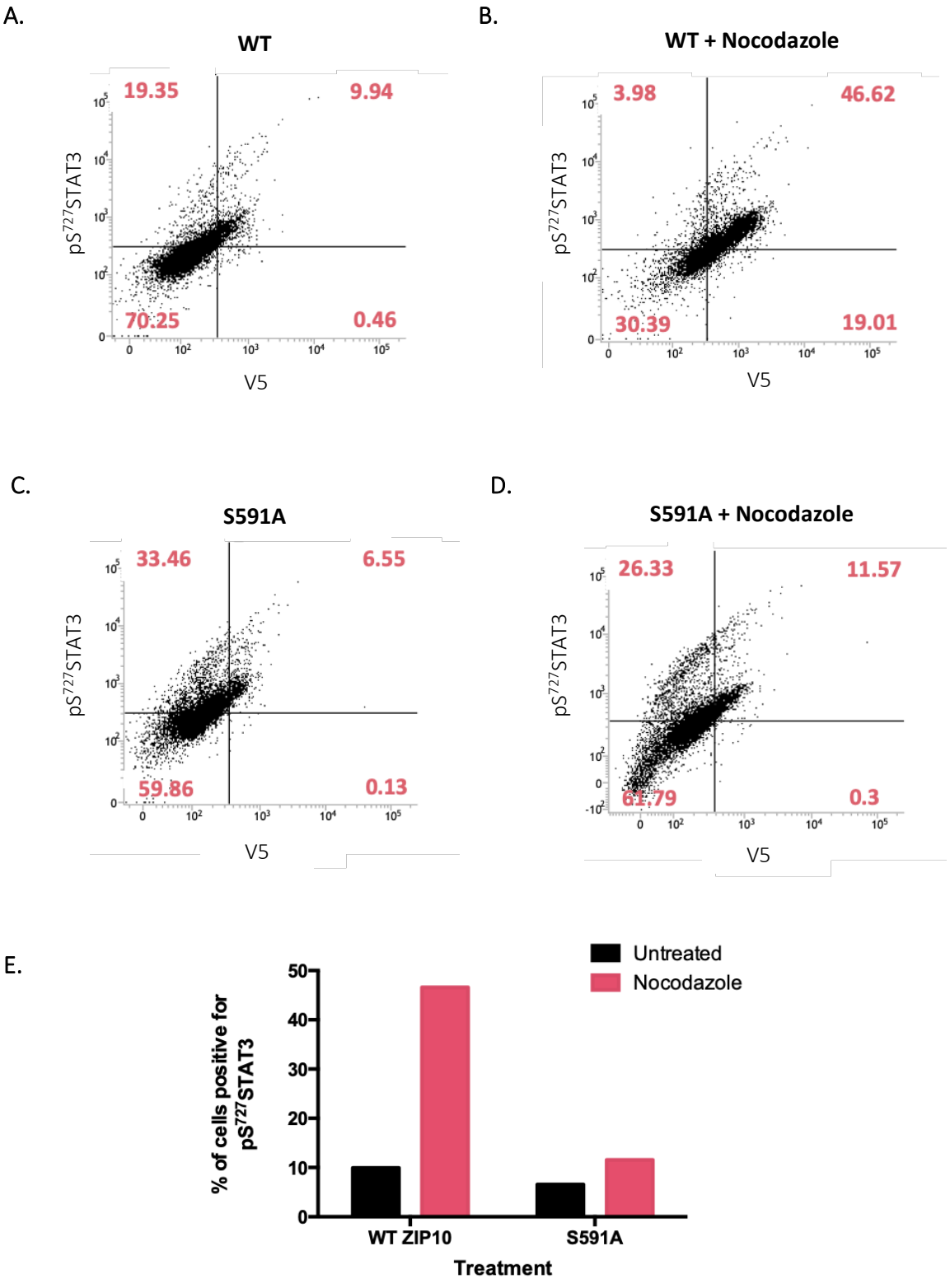

*Dot plots show the fluorescence intensity of both V5 (x axis) and pS^{727}STAT3 (y axis) in individual cells transfected with WT ZIP10 untreated (**A**) or treated with nocodazole (**B**) or transfected with the S591A mutant untreated (**C**) or treated with nocodazole (**D**). Quadrants were drawn on the dot plots to separate cells negative for both proteins (LL, lower left), positive for V5 only (LR, lower right), positive for pS^{727}STAT3 only (UL, upper left) or positive for both proteins (UR, upper right). **E**: The percentage of cells positive for both V5 and pS^{727}STAT3 in each sample (UR quadrants only) is presented in a bar graph. No statistical analysis was performed owing to the sample size (n = 1).*

It is important to note there was a small increase in S591A-expressing cells which were positive for pS^{727}STAT3 when treated with nocodazole (6.55% to 11.57%; figure 4.8E). This may be due to the endogenous protein, which is still expressed in transfected cells, and functioning as normal, though it could also be due to the upregulation of ZIP6, as a compensatory mechanism for the non-functioning ZIP10. The role of ZIP transporters in response to absence of other ZIPs is yet to be explored in detail.

4.4.5. ZIP10 interaction with CDK1

The investigation into ZIP10 serine phosphorylation on residue 591 suggested that phosphorylation has a role in ZIP10 activation, allowing zinc-induced initiation of mitosis. CDK1, which promotes cell cycle progression from G2 to M was the kinase predicted to phosphorylate S591 (table 4.1) making it a possible candidate for ZIP10 activation in mitosis. An investigation was carried out to assess the binding of ZIP10 to CDK1 in mitosis. MCF7 cells were treated with nocodazole and analysed using proximity ligation assay with antibodies directed to the intracellular region of ZIP10 and total CDK1 (figure 4.9A). The total CDK1 antibody was raised in mouse and therefore the ZIP10 L4 antibody, which was raised in rabbit, was used in conjunction. The images show an increase in the number of dots associated with mitotic cells (white arrows) compared with non-mitotic cells suggesting the binding together of ZIP10 and CDK1 in mitosis. This was confirmed by counting the dots; there was an average of 28 dots (s = 16.5 dots) per mitotic cell compared with 2 dots (s = 0.5 dots) per non-mitotic cell (figure 4.9B), albeit this was not statistically significant (p = 0.051).

Control experiments were carried out using each antibody individually and very few dots could be seen across the images (figure 4.9C) confirming the absence of background staining from either antibody. An average of less than 1 dot per cell was calculated when either antibody was used alone (figure 4.9B).

Figure 4.9. ZIP10 interaction with total CDK1

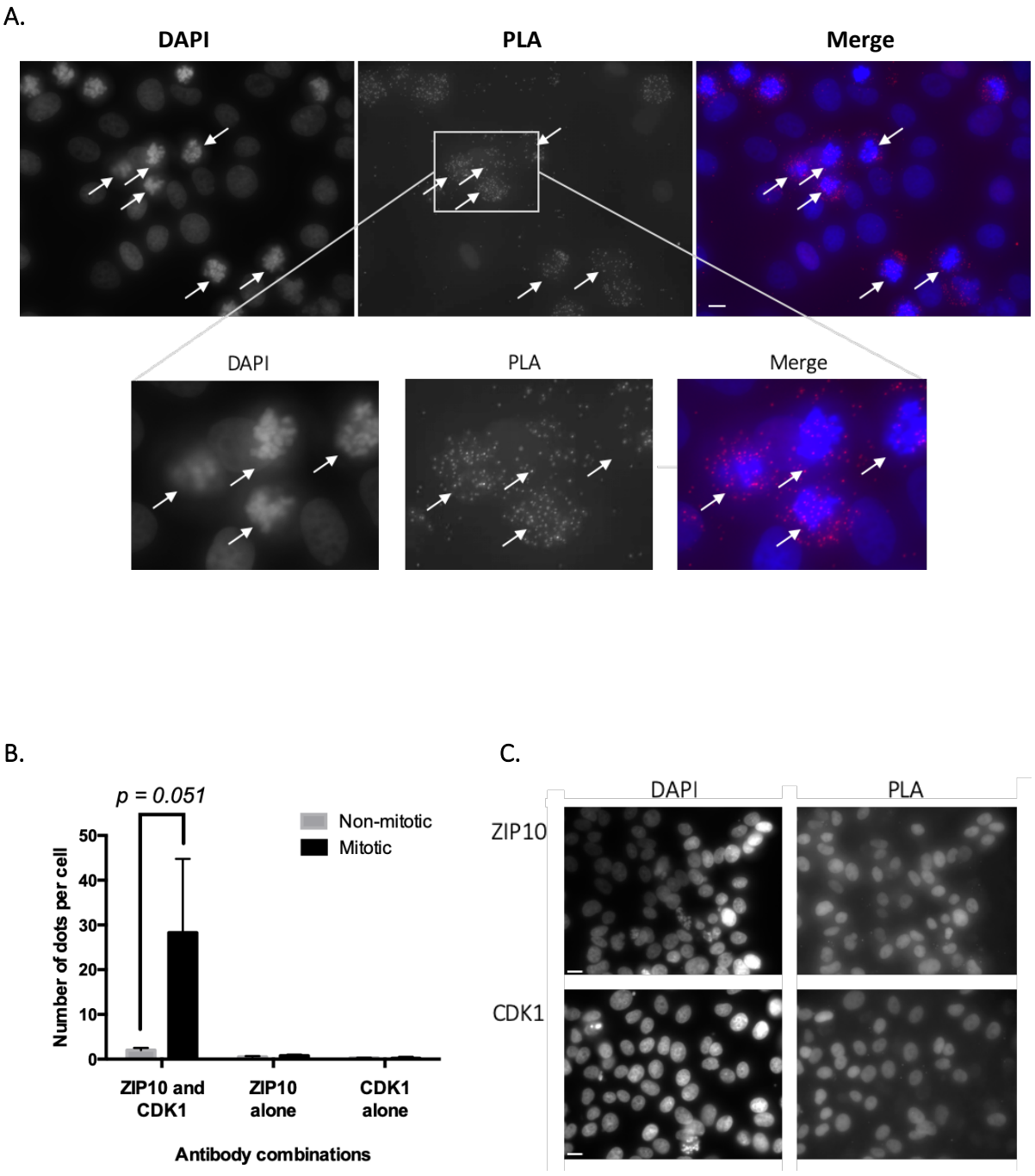

*Proximity ligation assay using anti-ZIP10 (L4) and -total CDK1 antibodies in MCF7 cells treated with nocodazole. Twenty-five images were taken at 3 μm apart and were merged for quantification of dots. Each cell population was imaged in three separate fields of view and a representative image is shown (**A**). Dots represent instances where the proteins of interest are within 40 nm of each other. Nuclei were stained with DAPI (blue). White arrows indicate mitotic cells. Scale bars: 10 μm. **B**. The number of dots per non-mitotic/mitotic cell was counted and the data presented as mean ± standard error (n = 3). Statistical significance was measured using a paired t-test. **C**. Negative control experiments were carried out using the anti-ZIP10 (L4) and -total CDK1 antibodies individually. A representative image is shown. Scale bars: 10 μm.*

The PLA data presented here suggest that ZIP10 is bound to CDK1 in mitosis. To investigate this further, a second PLA experiment was carried out to determine the form of CDK1 to which ZIP10 was bound, using antibodies targeted to the intracellular loop of ZIP10 and pY^{15}CDK1 (figure 4.10A). Phosphorylation of CDK1 of Y15 renders the protein inactive; dephosphorylation at the onset of mitosis causes activation and kinase activity (Parker and Piwnica-Worms, 1992; Mueller *et al.*, 1995). The ZIP10 L5 antibody, which was raised in mouse, was used here because the pY^{15}CDK1 antibody was raised in rabbit. There did not appear to be an increased number of dots associated with mitotic cells (white arrows) compared to non-mitotic cells (figure 4.10A). The average number of dots per mitotic cell was 5 (s = 2 dots) compared with 2 (s = 1 dot) in the non-mitotic cells (figure 4.10B) and no statistical significance was found between the two groups suggesting that ZIP10 does not bind pY^{15}CDK1 in mitosis.

In fact, the number of dots in mitotic cells was 5-times lower than the number of dots in mitotic cells when the total CDK1 antibody was used (figure 4.9B). This suggests that activation of CDK1 by dephosphorylation at Y15 precedes the interaction of CDK1 with ZIP10 and supports the hypothesis that CDK1 exerts its kinase activity on ZIP10 in mitosis. Less than 1 dot per cell was seen when either antibody was used individually (figure 4.10C) confirming the absence of background staining from either antibody.

A further software analysis of the ZIP10 protein sequence revealed several consensus CDK1 docking motifs (figure 4.11). These sequences are however located in the extracellular N-terminus of ZIP10 and given that CDK1 is an intracellular protein it seems unlikely that CDK1 is interacting with ZIP10 anywhere other than the predicted S591 phosphorylation site.

The data presented here implicate CDK1 in the phosphorylation of ZIP10 on S591, in mitosis. CDK1 is a highly regulated protein with roles in many signalling pathways and it is therefore likely that the relationship between these two proteins is more complex and requires further experimental investigation.

Figure 4.10. ZIP10 interaction with inactive CDK1

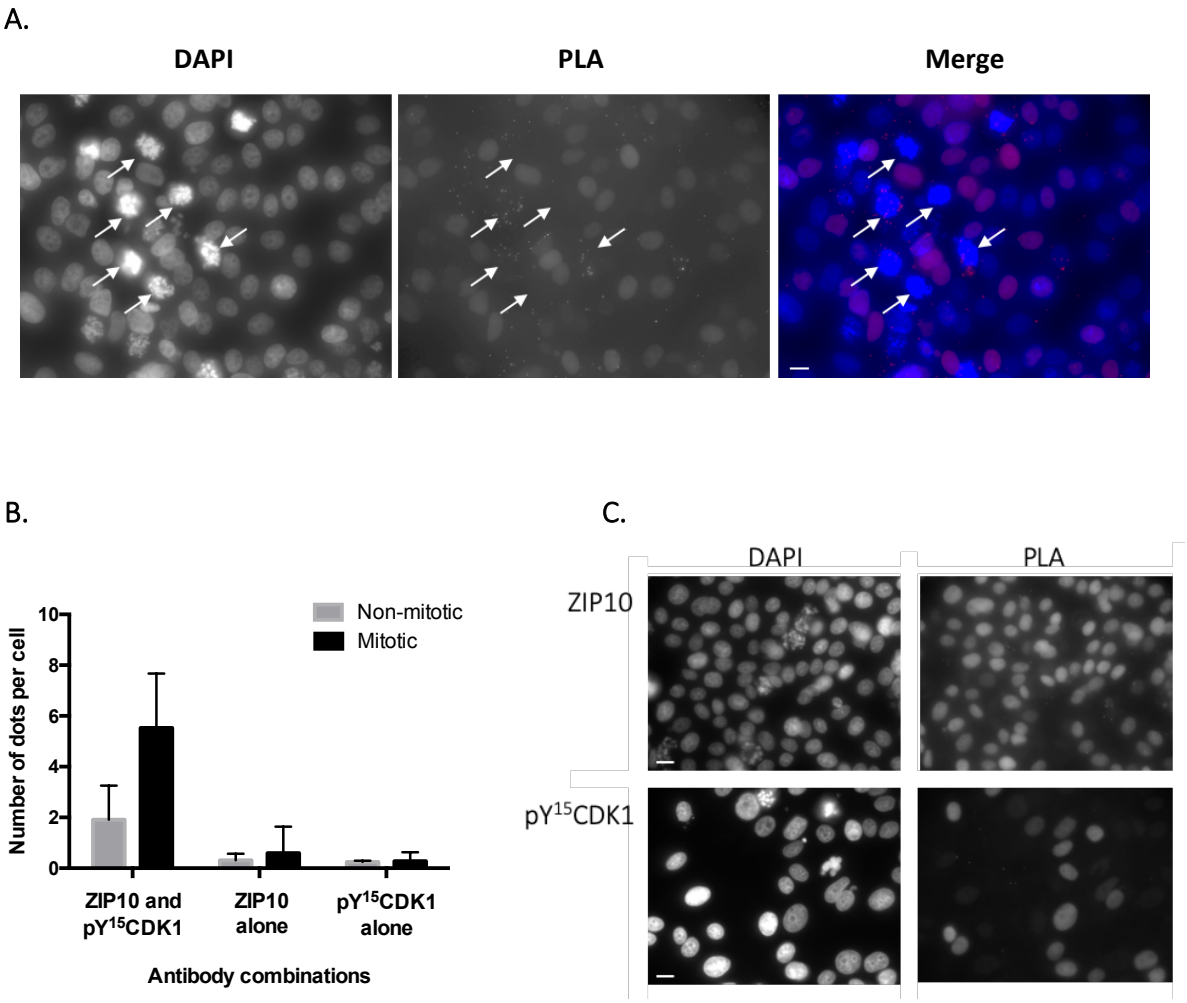

*Proximity ligation assay using anti-ZIP10 (L5) and -pY^{15}CDK1 antibodies in MCF7 cells treated with nocodazole. Twenty-five images were taken at 3 μm apart and were merged for quantification of dots. Each cell population was imaged in three separate fields of view and a representative image is shown (**A**). Dots represent instances where the proteins of interest are within 40 nm of each other. Nuclei were stained with DAPI (blue). White arrows indicate mitotic cells. Scale bars: 10 μm **B**. The number of dots per non-mitotic/mitotic cell was counted and the data presented as mean ± standard error (n = 3). Statistical significance was measured using a paired t-test, but no significance was found. **C**. Negative control experiments were carried out using the anti-ZIP10 (L5) and -pY^{15}CDK1 antibodies individually. A representative image is shown. Scale bars: 10 μm.*

Figure 4.11. Predicted interactions between ZIP10 and CDK1

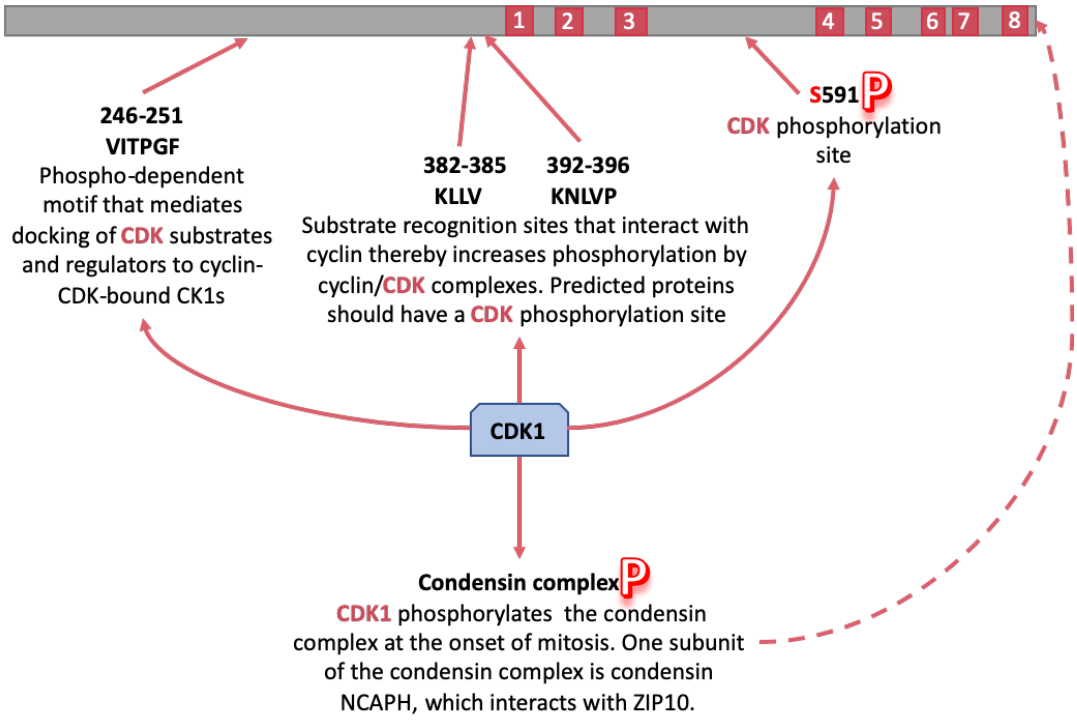

A software analysis of the human ZIP10 sequence was carried out using ELM (Dinkel *et al.*, 2016) *to identify predicted sites of CDK1 interaction.*

4.4.6. ZIP10 interaction with PLK1

The software analysis of ZIP10 phosphorylation carried out earlier in this chapter revealed potential phosphorylation by the PLK family of kinases on three residues; S539, T540 and S570 (table 4.1). One of the main aims of this project was to investigate ZIP10 regulation in mitosis, and as PLK1 has well-established roles in mitosis (Lee, Jang and Lee, 2014) it was chosen as a suitable candidate for ZIP10 regulation by phosphorylation. MCF7 cells were treated with nocodazole and a proximity ligation assay was carried out using antibodies directed to the intracellular region of ZIP10 and total PLK1 (figure 4.12A). The total PLK1 antibody was raised in mouse and therefore the ZIP10 L4 antibody, which was raised in rabbit, was used in conjunction. There was a clear increase in the number of dots associated with mitotic cells (white arrows) compared with non-mitotic cells (figure 4.12A). The dots were counted and an average of 112 dots (s = 48 dots) per mitotic cell was calculated compared with just 9.5 dots (s = 7 dots) in non-mitotic cells ($p < 0.01$) (figure 4.12B), confirming interaction of ZIP10 and PLK1 in mitosis.

Control experiments were carried out using each antibody individually (figure 4.12B-C). Less than 1 dot per cell was counted with the ZIP10 L4 antibody alone, and less than 3 dots per cell with the total PLK1 antibody alone, confirming the number of dots counted when both antibodies were used together was due to the proteins being in close proximity, and not due to background staining.

PLK1 is activated by phosphorylation on threonine residue 210 in mitosis, which increases its kinase activity (Akopyan *et al.*, 2014). For this reason, the proximity ligation assay was repeated using antibodies targeted to the intracellular region of ZIP10 and pT^{210}PLK1. The anti-pT^{210}PLK1 antibody was raised in rabbit therefore the anti-ZIP10 L5 antibody, which was raised in mouse was used in conjunction. Alike the PLA carried out with the total PLK1 antibody, there was an increase in the number of dots associated with mitotic cells (white arrows) compared with non-mitotic cells (figure 4.13A). The average number of dots per mitotic cell was 26.2 (s = 12 dots), significantly more than the average of 1.6 dots (s = 1 dot) counted in the non-mitotic cells ($p < 0.05$) (figure 4.13B), suggesting the binding of activated PLK1 and ZIP10 in mitosis.

Control experiments were carried out using each antibody individually (figure 4.13C) and less than 1 dot per cell was counted for both antibodies (figure 4.13B) confirming the

absence of background staining. The data indicate that ZIP10 is a substrate for PLK1 phosphorylation in mitosis.

To identify which residue(s) of ZIP10 may be phosphorylated by PLK1, three recombinant ZIP10 constructs were made, each with a different phospho-residue mutated to alanine; S539, T540 and S570. Successful mutagenesis was confirmed by DNA sequencing (figure 4.1).

MCF7 cells were transfected with either WT ZIP10, or one of the mutant constructs, in the presence of nocodazole. The cells were lysed, and the recombinant protein immunoprecipitated with an anti-V5 antibody. The immunoprecipitated proteins were analysed by SDS-PAGE and western blot (figure 4.14), to determine the presence (if any) of PLK1 in the samples, and therefore the association of PLK1 with recombinant ZIP10. There is a suggestion of a decrease of the S570A mutant interacting with total PLK1, though this was not a complete reduction (figure 4.14). Similarly, to the immunoprecipitation experiment in chapter 3 (figure 3.21C), there appears to be a problem with the negative controls; the anti-V5 antibody should not detect anything in these samples because the V5 tag is not present. Owing to this issue with the negative controls in this experiment the data cannot be completely trusted and the binding of ZIP10 to PLK1 via any of the investigated residues should not be ruled out.

Figure 4.12. ZIP10 interaction with total PLK1

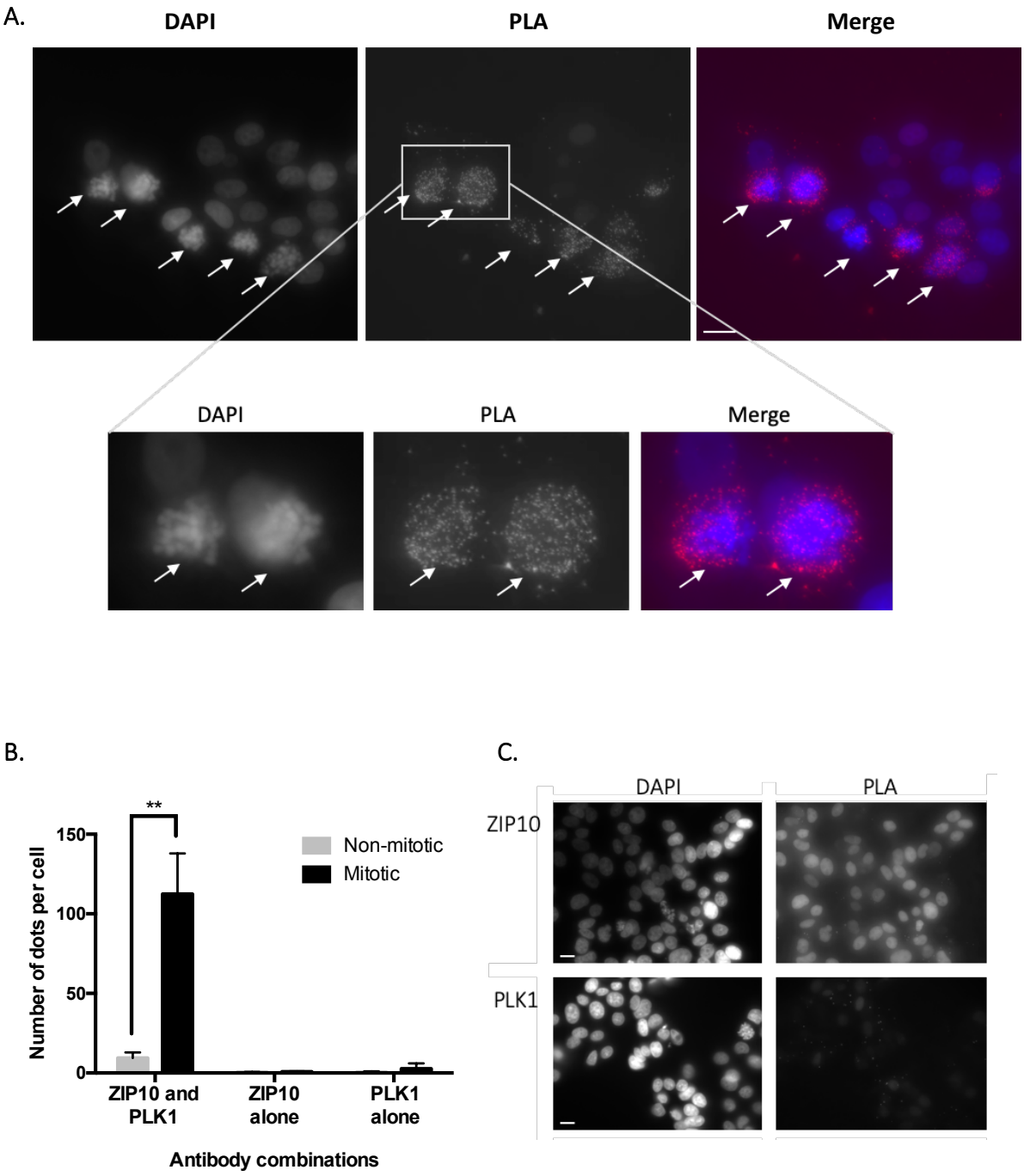

*Proximity ligation assay using anti-ZIP10 (L4) and -total PLK1 antibodies in MCF7 cells treated with nocodazole. Twenty-five images were taken at 3 μm apart and were merged for quantification of dots. Each cell population was imaged in three separate fields of view and a representative image is shown (**A**). Dots represent instances where the proteins of interest are within 40 nm of each other. Nuclei were stained with DAPI (blue). White arrows indicate mitotic cells. Scale bars: 10 μm. **B**. The number of dots per non-mitotic/mitotic cell was counted and the data presented as mean ± standard error (n = 3). Statistical significance was measured using a paired t-test. ** $p < 0.01$. **C**. Negative control experiments were carried out using the anti-ZIP10 (L4) and -total PLK1 antibodies individually. A representative image is shown. Scale bars: 10 μm.*

Figure 4.13. ZIP10 interaction with active PLK1

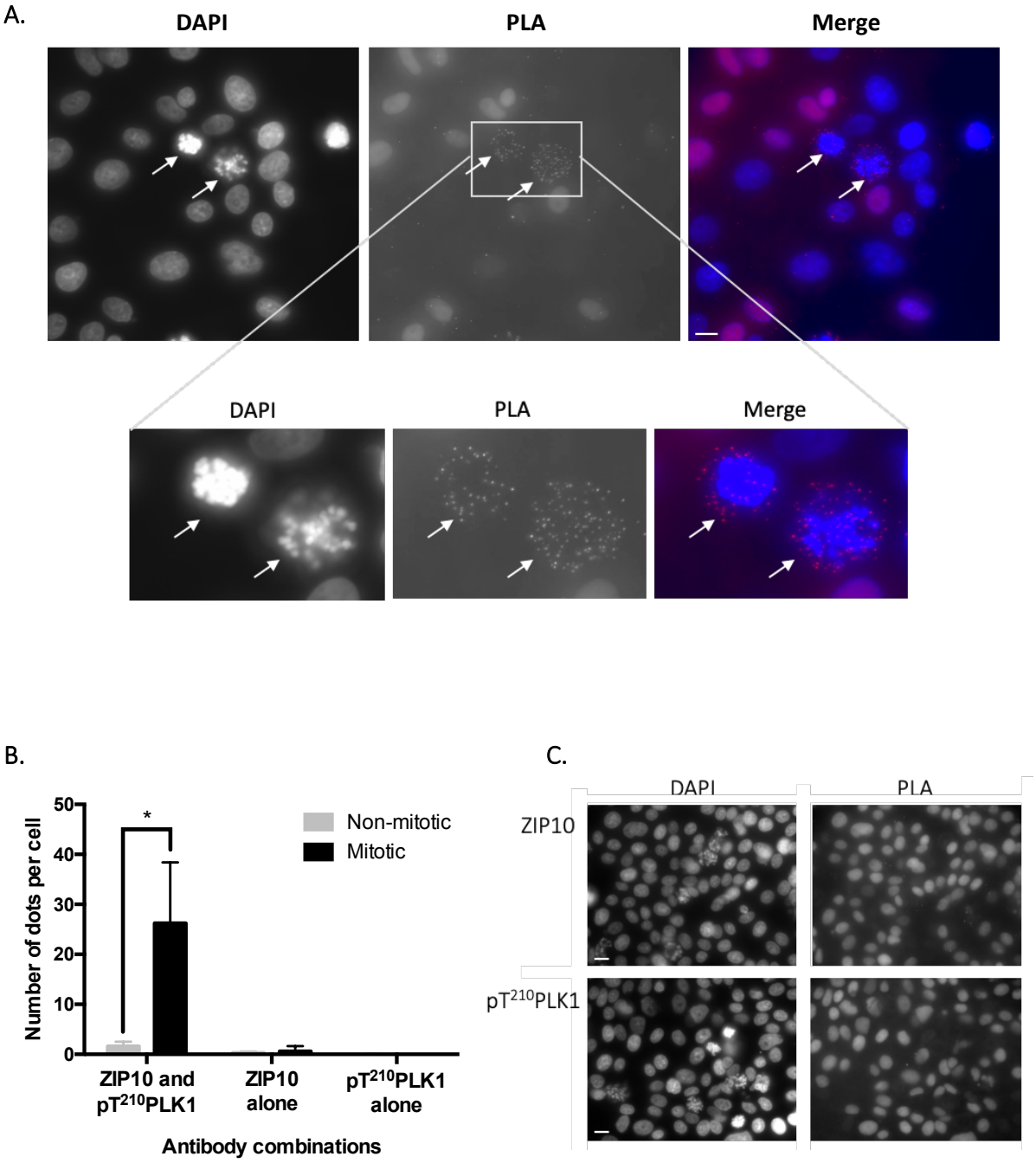

*Proximity ligation assay using anti-ZIP10 (L5) and -pT210PLK1 antibodies in MCF7 cells treated with nocodazole. Twenty-five images were taken at 3 μm apart and were merged for quantification of dots. Each cell population was imaged in three separate fields of view and a representative image is shown (**A**). Dots represent instances where the proteins of interest are within 40 nm of each other. Nuclei were stained with DAPI (blue). White arrows indicate mitotic cells. Scale bars: 10 μm. **B**. The number of dots per non-mitotic/mitotic cell was counted and the data presented as mean ± standard error (n = 3). Statistical significance was measured using a paired t-test. * $p < 0.05$. **C**. Negative control experiments were carried out using the anti-ZIP10 (L5) and -pT^{210}PLK1 antibodies individually. A representative image is shown. Scale bars: 10 μm.*

Figure 4.14. Recombinant ZIP10 interaction with PLK1

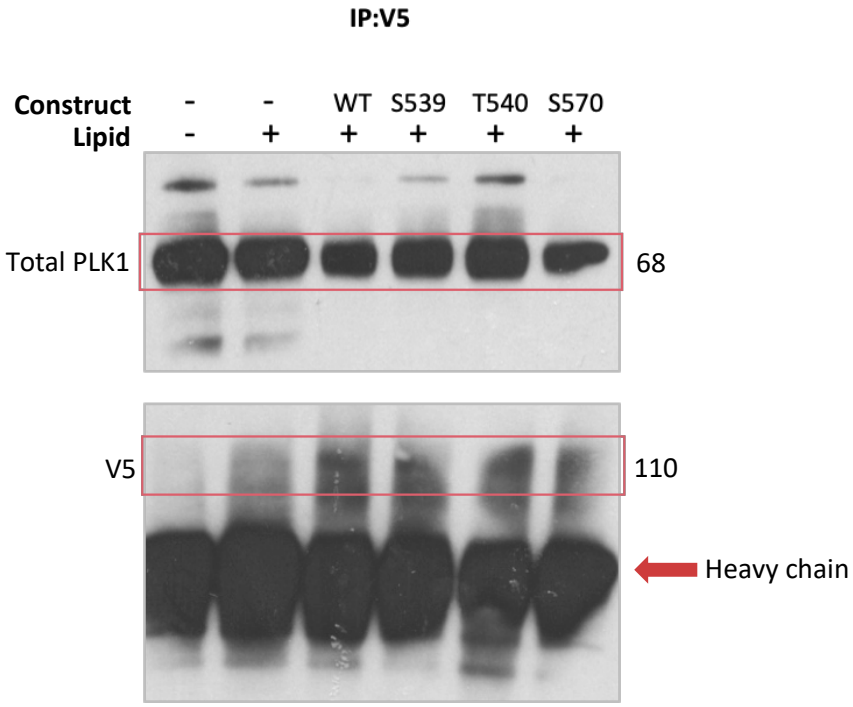

MCF7 cells were transfected with either WT ZIP10 or an S539A, T540A or S570A mutant ZIP10 construct. The recombinant protein was immunoprecipitated using an anti-V5 antibody and analysed by SDS-PAGE and western blot. Antibodies against total PLK1 and V5 were used to detect PLK1 association with recombinant ZIP10 (n = 1). Numbers represent molecular mass of protein bands kDa. Specfic bands are highlighted by the pink boxes.

4.4.7. Serine 546 phosphorylation of ZIP10

The data presented in this chapter so far have focused on ZIP10 regulation by phosphorylation specifically in mitosis. However, it was interesting that the software analysis of the ZIP10 protein sequence highlighted the phosphorylation of S546 in both mitosis and the G1 phase of the cell cycle. The prediction score for S546 phosphorylation in PHOSIDA was 1.2 for mitosis and 3.26 for G1, both of which are above the threshold score set by the database of 0.75 (Gnad *et al.*, 2007), which reflects the increased chance that the residue is modified, based on its fragmentation spectra. Interestingly, intracellular zinc fluctuations have been measured throughout the cell cycle. A peak in G1 was specifically attributed to zinc influx from outside the cell (Li and Maret, 2009), implicating a role for ZIP transporters on the plasma membrane in G1 and may provide an explanation for the potential phosphorylation of ZIP10 on S546 at this timepoint.

To understand whether ZIP10 has a specific role in G1, MCF7 cells were synchronised in mitosis over a 20-hour period. Cells were halted in prophase using nocodazole treatment for the full 20 hours, or the treatment was removed for a 1- (N +1), 2- (N +2) or 3-hour period (N +3) to allow cells to progress through mitosis into G1. During the recovery period, nocodazole was removed and replaced with fresh growth medium. The cell lysates were analysed by SDS-PAGE and western blot and the protein expression of pS^{10}Histone H3 was assessed to confirm synchronisation in G1 (figure 4.15A). pS^{10}Histone H3 was significantly increased in cells treated with nocodazole ($p < 0.01$) and those which had nocodazole removed for one hour ($p < 0.01$) compared with the untreated population (figure 4.15B). The level of pS^{10}Histone H3 decreased with increasing recovery time suggesting movement of cells through mitosis and the nocodazole +3 population is synchronised in G1.

The cell lysates of MCF7 cells in G1 were then assessed for ZIP10 protein expression using intracellular anti-ZIP10 antibodies. Intracellular ZIP10 antibodies were used here because the N-terminus is shed during mitosis as was demonstrated in the previous chapter. Therefore, only the TMD region of ZIP10 is expected to remain on the plasma membrane during G1. The epitopes of the ZIP10 L4 and L5 antibodies used here are shown in figure 4.16A with a reminder of the band sizes detected by each antibody in the previous chapter. There were two potential cleavages that generated the 44 kDa band and as of yet it is unclear which one is real, so both are shown in the figure 4.16A.

The amount of the 44 kDa band detected with antibody L4 did not change during mitosis or G1 (figure 4.16B-C). However, the 68 kDa band detected using antibody L5 increased significantly ($p < 0.05$) in the cells synchronised in G1 (figure 4.16D-E), suggesting the increased proteolytic cleavage at residue R637 in G1 (based on the prediction of proteolytic cleavage sites in figure 3.5 of the previous chapter). The data suggest there is regulation of ZIP10 by cleavage in G1, in addition to phosphorylation.

To investigate ZIP10 phosphorylation on serine 546, a recombinant mutant construct was made, in which serine 546 was mutated to alanine (S546A). The successful mutation was confirmed by DNA sequencing (figure 4.1C). MCF7 cells were transfected with WT ZIP10 or S546A ZIP10 mutant and were synchronised in either mitosis or G1 using nocodazole treatment which was removed for up to 6 hours before the cells were lysed. The cell lysates were analysed by SDS-PAGE and western blot for the presence of phospho-serine (figure 4.17A).

Upon initial inspection of the membrane, the level of phospho-serine did not appear to change depending on the ZIP10 construct that the cells were expressing, or across time-points (figure 4.17A). To quantify the phospho-serine, an anti-V5 antibody was used to probe for the recombinant ZIP10 constructs. However, instead of the expected band at 63 kDa which had been detected in the previous chapter, a band at 57.5 kDa was detected in the cells expressing the S546A mutant (figure 4.17A). The band was significantly increased in the mutant-expressing cells in G1 compared with the cells in mitosis ($p < 0.01$; figure 4.17B). The 57.5 kDa V5 band was not detected in the cells expressing WT ZIP10, suggesting that mutation of serine 546 caused an abnormal cleavage of ZIP10. To determine whether the 63 kDa recombinant ZIP10 which had been seen in the previous chapter could still be detected in these cells, the membrane was re-probed with a more sensitive detection reagent (Femto). This resulted in the detection of the 63 kDa band in both cells transfected with WT ZIP10 and the S546A mutant (figure 4.17C). The 63 kDa band could not be quantified however, due to the overlapping signal from the 57.5 kDa band which was present in abundance in the cells expressing the S546A mutant.

Figure 4.15. G1 synchronisation of MCF7 cells

A.

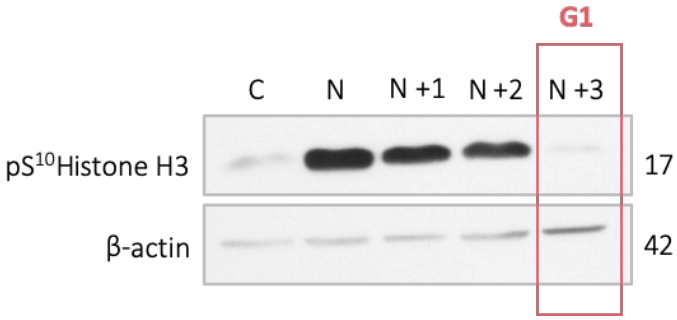

B.

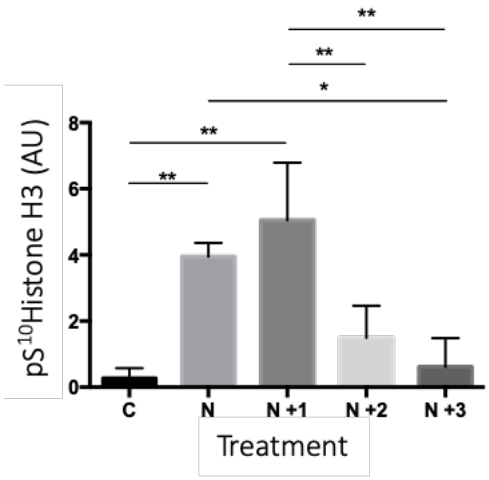

*MCF7 cells were treated with nocodazole (N) for 20 hours or the treatment was removed to allow 1 (N + 1), 2 (N + 2), or 3 (N + 3) hours recovery. C, control (untreated). The cells were lysed and analysed by SDS-PAGE and western blot. The level of pS[10]Histone H3 was determined in each sample (**A**). Numbers represent the molecular mass of the protein bands in kDa. The cell population in G1 is highlighted by the pink box. pS[10]Histone H3 was normalised to β-actin (**B**) and is presented as mean ± standard error (n = 3). Statistical significance was measured using ANoVA, comparing to the untreated population. * p < 0.05, ** p < 0.01. AU, arbitrary unit.*

Figure 4.16 Effect of G1 cell synchronisation on ZIP10

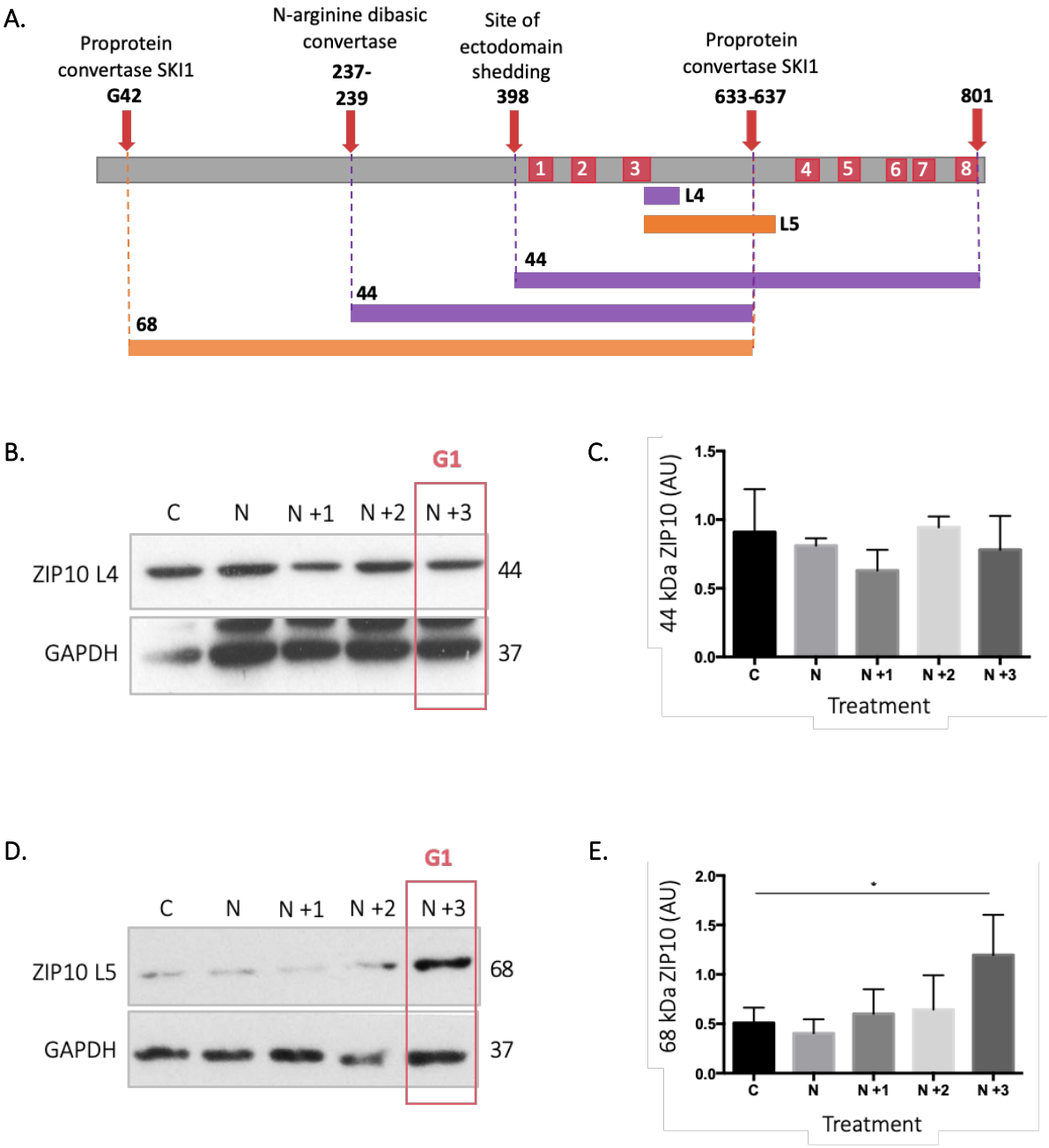

A*. ZIP10 L4 and L5 antibody epitopes are shown with a purple and orange bar respectively. The molecular mass of bands detected on western blots using these antibodies in the previous chapter are shown and the speculative ZIP10 cleavage sites from which they are generated are highlighted with pink arrows.* ***B-E****. MCF7 cells were treated with nocodazole (N) for 20 hours or the treatment was removed to allow 1 (N + 1), 2 (N + 2), or 3 (N + 3) hours recovery. C, control (untreated). The cells were lysed and analysed by SDS-PAGE and western blot. The level of ZIP10 L4 was determined in each sample (B) and normalised to GAPDH (C). The level of ZIP10 L5 was determined in each sample (D) and normalised to GAPDH (E). Numbers represent the molecular mass of the protein bands in kDa. The cell populations in G1 is highlighted by the pink boxes. Graphs are presented as mean ± standard error (n = 3). Statistical significance was measured using ANoVA, comparing to the untreated population. * $p < 0.05$. AU, arbitrary unit.*

Figure 4.17. Effect of G1 synchronisation on ZIP10

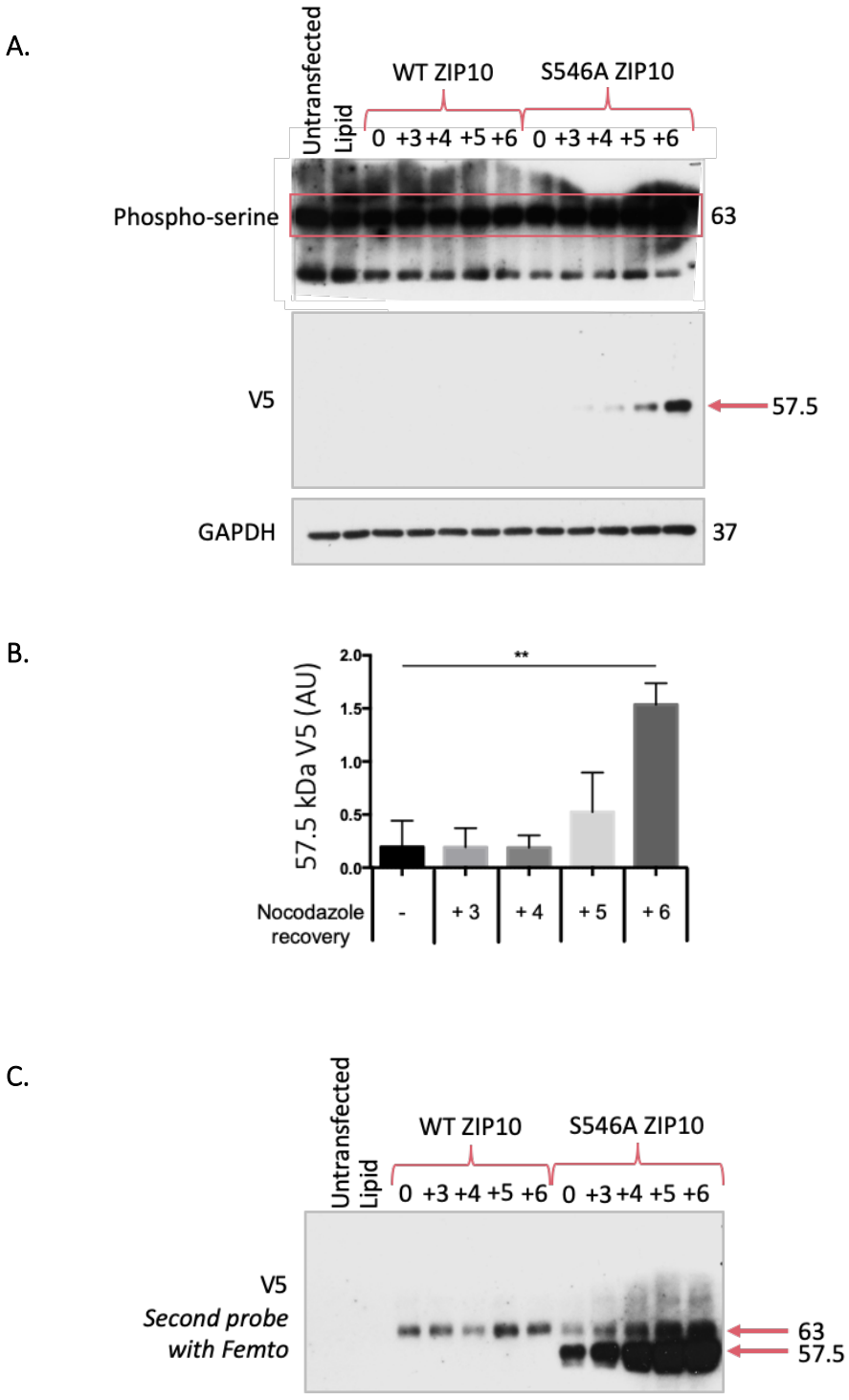

MCF7 cells were transfected with either WT ZIP10 or the S546A mutant. Cells were synchronised in mitosis with nocodazole for 18 hours, or the treatment was removed to allow 3 (+3), 4 (+4), 5 (+5) or 6 (+6) hours recovery. The cells were lysed and analysed by SDS-PAGE and western blot. ***A****. Phospho-serine, V5 and GAPDH were detected using specific antibodies. Numbers represent the molecular mass of protein bands in kDa. The pink box highlights the phospho-serine band that matches the expected 63 kDa band of V5.* ***B****. The level of V5 was normalised to GAPDH and is presented as mean ± standard error (n = 3). Statistical significance was measured using ANoVA, comparing to the cells treated with nocodazole with no recovery. ** p < 0.01. AU, arbitrary unit.* ***C****. The membrane was re-probed for V5 using a stronger detection reagent, Femto.*

Taking into consideration the 5 kDa mass of the V5 tag, the 57.5 kDa band seen in figure 4.17A is a C-terminal fragment of ZIP10 weighing 52.5 kDa (57.5 minus 5). This is demonstrated in the schematic in figure 4.18. Using the compute pI/Mw tool it was possible to determine that this fragment would be the product of proteolytic cleavage at approximately residue 357 (figure 4.18), immediately upstream of the *CPALLY* motif. There were no predicted cleavage sites in this region (table 3.1), suggesting that the cleavage may be part of the degradation of ZIP10 due to abnormal folding and/or function. The western blot data suggest that the abnormal 57.5 kDa band (52.5 kDa without the V5 tag) is the dominant form of recombinant ZIP10 when S546 is mutated to alanine, suggesting this residue is potentially important in ZIP10 regulation.

4.4.8. ZIP10 interaction with PKA, PIM1 and PIM3

The data presented in this chapter so far suggest that ZIP10 may undergo regulation by phosphorylation on S546. The initial software analysis predicted that this residue is phosphorylated in mitosis as well as G1. Since these two phases border each other in the cell cycle it is plausible that S546 is phosphorylated in mitosis and the phospho-residue remains throughout G1 until dephosphorylation. Therefore, the kinase responsible for phosphorylation is expected to be active in mitosis.

PKA (protein kinase A), PIM1 and PIM3 were all predicted to phosphorylate S546 (table 4.1). To investigate whether any of these kinases interact with ZIP10 in mitosis, WT ZIP10 and the S546A mutant constructs were transfected into MCF7 cells with or without nocodazole. The cells were lysed, and the recombinant protein immunoprecipitated with an anti-V5 antibody. The immunoprecipitated proteins were analysed for PKA, PIM1 and PIM3 by SDS-PAGE and western blot (figure 4.19).

In the cells transfected with the S546A mutant, the amount of PKA and PIM1 that precipitated with the recombinant protein did not appear to be different to that of the cells transfected with WT ZIP10 (figure 4.19). An abundance of PIM3 immunoprecipitated with WT ZIP10 in both control and mitotic populations, as well as the control S546A mutant. However, the amount of PIM3 that immunoprecipitated with the S546A mutant was substantially decreased following treatment with nocodazole (figure 4.19; pink box). These data suggest that PIM3 interacts with ZIP10 serine residue 546 in mitosis. Further experimental research will determine whether this decrease in PIM3 interaction with the ZIP10 mutant compared with WT ZIP10, is significant, and synchronisation of this cell

population in G1 will determine whether the interaction occurs only in mitosis or not. It seems likely that ZIP10 is phosphorylated by PIM3 on S546 in mitosis, and that the modification remains in place through G1.

Figure 4.18. Abnormal ZIP10 cleavage in S546A mutant

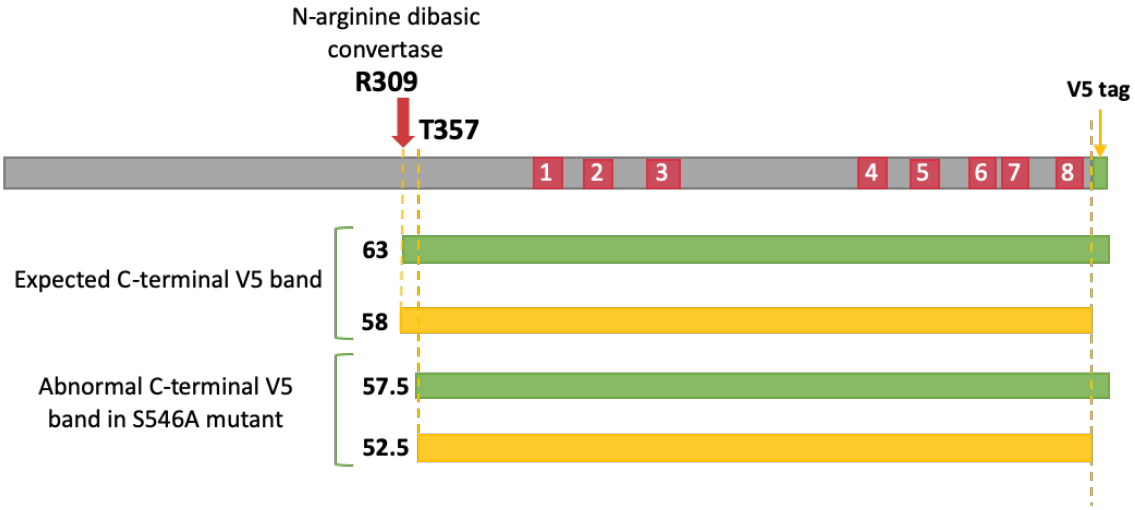

The potential ZIP10 cleavage site of the 57.5 kDa S546A ZIP10 band was determined using Compute pI/Mw (Bjellqvist et al., 1993). The green bands represent the full size of the band detected on western blot, and the yellow bands are the actual mass of the ZIP10 fragment with the 5 kDa when the 5 kDa V5 tag has been taken into account. The protease predicted to cleave ZIP10 at R309 is highlighted with the pink arrow.

Figure 4.19. Recombinant ZIP10 interaction with PKA, PIM1 and PIM3

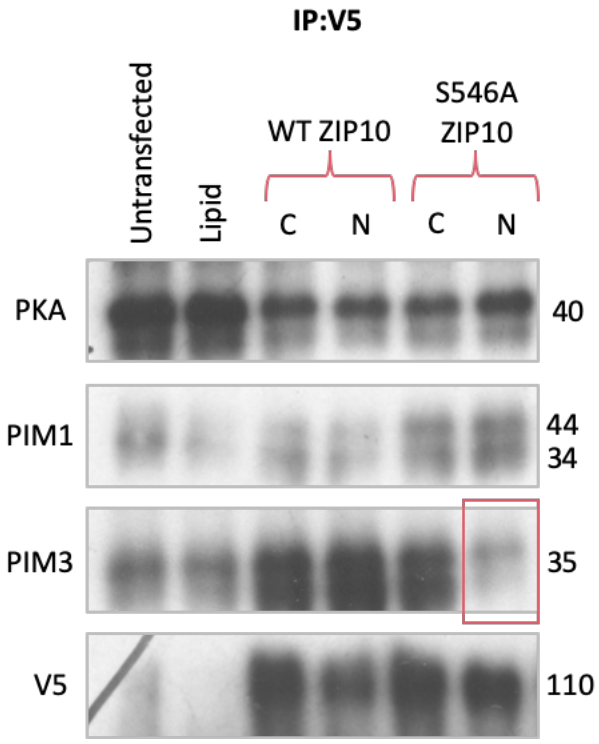

MCF7 cells were transfected with either WT ZIP10 or the S546A mutant ZIP10 and cells were treated with nocodazole (N) or left untreated (C, control). The recombinant protein was immunoprecipitated using an anti-V5 antibody and analysed by SDS-PAGE and western blot. Antibodies against total-PKA, -PIM1 and -PIM3 were used to detect PKA, PIM1 and PIM3 association with recombinant ZIP10 (n = 1). An antibody against V5 was used to confirm sucessful immunprecipitaiton of the recombinant protien. Numbers represent the molecular mass of protein bands in kDa. Decreased PIM3 association with the S546A mutant ZIP10 in mitosis is highlighted in the pink box.

4.5. Discussion

4.5.1. Location of ZIP10 phosphorylation sites

The focus of this chapter was a detailed investigation into the regulation of ZIP10 by phosphorylation, a modification that can change the conformation of a protein and subsequently its interaction with several proteins in multiple signalling pathways (Ardito *et al.*, 2017). The initial database search of the human ZIP10 protein sequence identified phosphorylation sites in two specific areas; the extracellular N-terminus, and the intracellular loop between TMD3 and TMD4. This supports the evidence in the previous chapter that the N-terminus and long intracellular loops are key regions involved in the regulation of ZIP10 activity; most of the predicted cleavage sites were also in these regions.

Extracellular phosphorylation of a ZIP transporter has not been studied before, however there were four residues in the N-terminus of ZIP10 predicted to be phosphorylated (table 4.1). It is important to note that each of the residues had only 1 record citing mass spectrometry data and they may be false 'hits'. If they are genuine phosphorylated residues of ZIP10, the process of phosphorylation must be considered. Proteins which are targeted to the plasma membrane or are secreted, commonly undergo phosphorylation in the Golgi lumen (Capasso *et al.*, 1989), though extracellular kinase activity has also been detected (Redegeld, Caldwell and Sitkovsky, 1999). It is unclear at which point in the secretory pathway ZIP10 undergoes N-terminal phosphorylation, or the role this plays in its regulation, though it may be linked to the widely speculated interaction of ZIP transporter N-termini with TMD5 (chapter 1). It is possible that phosphorylation of residues in the N-terminus alters the tertiary structure of the transporter on the outside of the cell either to activate or inactivate the transporter. In the previous chapter, it was demonstrated that ZIP10 undergoes N-terminal ectodomain shedding, which may also be linked to N-terminal phosphorylation. Since cleaved extracellular fragments of membrane-bound proteins have been found in phosphorylated form (reviewed by Klement and Medzihradszky, 2017), it is possible that further analysis of the ZIP10 ectodomain will reveal a phosphorylated residue within the fragment. Fibroblast growth factor 23 is regulated by the balanced crosstalk of glycosylation, phosphorylation and proteolytic cleavage by proprotein convertase (Tagliabracci *et al.*, 2014), highlighting how protein activity is carefully managed by a series of events each dependent on the previous event. ZIP10 undergoes both glycosylation and proteolytic cleavage in the extracellular N-terminal domain, so it is possible that phosphorylation could occur here, too.

The second region of phosphorylation in the ZIP10 protein is the intracellular loop between TMD3 and TMD4. Not only is this the site for the activating phosphorylation of ZIP7 (Taylor *et al.*, 2012), seven members of the LIV-1 family of ZIP transporters have predicted phosphorylation sites in this region (table 4.5) highlighting the conserved importance of this region in the regulation of this family of transporters. The long intracellular loop of ZIP4 senses intracellular zinc to regulate plasma membrane levels of ZIP4 (Bafaro *et al.*, 2015), so clearly this region is key to the ability of ZIP transporters to maintain zinc homeostasis, and phosphorylation in this region may be crucial to this function.

4.5.2. Close proximity of several ZIP10 phosphorylation sites

In ZIP10, 11 phosphorylation sites were identified in the long intracellular loop between TMD3 and TMD4, all of which were positive for mass spectrometry data. The prediction of phosphorylation of several residues by mitotic kinases (e.g. CDK1, PLK1 and PIM kinases) indicates that more than one site may be phosphorylated during mitosis and their close proximity suggests that ZIP10 may also be subject to hierarchical phosphorylation. This is the process by which phosphorylation of a protein on one residue, known as a 'priming phosphorylation' allows a second phosphorylation to occur on another residue of the same protein. For example, CK2 phosphorylation of glycogen synthase does not affect enzyme activity but is essential for the subsequent phosphorylation by GSK3 (Picton *et al.*, 1982), which leads to complete enzyme inactivation. In this case, CK2 acts as the 'priming' kinase. In addition, CK2 phosphorylates stem loop binding protein only after it has been phosphorylated by the CDK1/cyclin B complex (Koseoglu, Graves and Marzluff, 2008). Here, CK2 acts as the 'primed' kinase, as the substrate has been primed for CK2 phosphorylation (figure 4.20). PLK1 is the priming kinase involved in the phosphorylation of the DNA repair protein RAD51, which is subsequently phosphorylated by CK2 (Yata *et al.*, 2012). PLK1 can also act as the primed kinase in the phosphorylation of vimentin, a cytoskeletal protein which undergoes significant reorganisation in mitosis. Vimentin is first phosphorylated by CDK1 before subsequent modification by PLK1 (Yamaguchi *et al.*, 2005). ZIP10 is predicted to be phosphorylated by each of the kinases mentioned here (CK2 [S556, S573, T583], GSK [S539], CDK1 [S539, S591], PLK1 [S539, T540, S570]) implicating a possible role for hierarchical phosphorylation in the activation of ZIP10.

Table 4.5. TMD3–4 ICL phosphorylation sites in members of the LIV-1 family of ZIP transporters

ZIP	No. of residues with predicted phospho-sites in TMD3–4 ICL	No. of records citing MS data
4	2	2
5	1	2
6	13	248
7	4	51
8	3	5
10	11	62
14	5	10

Phospho-sites in the intracellular loop between TMD3 and TMD4 of the LIV-1 family of ZIP transporters were predicted using PhosphoSitePlus® (Hornbeck et al., 2004). The number of records citing MS data is the collective number of citations for all sites listed. ICL, intracellular loop; MS, mass spectrometry; No., number.

Figure 4.20. Hierarchical phosphorylation by CK2

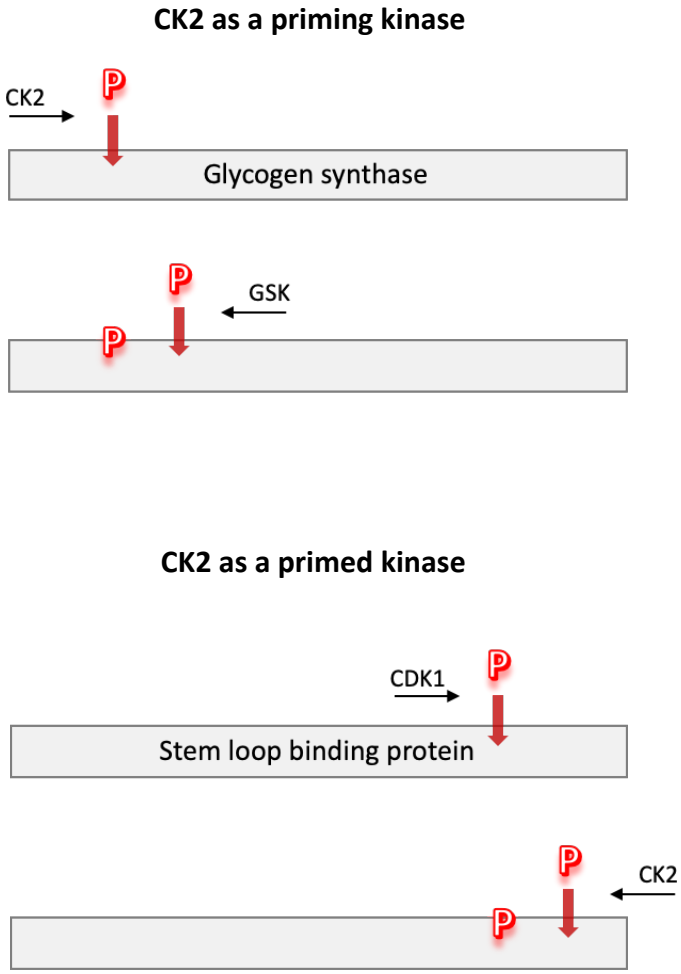

CK2 phosphorylates glycogen synthase to prime glycogen synthase for phosphorylation by GSK. In contrast, stem loop binding protein is first phosphorylated by CDK1 before recognition by CK2 which acts as the primed kinase in this case.

The consensus sequence for CK2 phosphorylation is *S/T-X-X-D/E*, where *S/T* is the phosphorylated residue, and *X* is any amino acid (St-Denis *et al.*, 2015). However, a phospho-serine can replace the acidic residue in the +3 position (D/E), allowing CK2 to phosphorylate a protein in a hierarchical manner (W. Litchfield *et al.*, 1990). The consensus sequence for CK2 phosphorylation is then *S/T-X-X-pS* where *pS* is the primed serine phosphorylation that CK2 recognises and *S/T* is the residue that CK2 subsequently phosphorylates. A phospho-threonine (*pT*) replacement of the +3 residue does not allow CK2 hierarchical phosphorylation. The human ZIP10 protein sequence contains three potential CK2 phosphorylation sites in the intracellular loop between TMD3 and TMD4 (figure 4.21). The consensus sequences for each of the CK2 phosphorylation sites were analysed for serine in the +3 position though there were none present (figure 4.21; grey circle). This suggests that, if CK2 is involved in hierarchical phosphorylation of ZIP10, it may act as the 'priming' kinase, allowing further phosphorylation to take place by another kinase.

The involvement of CK2 in ZIP transporter signalling pathways is an important finding, due to the known role of CK2 in promoting cell survival (Piazza *et al.*, 2012). Protein expression of CK2 is increased in cancers such as breast (Landesman-Bollag *et al.*, 2001), prostate (Yenice *et al.*, 1994) and lung (Daya-Makin *et al.*, 1994). The CK2 inhibitor, CX-4945 with anti-tumour efficacy in mice (Siddiqui-Jain *et al.*, 2010; Pierre *et al.*, 2011) is currently being used in phase I and II clinical trials for a novel cancer therapeutic (Clinicaltrials.gov identifier: NCT02128282). It is possible that one of the mechanisms of action of CX-4945 is through inhibition of zinc signalling pathways in which ZIP7, ZIP6 and/or ZIP10 are also involved.

The prediction of phosphorylation of ZIP10 on two adjacent residues, S539 and T540, echoes that which has been shown in ZIP7; phosphorylation of S275 and S276 activates the transporter to release zinc from intracellular stores (Taylor *et al.*, 2012), and that which has been predicted in ZIP6 (table 4.3). This is further evidence of the similarities between ZIP7, ZIP6, and ZIP10, the most widely studied ZIP transporters for their association with cancer. To investigate the double phosphorylation of ZIP10 in more detail, a mutant recombinant ZIP10 plasmid has been made, in which S539 and T540 have both been mutated to alanine (S539A/T540A) (appendix 10). This construct will be used to determine the effect of ZIP10 phosphorylation status in mitosis, and binding of ZIP10 to the PLK1 family of kinases, predicted to phosphorylate both residues.

Figure 4.21. Predicted ZIP10 phosphorylation by CK2

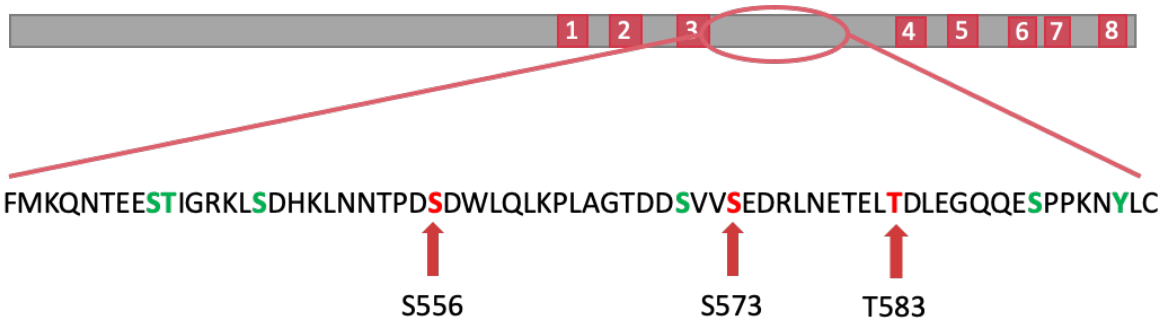

Residue	+1	+2	+3
S556	D	W	L
S573	E	D	R
T583	D	L	E

ZIP10 phosphorylation sites in the long intracellular loop are highlighted in red. Residues in green are predicted to be phosphorylated but not by CK2. Sites which are predicted to be phosphorylated by CK2 are indicated with arrows. The consensus sequence of these three sites has been analysed further, in particular to determine whether a serine is present in the +3 position (circled).

4.5.3. Phosphorylation of ZIP10 by cell cycle kinases

The potential phosphorylation of ZIP10 by several kinases involved in cell cycle regulation (e.g. CDK, PIM, PLK), as evidenced in table 4.1, is a strong indication that ZIP10 may have a role in cell cycle regulation. The PLA data in this chapter have evidenced the binding of PLK1 and ZIP10 in mitosis. During late G2 and prophase, PLK1 is located at the centrosomes where it recruits centrosome proteins such as ɣ-tubulin (Donaldson *et al.*, 2001; Morris *et al.*, 2017). Later in mitosis, PLK1 localises to the kinetochore (Ahonen *et al.*, 2005), a complex of proteins involved in attaching the chromatids to the mitotic spindle. It is interesting that the data in the previous chapter indicated the interaction of ZIP10 with at least three other proteins involved in the kinetochore; Borealin, centromere protein O (CENPO) and KIF18A. There is growing evidence to suggest the interaction of ZIP10 with several proteins involved in pathways including mitotic spindle assembly and chromosome stabilisation.

The PLA data presented here also showed that ZIP10 interacts with CDK1 in mitosis. Together with the high number of references that cited S591 phosphorylation and the prediction of phosphorylation of this residue by CDK1, it is probable that the interaction of these two proteins in mitosis is due to CDK1 phosphorylation of ZIP10. In fact, one of the references which cited S591 phosphorylation using mass spectrometry looked specifically at nocodazole-treated cells (Franz-Wachtel *et al.*, 2012) and another cited significant upregulation of this phospho-site in mitosis (Yamazaki, Kosako and Yoshimura, 2020). Furthermore, the breast cancer cells expressing the S591A mutant construct had a lower zinc content and less pS^{727}STAT3 compared with the cells expressing WT ZIP10, implicating S591 phosphorylation as an activating modification of ZIP10 in mitosis.

The software analysis revealed that CDK1 phosphorylates condensin complex I at the onset of mitosis (Kimura *et al.*, 1998). Condensin complex I is a complex of proteins associated with the chromatids in mitosis. It is present in the cytoplasm until the end of prophase when the nuclear membrane breaks down and it can access the nuclear material (Gerlich *et al.*, 2006). Interestingly, the regulatory subunit of this complex is NCAPH (Kim *et al.*, 2019), also shown to interact with ZIP10 (table 3.3; Hein et al., 2015). It is possible that CDK1 phosphorylates both condensin complex I and ZIP10 simultaneously during prophase. It is expected that ZIP10 would be active before prophase however, and therefore this phosphorylation may deactivate ZIP10. Furthermore, CDK1 phosphorylates STAT3 on serine 727 in mitosis (Shi *et al.*, 2006), another protein with which the ZIP6/ZIP10 heteromer interacts (Nimmanon *et al.*, 2020). The diagram in figure 4.22 highlights the interactions of

ZIP10 with other proteins in mitosis, using both experimentally confirmed data and database predictions. Proximity ligation assay and immunoprecipitation are useful tools to explore more of these interactions in the future.

4.5.4. Phosphorylation of ZIP10 in G1

Zinc is required at different timepoints in the cell cycle (Chesters, Petrie and Vint, 1989; Chesters and Petrie, 1999; Haase and Maret, 2003) and analysis of intracellular zinc fluctuations by Li and Maret (2009) determined that there are two large influxes of zinc in the cell cycle. The first influx of zinc is in G1 (figure 4.23), and comes from an extracellular source, implicating a ZIP transporter on the plasma membrane in G1. If the zinc requirement in G1 is not satisfied, cells are unable to move into S phase (Chesters, Petrie and Vint, 1989). It is particularly interesting that the PHOSIDA software strongly predicted ZIP10 phosphorylation in G1 (and mitosis) (figure 4.23) and that the synchronisation of cells in G1 led to a significant increase in the 68 kDa ZIP10 band detected with the ZIP10 L5 antibody. Western blot data from the previous chapter indicated that this 68 kDa ZIP10 fragment was generated from cleavage at approximately residue R637 in the long intracellular loop and encompasses most of the N-terminus and TMDs1–3 (figure 3.5). The significant increase in this band in G1 suggests that, following ectodomain shedding of the N-terminus (approximately 45 kDa) at the start of mitosis, the remaining protein (containing all 8 transmembrane domains and the C-terminus; approximately 50 kDa) is internalised and degraded. The full-length protein is then re-made and localised to the plasma membrane in G1 at which time cleavage at R309 occurs (figure 4.24).

Figure 4.22. ZIP10 interaction with mitotic proteins

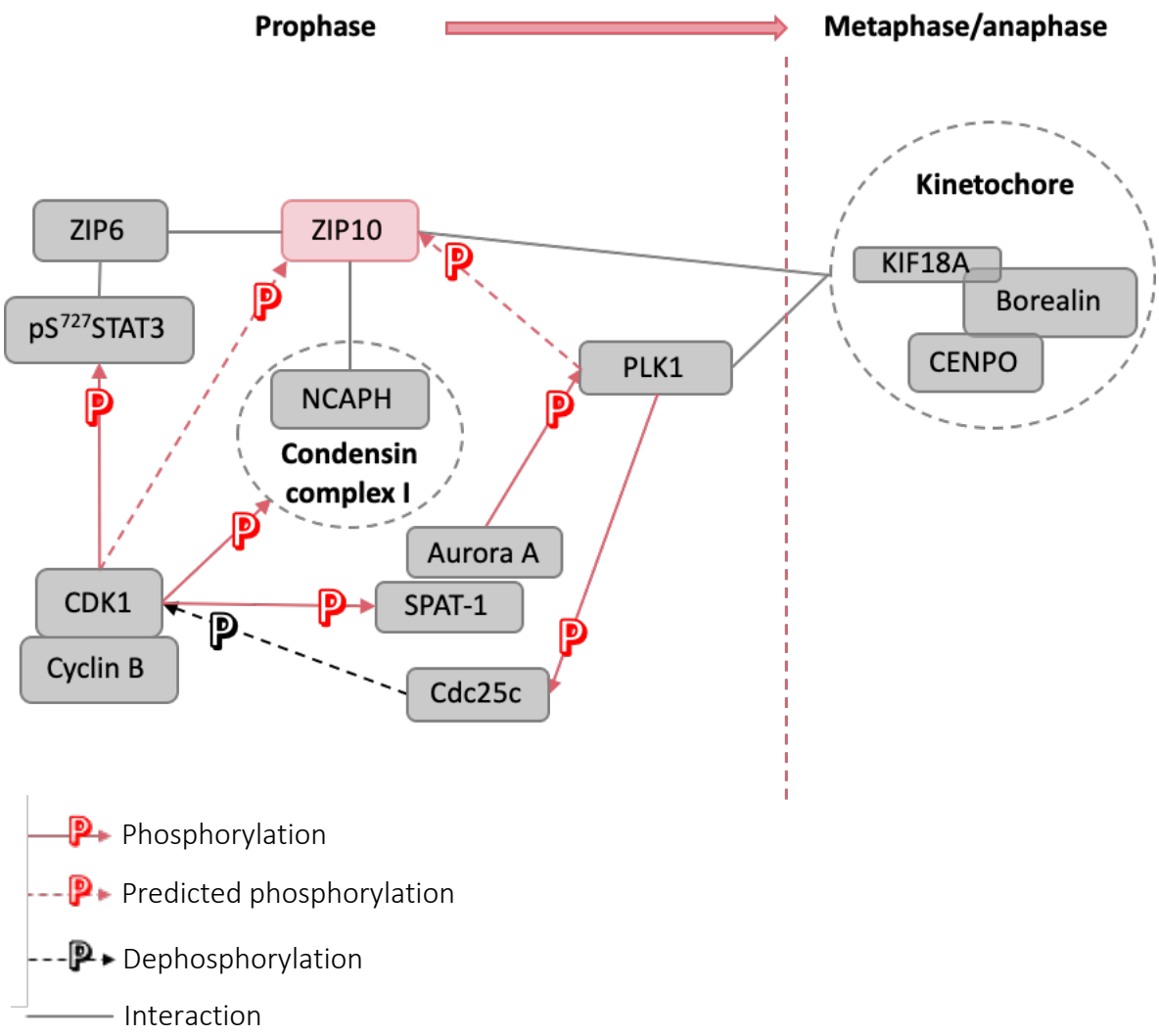

Interaction of ZIP10 with mitotic proteins and predicted interactions from the data presented in this project so far. ZIP10 interacts with ZIP6, STAT3, KIF18A, CENPO, Borealin, and NCAPH, and is predicted to be phosphorylated by PLK1 and CDK1. PLK1 and CDK1 regulate themselves through activation of Cdc25c (Toyoshima-Morimoto, Taniguchi and Nishida, 2002), and the activation of the SPAT1/Aurora A complex (Tavernier, Noatynska, *et al.*, 2015; Tavernier, Panbianco, *et al.*, 2015).

Phosphorylation of ZIP10 S546 may promote a conformational change that reveals the R309 cleavage site to the appropriate protease, thus S546 phosphorylation causes ZIP10 cleavage. In addition, it is particularly interesting that in cells expressing the S546A mutant, there was a significant increase in a previously unseen V5 band at 57.5 kDa after recovery from nocodazole for 6 hours. It is possible that, at a time when S546 would normally be phosphorylated to activate ZIP10 cleavage, if the phospho-site is unavailable the cleavage site is not exposed and therefore ZIP10 becomes cleaved at approximately T357 instead. Furthermore, there is a major requirement for zinc in cells approximately 8 hours into G1 (Chesters, Petrie and Vint, 1989) which is close to the time that the MCF7 cells were in this experiment.

The second influx of zinc is measured in S phase and comes from an intracellular source (Li and Maret, 2009), implicating a ZIP transporter on an intracellular membrane. PHOSIDA predicts the phosphorylation of ZIP7 residues S275 and S276 at the G1/S transition with a prediction score of 3.03 (figure 4.23), higher than the score for ZIP7 phosphorylation of S275/S276, which has been proven (Taylor *et al.*, 2012). The phosphorylation of these residues activates ZIP7-mediated zinc release from the endoplasmic reticulum (Taylor *et al.*, 2012). Together, the evidence suggests the cyclic regulation of intracellular zinc through the orchestrated activity of ZIP transporters ZIP7 and ZIP10 and this is supported by the data presented in this chapter that implicate ZIP10 phosphorylation and regulation in G1.

ZIP10 serine 546 was predicted to be phosphorylated by the PIM family of serine/threonine kinases or PKA. The immunoprecipitation data presented in this chapter indicate reduced interaction of PIM3 with recombinant mutant ZIP10 (S546A) in mitosis. PIM3 inhibits tumour suppressor protein $p27^{KIP1}$ by phosphorylation, preventing its binding to the cyclin E/cdk2 complex, and allowing cells to move through the G1/S phase transition of the cell cycle (Sheaff, Groudine and Roberts, 1997). In addition, PIM3 is linked to cancer development through its ability to inhibit apoptosis pathways (Fujii *et al.*, 2005; Li *et al.*, 2006; Popivanova *et al.*, 2007). Further residues in ZIP10 were predicted to be phosphorylated by PIM kinases (S323, S539 and S570) suggesting there may be a more prominent role for ZIP10 in cell survival through PIM signalling pathways.

Figure 4.23. ZIP transporter phosphorylation and zinc fluctuations throughout the cell cycle

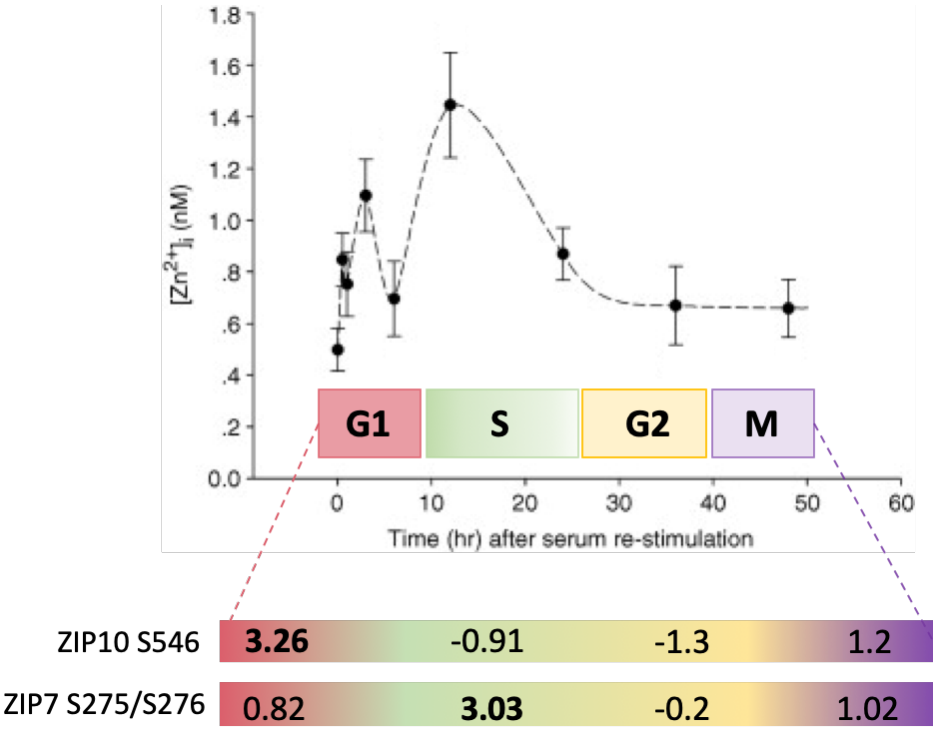

Intracellular zinc levels in PC12 (rat adrenal) cells measured at different time points following re-stimulation with serum (Li and Maret, 2009). *The graph has been overlaid with the phase of the cell cycle that the cells are in, and the phosphorylation prediction score for S546 (ZIP10) and S275/S276 (ZIP7) at each stage. Prediction scores were taken from PHOSIDA* (Gnad *et al.*, 2007). *Graph adapted from* Li and Maret (2009).

Figure 4.24. ZIP10 cleavage in mitosis and G1

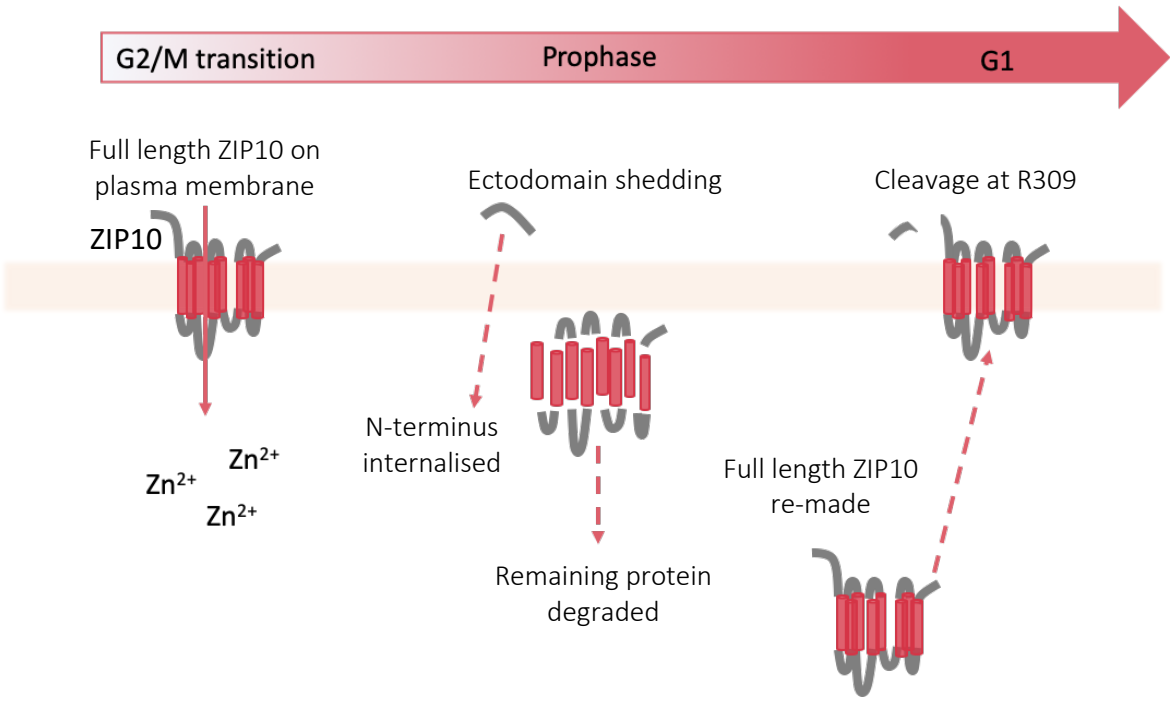

Proposed regulation of ZIP10 through the G2/M transition, and the M/G1 transition. ZIP10 is predicted to undergo ectodomain shedding in prophase to stop zinc influx, following which the rest of the ZIP10 protein is degraded. In G1, the full length of ZIP10 is re-made, and returned to the plasma membrane before cleavage at approximately residue R309.

4.5.5 Tyrosine phosphorylation of ZIP10

Tyrosine phosphorylation of members of the LIV-1 family of ZIP transporters has not yet been proven, despite its prediction in not only ZIP10, but ZIP4, ZIP6, ZIP12 and ZIP14 also (table 4.4). It is astounding to find that ZIP6 residue Y528 has over 100 citations for phosphorylation, by mass spectrometry, and another tyrosine residue in close proximity (Y531) has over 60. These data represent an exciting opportunity to explore a new mechanism of ZIP transporter regulation. Zinc causes widespread tyrosine phosphatase inhibition (Haase and Maret, 2003) which leads to the hypothesis that, if ZIP10 is activated by tyrosine phosphorylation, zinc entry into the cell via ZIP10 could inhibit the phosphatase responsible for ZIP10 de-activation, prolonging the activation of ZIP10 itself, and leading to further zinc influx (figure 4.25). This is another example of how ZIP10 may regulate its own activity, this time through a positive feedback loop.

This hypothesis of '*zinc-induced zinc influx*' echoes a similar process in which calcium promotes calcium release from intracellular stores, by binding the ryanodine receptor on the membrane of the endoplasmic or sarcoplasmic reticulum (Endo, 2009). Since the revelation that zinc acts as a second messenger in the cell (Yamasaki *et al.*, 2007) there has been growing evidence that zinc and calcium act in a similar way across multiple cell signalling pathways. In the myocardium, an action potential changes the electrochemical gradient of calcium across the membrane which triggers a cellular response and it has been speculated that zinc acts in a similar manner (Pitt and Stewart, 2015). The phosphorylation of ZIP10 Y596 would be interesting to explore in the future, using a recombinant phospho-ablative mutant.

Figure 4.25. ZIP7/ZIP10-mediated zinc induced zinc release

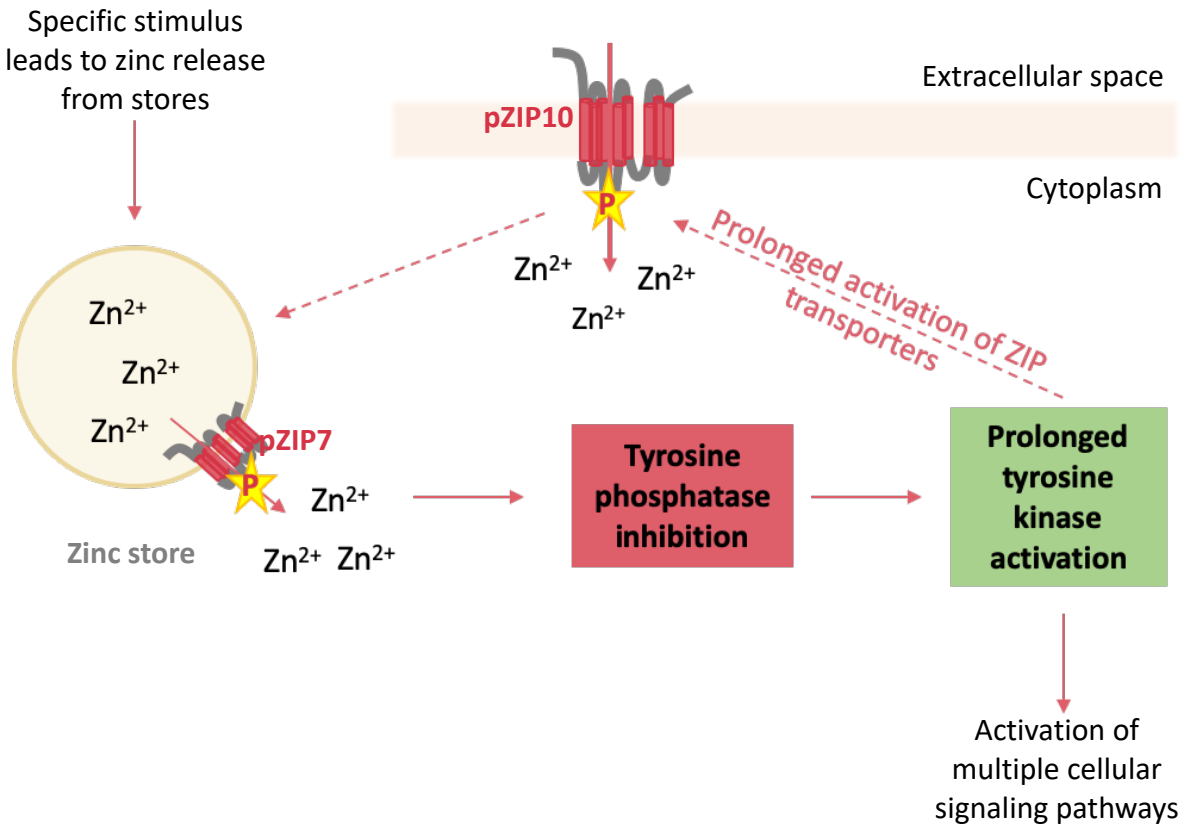

A stimulus that leads to zinc release from stores via activated ZIP7 causes widespread tyrosine phosphatase inhibition. Simultaneously, ZIP10 is activated by tyrosine phosphorylation on Y596 which is prolonged due to the inhibition of the tyrosine phosphatase responsible for its dephosphorylation. This positive feedback loop leads to an increase in intracellular free zinc ions within the cell which could activate multiple signalling pathways.

4.5.6. Chapter summary and conclusions

In this chapter, database analysis of ZIP10 phosphorylation sites has identified several potential phosphorylation sites of interest in the long intracellular loop between TMD3 and TMD4. Site-directed mutagenesis of S591 in a recombinant ZIP10 construct and FACS analysis indicated that S591 phosphorylation activates ZIP10 in mitosis leading to zinc influx and S727 phosphorylation of STAT3. Proximity ligation assay data highlighted the binding together of ZIP10 with CDK1 in mitosis, which, together with the data from the software analysis makes CDK1 a likely candidate for phosphorylation of ZIP10 S591 in mitosis. Proximity ligation assay and immunoprecipitation also highlighted binding together of ZIP10 and activated PLK1 in mitosis; PLK1 is a likely candidate for phosphorylation of ZIP10 S539, T540 and S570. The potential double phosphorylation of S539 and T540 was also discussed. Synchronisation of breast cancer cells in G1 led to some interesting findings regarding ZIP10 proteolytic cleavage in G1. ZIP10 phosphorylation of S546 is predicted in G1 and a potential candidate kinase for this phosphorylation is PIM3. Regulation of ZIP10 in G1 is supported by a model of intracellular zinc fluctuations throughout the cell cycle, in which there is a large increase of zinc during G1.

So far, this project has generated data in support of post-translational modification of ZIP10 in mitosis. Since ZIP10 has been linked to cancer development and progression, the following chapter will focus on novel antibodies targeted to ZIP10 (and ZIP6) to investigate whether ZIP transporters can be inhibited to prevent cell division and be used as a therapeutic agent in cancer treatment.

Chapter 5. Inhibition of ZIP transporter-mediated mitosis

5.1. Introduction

Intracellular zinc fluctuations throughout the cell cycle indicate a role for zinc in cell cycle control (Li and Maret, 2009), specifically in the movement from one phase of the cell cycle to the next. The cell cycle is halted at the G1/S transition by metal-chelating agent 1,10-phenanthroline, and this is reversed by the addition of zinc (Falchuk, Krishan and Sullivan, 1977). Passage through the G2/M transition is also zinc-dependent (Chesters, Petrie and Vint, 1989; Chesters and Petrie, 1999) and the authors of these studies suggested a role for zinc in the transcription of cyclins, a group of proteins associated with cell cycle progression (Malumbres and Barbacid, 2009). In addition, zinc is required for meiotic maturation of the oocyte (Bernhardt *et al.*, 2011, 2012), a type of cell division that occurs only in gametes. More specifically, disruption of ZIP6 and ZIP10 in oocytes causes a phenotype that reflects zinc deficiency in these cells (Kong *et al.*, 2014), highlighting the importance of ZIP6 and ZIP10 in zinc-mediated meiotic maturation.

Our group have demonstrated that MCF7 breast cancer cells undergoing mitosis have more free zinc, evidenced by increased FluoZin™-3 fluorescence intensity in mitotic cells (Nimmanon *et al*., 2020) and that ZIP6 and ZIP10 are upregulated in mitosis (Nimmanon *et al*., 2020). This evidence implicates both transporters as important regulators of zinc-mediated cell division in cancer cells as well as oocytes. Both transporters are required for epithelial to mesenchymal transition (Hogstrand *et al.*, 2013), the first stage of which is cell rounding and detachment through the loss of cell-adhesion proteins (Pickup, Novitskiy and Moses, 2013). The process of cell rounding and detachment is comparable to the first stage of mitosis (Pugacheva, Roegiers and Golemis, 2006). Taken together, these data lead to the hypothesis that ZIP6 and ZIP10 could be therapeutic targets in diseases of uncontrolled cell division including cancer.

The work in this chapter focuses on understanding the mechanism surrounding ZIP6- and ZIP10-dependent zinc entry in mitosis and investigates whether the mechanism can be inhibited using our custom-made antibodies.

5.2. Aims and objectives

The aim of this chapter is to investigate the potential for ZIP6 and ZIP10 to be therapeutic targets in cancer.

The objectives of this chapter are:

a. To determine whether anti-ZIP6 and -ZIP10 antibodies can inhibit cell division in multiple cancer cell lines

b. To determine whether long-term growth of cancer cells is suppressed in the presence of the antibodies

c. To confirm the antibodies are specific for their target proteins *in vitro*

d. To investigate how cells process the antibodies following treatment

e. To determine the effect of the antibodies on healthy, non-cancerous cells

f. To assess tumour growth in xenograft models of breast cancer in response to antibody treatment.

5.3. Methods

5.3.1. Antibody inhibition of nocodazole-dependent mitosis

To assess the ability of our in-house anti-ZIP6 and -ZIP10 antibodies (figure 2.1) to inhibit cell division, cells were treated at 70% confluency with 150 nM nocodazole, with or without anti-ZIP6, or -ZIP10 antibodies (table 2.2), or non-specific IgG control antibodies for 18 hours (table 2.3). Following treatment, cells were fixed and stained for pS^{10}Histone H3 and DAPI. For each treatment, a total of 6 fields of view were imaged. The total number of cells and the number of mitotic cells was counted, and the percentage of mitotic cells calculated. This process is outlined in figure 5.1. Cell lysates of antibody-treated cells were analysed by SDS-PAGE and western blot using antibodies targeted to pS^{10}Histone H3, pS^{727}STAT3, and HRP-conjugated GAPDH (table 2.3).

5.3.2. Antibody inhibition of cell growth

To assess the ability of the anti-ZIP10 antibody to suppress cell growth, MCF7 cells were seeded in 46-well plates (day 0). Antibody treatment was added on day 1. The medium was replaced on day 4 for the 7-day growth studies, and on day 5 for the 10-day growth studies.

5.3.3. Development and investigation of a ZIP6 KO cell line

ZIP6 knock-out cells were generated using the second generation CRISPR/Cas9 (clustered regularly interspaced short palindromic repeats/Cas9) technique (figure 5.2) by Schmitt-Ulms *et al.* at the Centre for Research in Neurodegeneration, University of Toronto, and were kindly donated to our group for use in this project. NMuMG (normal murine mammary gland) cells were transfected with a construct coding for point mutated Cas9-D10A nickase and a pair of guide RNAs that targeted the complex to specific sites in the ZIP6 gene (SLC39A6). The generation of nearby nicks in the DNA triggers the non-homologous end-joining pathway which repairs double-stranded breaks in DNA. Clones were isolated by serial dilution and western blot analysis was used to identify clones which were negative for ZIP6 following TGFβ1 (transforming growth factor beta) exposure (Brethour *et al.*, 2017). Sequencing of the gene in this clone revealed a two-nucleotide deletion and subsequent generation of a stop codon due to a shift in the open reading frame of the ZIP6 gene.

The effect of ZIP6 KO on ZIP5 was analysed by SDS-PAGE and western blot, using antibodies against ZIP5 and HRP-conjugated GAPDH (table 2.3).

5.3.4. Antibody inhibition of tumour growth *in-vivo*

Animal studies were carried out by Gillian Seaton at the School of Biosciences, Cardiff University. The work was performed in accordance with the Animals (Scientific Procedures) Act 1986 and approved by the UK Home Office (PPL 30/3433). Xenograft Athymic Nude mice were injected intraperitoneally with anti-ZIP6 antibody once tumours were a minimum volume of 4 mm^3. Antibody treatment was administered every 4 days and the tumours measured every 4 days for 20 days. Mice were harvested 20 days after their first injection.

Figure 5.1. The process of MCF7 cell antibody treatment and staining for pS[10]Histone H3

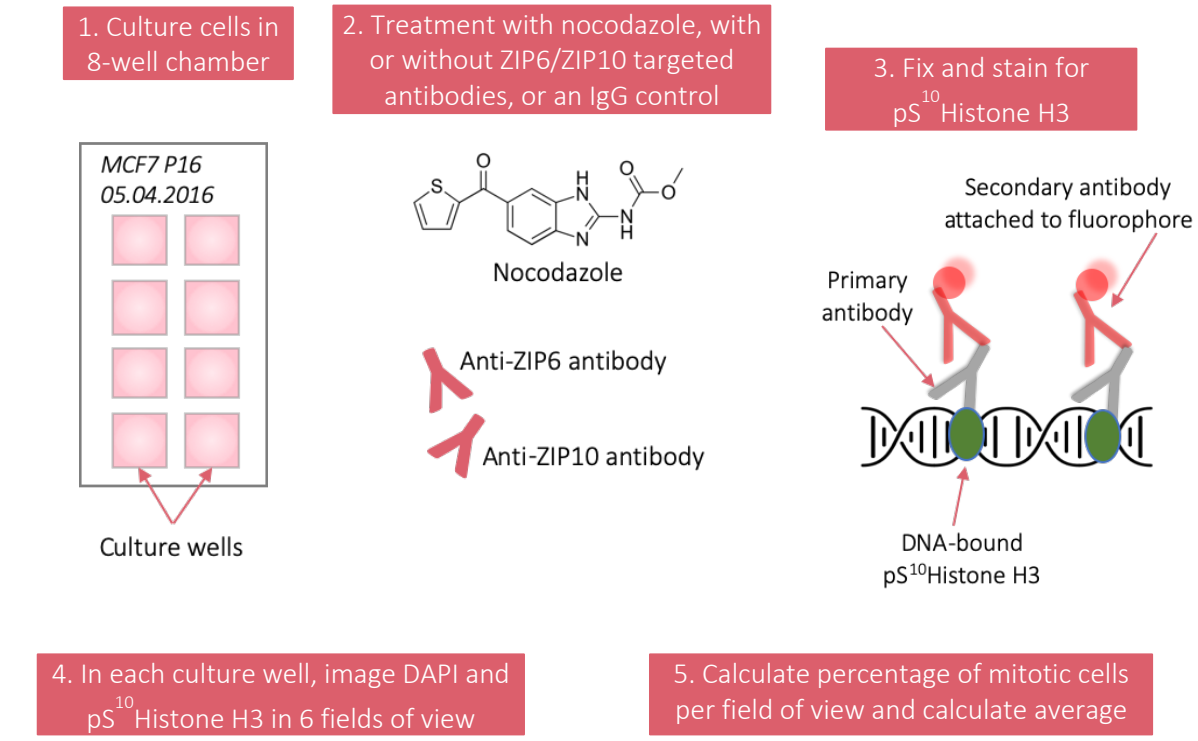

Field of view	Total cells	Mitotic cells	Percentage of mitotic cells
1	17	4	23.5
2	21	6	28.6
3			
4			
5			
6			

Cells were grown in 8-well chambers (1) and each well was treated with nocodazole, with or without anti-ZIP6 or -ZIP10 antibodies or a non-specific IgG control (2). The cells were fixed in 3.7% paraformaldehyde and stained for pS[10]Histone H3 and a fluorophore-conjugated secondary antibody (3), and DAPI to stain the cell nuclei. For details of the antibodies used, see table 2.3. Six images from different fields of view were taken from each well using an epi-fluorescent microscope (4). The total number of cells and the total number of mitotic cells was counted, and the percentage of mitotic cells calculated (5). Steps 1–5 were repeated for three separate biological repeats and the percentage of mitotic cells in each treatment group averaged.

Figure 5.2. Schematic demonstrating the CRISPR/Cas9 knock-out technique

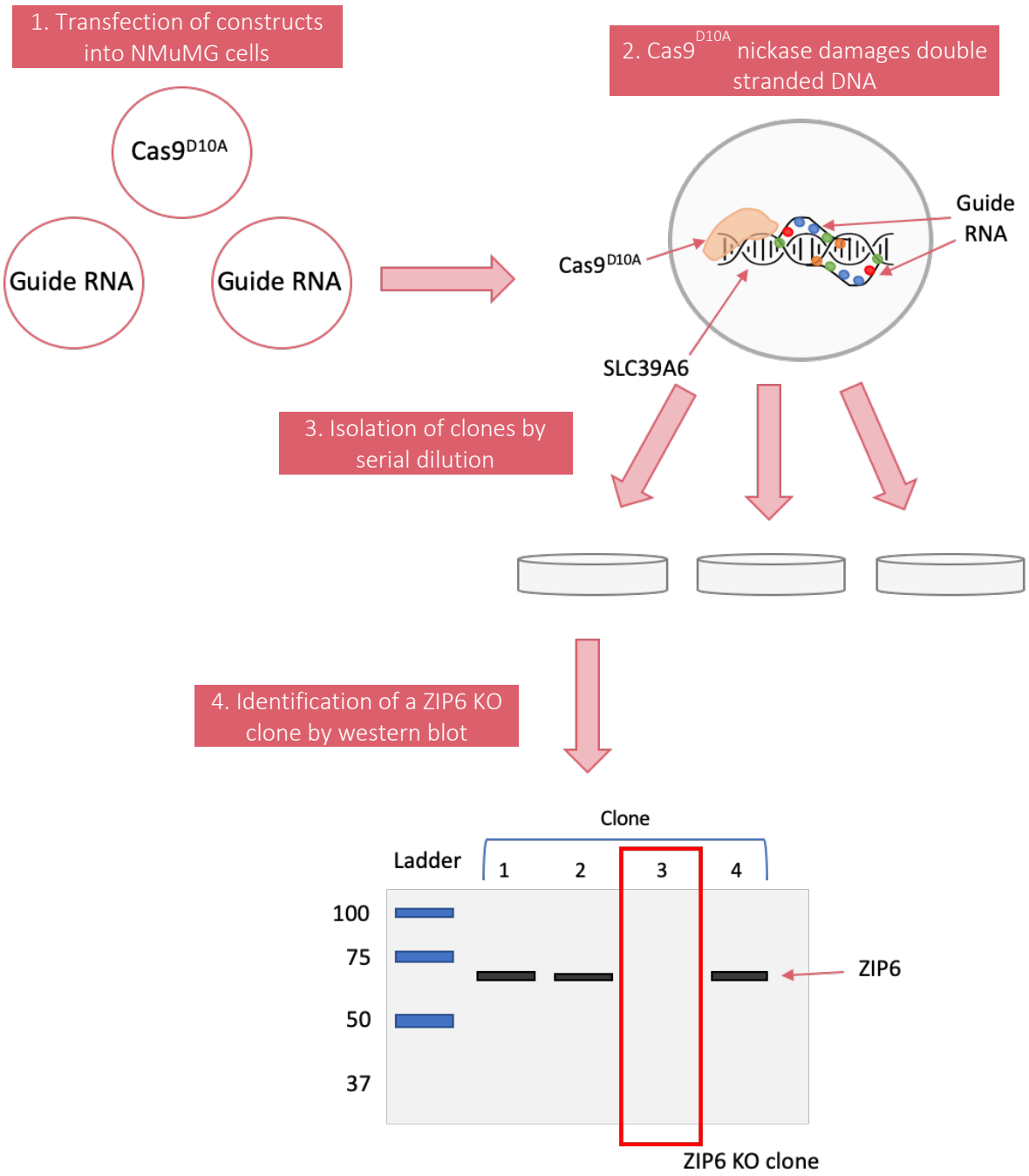

NMuMG cells are transfected with Cas9^{D10A} and guide RNA constructs that direct the Cas9 protein to the target DNA of the ZIP6 gene (SLC39A6). The Cas9^{D10A} protein causes double-stranded breaks in the DNA which the cell repairs. Isolation of different clones and western blot analysis allows the identification of a clone which does not contain ZIP6 due to the cell incorrectly repairing the damaged DNA.

5.4. Results

5.4.1. Anti-ZIP6 and -ZIP10 antibodies inhibit mitosis in MCF7 cells

To test the hypothesis that ZIP6 and ZIP10 can be targeted to inhibit cell division in cancer, MCF7 breast cancer cells were treated with nocodazole with or without the N-terminal targeted ZIP6 Y3 or ZIP10 N1 antibodies (the epitopes of these antibodies are shown in figure 2.1). The cells were stained using immunofluorescence with an antibody against pS^{10}Histone H3 to identify mitotic cells, and DAPI was used to stain all cell nuclei. The percentage of mitotic cells in each treatment group was then calculated.

5.4.1.1. Anti-ZIP6 antibody inhibition of mitosis

In the population of cells treated only with nocodazole, 27% (s = 0.3%) of cells were mitotic, compared with just 2% (s = 0.1) of cells in the untreated population (figure 5.3A-B; $p < 0.001$). The addition of the N-terminal anti-ZIP6 antibody at a range of concentrations (0.4–4 μg/mL) decreased the percentage of mitotic cells in an antibody-concentration dependent manner (figure 5.3B). 0.4 and 0.8 μg/mL antibody decreased the percentage of cells in mitosis to 18% (s = 3%) and 17.5% (s = 5%) respectively, though these were not significant. Following treatment with 2 and 4 μg/mL of antibody, the percentage of cells in mitosis was 8% (s = 3%; $p < 0.05$) and 6% (s = 2%; $p < 0.001$) respectively. At the highest concentration of antibody (4 μg/mL), statistically, the percentage of cells in mitosis was not different to the percentage of mitotic cells in the untreated population.

To confirm that the observed inhibition of mitosis with the anti-ZIP6 antibody was specifically due to ZIP6 binding of the antibody and not an aberrant effect of the IgG, the cells were treated with a normal mouse IgG antibody in the presence of nocodazole. The concentration of antibody used was 4 μg/mL to match that of the anti-ZIP6 antibody which had the greatest effect on mitosis. The percentage of cells in mitosis following treatment with the control IgG antibody was 28% (s = 3%) and this was not significantly different to the percentage of cells in mitosis with nocodazole treatment alone, confirming the observed ability of the anti-ZIP6 antibody to inhibit mitosis was due to specific binding.

Figure 5.3. Anti-ZIP6 antibody inhibition of mitosis in MCF7 cells

A.

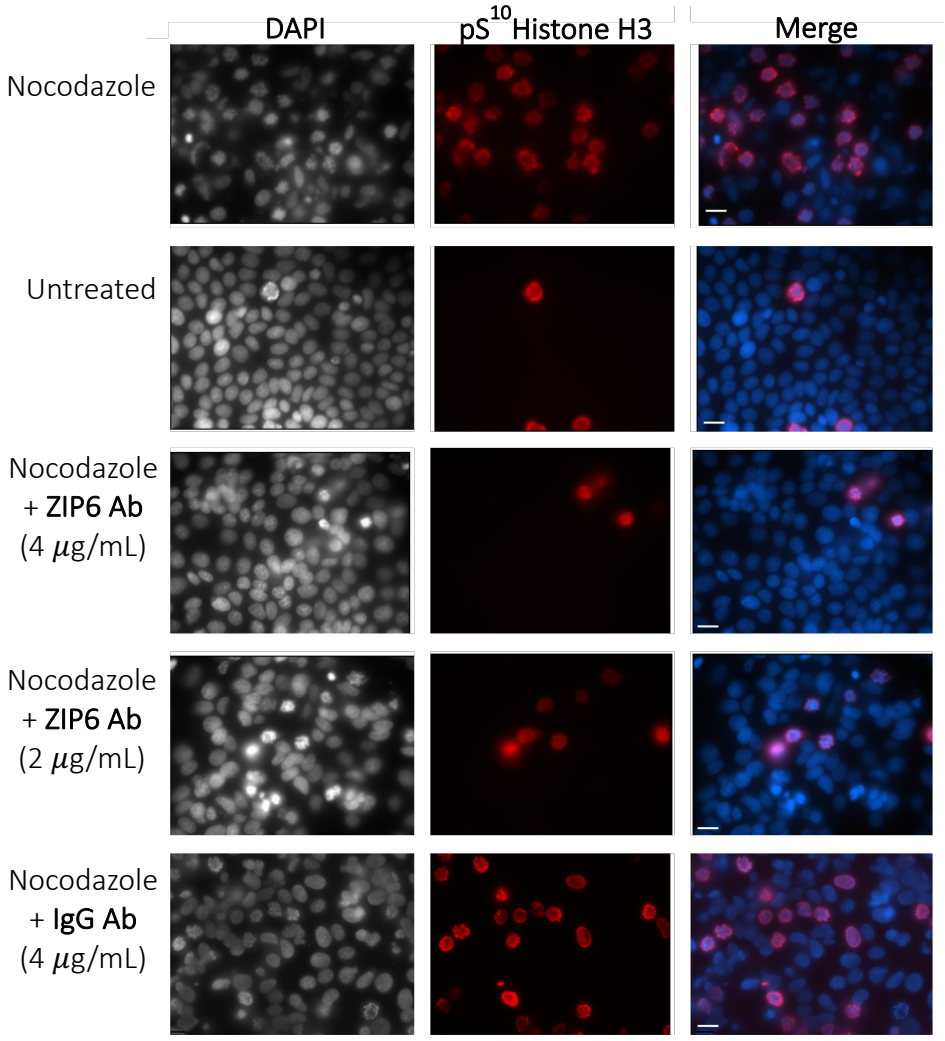

B.

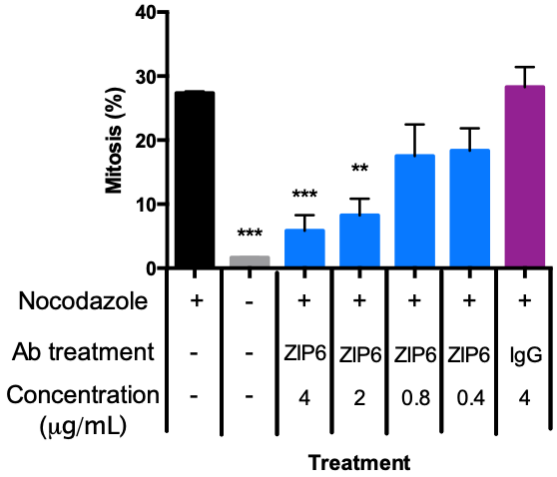

***A**. MCF7 cells were treated with 150 nM nocodazole for 18 hours with or without anti-ZIP6 (Y3) or -IgG control antibodies. The cells were stained for pS[10]Histone H3 (red) and DAPI (blue). A representative image of each population is shown. Ab, antibody. Scale bars: 10 μm.*
***B**. Percentages of cells in mitosis are presented as mean ± standard error (n = 3). Statistical significance was measured using ANoVA, comparing to nocodazole treatment alone. ** p < 0.01, *** p < 0.001.*

5.4.1.2. Anti-ZIP10 antibody inhibition of mitosis

To investigate whether the observed ZIP6 antibody inhibition of mitosis could be replicated with the N-terminal anti-ZIP10 antibody, cells were treated with the ZIP10 antibody at a range of concentrations (1–10 μg/mL) in the presence of nocodazole (figure 5.4A). The addition of the anti-ZIP10 antibody at the lowest concentrations (1 and 2 μg/mL) did not significantly affect the percentage of mitotic cells; 31.5% (s = 5%) and 19% (s = 10%) respectively, compared to 31% (s = 8%) in the cells treated with nocodazole alone (figure 5.4B). Treatment with the antibody at 5 μg/mL decreased the percentage of mitotic cells to 5% (s = 2%; $p < 0.05$) and the greatest effect was seen at 10 μg/mL which decreased the percentage of mitotic cells to 2% (s = 1%; $p < 0.01$). The latter value was not significantly different to the percentage of cells in mitosis in the untreated population. The observed inhibition of mitosis with the anti-ZIP10 antibody was antibody concentration-dependent, which was similar to the effect of the anti-ZIP6 antibody.

Following treatment of cells with a normal rabbit IgG antibody at 10 μg/mL the percentage of cells in mitosis was 19% (s = 2%; figure 5.4B). This was not significantly different from that of cells treated with nocodazole alone, confirming the observed mitotic inhibition with the anti-ZIP10 antibody was due to specific binding to ZIP10. These data show that nocodazole induced mitosis can be inhibited in MCF7 breast cancer cells by treatment with an N-terminal targeted anti- ZIP6 or -ZIP10 antibody.

Western blot analysis of the ZIP10 antibody-treated MCF7 cells (figure 5.5A) confirmed the decrease in pS^{10}Histone H3, and hence the decrease in mitosis, at 10 μg/mL ($p < 0.01$) and 5 μg/mL ($p < 0.01$) compared with the nocodazole-treated population (figure 5.5B). In addition, there was significantly less pS^{727}STAT3 in the antibody-treated populations ($p < 0.05$ for both 10 μg/mL and 5 μg/mL) compared with the nocodazole-treated population (figure 5.5C). pS^{727}STAT3 in these samples was not significantly different compared to the untreated cells. Lower amounts of pS^{10}Histone H3 (Hendzel *et al.*, 1997) and pS^{727}STAT3 (Nimmanon *et al*., 2020) is consistent with a population in which there are fewer mitotic cells, confirming the ability of the anti-ZIP10 antibody to inhibit nocodazole-induced mitosis.

Figure 5.4. Anti-ZIP10 antibody inhibition of mitosis in MCF7 cells

A.

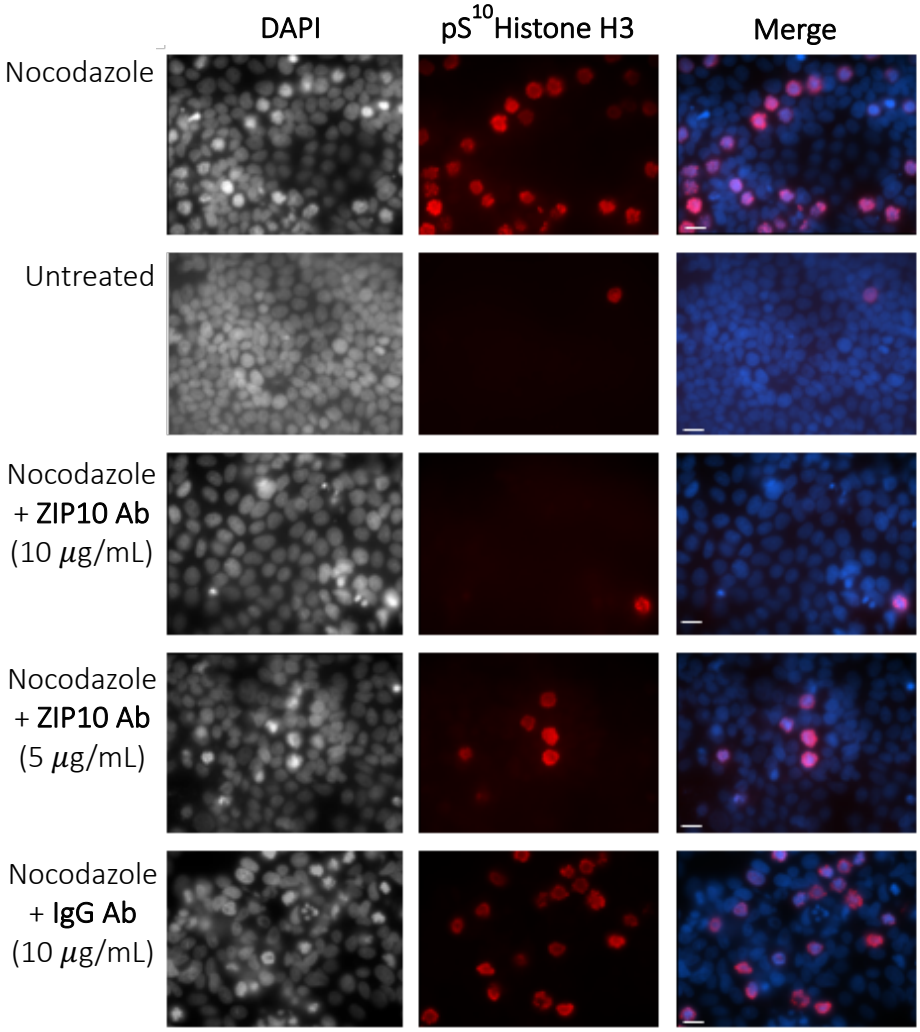

B.

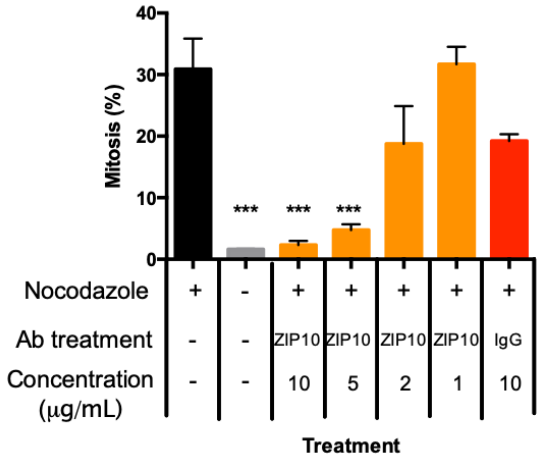

A. *MCF7 cells were treated with 150 nM nocodazole for 18 hours with or without anti-ZIP10 (N1) or -IgG control antibodies. The cells were stained for pS[10]Histone H3 (red) and DAPI (blue). A representative image of each population is shown. Ab, antibody. Scale bars: 10 μm.*
B. *Percentages of cells in mitosis are presented as mean ± standard error (n = 3). Statistical significance was measured using ANoVA, comparing to nocodazole treatment alone. * p < 0.05, ** p < 0.01, *** p < 0.001.*

Figure 5.5. Western blot analysis of anti-ZIP10 antibody treated MCF7 cells

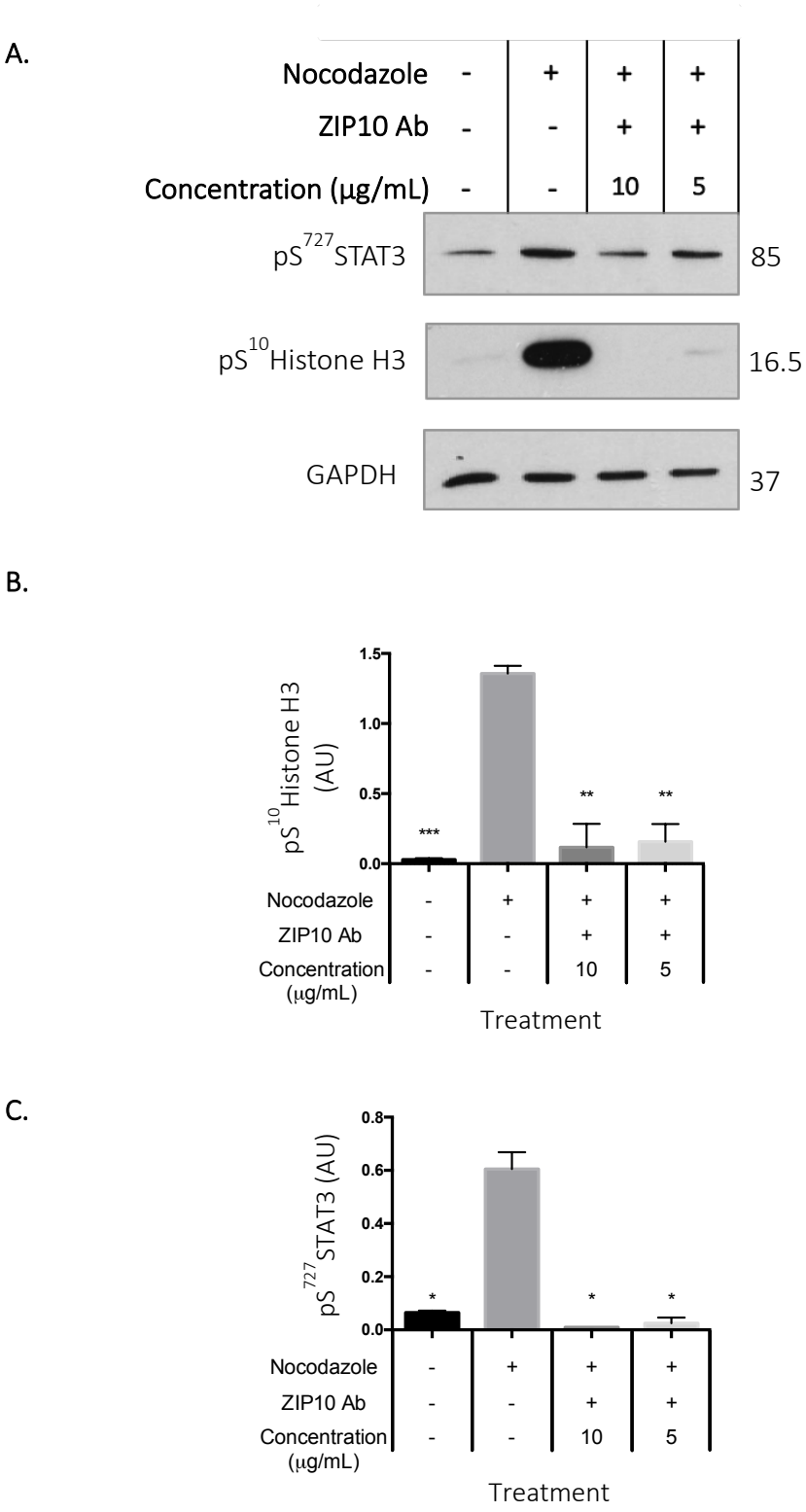

***A**. Western blot analysis of pS[10]Histone H3 and pS[727]STAT3 in anti-ZIP10 antibody-treated MCF7 cells. Numbers represent the molecular mass of protein bands in kDa. Protein expression of pS[10]Histone H3 (**B**) and pS[727]STAT3 (**C**) were normalised to GAPDH expression and are presented in a bar graph as mean ± standard error (n = 3). AU, arbitrary unit. Statistical significance was measured using ANoVA, comparing to the population treated with nocodazole alone. * p < 0.05, ** p < 0.01, *** p < 0.001.*

5.4.2. Investigation of the anti-ZIP10 antibody processing after treatment

Thus far, this chapter has demonstrated the ability of the anti-ZIP6 and -ZIP10 antibodies to inhibit nocodazole-induced mitosis in an antibody-concentration dependent manner. Data in chapter 3 showed N-terminal ectodomain shedding of ZIP10 in mitosis; therefore, it was interesting to investigate how the anti-ZIP10 antibody binding to ZIP10 in mitosis affected ectodomain shedding of ZIP10.

MCF7 cells were treated with nocodazole and the ZIP10 targeted antibody (produced in rabbit) for 18 hours and fixed with 3.7% paraformaldehyde. pS^{10}Histone H3 was stained with a mouse primary antibody (table 2.3) and an anti-mouse Alexa Fluor® 594 (red) conjugated secondary antibody. An anti-rabbit Alexa Fluor® 488 (green) conjugated secondary antibody was also used during this process, to detect the anti-ZIP10 antibody which had been used to treat the cells (figure 5.6A).

The staining demonstrated plasma membrane localisation of the anti-ZIP10 treatment antibody in non-mitotic cells (figure 5.6B-C), which were identified owing to their absence for pS^{10}Histone H3. Further analysis of the coverslip revealed punctate staining of pS^{10}Histone H3 in the nucleus of cells which were positive for the anti-ZIP10 antibody (figure 5.6D), indicating that the full-size ZIP10 protein is present on the plasma membrane before the onset of mitosis, and at the same time serine 10 phosphorylation of Histone H3 is initiated, in late G2 (Hendzel *et al.*, 1997). The mitotic cells in figures 5.6B and 5.6D (labelled with white arrows) are negative for ZIP10, which could indicate that (a) the ectodomain has already been shed before the antibody was able to bind during treatment, or (b) antibody binding caused degradation of ZIP10 because the protein was no longer functional.

Figure 5.6. Immunofluorescent staining of the anti-ZIP10 antibody in MCF7 cells

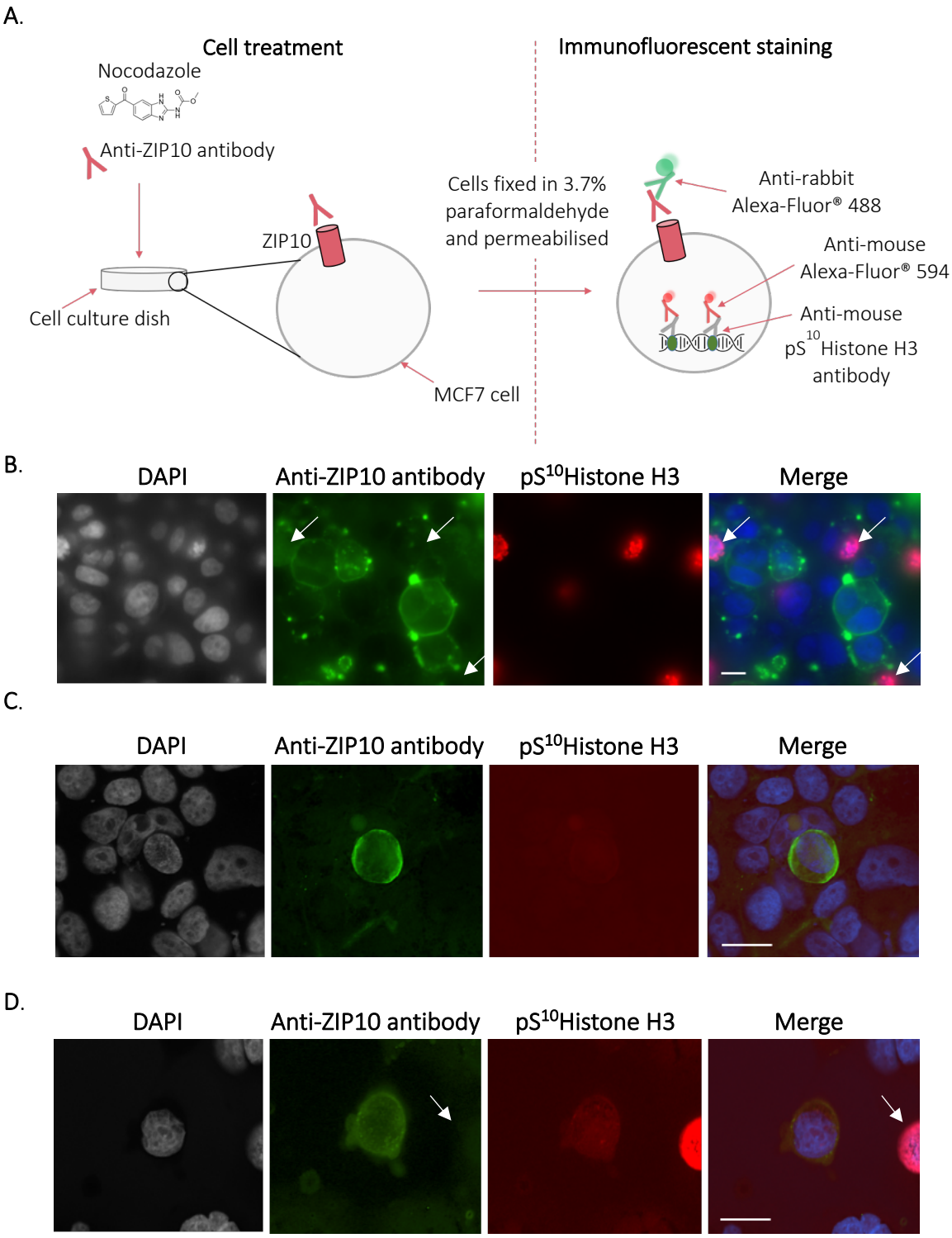

A. *The process by which the anti-ZIP10 antibody (rabbit) was detected following treatment of MCF7 cells for 18 hours. A mouse primary antibody was used to detect pS[10]Histone H3 and an anti-mouse Alexa Fluor® 594 conjugated secondary antibody (red) to counterstain. An anti-rabbit Alexa Fluor® 488 conjugated secondary antibody was used to detect the anti-ZIP10 treatment antibody. Cells were stained for DAPI to visualise the nuclei (blue).* ***B-D.*** *Immunofluorescence staining of the anti-ZIP10 (N1) antibody in MCF7 cells. Scale bars: 10 μm. White arrows indicate mitotic cells. Images are of 3 separate fields of view from a representative coverslip.*

5.4.3. ZIP10 targeted antibody treatment inhibits MCF7 cell growth

The ability of ZIP6 and ZIP10 targeted antibodies to inhibit mitosis in MCF7 cells highlights their potential to be used as a therapeutic target in breast cancer. However, these experiments were conducted over an 18-hour period and do not give an indication of how cells might respond with longer-term treatment in a clinical setting. Previous data from our lab suggest that the antibodies are able to suppress the growth of MCF7 cells over a 4-day period of constant exposure at an antibody concentration of 4 μg/mL for anti-ZIP6 and 10.5 μg/mL for anti-ZIP10 (Nimmanon *et al.*, 2020). It was interesting to investigate whether a lower concentration of the antibody was effective in inhibiting cell growth over a longer period of time because, if so, it could mean a lower dose could be given to a patient and thus limiting any potential off-target side effects.

MCF7 cells were seeded into 48-well plates (day 0) and treated with the anti-ZIP10 antibody at two different concentrations (5 μg/mL and 2.8 μg/mL) on day 1. Cells were counted every day for 7 days. The growth medium/antibody treatment was replaced on day 4. The growth of cells treated with 5 μg/mL was slower after day 2, and the total number of cells was significantly less on days 5 ($p < 0.05$), 6 ($p < 0.01$), and 7 ($p < 0.001$) (figure 5.7A). The total number of cells at day 7 was only half that of the untreated cells (316,000 [s = 45,900] and 611,000 [s = 62,000] respectively). In addition, the growth curve of cells treated with the lower concentration of antibody (2.8 μg/mL) did not differ significantly from the untreated cells. These results highlight the ability of the ZIP10 targeted antibody to slow growth of breast cancer cells over a 7-day period, at half the concentration that was used in the previous inhibition experiments. The decreased rate of cell growth was also in an antibody-concentration dependent manner, as seen in the previous experiments. Furthermore, in the growth experiment, cells were not chemically synchronised in mitosis, confirming the inhibition of mitosis is not an aberrant effect of nocodazole.

To determine whether MCF7 cells could recover from anti-ZIP10 antibody treatment, the cells were grown for a total of 10 days, and the antibody treatment replaced with fresh growth medium on day 5 (figure 5.7B). The data show that when the treatment was removed at day 5, the cells continued to grow at a similar rate to those which had been exposed to the antibody for the full 10 days. The number of cells at day 10 in both antibody-treated populations is less than those in the untreated population, though there was no statistical significance on this day. These data suggest that the cells were able to recover from 5 μg/mL antibody treatment, suggesting that the antibody is cytostatic, not cytotoxic.

Figure 5.7. Anti-ZIP10 antibody inhibition of MCF7 cell growth

A.

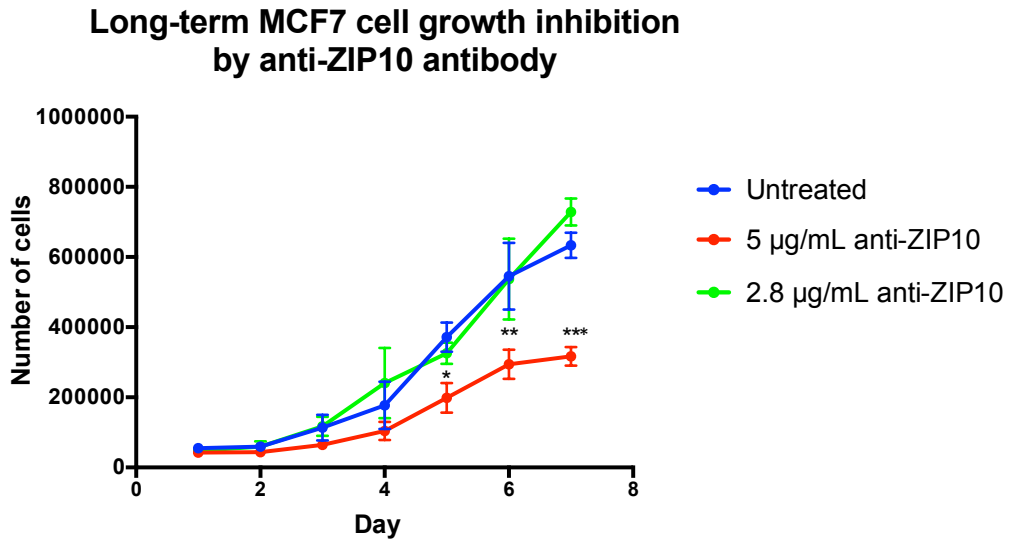

B.

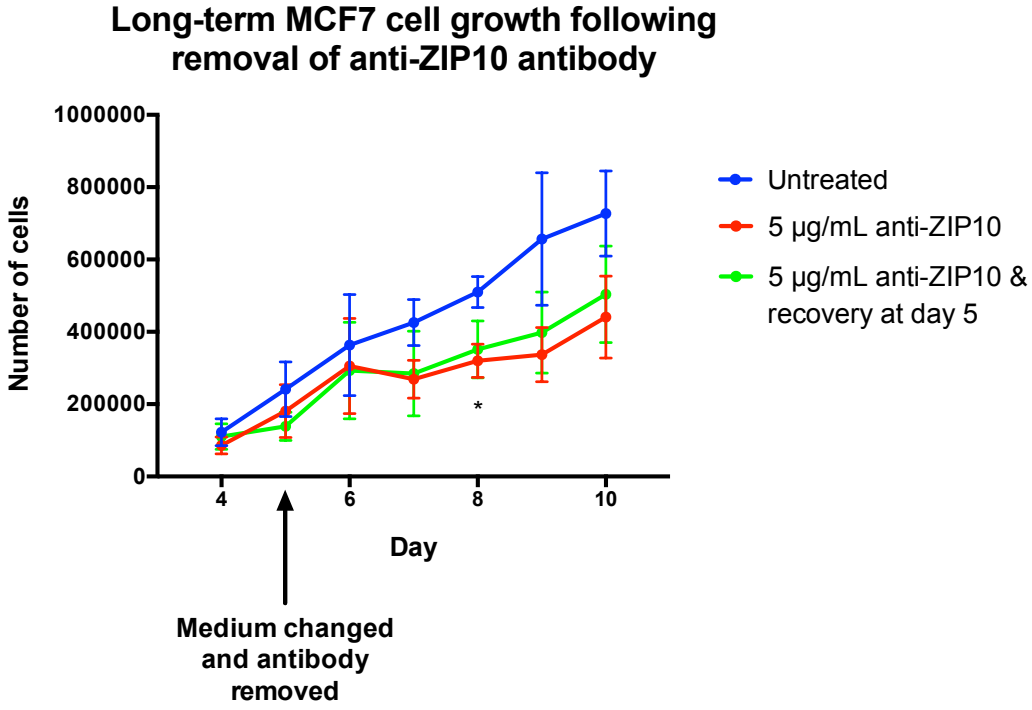

MCF7 cells were seeded in 46-well plates (day 0) and treated with anti-ZIP10 (N1) antibody on day 1. ***A.*** *Cells were counted daily for 7 days and the growth medium/antibody was replaced on day 4.* ***B.*** *Cells were counted daily from day 4 onwards, and the antibody was either replaced with growth medium or removed on day 5. Results are presented in a line graph as mean ± standard error (n = 3). Statistical significance was measured using ANoVA, comparing to the untreated population. * $p < 0.05$, ** $p < 0.01$, *** $p < 0.001$.*

5.4.4. Anti-ZIP6 and ZIP10 antibodies inhibit mitosis in several cancer cell lines

The data presented in this chapter so far demonstrate the potential for ZIP6 and ZIP10 targeted antibodies to inhibit breast cancer cell division and growth. To determine whether these transporters could also be targeted to inhibit cell division in other cancer types, the antibodies were used to treat DU145 prostate cancer cells and SK-MEL-29 melanoma cells as well. These cell lines were chosen due to the known dysregulation of zinc and/or ZIP6 and ZIP10 in these cancer types (chapter 1). Before treatment with the antibodies, it was important to confirm the presence of ZIP6 and ZIP10 in these cell lines. Cells were synchronised in mitosis by treatment with nocodazole and stained using an anti-pS^{10}Histone H3 antibody to stain mitotic cells and either an anti-ZIP6 or -ZIP10 antibody to detect ZIP6 or ZIP10 respectively.

Mitotic SK-MEL-29 cells showed increased ZIP10 fluorescence compared with non-mitotic cells (figure 5.8A) suggesting that ZIP10 is involved in mitosis of melanoma cells. Interestingly, mitotic DU145 cells showed the same amount of ZIP10 fluorescence as the non-mitotic DU145 cells (figure 5.8B). However, it was apparent that the localisation of ZIP10 was different in mitotic (plasma membrane) and non-mitotic (intracellular) cells. To investigate this further, the RGB Profiler tool for ImageJ was used to generate a fluorescence intensity profile of ZIP10 (green) and DAPI (blue) in non-mitotic (figure 5.8C) and mitotic (figure 5.8D) DU145 cells. In a non-mitotic cell, the peak fluorescence of ZIP10 is adjacent to the nucleus and decreases towards the outside of the cell (figure 5.8C). In a mitotic cell, the peak fluorescence of ZIP10 is not adjacent to the nucleus but further away (figure 5.8D) and drops more abruptly than in the non-mitotic cell, suggesting its presence on the outside edge of the cell (plasma membrane). Furthermore, the ZIP10 staining was carried out with an N-terminal anti-ZIP10 antibody (N1) and its presence on the plasma membrane can be seen in a cell in metaphase (figure 5.8D). This suggests that ZIP10 does not undergo ectodomain shedding in mitosis in DU145 cells and may reflect the increased need for zinc in prostate cells; ZIP10 remains active for a longer period of time.

In addition to the ZIP10, there was increased ZIP6 in SK-MEL-29 cells (figure 5.9A) and in DU145 cells (figure 5.9B), compared with the non-mitotic cells. These data suggest that both ZIP6 and ZIP10 play a role in mitosis in both DU145 and SK-MEL-29 cells and therefore treatment with our novel antibodies may prevent cell division, as it does in the MCF7 cells.

Figure 5.8. Immunofluorescent staining of ZIP10 in SK-MEL-29 and DU145 cells

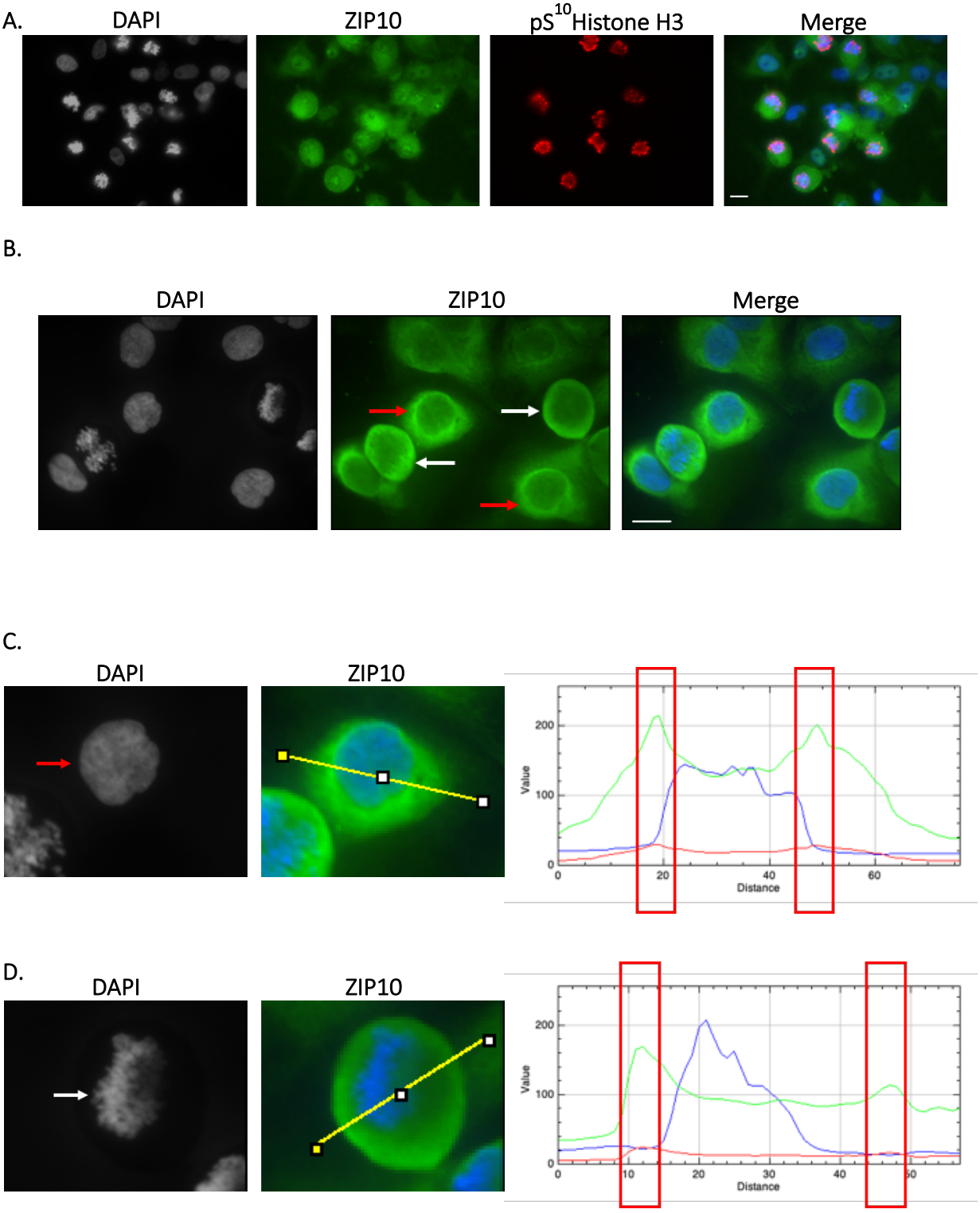

*SK-MEL-29 melanoma cells (**A**) and DU145 prostate cancer cells (**B**) were treated with 150 nM nocodazole and fixed with 3.7% paraformaldehyde. Cells were stained for using ZIP6 (Y3) or ZIP10 (N1) and pS[10]Histone H3 primary antibodies with anti-rabbit Alexa Fluor® 488 (green) and anti-mouse Alexa Fluor® 594 (red) secondary antibodies, respectively. Cell nuclei were stained with DAPI (blue). Scale bars: (A) 10 μm, (B) 20 μm. The RGB Profiler for Image J was used to generate a fluorescence intensity profile for ZIP10 and DAPI in a non-mitotic (**C**) and mitotic (**D**) DU145 cell. White arrows indicate mitotic cells and red arrows indicate non-mitotic cells. The yellow lines indicate where the profile was generated on the image. The red boxes indicate the fluorescence peaks of ZIP10.*

Figure 5.9. Immunofluorescent staining of ZIP6 in SK-MEL-29 and DU145 cells

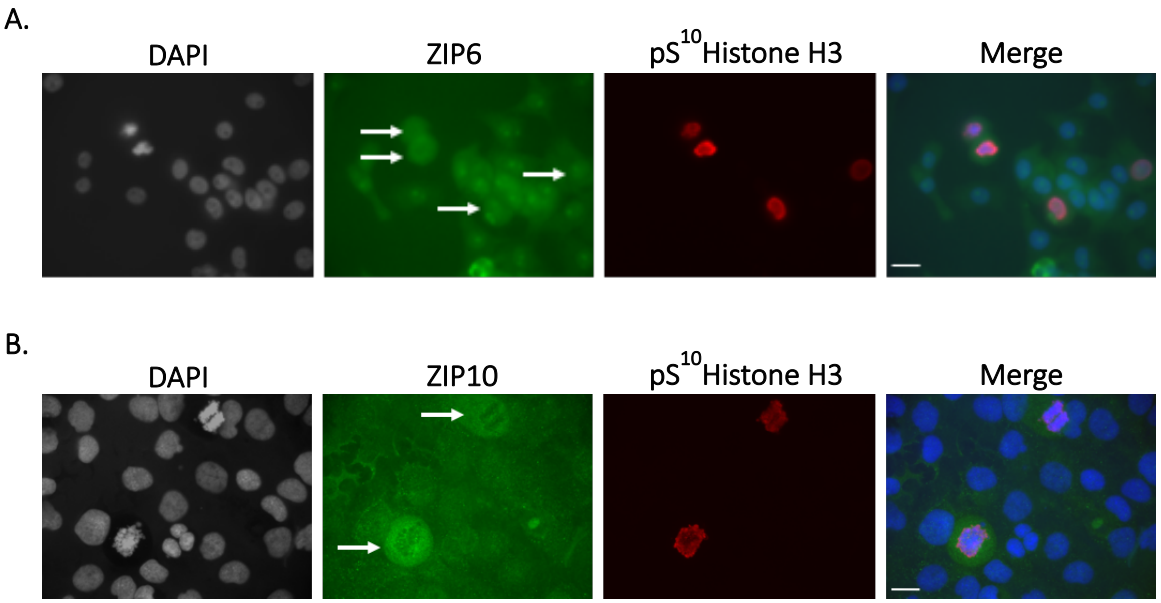

*SK-MEL-29 melanoma cells (**A**) and DU145 prostate cancer cells (**B**) were treated with 150 nM nocodazole and fixed with 3.7% paraformaldehyde. Cells were stained for using ZIP6 (Y3) or ZIP10 (N1) and pS[10]Histone H3 primary antibodies, with anti-rabbit Alexa Fluor® 488 (green) and anti-mouse Alexa Fluor® 594 (red) secondary antibodies, respectively. Cell nuclei are stained with DAPI (blue). White arrows indicate mitotic cells. Scale bars: (A) 10 μm, (B) 20 μm.*

Twenty-eight percent (s = 2%) of nocodazole-treated DU145 cells were mitotic, compared with 3% (s = 1%) of the untreated population (figure 5.10A). Addition of the anti-ZIP6 antibody at a 4 μg/mL concentration significantly decreased the percentage of cells in mitosis to 3% ((s = 2%; $p < 0.01$), while treatment with the anti-ZIP10 antibody at a 10 μg/mL concentration reduced the percentage of cells in mitosis to 10% (s = 3%; $p < 0.05$) (figure 5.10B). The percentage of DU145 cells in mitosis following treatment with either antibody was not significantly different to that of the untreated cells. Both the ZIP6 and ZIP10 targeted antibodies successfully inhibited nocodazole-induced mitosis in DU145 prostate cancer cells, at the same respective concentrations that inhibited mitosis in the MCF7 cells.

In the nocodazole-treated SK-MEL-29 population, 21% (s = 5%) of cells were mitotic, compared with 3% (s = 1%) in the untreated population (figure 5.11A). Addition of the anti-ZIP6 antibody at a 4 μg/mL concentration significantly reduced the percentage of mitotic cells to 5% (s = 3%; figure 5.11B; $p < 0.01$). However, the addition of the anti-ZIP10 antibody at the highest concentration used in previous cell lines (10 μg/mL), caused widespread cell death and detachment from the coverslip on which they were treated. Therefore, these cells could not be fixed and stained for counting. The concentration of antibody was reduced to determine whether a lower amount could successfully inhibit cell division while the cells remained adhered to the coverslip. A concentration of 2 μg/mL was found to reduce the percentage of cells in mitosis to 2% (s = 1%), which was significantly less than the population treated with nocodazole alone ($p < 0.05$). The percentage of SK-MEL-29 cells in mitosis following treatment with either antibody was not significantly different to that of the untreated cells. These data highlight the potential of targeting ZIP6 and ZIP10 in both prostate cancer and melanoma to inhibit cell division. In addition, the data suggest that melanoma cells may be more sensitive to zinc signalling pathways, in particular those involving ZIP10, than breast or prostate cancer cells.

Figure 5.10. Anti-ZIP6 and -ZIP10 antibody inhibition of mitosis in DU145 cells

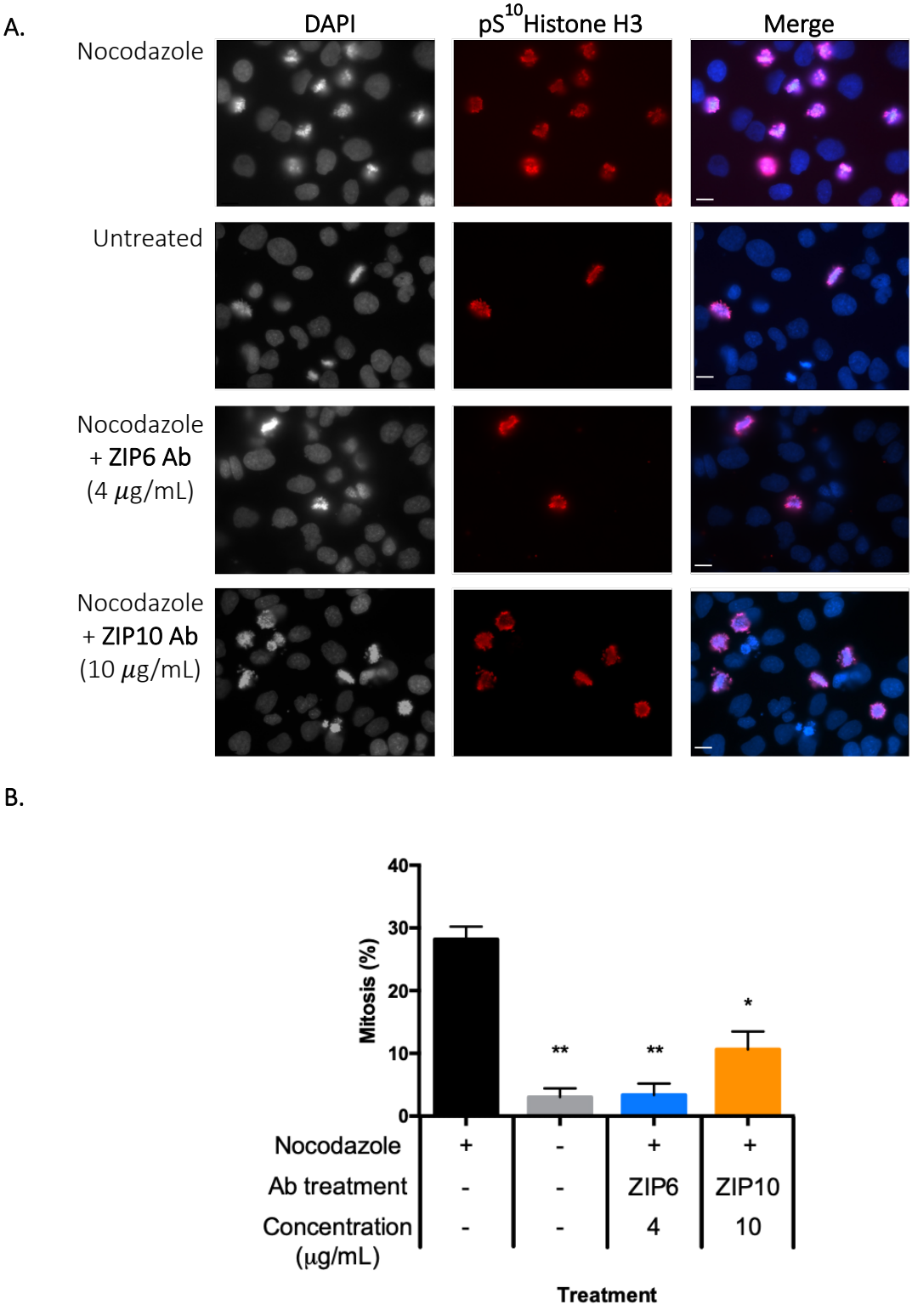

***A**. DU145 cells were treated with 150 nM nocodazole for 18 hours with or without anti-ZIP6 (Y3) or anti-ZIP10 (N1) antibodies. The cells were stained for pS[10]Histone H3 (red) and DAPI (blue). A representative image of each population is shown. Ab, antibody. Scale bars: 20 μm. **B**. Percentages of cells in mitosis are presented as mean ± standard error (n = 3). Statistical significance was measured using ANoVA, comparing to the population treated with nocodazole alone. * $p < 0.05$, ** $p < 0.01$.*

Figure 5.11. Anti-ZIP6 and -ZIP10 antibody inhibition of mitosis in SK-MEL-29 cells

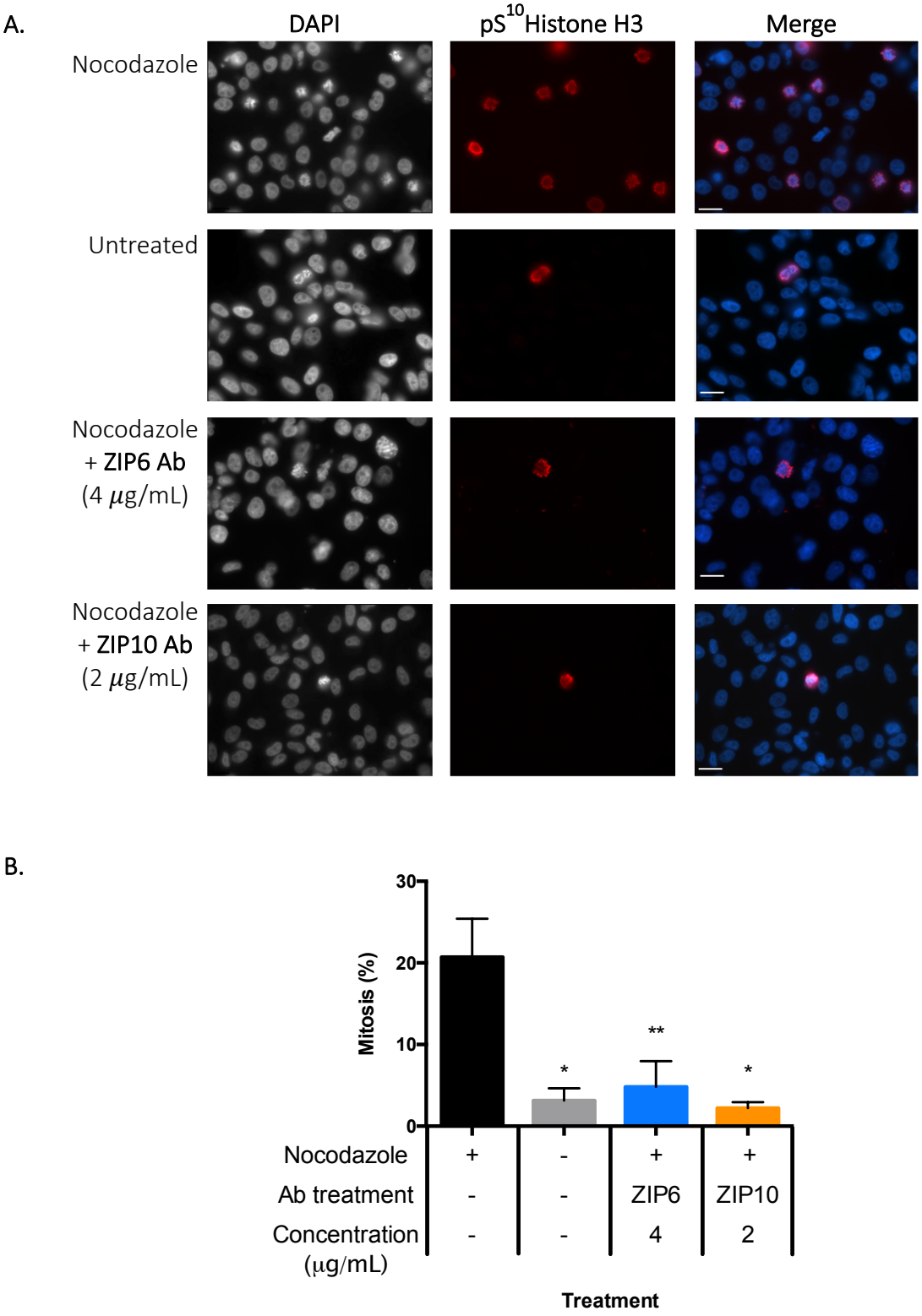

***A**. SK-MEL-29 cells were treated with 150 nM nocodazole for 18 hours with or without anti-ZIP6 (Y3) or anti-ZIP10 (N1) antibodies. The cells were stained for pS[10]Histone H3 (red) and DAPI (blue). A representative image of each population is shown. Ab, antibody. Scale bars: 10 μm. **B**. Percentages of cells in mitosis are presented as mean ± standard error (n = 3). Statistical significance was measured using ANoVA, comparing to the population treated with nocodazole alone. * $p < 0.05$, ** $p < 0.01$.*

5.4.5. Investigation of ZIP10 processing in DU145 prostate cancer cells

Immunofluorescent staining of DU145 prostate cancer cells in the previous section indicated that ZIP10 may not undergo ectodomain shedding in this cell line. The N-terminal ZIP10 antibody was able to detect ZIP10 on the plasma membrane of cells in prophase and later in mitosis, unlike the MCF7 cells, in which the N-terminal antibody was unable to detect ZIP10 on the plasma membrane after prophase. Despite this difference in ZIP10 regulation, the antibody successfully inhibited mitosis in both cell lines. To gain a deeper understanding of the regulation of ZIP10 in mitosis of DU145 cells, the cells were treated with the anti-ZIP10 antibody in the presence of nocodazole for 18 hours, to inhibit nocodazole-induced mitosis. The cells were fixed and stained for pS^{10}Histone H3 using an anti-mouse Alexa Fluor® 594 antibody to counterstain. During the counterstain process, an anti-rabbit Alexa Fluor® 488 antibody was also used, to detect the anti-ZIP10 antibody that was used in the earlier treatment. A schematic of this process is shown in figure 5.6A.

The staining of the anti-ZIP10 antibody highlighted its localisation with what appeared to be the mitotic spindles of mitotic cells (figure 5.12A-B). There was no anti-ZIP10 antibody staining in the non-mitotic cells. To investigate whether the association of the anti-ZIP10 antibody with the mitotic spindle was an aberrant effect of the IgG, the cells were treated with a normal rabbit IgG control antibody in the presence of nocodazole, for 18 hours, and the staining with the anti-rabbit Alexa Fluor® 488 was repeated (figure 5.12C). The IgG antibody was increased in mitotic DU145 cells, though the staining was not specific to the spindles. The increase of the anti-rabbit IgG in the mitotic DU145 cells is unexpected, however the non-specificity of the staining does suggest that the anti-ZIP10 antibody associating with the mitotic spindles is a real result. Data from chapter 3 highlighted the potential for ZIP10 to interact with several proteins which are involved with stabilisation of the mitotic spindle (table 3.3) which is supported by the finding presented here in DU145 cells.

As the cells in which ZIP10 appears to be associated with the spindles are in prophase, and in this stage of mitosis, the nuclear membrane has not yet completely broken down, the protein sequence of ZIP10 was analysed for the presence of a nuclear localisation signal (NLS), a sequence that 'tags' a protein for import to the nucleus. The search predicted a 10 amino acid NLS in the N-terminal region of ZIP10 (figure 5.12D), suggesting the localisation of at least an N-terminal fragment of ZIP10 to the nucleus during mitosis in DU145 cells.

Figure 5.12. Immunofluorescent staining of the anti-ZIP10 antibody in DU145 cells

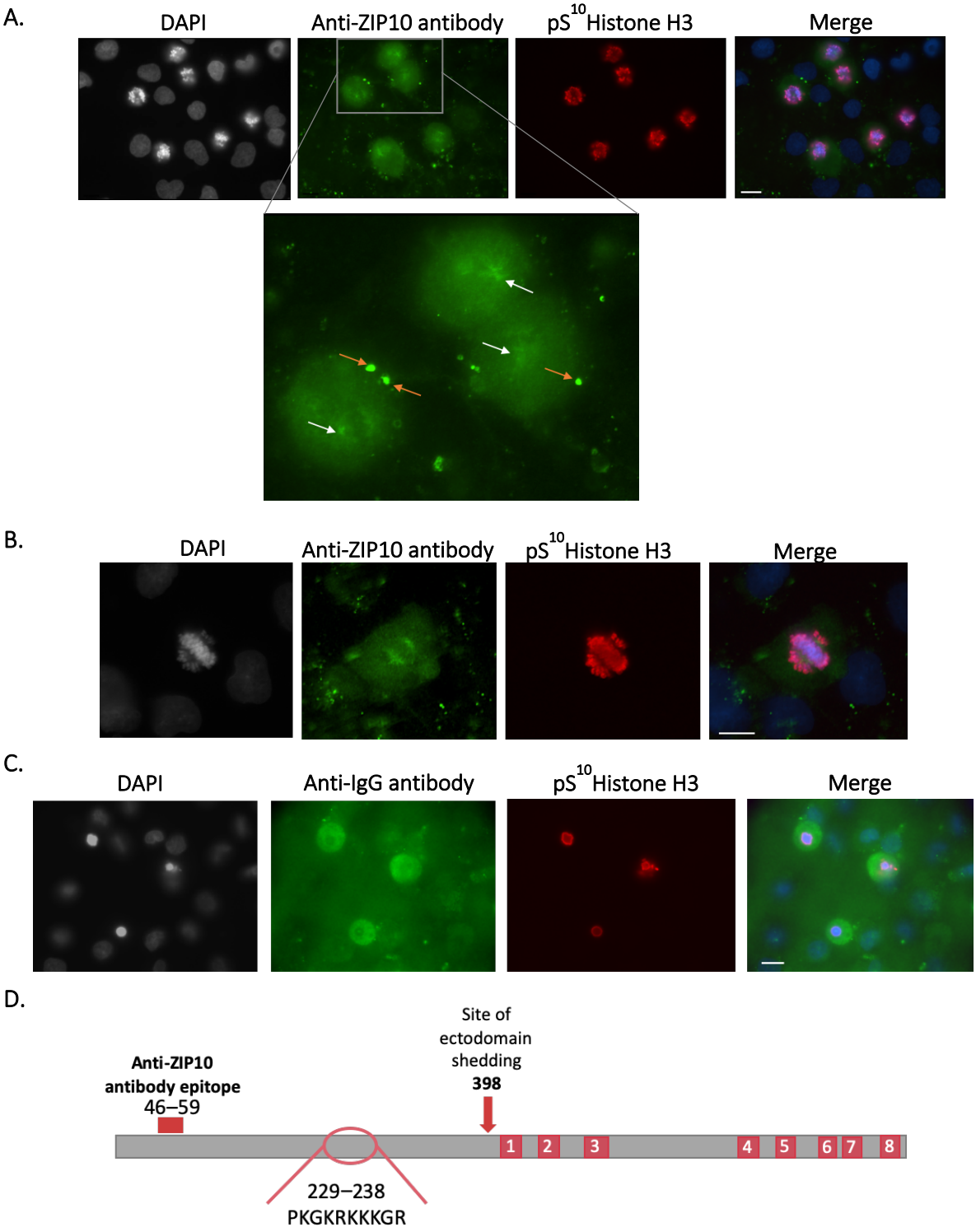

*MCF7 cells were treated with the anti-ZIP10 (**A-B**) or anti-rabbit IgG (**C**) antibody for 18 hours in the presence of nocodazole. Cells were fixed and stained using an anti-mouse pS[10]Histone H3 antibody. Fluorophore conjugated Alexa Fluor® secondary antibodies were used to detect pS[10]Histone H3 (red) and the anti-ZIP10 or -IgG treatment antibodies (green). White arrows indicate mitotic spindle-like structures and orange arrows indicate bright green spots which are likely to be cell debris due to stress following antibody treatment. Scale bars: 20 μm. **D.** Nuclear localisation signal in human ZIP10, identified using cNLS Mapper* (Kosugi *et al.*, 2009).

However, this finding does not agree with the ZIP10 staining in DU145 cells in figure 5.8D that showed plasma membrane staining throughout mitosis. The data suggest that ZIP10 does undergo ectodomain shedding in these cells, but only upon antibody binding (or potentially the interaction of another foreign body) that may prevent ZIP10 functioning.

5.4.6. *In vivo* study of the anti-ZIP6 antibody

Thus far, the ability of ZIP6 and ZIP10 targeted antibodies to inhibit mitosis in several cancer cell lines has been demonstrated. Preliminary studies in cell line-derived xenograft models of breast cancer were carried out to test the ability of the anti-ZIP6 antibody to slow tumour growth. A triple-negative (oestrogen receptor, progesterone receptor and HER2 negative) breast cancer cell line was chosen for the study due to (a) its ability to form tumours, and (b) the successful inhibition of mitosis in this cell line using the anti-ZIP6 antibody (Nimmanon *et al.* 2020). Once the cells had formed palpable tumours, the purified anti-ZIP6 antibody diluted in PBS was injected intraperitoneally at 4-day intervals. The effect of the antibody was assessed by tumour volume.

At day 20, the average tumour volume (normalised to that at the time of the first injection) in the untreated mice was 23 mm^3 (figure 5.13; black line), compared with 16 mm^3 in those treated only with PBS (figure 5.13; blue line). In contrast, when treated with the anti-ZIP6 antibody at a 1 mg/kg concentration, the average tumour volume at day 20 was 9 mm^3 (figure 5.13; orange line), almost half the volume in the mice treated with PBS alone, indicating the anti-ZIP6 antibody reduced breast tumour growth *in vivo*. In the anti-ZIP6 antibody-treated mice the average tumour size remained similar to the untreated and PBS control mice, until day 12 when it measured 3 mm^3 (compared with 6 mm^3 and 11 mm^3 in the untreated and PBS control mice, respectively). These data suggest that the anti-ZIP6 antibody slows tumour growth *in vivo* after 8 days of exposure. It is important to note that the animals treated with the anti-ZIP6 antibody did not experience such major side effects that they had to be sacrificed before the 20-day treatment period ended. This is promising as it suggests that the therapeutic level is within the limits of the tolerated dose. These results will be used for the design and execution of further animal models of breast cancer to test the efficacy of both the anti-ZIP6 and -ZIP10 antibodies in inhibiting tumour growth.

Figure 5.13. Effect of anti-ZIP6 antibody on tumour volume in Athymic Nude mice

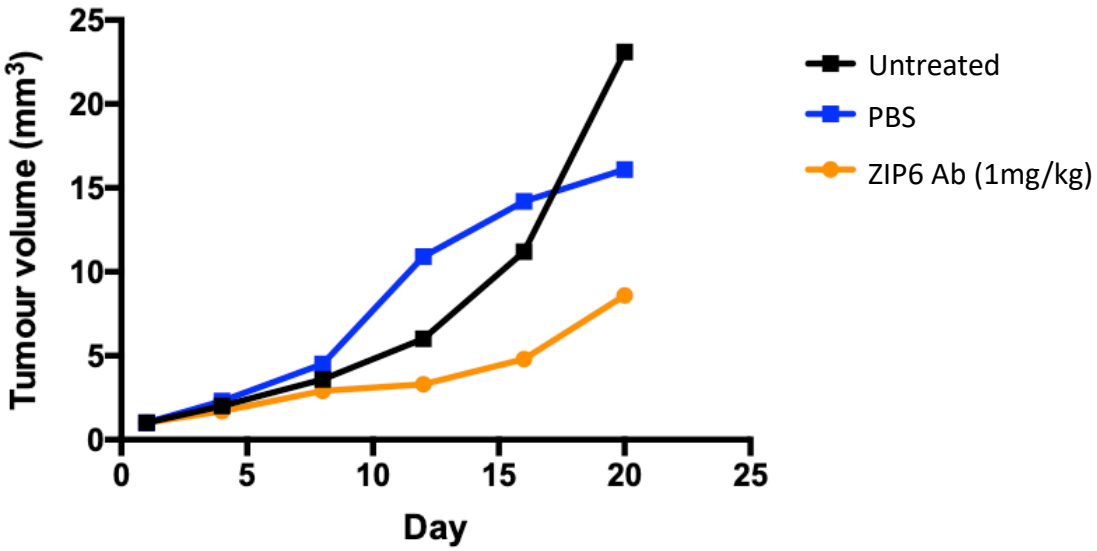

Seven xenograft Athymic Nude mice were treated with the anti-ZIP6 antibody (4 mice), PBS (2 mice) by intraperitoneal injection every 4 days. One mouse was left untreated. Tumour volume was measured every 4 days and is presented as mean tumour volume normalised to the size of tumour at the beginning of treatment. No statistical analysis was performed owing to the different number of mice across treatment groups. Ab, antibody.

5.4.7. Anti-ZIP6 and -ZIP10 antibodies inhibit mitosis in non-cancerous cells

It is important to consider whether the potential treatment of cancer with anti-ZIP6 and -ZIP10 antibodies would also influence non-cancerous (healthy) cells as this will have major implications on the clinical use of the therapies. Treatments that are not specific for tumour cells are associated with side effects which may result in withdrawal from a treatment regimen early. NMuMG (normal murine mammary gland) cells were used here as a model of non-cancerous cells to determine the efficacy of the anti-ZIP6 and -ZIP10 antibodies in inhibiting mitosis.

The anti-ZIP6 and -ZIP10 antibodies were raised against the human epitopes of their respective proteins. Therefore, prior to treatment, it was important to determine whether they could still bind to the mouse respective proteins. An alignment of the antibody epitopes in each species was performed (figure 5.14A). The human and mouse ZIP6 epitope differ by only 1 amino acid (glycine is replaced by serine in the mouse protein), whereas there are 4 amino acid differences in the human and mouse ZIP10 sequence (leucine and proline are both replaced with serine, lysine with valine and alanine with aspartic acid). Immunofluorescent staining was carried out in NMuMG cells treated with nocodazole to confirm the antibodies could still detect their target proteins despite these changes in the epitope sequences (figure 5.14B-C). Protein expression of ZIP6 and ZIP10 was increased in the mitotic cells as determined by positivity for pS^{10}Histone H3. The cells were also stained for pS^{727}STAT3 (figure 5.14D) as this is a potentially important protein in ZIP6/ZIP10-mediated mitosis through its interaction with ZIP6. There was increased pS^{727}STAT3 in the mitotic cells, further highlighting the use of zinc signalling pathways in normal cells as well as cancer cells.

Figure 5.14. Characterisation of ZIP6, ZIP10 and pS^{727}STAT3 in NMuMG cells

A.

```
Human ZIP6      VSEPRKGFMYSRNTN
Mouse ZIP6      VSEPRKSFMYSRNTN

Human ZIP10     LEPSKFSKQAAENE
Mouse ZIP10     SESSKFSVQDAENE
```

B.

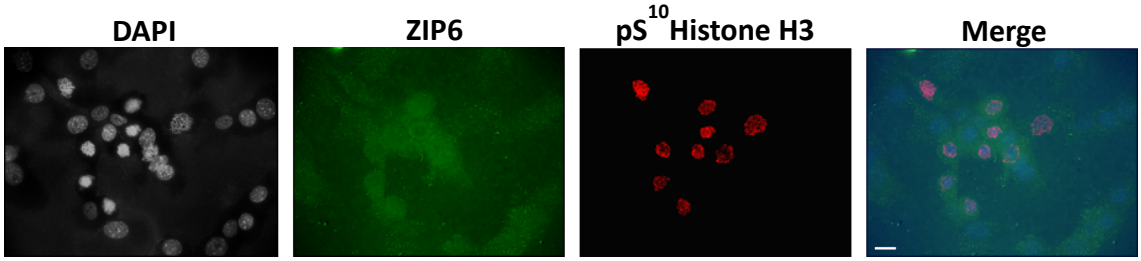

C.

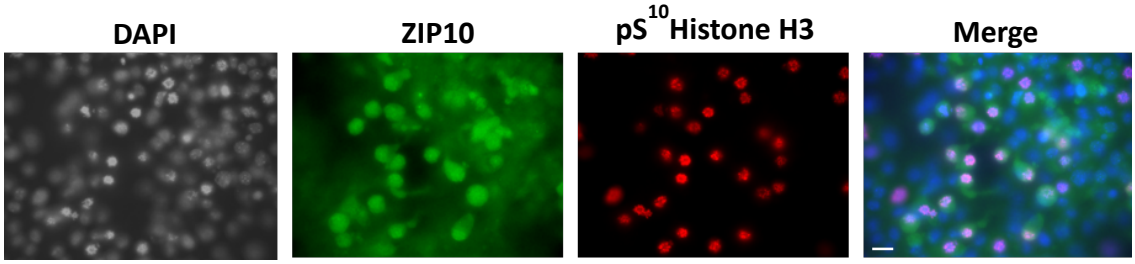

D.

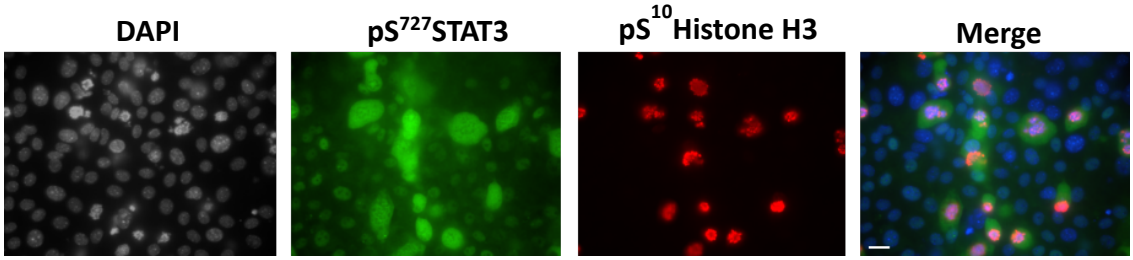

***A**. The human epitopes of the anti-ZIP6 (Y3) and -ZIP10 (N1) antibodies in FASTA format were aligned with the mouse sequences using Kalign* (Li *et al.*, 2015). *NMuMG murine mammary cells were treated with 150 nM nocodazole and stained with anti-pS^{10}Histone H3, -ZIP6 (Y3) (**B**), anti-ZIP10 (N1) (**C**) and anti-pS^{727}STAT3 (**D**) antibodies. Fluorophore-conjugated Alexa Fluor® 488 (green) and 594 (red) secondary antibodies were used to detect proteins of interest. Cell nuclei were stained with DAPI (blue). Scale bars: 10 μm.*

To determine whether the ZIP6 and ZIP10 targeted antibodies could inhibit mitosis in non-cancerous cells, they were used to treat the NMuMG cells in the presence of nocodazole. It should be noted at this stage that new batches of ZIP6 (Y3) and ZIP10 (N1) antibody were prepared by Biogenes GmbH to replenish our stock. These batches were used from then on in this project; however, the concentration of the antibody in the new batches did differ from that of the previous ones. Preliminary experiments were carried out to determine a concentration of the new antibody batches which successfully inhibited mitosis.

The cells were fixed in 3.7% paraformaldehyde after 18 hours of treatment and stained for pS^{10}Histone H3, as a marker of mitosis (figure 5.15A). Initially, these data were analysed using the number of mitotic cells as a percentage of the whole population, to reflect the data from other cell lines used in this chapter. However, it was found that nocodazole treatment in this cell line was variable between biological replicates resulting in large error bars when the data were plotted into a bar graph. This made it difficult to conclude whether the antibody treatment had influenced mitosis or not. For this reason, the number of mitotic cells in each of the antibody-treated populations have been calculated as a percentage of the mitotic cells with nocodazole treatment alone (figure 5.15B).

The number of mitotic cells in the untreated population was 10% (s = 5%) of that in the population treated with nocodazole. With the addition of the anti-ZIP6 antibody at a 3 μg/mL concentration, the number of mitotic cells was 32% (s = 5%) of that in the nocodazole-treated population ($p < 0.01$; figure 5.15B), and treatment with the anti-ZIP10 antibody at a 28 μg/mL concentration decreased the number of mitotic cells to 20% (s = 17%) of that in the population treated with nocodazole alone ($p < 0.05$; figure 5.15B). These data demonstrate that the anti-ZIP6 and -ZIP10 antibodies inhibit cell division in non-cancerous cells and that the ZIP6/ZIP10-induced mechanism for mitosis is relevant in both healthy and diseased cells.

The percentage decrease in mitotic cells following treatment with the anti-ZIP6 or -ZIP10 antibodies in all cell lines is presented in a bar graph in figure 5.16. In all the cancer cell lines there was over 60% reduction in mitotic cells following treatment with either antibody compared with nocodazole treatment alone, which supports the hypothesis that these antibodies could be used to target cell division in a diverse range of cancers.

Figure 5.15. Anti-ZIP6 and -ZIP10 antibody inhibition of mitosis in NMuMG cells

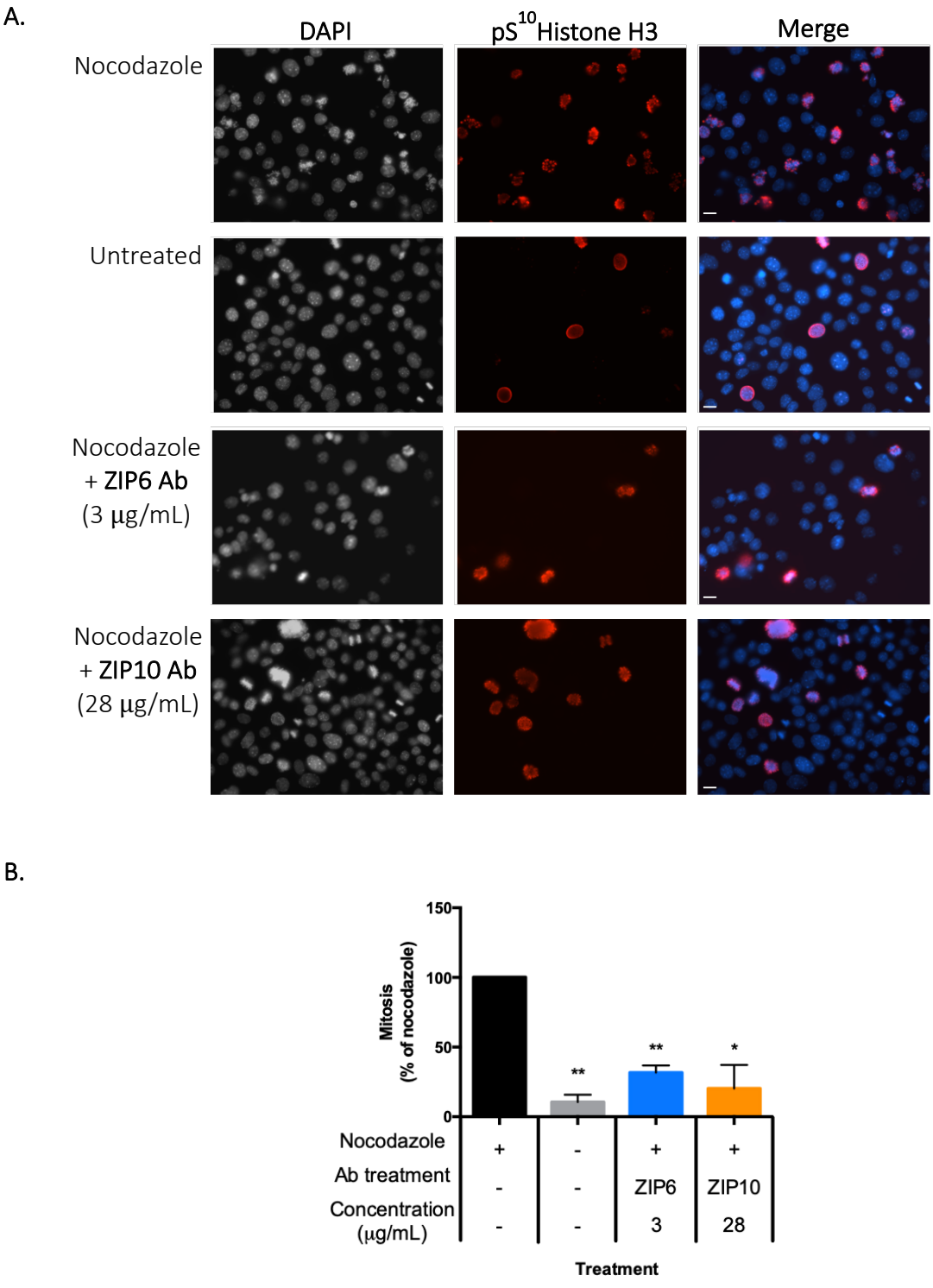

A. *NMuMG cells were treated with 150 nM nocodazole for 18 hours with or without the anti-ZIP6 (Y3) or anti-ZIP10 (N1) antibodies. The cells were stained for pS[10]Histone H3 (red) and DAPI (blue). A representative image of each population is shown. Ab, antibody. Scale bars: 10 µm.* ***B.*** *The number of mitotic cells as a percentage of the mitotic cells following nocodazole treatment alone is presented as mean ± standard error (n = 3). Statistical significance was measured using ANoVA, comparing to the population treated with nocodazole alone. * $p < 0.05$, ** $p < 0.01$.*

Figure 5.16. Percentage decrease in mitotic cells following antibody treatment

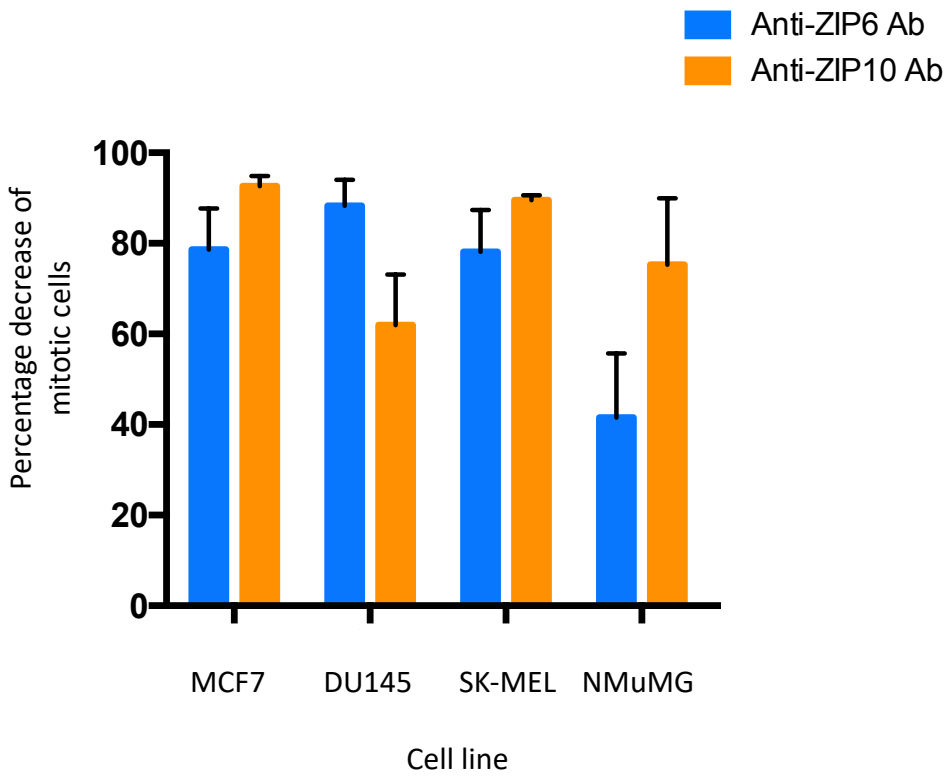

The percentage decrease of mitotic cells following anti-ZIP6 antibody (blue) and anti-ZIP10 antibody (orange) treatment is presented as mean ± standard error (n = 3). Percentage decrease was calculated using the percentage of mitotic cells following nocodazole treatment alone for each respective cell line. Ab, antibody.

5.4.8. The anti-ZIP6 antibody is specific to its target protein

The data in the previous section demonstrate that ZIP6 and ZIP10 targeted antibodies can inhibit mitosis in the non-cancerous cell line, NMuMG. Using the CRISPR-Cas9 technique, a ZIP6 knock-out cell line was generated by *Schmitt-Ulms et al*. at the University of Toronto and was kindly gifted to us for use in this project. The knock-out cell line (NMuMG ZIP6 KO) was a useful tool to determine the specificity of the anti-ZIP6 antibody for the ZIP6 protein.

The NMuMG ZIP6 KO cell line was confirmed to be negative for ZIP6 in mitotic (and non-mitotic) cells (figure 5.17A). However, the protein expression of ZIP10 (figure 5.17B) and pS^{727}STAT3 (figure 5.17C) is retained in mitotic cells even in the absence of ZIP6. Both proteins were increased in the mitotic NMuMG ZIP6 KO cells compared with the non-mitotic cells, suggesting that in the absence of ZIP6, zinc signalling pathways are still being used in mitosis.

To confirm the specificity of the anti-ZIP6 antibody for the ZIP6 protein, the NMuMG ZIP6 KO cells were treated with 150 nM nocodazole with or without the anti-ZIP6 antibody. The cells were fixed and stained for pS^{10}Histone H3 to indicate the mitotic cells (figure 5.18A) and the total number of mitotic cells was calculated as a percentage of the mitotic cells in the population treated with nocodazole only.

In the untreated population, the number of mitotic cells was only 24% (s = 8%) of those following treatment with nocodazole alone (figure 5.18B; $p < 0.01$). In the population treated with both nocodazole and the anti-ZIP6 antibody, the percentage of mitotic cells was not significantly different from the percentage of mitotic cells following nocodazole treatment alone. The inability of the ZIP6 targeted antibody to inhibit mitosis in the NMuMG ZIP6 KO cells confirms that (a) they are ZIP6 negative, and (b) the anti-ZIP6 antibody is specific for the ZIP6 protein. In contrast, the percentage of cells in mitosis following treatment with nocodazole and the anti-ZIP10 antibody was 22% (s = 12%) of that following nocodazole treatment alone (figure 5.18B; $p < 0.01$). The anti-ZIP10 antibody inhibited mitosis to a similar extent in both the WT NMuMG cells and the NMuMG ZIP6 KO cells highlighting that its effect is independent of ZIP6 and is not altered by increased protein expression of ZIP10, a phenotype which the NMuMG ZIP6 KO cells exhibit (Ziliotto, 2018).

Comparing the anti-ZIP6 antibody treatments in the WT NMuMG and NMuMG ZIP6 KO cell lines (figure 5.19), there is a significant increase in the number of mitotic cells in the ZIP6 KO

cells compared to the WT cells ($p < 0.01$). This further confirms that the anti-ZIP6 antibody does not have an effect when ZIP6 is absent.

Figure 5.17. Characterisation of ZIP6, ZIP10 and pS^{727}STAT3 in NMuMG ZIP6 KO cells

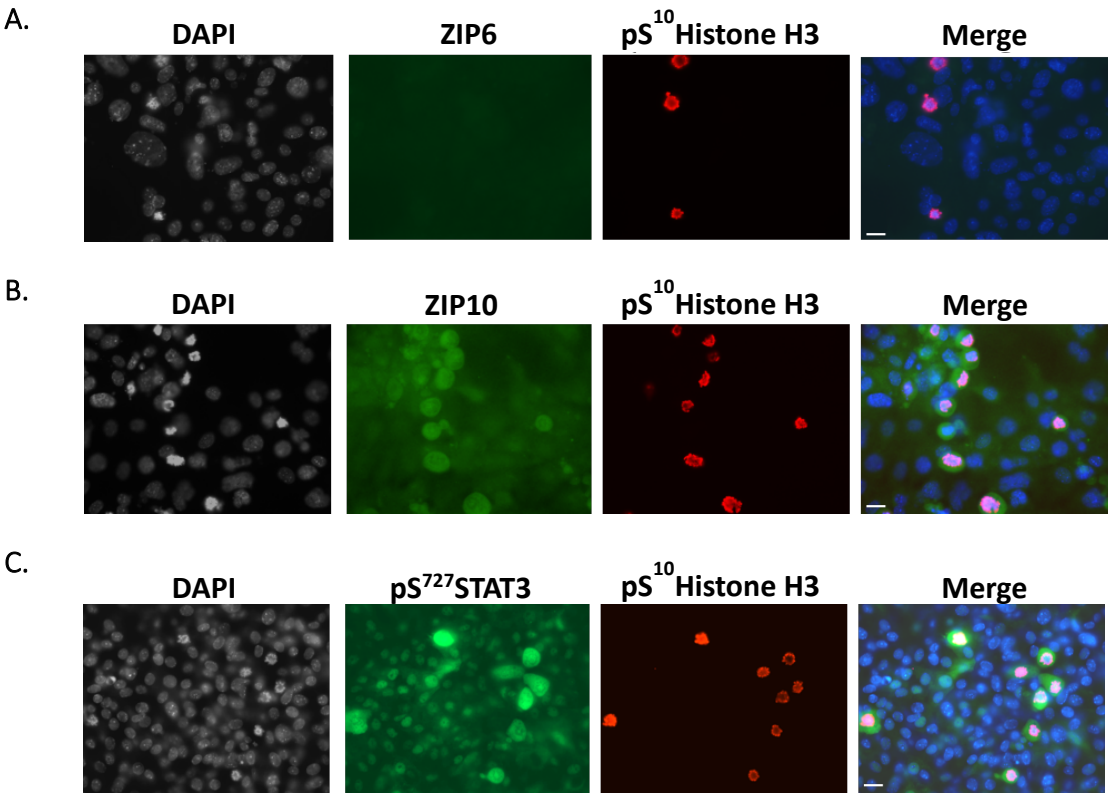

*NMuMG ZIP6 KO cells were treated with 150 nM nocodazole and stained using anti-ZIP6 (Y3) (**A**), anti-ZIP10 (N1) (**B**), and pS^{727}STAT3 (**C**) and an Alexa Fluor® 488 (green) secondary antibody. Cells were also stained using an anti-pS^{10}Histone H3 primary and Alexa Fluor® 594 (red) secondary antibody. Cell nuclei were stained with DAPI (blue). Scale bars: 10 μm.*

Figure 5.18. Anti-ZIP6 and -ZIP10 antibody inhibition of mitosis in NMuMG ZIP6 KO cells

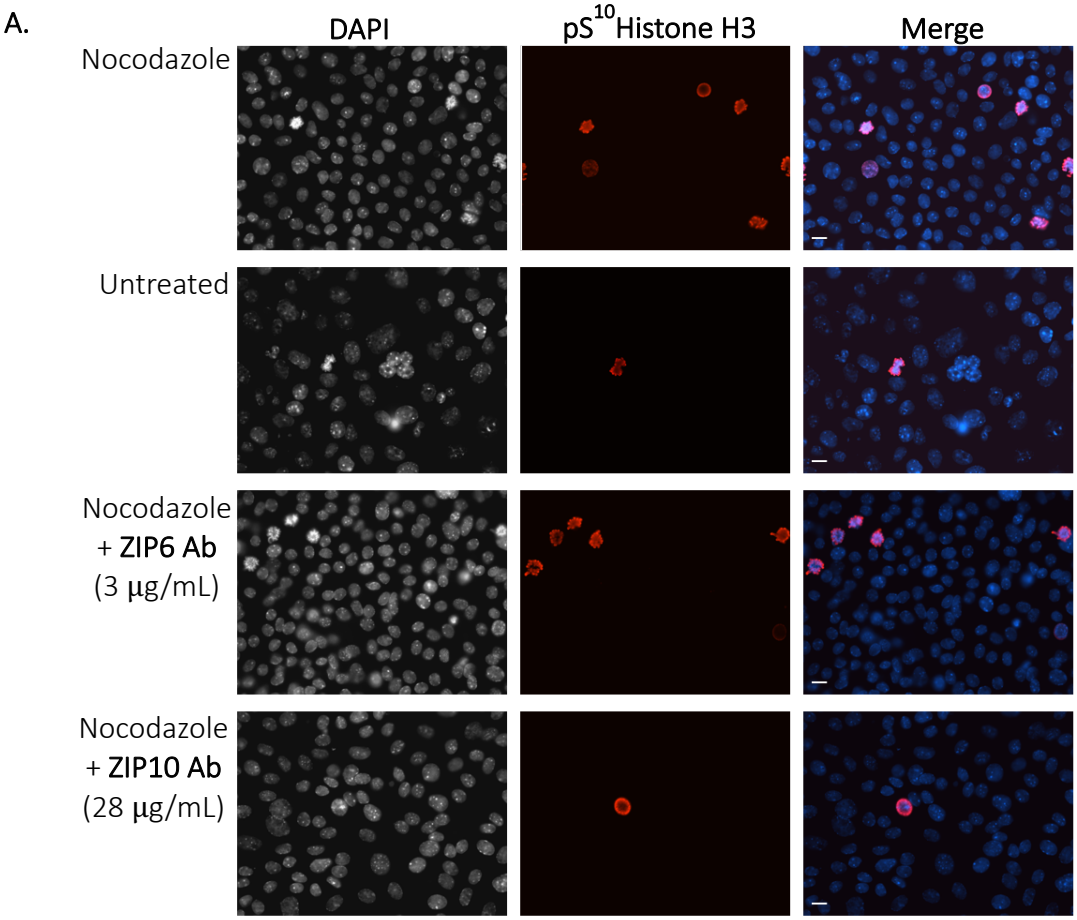

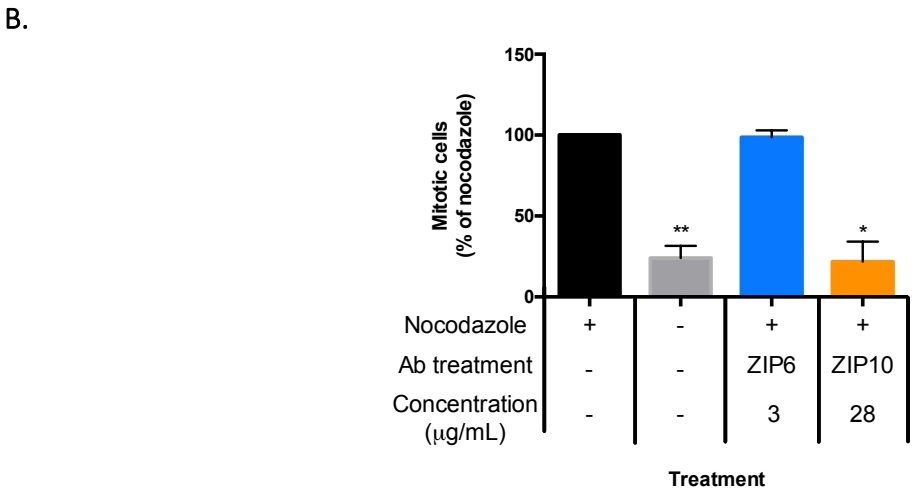

A. *NMuMG ZIP6 KO cells were treated with 150 nM nocodazole for 18 hours with or without the anti-ZIP6 (Y3) or anti-ZIP10 (N1) antibodies. The cells were stained for pS[10]Histone H3 (red) and DAPI (blue). A representative image of each population is shown. Ab, antibody. Scale bars: 10 µm.* ***B***. *Number of mitotic cells as a percentage of the mitotic cells in nocodazole treatment arm is presented as mean ± standard error (n = 3). Statistical significance was measured using ANoVA, comparing to the population treated with nocodazole alone. * p < 0.05, ** p < 0.01.*

Figure 5.19. Anti-ZIP6 antibody inhibition of mitosis in NMuMG cells vs NMuMG ZIP6 KO cells

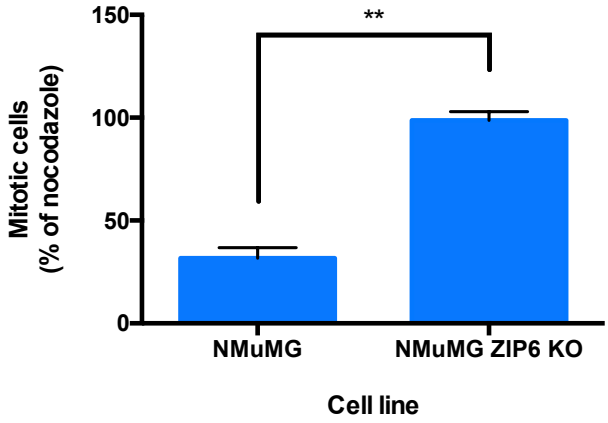

*The number of mitotic cells with anti-ZIP6 antibody treatment as a percentage of the mitotic cells in nocodazole treatment arm in both the NMuMG and NMuMG ZIP6 KO cell line is presented as mean ± standard error (n = 3). Statistical significance was measured using a paired t-test. ** $p < 0.01$.*

5.4.9. The effect of ZIP6 knock-out on ZIP5

The ability of the anti-ZIP10 antibody to inhibit mitosis in the absence of ZIP6 suggests that ZIP10 still functions to initiate mitosis when it is not in a heteromer with ZIP6. It is possible that, in this case, ZIP10 forms a homodimer, or it pairs with another ZIP transporter, not previously explored in mitosis. ZIP5 is the closest ZIP family member to ZIP6 and ZIP10 according to the phylogenetic tree in figure 1.3A. The investigation of protein-protein interaction in chapter 3 identified that ZIP10 interacts with ZIP5 (figure 3.22). In addition, according to the Biological General Repository for Interaction Datasets (BIoGRID) database, ZIP6 also interacts with ZIP5, suggesting that ZIP5 may interact with the ZIP6/ZIP10 heteromer in mitosis. The NMuMG ZIP6 KO cell model was used here to investigate the potential impact that ZIP6 knock-out had on ZIP5 protein expression.

Both WT NMuMG and NMuMG ZIP6 KO cells were treated with nocodazole and the cell lysates were analysed for ZIP5 on a western blot. There appeared to be an increase in the amount of ZIP5 protein in the WT cells treated with nocodazole (figure 5.20A), suggesting that ZIP5 may also play a role in mitosis. However, in both the untreated ZIP6 KO cells and those treated with nocodazole there was a decrease in the amount of ZIP5 protein (figure 5.20A) compared with the WT cells. This decrease was statistically significant in KO cells treated with nocodazole ($p < 0.05$; figure 5.20B). The loss of ZIP5 in ZIP6 KO cells indicates that ZIP5 protein expression is dependent on ZIP6 protein expression, and therefore ZIP5 activity is not able to compensate for the loss of ZIP6. It is possible that ZIP5 binds the ZIP6/ZIP10 heteromer in mitosis but requires ZIP6 binding before it can bind ZIP10, consequently therefore it cannot directly bind ZIP10 in the absence of ZIP6.

Figure 5.20. ZIP5 protein expression in NMuMG and NMuMG ZIP6 KO cells

A.

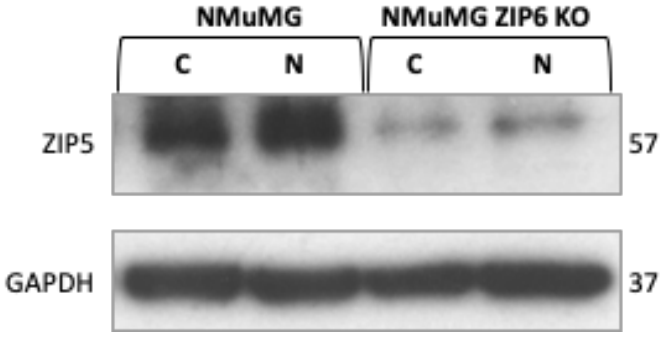

B.

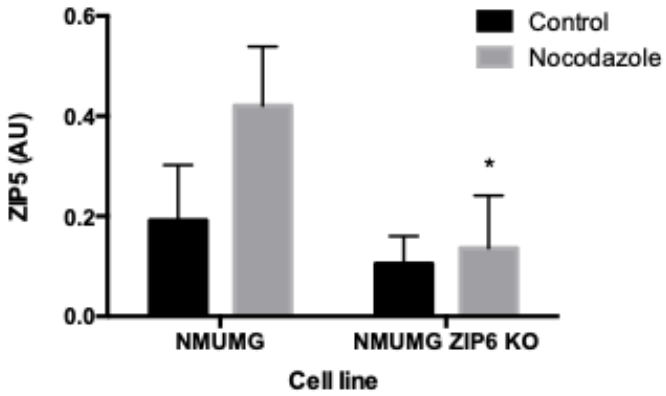

***A**. Western blot analysis of ZIP5 in nocodazole-treated NMuMG and NMuMG ZIP6 KO cells. Numbers represent the molecular mass of protein bands in kDa. C, control (untreated); N, nocodazole. **B**. Protein expression of ZIP5 was normalised to GAPDH expression and is presented in a bar graph as mean ± standard error (n = 3). Statistical significance was measured using ANoVA comparing to the NMuMG cells treated with nocodazole. * $p < 0.05$. AU, arbitrary unit.*

5.4.10. Synergistic targeting of ZIP6 and ZIP10 to inhibit mitosis

So far, this chapter has highlighted the ability of the anti-ZIP6 and -ZIP10 antibodies individually to inhibit mitosis. The next investigation carried out was to assess the ability of a mixture of the anti-ZIP6 and -ZIP10 antibodies to offer greater therapeutic benefit than either antibody alone.

For treatment with each antibody individually, a concentration which reduced mitosis by approximately 50% compared with nocodazole treatment alone was chosen (figure 5.21A). This would allow for a further decrease in the percentage of mitotic cells when the antibodies were used together to be seen more clearly than if each antibody was used at a concentration that reduced mitosis to their maximum effect. A concentration of 2 μg/uL was chosen for the anti-ZIP6 antibody and a concentration of 15 μg/uL for the anti-ZIP10 antibody (figure 5.21A). The cells were stained for pS^{10}Histone H3 to indicate the mitotic cells (figure 5.21B) and the percentage of mitotic cells in each treatment group was calculated (figure 5.21C).

In the population of cells treated with the anti-ZIP6 antibody alone, 11% (s = 2%) of cells were mitotic, and 12.2% (s = 3%) were mitotic in the population treated with the anti-ZIP10 antibody alone (figure 5.21C). When the two antibodies were added together, there was a significant decrease in the percentage of mitotic cells (3.9% [s = 1%]) compared with the percentage of mitotic cells with the anti-ZIP6 ($p < 0.05$) or anti-ZIP10 ($p < 0.01$) antibodies individually. Furthermore, the percentage of cells in mitosis following treatment with both antibodies together was significantly less ($p < 0.001$) than treatment with nocodazole alone (figure 5.21C). These data offer proof of principle that both antibodies could be used together to inhibit mitosis, and this may be important if one antibody caused greater side effects *in vivo* than the other; the concentrations of both antibodies could be adjusted accordingly.

Figure 5.21. Inhibition of mitosis in MCF7 cells using anti-ZIP6 and -ZIP10 antibodies together

A.

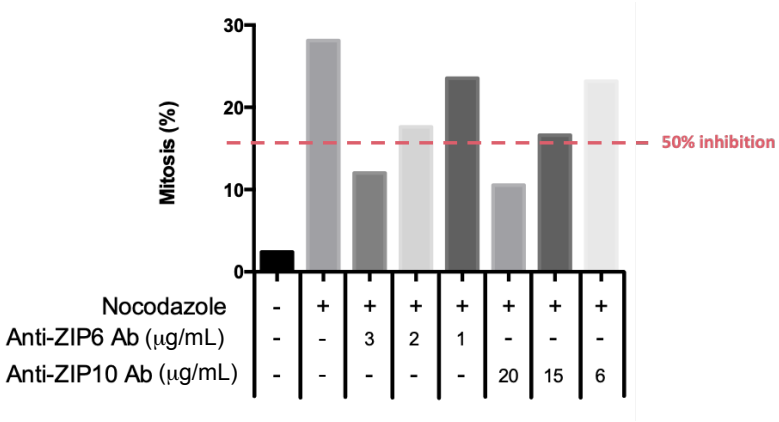

B.

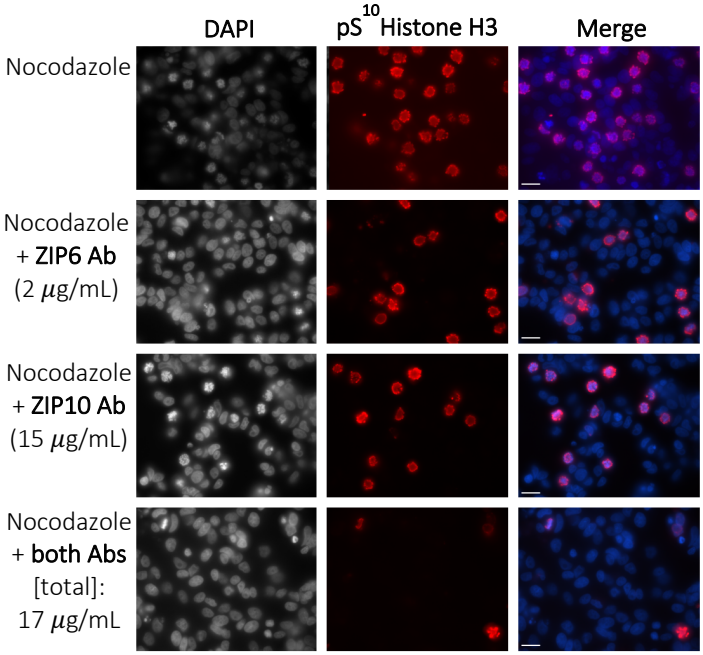

C.

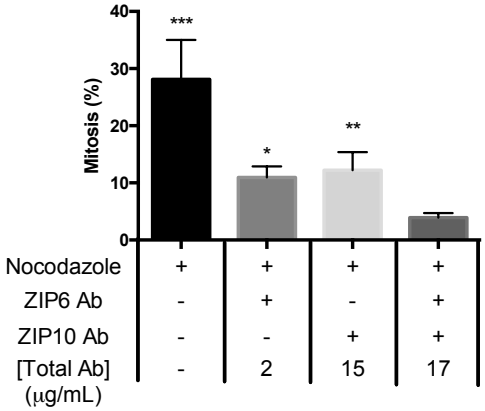

MCF7 cells were treated with 150 nM nocodazole for 18 hours in the presence of the anti-ZIP6 (Y3) or -ZIP10 (N1) antibody. ***A****. The percentage of cells in mitosis was calculated and the dose of antibody that gave approximately a 50% reduction of the cells in mitosis (pink line) was selected for use in experiments to target mitosis with both antibodies together.* ***B****. MCF7 cells were treated with 150 nM nocodazole for 18 hours with or without the anti-ZIP6 (Y3) or anti-ZIP10 (N1) antibodies or a mixture of the two. The cells were stained for pS[10]Histone H3 (red) and DAPI (blue). A representative image of each population is shown. Square brackets denote total concentration of the two antibodies together. Scale bars: 10 μm. B. Percentages of cells in mitosis are presented as mean ± standard error (n = 3). Statistical significance was measured using ANoVA, comparing to the population treated with both antibodies together. * p < 0.05, ** p < 0.01, *** p < 0.001.*

5.5. Discussion

The focus of this chapter was the investigation of novel anti-ZIP6 and -ZIP10 antibodies and their ability to inhibit cell division. The cytostatic ability of the antibodies was measured using immunofluorescence, western blot and cell growth assays. Several cancer lines were used to determine the cytostatic ability in several cancers, and non-cancerous cell lines were used to not only determine the potential off-target effect of antibody treatment in cancer therapy but also to understand the importance of ZIP6- and ZIP0-mediated mitosis in normal cell division. Finally, animal models of breast cancer were used in a preliminary study to investigate the ability of the antibodies to slow the growth of solid tumours.

5.5.1. The specificity of the antibodies

Treatment of several cancer cell lines with anti-ZIP6 and -ZIP10 antibodies successfully inhibited nocodazole-induced mitosis, however, it should be noted that the concentration of the anti-ZIP10 antibody used was greater than that of the anti-ZIP6 antibody. The anti-ZIP6 antibody is a monoclonal antibody, generated from one specific immune cell type resulting in a solution of identical antibody molecules which bind the same epitope within an antigen (Ascoli and Aggeler, 2018). In contrast, the anti-ZIP10 antibody is polyclonal, meaning it is a heterogeneous mix of antibodies collected from the serum of the animal in which it was generated (in this case, rabbit). The different antibodies in the mix recognise different epitopes within the same antigen (Ascoli and Aggeler, 2018) so some antibodies may bind to a specific site which is not critical for ZIP10 function. Furthermore, the ZIP10 peptide, when injected into an animal may fold differently to how it folds when it is (a) attached to the rest of the ZIP10 protein and (b) bound to ZIP6 in a heteromer. Therefore, the specific binding sites of some antibodies in the heterogeneous mix may not be accessible to the antibody *in vitro*. The factors described here are likely to contribute to the lower overall efficacy of the anti-ZIP10 polyclonal antibody and hence a higher concentration was needed to inhibit cell division to the same extent as the anti-ZIP6 monoclonal antibody.

The NMuMG ZIP6 KO cell model was a useful tool for investigating the specificity of the anti-ZIP6 antibody for the ZIP6 protein. It was promising that the antibody was not able to inhibit mitosis in this cell model, confirming that inhibition of mitosis is due to the binding of the ZIP6 antibody to the ZIP6 epitope and that other proteins in the cell do not act as targets for the antibody to bind and elicit a secondary effect. IgG molecules bind free zinc ions (Yamanaka *et al.*, 2016) via their F(c) region which may have caused mitosis inhibition by

binding zinc outside the cell and preventing its entry. However, in the absence of ZIP6 (in the ZIP6 KO cell model), the anti-ZIP6 antibody could still bind zinc outside the cell, though this treatment had no effect on mitosis. This confirms the antibody does not prevent mitosis by binding zinc and preventing its entry into the cell. Interestingly, although the NMuMG ZIP6 KO cells have significantly increased protein expression of ZIP10 (Ziliotto, 2018), they also have less zinc, suggesting that ZIP10 is upregulated to increase zinc entry into the cell but that it is unable to fully compensate for the loss of ZIP6. The anti-ZIP10 antibody was as successful at inhibiting mitosis in these cells as it was at inhibiting mitosis in cells expressing ZIP6, highlighting that the increased presence of ZIP10 at the plasma membrane does not make them more sensitive to anti-ZIP10 antibody treatment.

Remarkably, in the NMuMG ZIP6 KO cell line there was reduced protein expression of ZIP5, suggesting protein expression of ZIP5 is dependent on the presence of ZIP6. The BioGRID software (Oughtred *et al.*, 2019) lists ZIP5 as binding both ZIP6 and ZIP10. ZIP5 is linked with cell proliferation in oesophageal cancer (Jin *et al.*, 2015), and the evidence suggests its involvement in proliferation may be via the ZIP6/ZIP10 complex which forms in mitosis. In addition, ZIP5 is the most closely related ZIP transporter to ZIP6 and ZIP10 according to the phylogenetic tree in figure 1.3A and is an interesting protein to investigate further for a role in ZIP6-mediated mitosis.

5.5.2. *In vitro* inhibition of nocodazole-induced mitosis

In vitro, breast cancer, prostate cancer and melanoma cells were all prevented from entering nocodazole-induced mitosis after treatment with the anti-ZIP6 and/or -ZIP10 antibodies. The data implicate a role for ZIP6 and ZIP10 in cell division in each cancer.

Both transporters have been associated with oestrogen receptor-positive breast cancer (Manning *et al.*, 1993; Perou *et al.*, 2000; Dressman *et al.*, 2001; Tozlu *et al.*, 2006; Kagara *et al.*, 2007), which is supported by the data in this chapter as MCF7 cells are a model of this type of breast cancer. Expression of the ZIP6 gene is induced by oestrogen treatment in the ZR-75 human breast cancer cell line (Manning *et al.*, 1988) indicating that the role of ZIP6 in breast cancer cell division is dependent on oestrogen. However, further data from our lab have demonstrated the ability of both antibodies to inhibit cell division in a range of breast cancer cell lines (Nimmanon *et al.*, 2020) including those which are not reliant upon oestrogen for their growth (oestrogen receptor-negative). In these types of breast cancer, ZIP6 may rely upon different signals to initiate activation and zinc transport in mitosis. These

data do suggest that ZIP6 and ZIP10 targeted antibodies could offer therapeutic potential in a wider range of breast cancers.

The idea that ZIP6 and ZIP10 are involved in mitosis independently of other signalling pathways that regulate growth is even more apparent in the prostate cancer cell line. Intracellular zinc is known to decrease in prostate cancer cells due to the loss of ZIP1 impeding their ability to accumulate zinc (Franklin *et al.*, 2005). The loss of zinc accumulation is an early event in the development of prostate cancer, however, the data presented here provide evidence that prostate cancer cells maintain the need for ZIP6 and ZIP10 to enter mitosis. It is likely that the efficacy of the antibody treatment is dependent on other cellular factors at the time of binding i.e. the cells having the machinery in place to begin mitosis when the zinc enters. Exposure of prostate cancer cells to physiological concentrations of zinc is cytotoxic (Liang *et al.*, 1999) implicating not only their ability to survive in low zinc concentrations but their dependency on it. This is further evidence that targeting the ZIP6 and ZIP10 transporters effects an independent signalling pathway specific to mitosis, and not the well-established zinc-dependent pathway that maintains male reproductive health (figure 5.22). Therefore, targeting ZIP6 and ZIP10 in prostate cancer cells could successfully inhibit cell division while maintaining the homeostatic balance of zinc required to maintain the integrity of sperm and subsequently, male fertility could be preserved.

The finding that the melanoma cell line was more sensitive to anti-ZIP10 antibody treatment than the other cell lines tested was particularly interesting. Unpublished data from our lab have shown that, in basal conditions, 100% of SK-MEL-29 cells are positive for activated ZIP7 (pZIP7), which releases zinc from intracellular stores (Taylor *et al.*, 2012). In contrast, only 10% of MCF7 cells in basal conditions are positive for pZIP7, suggesting the melanoma cells are actively using zinc signalling pathways more than the breast cancer cells which may explain their greater sensitivity to treatment with the anti-ZIP10 antibody. This is comparable to anti-hormone resistant breast cancer cells, in which protein expression of ZIP7 and activated ZIP7 is prevalent (Kathryn M. Taylor *et al.*, 2008; Ziliotto *et al.*, 2019). The potential to use a reduced dose of this antibody to treat melanoma would also reduce the risk of side effects, making it a more desirable treatment than many chemotherapies (the side effects of chemotherapy are discussed in more detail in the following chapter). Furthermore, STAT3 is constitutively phosphorylated on serine 727 in melanoma cells (Sakaguchi *et al.*, 2012), a phosphorylation typically associated only with mitosis (Nimmanon *et al.,* 2020). Treatment of melanoma cells with tumour promoting agent TPA (12-O-

tetradecanoylphorbol-13-acetate) is associated with increases of both pS^{727}STAT3 and ERK 1/2 (extracellular signal regulated kinase 1/2) the latter of which is also associated with cell cycle progression (Chambard *et al.*, 2007), implicating both proteins in the survival of skin cells (Oka *et al.*, 2004; Sakaguchi *et al.*, 2012). It is expected that inhibition of ZIP6 or ZIP10 with antibody treatment would decrease pS^{727}STAT3 activity in mitosis, since they are bound together in a complex, limiting the chance of cancer cell survival even further.

Interestingly, ERK activity is also upregulated in response to ZIP7-mediated zinc release from intracellular stores in breast cancer cells (Nimmanon *et al.*, 2017). This is an additional example of ZIP7 involvement in tumour progression pathways, and the potential crosstalk of ZIP7 activity with ZIP6 and ZIP10 to mediate cell proliferation.

An important finding of this chapter is the ability of the ZIP6 and ZIP10 targeted antibodies to inhibit mitosis in non-cancerous cells. These data support the hypothesis that ZIP6 and ZIP10 play a crucial role in cell division in all cell types. Therefore, cancer treatment with the antibodies would aim to take advantage of the increased proliferative ability of cancer cells compared with healthy cells (Feitelson *et al.*, 2015).

Figure 5.22. Hypothesis of zinc signalling pathways in the prostate

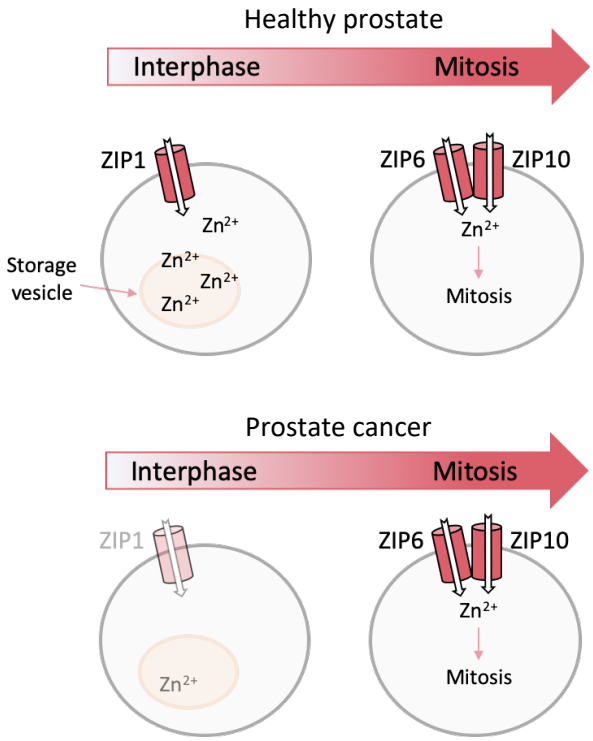

Schematic depicting the hypothesis that ZIP6- and ZIP10-mediated zinc transport in mitosis of prostate cells is independent of the zinc import required to maintain male reproductive health. In prostate cancer, the cells lose ZIP1 and therefore lose the ability to accumulate zinc but maintain the ability to divide through ZIP6- and ZIP10-mediated zinc entry in mitosis.

5.5.3. Targeting ZIP6 and ZIP10 at the same time

Addition of both the anti-ZIP6 and anti-ZIP10 antibodies to the same cells significantly decreased the percentage of mitotic cells, compared with treatment of each antibody individually and with nocodazole treatment alone. This data is proof of the principle that a cancer treatment could be made of a heterogeneous mix of both antibodies and it may prove to be more effective than the use of either antibody alone. It is unclear whether the antibodies in the mixture bind both ZIP6 and ZIP10 in the same heteromer, or whether the anti-ZIP6 antibody binds ZIP6 in one heteromer while the anti-ZIP10 antibody binds ZIP10 in a separate heteromer (figure 5.23A).

However, the data do provoke interesting discussion about the generation of a single antibody with the capability to bind both ZIP6 and ZIP10 at the same time, known as a bispecific antibody (Labrijn *et al.*, 2019) (figure 5.23B). A single antibody with an epitope for both ZIP6 and ZIP10 may be able to bind and completely inhibit one ZIP6/ZIP10 heteromer or have the ability to crosslink cells, by binding ZIP6 on one cell and binding ZIP10 on a nearby cell (figure 5.23C). Bispecific antibodies have been used clinically to bind antigens on different cells (e.g. a tumour cell and immune cell) to elicit an immune response and lysis specifically of the tumour cell (Offner *et al.*, 2006). One example of this is blinatumomab; which binds both the T cell receptor CD3 and the B lymphocyte antigen CD19. Blinatumomab gave very good clinical results for the treatment of B cell leukaemia (Gökbuget *et al.*, 2018) and patients had a much better survival rate compared to those on standard chemotherapy (Kantarjian *et al.*, 2017). It was marketed for the treatment of relapsed or refractory acute lymphoblastic leukaemia in the EU in 2015 (Labrijn *et al.*, 2019). In addition, the technology is not only limited to cancer treatment; emicizumab binds clotting factors 9 and 10 to mimic the actions of clotting factor 8 which is deficient in patients with haemophilia A (Oldenburg *et al.*, 2017), indicating that a bispecific ZIP6/ZIP10 antibody could also be used in other diseases of zinc dysregulation.

Figure 5.23. Targeting ZIP6 and ZIP10 at the same time to inhibit cell division

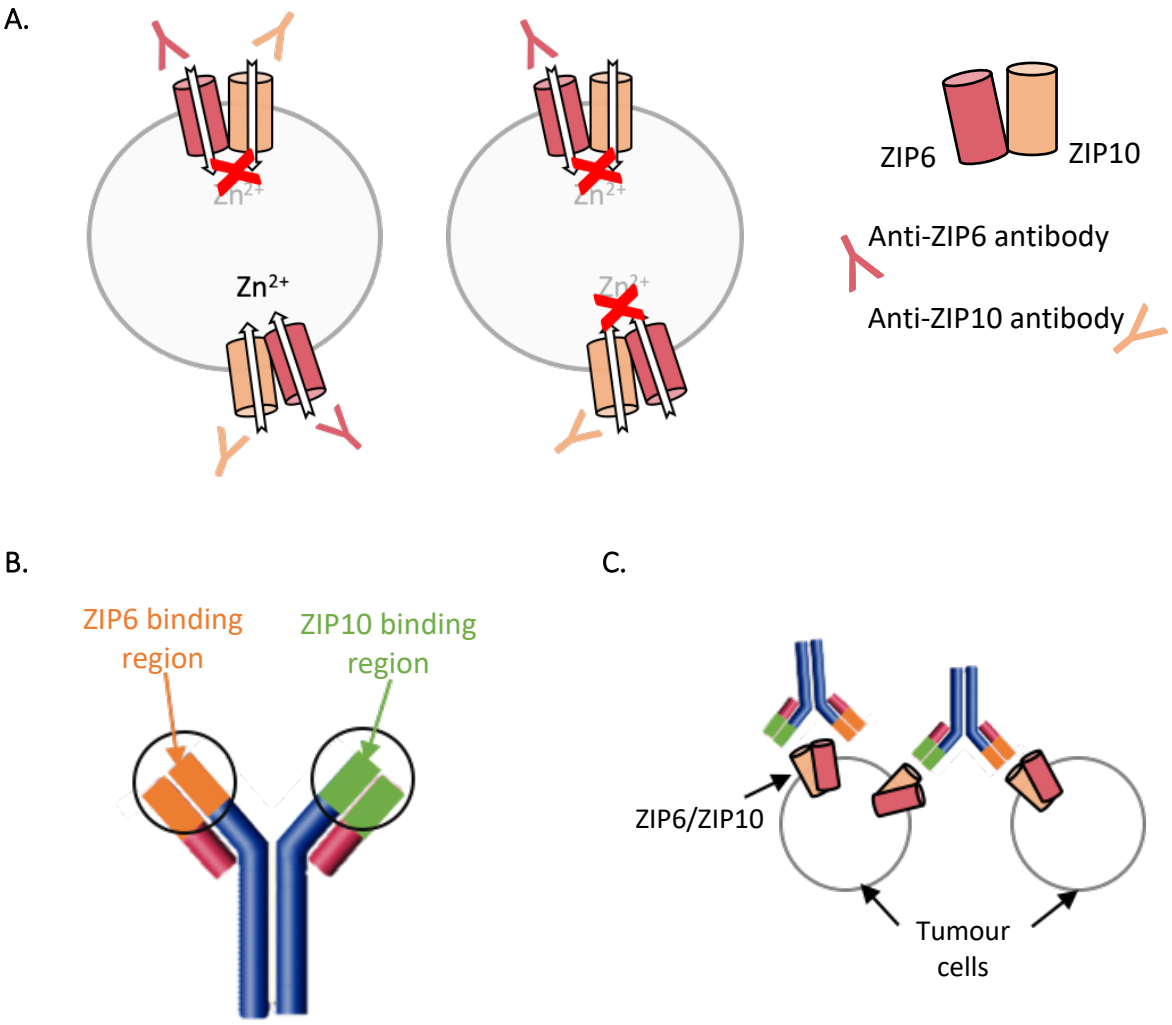

***A**. Antibodies may bind their respective targets in the same heteromer (left) to prevent zinc influx or bind their respective targets in separate heteromers on the same cell (right). **B**. The proposed structure of a bispecific antibody with binding regions for both ZIP6 (orange) and ZIP10 (green). **C**. A ZIP6/ZIP10 bispecific antibody could have the potential to bind both proteins in one ZIP6/ZIP10 heteromer or cross-link two heteromers on two tumour cells.*

5.5.4. Antibody inhibition of cell growth

As mitosis takes 1 hour of a much longer cell cycle (approximately 24 hours in MCF7 cells), no more than 5% of cells are usually in mitosis under basal conditions, therefore nocodazole treatment was used to synchronise cells in mitosis and allow the effect of the antibody treatments to be seen. However, both antibodies inhibit mitosis in MCF7 cells synchronised in mitosis by serum starvation in the absence of nocodazole (Nimmanon, 2016), confirming the inhibitory effect of the antibodies is not due to interaction with nocodazole preventing nocodazole-induced cell cycle arrest. This is an important finding because the use of chemicals to synchronise cells in mitosis does not necessarily reflect the development of solid tumours clinically.

Another way to overcome this problem was to test the ability of the antibodies to inhibit growth when cells are treated for several days. Treatment with either the anti-ZIP6 or -ZIP10 antibody significantly suppressed the growth of MFC7 breast cancer cells over a 4-day period (Nimmanon *et al*., 2020) and cyclin analysis of cells inhibited with the antibodies revealed the cells were arrested in the G2 phase of the cell cycle (Ziliotto, 2018). The results in this chapter show that removal of the anti-ZIP10 antibody following 5 days of treatment allows cells to re-enter the exponential phase of growth, implicating they do not die following 5 days of treatment. Furthermore, their ability to continue growth after removal of the antibody implies that the cells have not entered senescence (irreversible cell-cycle arrest) (Dodig, Cepelak and Pavic, 2019). In contrast, the cells may enter a state of quiescence, in which they maintain metabolic pathways but do not continue the cell cycle (Cho *et al.*, 2019). The maintenance of cancer cells in a quiescent state is a novel approach to the treatment of cancers, to prevent them from re-entering the cell cycle and ultimately causing apoptosis (Mackay *et al.*, 2012). This is particularly important in the prevention of metastatic cancer, in which a small number of cells settle in a different part of the body and become quiescent. These cells may not re-enter the cell cycle until years after the primary tumour is treated and therefore are completely undetected during initial follow-up in clinic (Wells *et al.*, 2013). The prognosis of metastatic tumours is much worse than those that remain in their primary site (Welch and Hurst, 2019). The anti-ZIP6 and -ZIP10 antibodies, therefore, may have the potential to maintain cancer cells in a quiescent state if sufficient doses were given to maintain the concentration of drug in the body.

5.5.5. *In vivo* inhibition of tumour growth

Having concluded that both the anti-ZIP6 and -ZIP10 antibodies can successfully inhibit cell division *in vitro*, the next step was to test this ability of the antibodies to reduce tumour growth *in vivo*. A triple-negative breast cancer cell line, MDA-MB-231, was used for the xenograft mouse models in this preliminary study due to their quick growth rate and ability to form tumours. This cell line represents a particularly aggressive form of breast cancer, for which there is an unmet clinical need (Nasrazadani *et al.*, 2018) and both the anti-ZIP6 and -ZIP10 antibodies do inhibit cell division in this cell line *in vitro* (Nimmanon *et al.,* 2020). The anti-ZIP6 antibody was used in this study at 1 mg/kg and was the same concentration used for an *in vivo* study of a humanised anti-ZIP6 antibody conjugated to a toxin (SGN-LIV1) (Sussman *et al.*, 2014).

The tumour tissue was excised from the mice following treatment and fixed in formalin. The tissue samples will be analysed using immunohistochemistry to assess the levels of cleaved caspase-3, to assess apoptosis (Nicholson *et al.*, 1995), the tumour proliferation marker ki67 (Brown *et al.,* 1990), and pS^{10}Histone H3, a marker of mitosis. These data will help to inform the discussion about the specific effect of the anti-ZIP6 antibody on tumour tissue. The inability of the anti-ZIP6 antibody to inhibit mitosis in the NMuMG ZIP6 KO cell line does highlight that the antibody is specific to its target protein and in particular, confirms that the effect is not due to the IgG binding zinc and preventing its entry into the cell that way, as IgG proteins are known to bind zinc (Yamanaka *et al.*, 2016). Distal organs were also harvested which will allow for preliminary studies into the toxicity of the antibody at the concentrations used. Finally, tumour tissue was homogenised and stored in RNAlater (a non-toxic tissue storage reagent that stabilizes RNA) to allow for the study of downstream signalling pathways at a transcriptional level, and how they have been affected by the drug.

5.5.6. Anti-ZIP6 and -ZIP10 antibody mechanism of action

Although there is no crystal structure available for a ZIP transporter, there is a structural model of the N-terminal ectodomain of ZIP4, which forms homodimers on the plasma membrane (Zhang, Sui and Hu, 2016). The authors determined that the ZIP4 dimerisation is centred around the *CPALLY* motif in the N-terminus of each ZIP4 protein. Using the structural model of ZIP4 homodimers, it is speculated that the N-terminal ectodomains of ZIP6 and ZIP10 are also intertwined around each other on the plasma membrane (figure 5.24), meaning that binding of either antibody affects the tertiary structure and therefore

transport ability of the heteromer. This hypothesis supports the data in this chapter that show that treatment of cells with only one antibody is sufficient to prevent nocodazole-induced mitosis.

The data in chapter 3 highlighted the probable "switching off" of ZIP10 by ectodomain shedding in breast cancer cells. However, in prostate cancer cells the full length of ZIP10 was present on the plasma membrane throughout mitosis, possibly reflecting the increased need for zinc in these cells (Zaichick, Sviridova and Zaichick, 1997). The association of the N-terminal fragment with intracellular structures after 18 hours of antibody treatment may reflect premature ectodomain shedding of ZIP10 in response to antibody binding in the prostate cancer cells. The ectodomain and the antibody may then have been internalised together.

Eighteen hours after treatment of breast cancer cells with the anti-ZIP10 antibody, the antibody was still present on the outside of non-mitotic cells suggesting that in this cell line antibody binding does not encourage premature ectodomain shedding but exerts an inhibitory effect on ZIP10 in another way. In chapter 1 the hypothesis that the spare cysteine residue in the N-terminus of LIV-1 transporters could bind the cysteine immediately prior to the *HEXPHE* motif in TMD5 to regulate zinc transport was introduced. In this case, antibody binding could disrupt the N-terminal interaction with TMD5 potentially causing the transporter to close. This is supported by the use of an N-terminal ZIP10 targeted antibody blocking the functional ability of ZIP10 to influx zinc in the maturing oocyte (Kong *et al.*, 2014). In addition, this experiment revealed ZIP10 positive cells which were positive for pS^{10}Histone H3 even though they had not entered prophase. Initiation of S10 phosphorylation of Histone H3 begins in late G2 and causes punctate staining before complete condensation of chromosomes in mitosis (Hendzel *et al.*, 1997). This supports the hypothesis of ZIP10 upregulation and presence at the plasma membrane at the end of G2, and the data presented in chapter 3 that suggested the both presence of the full-length ZIP10 on the plasma membrane before the onset of mitosis, and ectodomain shedding after mitosis has started to "switch off" zinc transport.

Furthermore, treatment with the ZIP10 antibody in MCF7 cells caused a significant decrease in the protein level of pS^{727}STAT3, which associates with the ZIP6/ZIP10 heteromer via the STAT3 binding site in the intracellular loop of ZIP6 (Nimmanon *et al.*, 2020). These data implicate pS^{727}STAT3 as a downstream protein in the ZIP6/ZIP10-mediated mitotic pathway

and is supported by the data that show zinc is required for S727 phosphorylation of STAT3 (Kitabayashi *et al.*, 2010).

Figure 5.24. The proposed structure of the ZIP6/ZIP10 heteromer on the plasma membrane

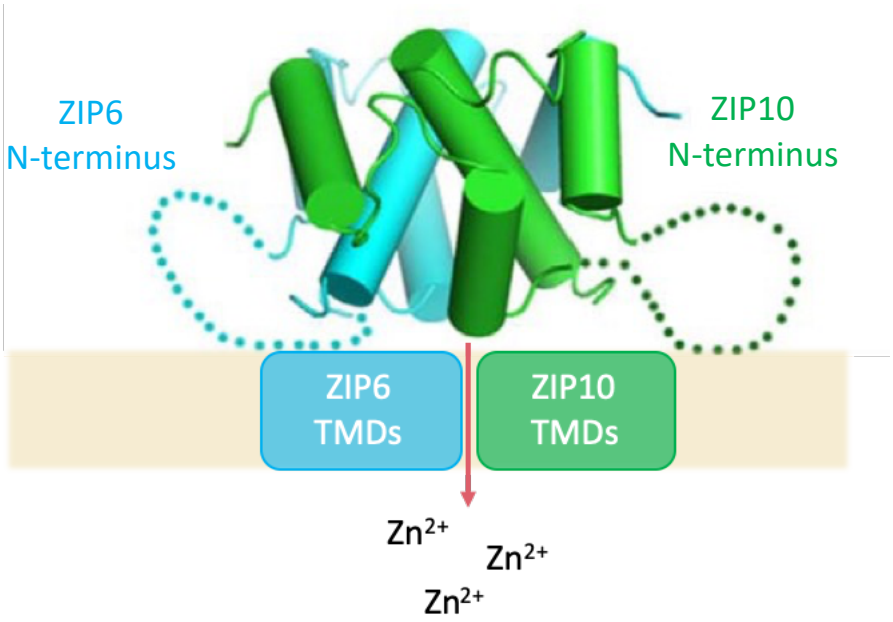

A structural model of the ZIP4 N-terminal ectodomains in the ZIP4 homodimer has been adapted to propose the structure of the ZIP6/ZIP10 heteromer on the plasma membrane. The ZIP6 N-terminus is shown in blue and the ZIP10 N-terminus in green. Adapted from Zhang, Sui & Hu (2016). TMD, transmembrane domain.

5.5.7. Chapter summary and conclusions

This chapter has highlighted the potential use of ZIP6 and ZIP10 targeted antibodies to prevent cell division in an antibody-concentration dependent manner. *In vitro,* both antibodies, both individually and together, successfully inhibited nocodazole-induced mitosis in breast cancer, prostate cancer, and melanoma cells. The antibodies also inhibited nocodazole-induced mitosis in normal (non-cancerous) cells, indicating ZIP-mediated cell division is important in all cell types. Furthermore, a ZIP6 KO cell model enabled the study of the specificity of the anti-ZIP6 antibody which did not inhibit mitosis in the absence of the ZIP6 protein. Cell growth assays showed that treatment with the anti-ZIP10 antibody slowed cell growth over a 7-day period, but that the effect was reversible as cells are able to re-enter the exponential phase of growth soon after the antibody is removed. *In vivo*, the anti-ZIP6 antibody slowed tumour growth of MDA-MB-231 tumour cells in xenograft mice models over a 20-day period, indicating the potential for this antibody to be used clinically in the treatment of breast cancer. Furthermore, a potential role for ZIP5 in mitosis was identified, its protein expression seemingly dependent on ZIP6 protein expression.

Taken together, the data presented in this project evidence the complex post-translational modification of ZIP transporter ZIP10 in mitosis and suggests a role for both ZIP6 and ZIP10 in mitosis of several cell types. This not only supports the evidence of an important role for zinc in cell cycle regulation but suggests that ZIP transporters could realistically become therapeutic targets in diseases of uncontrolled cell division.

Chapter 6. General discussion

As the data in the literature regarding zinc in human health expand, the number of diseases which have been attributed to zinc dysregulation has also grown. Zinc itself is a difficult metal to study due to the high proportion that is protein-bound. Attention has turned to zinc transporters as a measure of zinc signalling, and many, including ZIP6 and ZIP10, have since been associated with cancer.

To understand fully the link between ZIP10 and cancer and assess how appropriate ZIP10 may be as a therapeutic target, it is important to gain a broader understanding of ZIP10 regulation. In this project, various anti-ZIP10 antibodies were used to characterise proteolytic cleavage of ZIP10 in response to certain stimuli, and it was concluded that ZIP10 undergoes ectodomain shedding in both mitosis and in response to zinc starvation (chapter 3). Furthermore, ZIP10 is phosphorylated on serine 591 in mitosis, and cells expressing a mutant variant of ZIP10 in which this residue cannot be phosphorylated have less intracellular zinc (chapter 4). The project also confirmed that the ZIP6/ZIP10 heteromer can be inhibited to prevent cell division *in vitro* using specific N-terminal targeted antibodies and the anti-ZIP6 antibody slows tumour growth *in vivo* (chapter 5).

In this chapter, the implications of these results will be discussed in more detail, both in the context of cellular zinc biology and the clinical use of targeting zinc transporters in disease.

6.1. Regulation of ZIP transporters

This project has demonstrated the post-translational modification of ZIP10 by proteolytic cleavage, glycosylation and phosphorylation.

In particular, the finding that ZIP10 protein levels are controlled by zinc availability highlights the importance of this transporter in the maintenance of intracellular zinc homeostasis. Both ZIP4 and ZIP5, other members of the LIV-1 family of ZIP transporters, undergo protein regulation in response to zinc availability. Similarly to ZIP10, the presence of ZIP4 on the plasma membrane is increased in response to zinc starvation (Dufner-Beattie *et al.*, 2004) owing to decreased endocytosis and is rapidly degraded once zinc is replenished (Kim *et al.*, 2004; Mao *et al.*, 2007; Weaver *et al.*, 2007). Furthermore, ZIP4 mRNA becomes unstable when zinc levels are adequate and becomes stable during zinc deficiency (Dufner-Beattie *et al.*, 2004; Weaver *et al.*, 2007). In contrast, ZIP5, which is closely related to ZIP6 and ZIP10, is degraded in response to zinc deficiency and ZIP5 mRNA is translated when zinc levels are restored (Weaver *et al.*, 2007).

Another ZIP transporter that has been shown to be regulated by proteolytic cleavage is ZIP6, which undergoes cleavage at a PEST site approximately half-way along its N-terminus in the endoplasmic reticulum before it relocates to the plasma membrane (Hogstrand *et al.*, 2013). This plasma membrane form of ZIP6 is the active transporter that influxes zinc into cells (Hogstrand *et al.*, 2013). In the later stages of mitosis, the remainder of the ZIP6 N-terminus is cleaved (Nimmanon *et al.,* 2020), which may reflect a "switch off" mechanism for zinc transport via ZIP6 similar to the ectodomain shedding of ZIP10.

Collectively, the evidence shows that ZIP transporters are able to respond to zinc in their environment and that their responses to zinc availability differ across cell types. Conserved histidine-rich regions through the proteins are likely to be crucial for their zinc-sensing ability due to the known ability of histidine to bind zinc (Guerinot, 2000). The histidine content of ZIP10 is 10.8%, more than four-fold higher than the average histidine content of other proteins (Strohl, 2017). This implies an important role in the zinc sensing ability of ZIP10. The histidine-rich region in the intracellular loop between TMD3 and TMD4 is essential for the degradation of ZIP4 (Mao *et al.*, 2007), and is a region which is highly conserved among the LIV-1 family of zinc transporters (Taylor *et al.*, 2007). Furthermore, phosphorylation of histidine residues has recently emerged as a post-translational modification involved in signal transduction (Fuhs and Hunter, 2017). The instability of phosphorylated histidine residues makes them difficult to study (Attwood *et al.*, 2007), however it has been suggested that cells use phospho-histidine to coordinate metal ions within certain proteins e.g. the calcium-activated potassium channel KCa3.1 is stimulated by histidine phosphorylation of residue 358 (Srivastava *et al.*, 2016). In addition, many zinc-binding proteins have been identified as substrates for histidine phosphorylation (carbonic anhydrase II, zinc finger protein and kinase suppressor of Ras 1) (Fuhs and Hunter, 2017). The large number of histidine residues in ZIP transporters implicates the potential for histidine phosphorylation to be an important regulator of transporter activity.

In chapter 3 it was highlighted that ZIP10 is also regulated at a transcriptional level in response to zinc availability through zinc-activated metal transcription factor (MTF1). Interestingly, cadmium-activated MTF1 also binds to the ZIP10 promotor and causes downregulation of ZIP10, suggesting that ZIP10 responds to metals other than zinc (Wimmer *et al.*, 2005). Members of the ZIP family do transport other metals such as iron, manganese, cadmium, and copper (Eide *et al.*, 1996; Grotz *et al.*, 1998; Wintz *et al.*, 2003; Cohen, Garvin and Kochian, 2004; Pedas *et al.*, 2008; Lin *et al.*, 2009; Jenkitkasemwong *et al.*, 2012), albeit

to a lesser extent than zinc. ZIP2 and ZIP8 have been reported as zinc/HCO_3 cotransporters (Gaither and Eide, 2000), further highlighting the diversity of roles within the family. In ZIP8 and ZIP14, the *HEXPHE* motif in transmembrane domain 5 is modified slightly to *EEXXH* which is responsible for the loss of zinc selectivity of these transporters; ZIP8 has a preference for cadmium (Dalton *et al.*, 2005) and ZIP14 a preference for iron (Liuzzi *et al.*, 2006).

The ability of ZIP10 to be transcriptionally regulated by both zinc deficiency and zinc excess in different tissues, to respond to dietary zinc and the availability of other transition metals confirms its importance in a diverse range of signalling pathways. It is likely that the post-translational modification of ZIP10 is equally diverse in response to different stimuli.

6.2. Hub of zinc signalling in cells: ZIP10, ZIP6 and ZIP7

There is growing evidence that ZIP10 may act together with ZIP6 and ZIP7 to control cellular zinc homeostasis. For example, zinc released from intracellular stores via ZIP7 causes widespread tyrosine phosphatase inhibition (Haase and Maret, 2003). It is possible that one of the phosphatases inhibited dephosphorylates ZIP10 tyrosine 596, leading to zinc-induced zinc influx in a positive feedback loop. Tyrosine phosphorylation of ZIP transporters is currently an unexplored post-translational modification; however, it is potentially important in understanding zinc signalling pathways in cancer. Tyrosine phosphorylation of ZIP6 residue 528 has been demonstrated in 126 mass spectrometry screens (table 4.4), the largest number for any ZIP transporter tyrosine residue. The lack of prediction of a kinase that phosphorylates this residue (Nimmanon and Taylor, 2019) however, may be an indication that the sequence does not follow already recognised consensus sequences for tyrosine phosphorylation. Therefore, ZIP transporter tyrosine phosphorylation is an entirely new and exciting field of study.

Both ZIP6 and ZIP10 contribute to zinc-dependent inhibition of GSKβ in a pathway that leads to epithelial to mesenchymal transition (EMT) (Hogstrand *et al.*, 2013; Taylor *et al.*, 2016) through downregulation of E-cadherin. The first stage in EMT is cell rounding and detachment from other cells and/or stroma, which is also the first stage in mitosis (Pugacheva, Roegiers and Golemis, 2006). ZIP7-mediated zinc release from intracellular stores also deactivates GSKβ (Nimmanon *et al.*, 2017), which not only links ZIP7 to a role in EMT, but is the first evidence to suggest that ZIP7 may also play a role in mitosis (figure 6.1). The MAPK/ERK pathway which regulates cell growth and proliferation (Chambard *et al.*,

2007) is activated in response to ZIP7-mediated zinc release, further cementing a role for ZIP7 in cell cycle regulation alongside ZIP6 and ZIP10.

Furthermore, the data presented in chapter 4 highlight the potential cyclic regulation of intracellular zinc by ZIP10 and ZIP6 in mitosis, ZIP10 in G1 and ZIP7 in S phase. No other ZIP transporters have been implicated in cell cycle regulation and this fact taken together with the data presented here, does suggest that ZIP6, ZIP7 and ZIP10 may have a close relationship in maintaining zinc signalling pathways that allow cells to divide. Cancer therapies that target zinc signalling pathways may be of more benefit if they target each of these transporters. Furthermore, targeting each transporter may limit the risk that one transporter becomes upregulated in response to another not being available.

ZIP7 was recently identified as a regulatory protein in Notch signalling (Nolin *et al.*, 2019), a highly regulated pathway involved in development and differentiation (Hori, Sen and Artavanis-Tsakonas, 2013). This novel role for ZIP7 in plasma membrane protein trafficking in the endoplasmic reticulum is evidence of a zinc transporter involvement in a process not directly related to zinc. At the plasma membrane, Notch itself is regulated by ADAM-mediated ectodomain shedding (Hansson *et al.*, 2010), generating the substrate for a further cleavage by the γ-secretase complex (Huppert *et al.*, 2000). It is interesting that ZIP7 is involved in the trafficking of a protein regulated in the same way that was proposed for ZIP10, in chapter 3. Following ectodomain shedding, the intracellular region of Notch is trafficked to the cell nucleus where it exerts transcriptional activity (Hartmann, Herrlich and Herrlich, 2013), a process that is negatively regulated by zinc (Baek *et al.*, 2007). The Notch signalling pathway therefore is both positively and negatively regulated, by ZIP7 and zinc respectively, highlighting the diverse role of this second messenger and its transporters in the cell.

Figure 6.1. The crosstalk of ZIP10 with other ZIP transporters

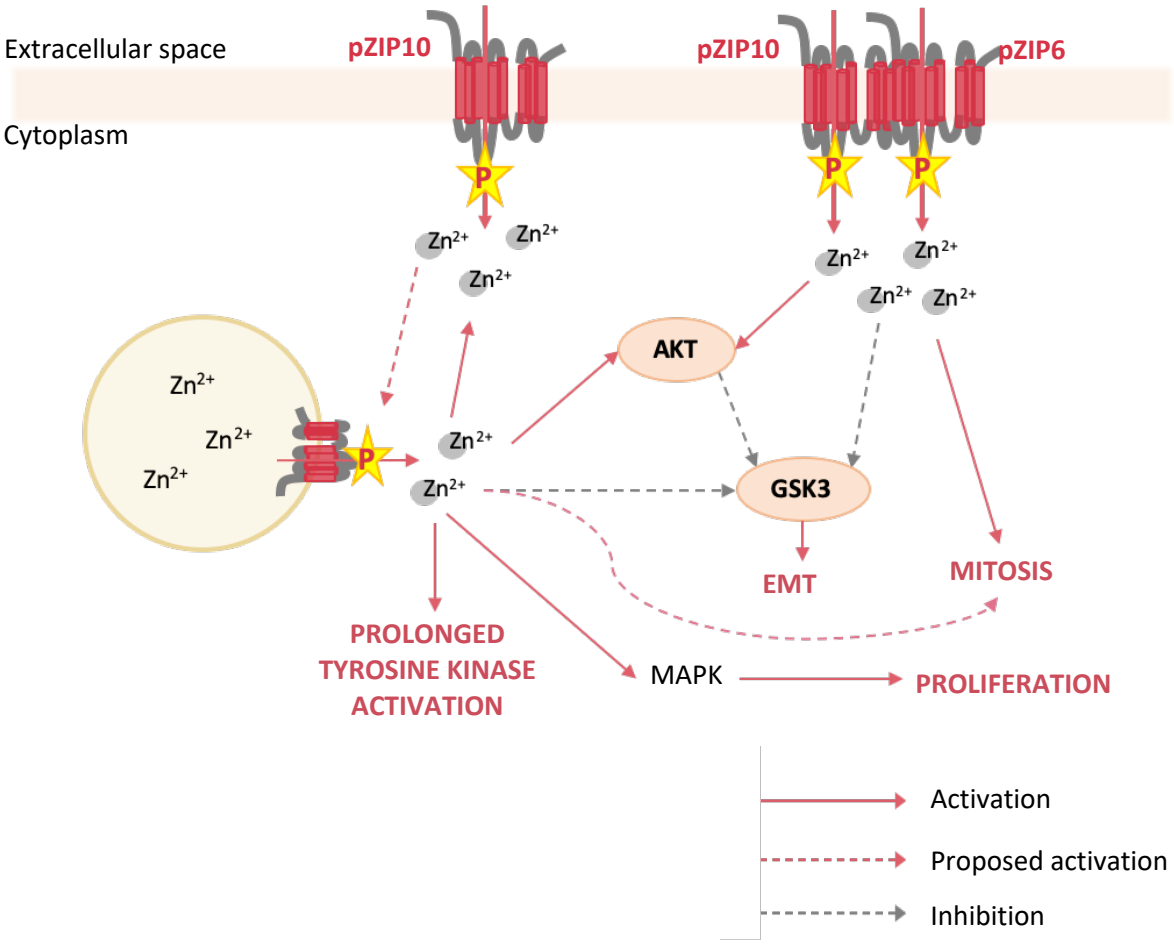

ZIP7-mediated zinc release from intracellular stores prolongs tyrosine kinase activation, which may be exacerbated by tyrosine 596 phosphorylation of ZIP10, increasing intracellular zinc concentration and further increasing ZIP7-mediated zinc release from stores. Increasing intracellular zinc concentration inhibits GSK3β activity directly, and indirectly through AKT activation, leading to EMT. Finally, zinc entry through ZIP6 and ZIP10 causes mitosis. Increased tyrosine kinase activity, EMT, and mitosis are all hallmarks of cancer.

6.3. The diversity of ZIP10

Although this project has investigated the role and regulation of ZIP10 mainly in mitosis, there is a wide range of evidence that shows the role of ZIP10 is not limited to cell division.

In B cells, ZIP10-mediated zinc entry promotes cell survival by inhibiting caspase activity (Miyai *et al.*, 2014). The role of ZIP10 in both anti-apoptotic signalling and cell cycle progression is likely to contribute to the development of several cancers in which its increased expression has been observed (chapter 1). ZIP10-mediated inhibition of caspase activity is regulated by STAT3/STAT5 activation; the promoter region of ZIP10 contains a binding site for the transcription factor pY^{705}STAT3 (Miyai *et al.*, 2014). pY^{705}STAT3 is a diverse protein with roles in many cellular processes including growth, differentiation and survival (Guanizo *et al.*, 2018) highlighting the wide range of signalling cascades in which ZIP10 transcription may be an outcome.

Zinc entry to the cell via ZIP10 is vital for successful meiosis during the oocyte-to-egg transition (Kong *et al.*, 2014). The viability and motility of sperm is dependent on a high intracellular zinc content (Yamaguchi *et al.*, 2009) and zinc-deficient mice have a lower testicular abundance of both ZIP6 and ZIP10 (Croxford, McCormick and Kelleher, 2011) implicating these transporters in the development of mature male gametes (spermatogenesis); essential for sexual reproduction.

Hypoxia in cardiomyocytes causes accumulation of free zinc but reoxygenation results in a loss of zinc and decreased cell viability, due to decreased ZIP proteins including ZIP10 (Bodiga *et al.*, 2017). ZIP10 is an important regulator of intracellular zinc in cardiomyocytes suggesting that its deregulation in hypoxia is involved in the pathogenesis of myocardial ischemia (Thokala *et al.*, 2019). Furthermore, zinc is essential for the development of red blood cells (erythropoiesis) and ZIP10 mRNA is increased after addition of the main erythropoiesis promoter, erythropoietin (EPO), to differentiating red blood cells (Ryu *et al.*, 2008). This suggests that ZIP10 is, at least partially, responsible for fulfilling the zinc requirement of red blood cell development and therefore key to the systemic delivery of oxygen to tissues.

Development of murine skin in embryogenesis has been attributed to ZIP10-dependent zinc supply to the metal binding sites in transcription factor p63 (Tichý *et al.*, 2013; Bin *et al.*, 2017). Furthermore, in keratinocytes, inhibition of ZIP10 downregulates histone

acetyltransferases (HATs) (Bin *et al.*, 2019) and modifies chromatin accessibility for transcription factor binding (Trisciuoglio, Di Martile and Del Bufalo, 2018). Therefore, ZIP10 controls gene expression of homeostatic factors including profilaggrin (Bin *et al.*, 2019), a structural protein in the epidermis; the body's first defence to external pathogens.

Both ZIP10 and ZIP6 have been implicated in the process of EMT though inhibition of GSKβ (Yamashita *et al.*, 2004; Hogstrand *et al.*, 2013; Taylor *et al.*, 2016) and regulation of the cell-adhesion molecule NCAM1 (Brethour *et al.*, 2017). EMT is caused by the loss of cell-cell adhesion molecules enabling cells to gain migratory properties (Kalluri and Weinberg, 2009). EMT is a vital stage of embryogenesis (Hay, 1995) and wound healing (Haensel and Dai, 2018); both of which are essential to maintain human growth and development. On the other hand, cancer cells that undergo EMT metastasize to distal organs (Kalluri and Weinberg, 2009), resulting in a disease state that is no longer curable. Both transporters are therefore implicated in cancers with more aggressive phenotypes. Knock-out of either ZIP6 or ZIP10 inhibits high glucose-induced cell migration (Takatani-Nakase, 2013; Takatani-Nakase *et al.*, 2014), implicating ZIP6 and ZIP10 in diabetic patients with breast cancer, who typically have a poorer prognosis than their non-diabetic counterparts (Peairs *et al.*, 2011).

The evidence presented here highlights that ZIP10 is involved in several processes across numerous cell types. ZIP10 regulation is likely to be specific to the cell type and this helps to explain the diversity in the mechanisms by which it is regulated that have been described throughout this project. It should be noted that the processes mentioned here may be affected following systemic treatment with an anti-ZIP10 antibody to treat cancer. If so, the knowledge will enable appropriate measures to be taken to maintain zinc homeostasis in other cell types, limiting the side effects experienced by the patient.

6.4. ZIP6- and ZIP10-mediated mitosis mechanism

This project has identified several proteins with which ZIP10 interacts, and this provides some clues as to the mechanism of ZIP6/ZIP10-mediated mitosis. The serine 727 phosphorylation of STAT3 (pS^{727}STAT3), is associated with mitosis (Shi *et al.*, 2006; Huang *et al.*, 2014) and has a reciprocal relationship with the tyrosine 705 phosphorylated form of STAT3 (pY^{705}STAT3) (Nimmanon *et al.,* 2020). Y705 phosphorylation of STAT3 causes STAT3 dimerisation and translocation to the nucleus where the homodimers act as transcription factors (Decker and Kovarik, 2000). The role of pS^{727}STAT3 has been studied to a much lesser extent though it is the predominant form of the protein in mitosis (Shi *et al.*, 2006; Silva and

Cassimeris, 2013). Binding of zinc to pY^{705}STAT3 alters the tertiary structure of pY^{705}STAT3 and inhibits its activity (Kitabayashi *et al.*, 2010). Together with the knowledge that transcription ceases in mitosis (Zaret, 2014) this evidence favours the hypothesis that zinc entry into the cell in mitosis via the ZIP6/ZIP10 heteromer causes the inhibition of Y705 STAT3 activity allowing S727 to be phosphorylated. In addition, ZIP6 binds pS^{727}STAT3 in mitosis (Nimmanon *et al.,* 2020) suggesting that ZIP6 regulates its own activity through zinc import allowing subsequent recruitment of pS^{727}STAT3 to the heteromer. This highlights the need for zinc influx before the serine phosphorylation of STAT3 can occur, confirming the need for an active zinc transporter at the plasma membrane, before mitosis can begin.

The exact role of pS^{727}STAT3 in this complex is yet to be determined though it has been demonstrated to bind pS^{38}Stathmin, a potent regulator of microtubule assembly in mitosis (Iancu *et al.*, 2001; Ng *et al.*, 2006), therefore providing a role for STAT3 in the microtubule arrangement required for mitosis. Interestingly, one identified downstream target of this complex is PLK1 (Silva and Cassimeris, 2013; Morris *et al.*, 2017), shown in this project to associate with ZIP10 in mitosis (figure 6.2A).

E2F, a transcription factor that regulates cell cycle progression and tumour growth (Chen, Tsai and Leone, 2009) and a known transcriptional activator of PLK1 (Bracken *et al.*, 2004), is inhibited by knock-down of ZIP10 using siRNA (Lichten *et al.*, 2011). E2F activity also regulates transcription of CDK1 (Ishida *et al.*, 2001), which itself is activated by PLK1. CDK1 activation leads to condensin association with chromosome arms and chromosome condensation, necessary for mitosis to begin (Abe *et al.*, 2011).

This project has highlighted the potential phosphorylation of ZIP10 by both CDK1 and PLK1 in mitosis (chapter 4). Cells expressing recombinant ZIP10 with a mutant CDK1 phosphorylation site (S591A) had less intracellular zinc suggesting that CDK1 phosphorylation of ZIP10 enhances ZIP10 zinc transport ability. At which stage CDK1 interacts with ZIP10 is unclear, however if CDK1 becomes activated as a result of ZIP10-mediated zinc influx it is possible to speculate CDK1 phosphorylates ZIP10 to increase zinc transport function further, in a positive feedback loop. The same mechanism may also be true for PLK1 and ZIP10 interaction in mitosis. The proposed ZIP6/ZIP10-mediated mitotic entry signalling pathway is shown in figure 6.2B.

The proposed mechanism of ZIP6/ZIP10 mediated mitosis in figure 6.2 enables a hypothesis to be formed concerning the mechanism of action of the anti-ZIP6 and -ZIP10 antibodies. This has been outlined in figure 6.3. Prevention of zinc entry into the cell via ZIP6 and ZIP10 would prevent the S727 phosphorylation of STAT3, thereby maintaining the Y705 phosphorylation of STAT3, which is not present in mitosis (Nimmanon *et al.,* 2020). In addition, inhibition of ZIP10 activity may lead to decreased E2F activity and prevention of PLK1 transcription. The end result is decreased CDK1/Cyclin B activation and an inability of cells to move into mitosis. This hypothesis is supported by the data that show antibody inhibition of ZIP6 and ZIP10 decreases levels of both PLK1 and cyclin B1 (Ziliotto, 2018) and pS^{727}STAT3. Cyclin B1 forms a complex with CDK1 and together they act as key regulators of mitotic entry (Roshak *et al.*, 2000). In contrast, there was no significant difference in the protein levels of cyclins E and A, both of which are implicated in S and G1 phase (Lew, Dulić and Reed, 1991; Pagano *et al.*, 1992), in MCF7 cells following antibody treatment (Ziliotto, 2018). PLK1 is a serine/threonine kinase with many roles in mitosis including chromosome condensation and spindle assembly (reviewed by Lee, Jang, and Lee 2014). This is the first evidence which implicates zinc in the PLK1 signalling pathway. Interestingly, PLK1 is known to phosphorylate Cdc25C (Toyoshima-Morimoto, Taniguchi and Nishida, 2002), a tyrosine phosphatase which is linked to cell cycle progression into M phase via activation of the CDK1/cyclin B complex. CDK1 is also the kinase responsible for the serine phosphorylation of STAT3 on residue 727 (Shi *et al.*, 2006).

In addition to directly preventing zinc influx, the anti-ZIP6 and -ZIP10 antibodies may prevent ZIP6/ZIP10 activation by preventing intracellular phosphorylation, as is the case with trastuzumab, a monoclonal antibody routinely used for the treatment of HER2 positive breast cancer (Figueroa-Magalhães *et al.*, 2014). Trastuzumab prevents intracellular HER2 phosphorylation and therefore activation of cell proliferation pathways (Molina *et al.*, 2001).

Through inhibition of the ZIP6 and ZIP10 transporters and the analysis of downstream signalling, it has been possible to gain a better understanding of how well-established mitotic signalling pathways involve zinc signalling pathways.

Figure 6.2. Proposed mechanism of ZIP6/ZIP10-mediated mitotic entry

A.

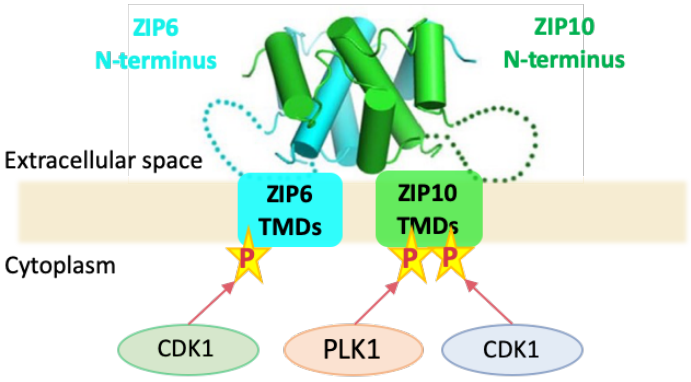

B.

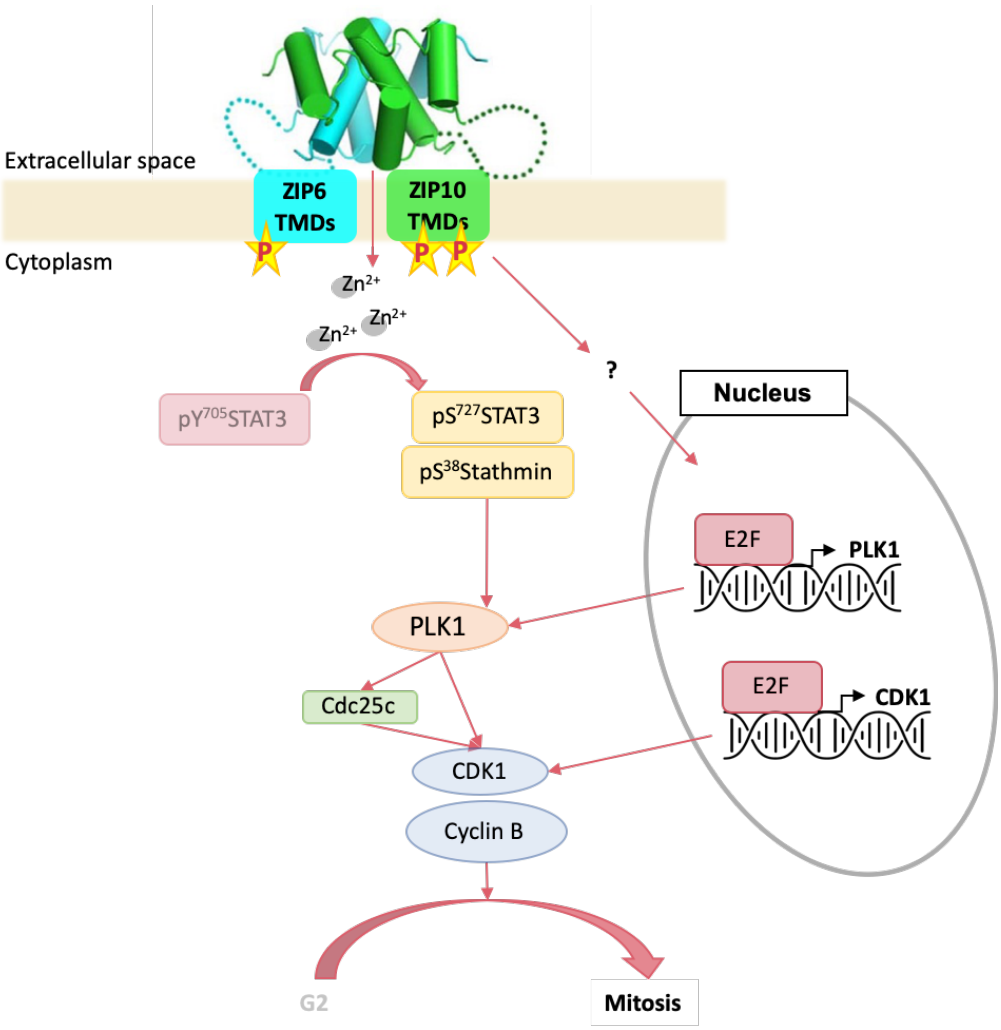

Proposed mechanism of ZIP6/ZIP10-mediated zinc entry in mitosis. ***A****. The heteromer is activated by phosphorylation of ZIP6 by CK2* (Ziliotto, 2018) *and phosphorylation of ZIP10 by CDK1 and PLK1.* ***B****. Activation causes zinc influx which leads to S727 phosphorylation of STAT3. Subsequent recruitment of pS*^{38}*Stathmin to pS*^{727}*STAT3 activates the PLK1/CDK1 pathway crucial to mitotic entry. In addition, ZIP10 has been linked to E2F activity, which is responsible for PLK1 and CDK1 transcription.*

Figure 6.3. Proposed mechanism of anti-ZIP6/ZIP10 antibody inhibition of mitosis

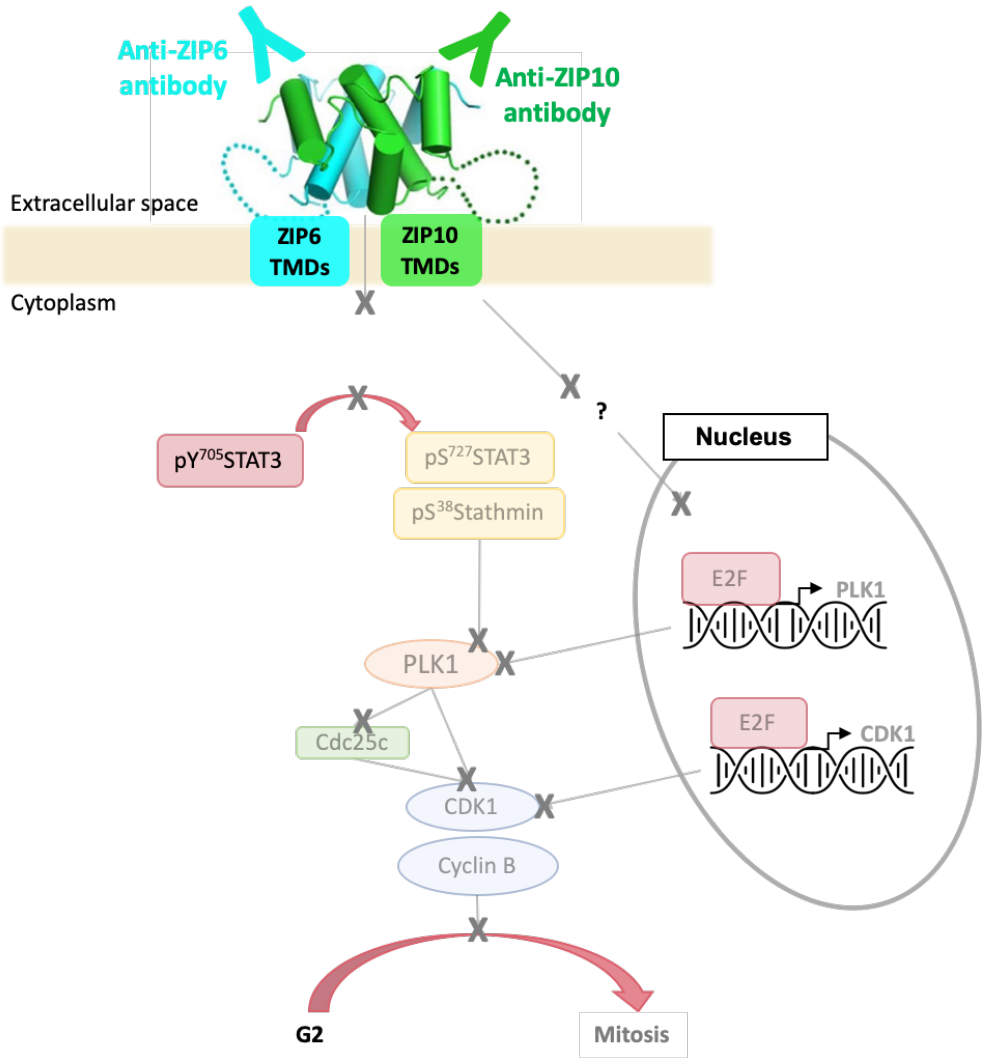

Anti-ZIP6 and -ZIP10 antibodies inhibit ZIP6/ZIP10 heteromer activation, preventing zinc influx. S727 phosphorylation of STAT3 does not occur, leaving pY^{705}STAT3 to continue transcriptional activity. Inhibition of ZIP10 also prevents E2F-mediated transcription of PLK1 and CDK1. CDK1 inhibition prevents chromosome condensation and therefore cells remain in the G2 phase of the cell cycle.

6.5. Current standards in cancer therapy

For a large part of the 20th century, the three main options for cancer therapy were surgery, radiotherapy and chemotherapy. Surgery is an effective method for completely removing a solid tumour and, if the cancer has not spread can cure a patient. Radiotherapy is the use of an electron beam to penetrate solid tumour tissue, causing enough DNA damage to induce cell death. In the mid 20th century the curability rates of many cancers plateaued, because neither of the aforementioned treatments are effective against metastasis (Arruebo *et al.*, 2011).

Chemotherapy was the first systemic treatment to be introduced, first being used for the treatment of leukaemia after it was noticed during the World Wars that soldiers who had been exposed to mustard gas had decreased leukocytes (Arruebo *et al.*, 2011). The term *chemotherapy* literally means the chemical treatment of disease and involves the delivery of chemicals that induce cell death. However, the systemic delivery of chemotherapy and the non-specific nature of the drugs for tumour cells means it is associated with toxicity (Schirrmacher, 2019) and side effects arise from the death of rapidly dividing cells; diarrhoea and vomiting (gastrointestinal cells), hair loss (follicular cells) and immunosuppression (blood cells in the bone marrow) (Nurgali, Jagoe and Abalo, 2018). In the 1980's it was suggested for the first time that adjuvant chemotherapy after surgery or radiotherapy could improve patient outcomes (Fisher and Wolmark, 1981). Breast cancer was the first cancer to be routinely treated in this way (Fisher and Wolmark, 1981), though nowadays a combination of therapies is used to treat many types of cancer (Arruebo *et al.*, 2011).

There are several types of chemotherapy and they differ by their mode of action: alkylating agents (e.g. cyclophosphamide and melphalan) attach an alkyl group to DNA which causes damage and prevents the cell from replicating itself; anti-metabolites (e.g. 5FU, gemcitabine and methotrexate) inhibit the normal metabolism of cells; and anthracyclines (e.g. doxorubicin and epirubicin) inhibit topoisomerase II (Huang *et al.*, 2017).

6.5.1. Anti-mitotic chemotherapy

Anti-microtubule agents are also known as anti-mitotic agents because they specifically act upon cells in mitosis. Vinca alkaloids (e.g. vincristine) inhibit spindle assembly in mitosis so chromosomes are unable to form proper attachments with the spindle (Rieder and Maiato, 2004), while taxanes (e.g. docetaxel) prevent microtubule function resulting in the inability of chromosomes to be separated in mitosis (Gradishar, 2012). Both these events result in permanent arrest at the spindle assembly checkpoint (SAC). In mitosis, the SAC ensures proper segregation of the chromosomes and is responsible for the cell exiting mitosis. It is active for only a matter of minutes to check chromosome attachment to the spindle and correct improper attachments (Matson and Stukenberg, 2011). During activation, the SAC inhibits the anaphase promoting complex (APC) (Ibrahim, 2015), a ubiquitin ligase responsible for cyclin B degradation (Hershko, 1999). The inhibition of APC maintains activity of the CDK1/cyclin B complex, which is degraded following SAC switch-off once the chromosomes are confirmed as properly attached to the spindle, allowing cells to progress to anaphase (Chang, Xu and Luo, 2003).

As with many types of chemotherapy, acquired resistance of the tumour to the treatment is a problem clinically. One mechanism which has been proposed for anti-microtubule agent resistance is 'mitotic slippage' in which the prolonged mitotic arrest leads to slow degradation of cyclin B causing cells to prematurely exit mitosis (Brito and Rieder, 2006), and continue through the cell cycle with unstable genomic material (Cheng and Crasta, 2017). This mechanism has been proposed in cervical (Ma *et al.*, 2012; Habu and Matsumoto, 2013; He *et al.*, 2016), ovarian (Fu *et al.*, 2007), liver (Ma *et al.*, 2012; He *et al.*, 2016) and lung (Ma *et al.*, 2012) cancer cells. Tumours that become resistant to one kind of treatment can be treated with different drugs, however in time, it is likely they will develop resistance to these as well (Rivera and Gomez, 2010). In the case of metastatic cancer, treatment options will eventually run out at which point the patient is transferred to palliative care.

Combination cancer therapies which include some element of chemotherapy remain the gold standard treatment for many types of treatment, despite their toxicity, problem of resistance and significant burden on a patient's quality of life (Nurgali, Jagoe and Abalo, 2018). This has led to a global push towards more targeted therapies such as small molecules or peptide-based drugs e.g. antibodies.

6.6. Emerging cancer therapies that target cell cycle regulation

Small molecules are organic molecules which, due to their small size (typically less than 900 daltons) and hydrophobicity are easily able to cross the cell membrane (Lavanya *et al.*, 2014). CDK4 and CDK6 have become targets for the development of small molecule inhibitors (Dickson, 2014; VanArsdale *et al.*, 2015). These are two of the most important cyclin dependent kinases in the G1/S phase transition (Asghar *et al.*, 2015) and their activity is controlled by association with cyclin D (Lim and Kaldis, 2013) (figure 6.4). Both CDK4 and CDK6 can phosphorylate the tumour suppressor retinoblastoma protein (RB) (Kato and Sherr, 1993; Matsushime *et al.*, 1994). RB is maintained in a non-phosphorylated form, binding and inhibiting transcription factors such as E2F (Harbour and Dean, 2000), and preventing the transcription of cell cycle progression proteins. When the cell is ready to divide, RB is phosphorylated by CDK4 or CDK6, causing the release of E2F and the activation of transcription of cell cycle progression proteins. Inappropriately phosphorylated RB protein is a major factor in several cancers (Du and Searle, 2009) hence the huge potential for targeting CDK4 and CDK6.

Palbociclib is a small molecule inhibitor of CDK4/CDK6 approved by the FDA for the treatment of oestrogen receptor-positive breast cancer (Fry et al. 2004; VanArsdale et al. 2015). Palbociclib has particularly good efficacy when used in combination with the aromatase inhibitor letrozole (Finn *et al.*, 2015) and has also now shown efficacy in treating triple-negative breast cancers prior to treatment with chemotherapy (Cretella *et al.*, 2019).

Small molecule inhibitors of CDK4 and CDK6 are well-tolerated clinically because neither is essential for cell viability (Malumbres *et al.*, 2004). The absolute requirement for other CDKs e.g. CDK1 in mitosis and CDK2 in S phase, and their expression across all cell types make them less suitable targets in cancer therapy. Indeed, CDK1 and CDK2 inhibitors have been less successful at demonstrating efficacy in clinical trials because their therapeutic index is too low i.e. their therapeutic dose is higher than the dose that causes toxicity (Blum *et al.*, 2010; Le Tourneau *et al.*, 2010).

Figure 6.4. The control of the cell cycle by cyclins and cyclin-dependent kinases

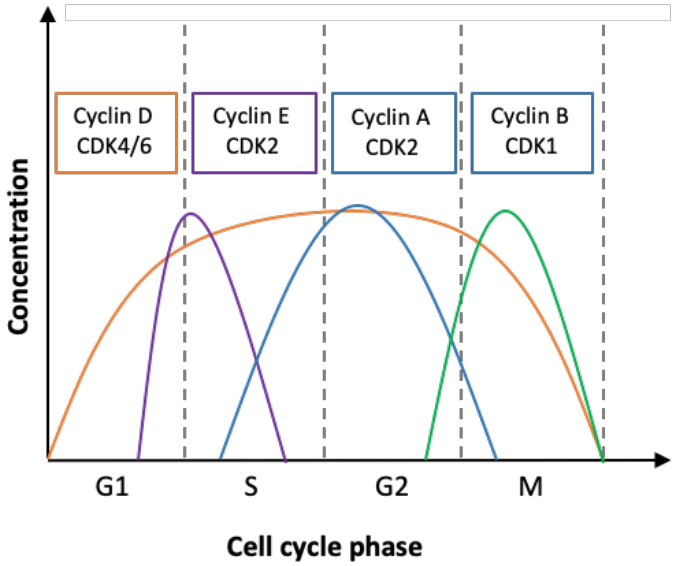

Progression through the cell cycle depends upon activation of specific cyclins and their binding to cyclin-dependent kinases (CDKs).

M phase entry is largely driven by both CDK1 and PLK1 (Roshak *et al.*, 2000), which makes PLK1 another desirable target for cancer treatment. Unfortunately, the *in vitro* data of PLK1 inhibitors and success of pre-clinical models have not translated into clinical trials and these inhibitors have already been associated with resistance (reviewed by Gutteridge et al. 2016), in addition to toxicity (Elsayed and Wang, 2019). New methods of targeting PLK1 involve combination therapy with other molecules that target the same pathway, a category in which anti-ZIP6 and -ZIP10 antibodies fall.

The nature of small molecule inhibitors enables them to target both extracellular and intracellular signalling proteins, giving huge diversity to their potential as targeted cancer therapeutics (Lavanya *et al.*, 2014).

6.7. Antibodies in cancer therapy

The use of peptide-based drugs such as antibodies is in its infancy compared to the use of conventional small molecule and chemotherapy cancer treatments. However, they have emerged as potentially very useful agents due to their high specificity for target proteins (Fosgerau and Hoffmann, 2015), resulting in fewer off-target effects. Binding of the antibody to its target antigen may induce the recruitment of immune cells which causes tumour cell lysis (Zafir-Lavie, Michaeli and Reiter, 2007). Additionally, antibodies may prevent signalling via the antigen by inhibiting function or promoting internalisation and degradation.

Rituximab was the first monoclonal antibody to be approved for the treatment of cancer. It is used specifically for B cell malignancies and lymphoma (Coiffier *et al.*, 2002; Hainsworth *et al.*, 2003; Hiddemann *et al.*, 2005) and binds CD20 (cluster of differentiation 20) on the surface of B cells to induce cell death via antibody-dependent cellular cytotoxicity (Reff *et al.*, 1994). Trastuzumab is a monoclonal antibody widely used in the treatment of HER2 positive breast cancer. Upon binding HER2, trastuzumab triggers HER2 internalisation and degradation (Klapper *et al.*, 2000), antibody-dependent cellular cytotoxicity (Clynes *et al.*, 2000; Arnould *et al.*, 2006; Musolino *et al.*, 2008) and downregulation of intracellular MAPK and PI3K/Akt signalling pathways (Nagata *et al.*, 2004; Dubská, Anděra and Sheard, 2005; Musolino *et al.*, 2008; Junttila *et al.*, 2009; Zhang *et al.*, 2011). Trastuzumab was approved by the FDA for the treatment of metastatic breast cancer in 1998, and the prognosis for women with this diagnosis has improved significantly since it was introduced (Miller and Schwartzberg, 2019).

Resistance to antibody treatments such as rituximab and trastuzumab has been described. The loss of CD20 expression at the plasma membrane confers resistance to rituximab (Pavanello, Zucca and Ghielmini, 2017) while signalling via alternative pathways such as IGFR (insulin-like growth factor receptor), p27 and EGFR renders breast cancers resistant to trastuzumab (Luque-Cabal *et al.*, 2016). Furthermore, expression of a truncated HER2 protein, p95HER2 (Codony-Servat *et al.*, 1999), which lacks the extracellular trastuzumab-binding domain but retains the intracellular kinase activity of HER2 (Christianson *et al.*, 1998) enables cells to continue to grow in the presence of trastuzumab. p95HER2 is generated from two mechanisms; translation of mRNA encoding HER2 from an alternative start codon (Josep and Serra, 2006) and the ectodomain shedding of HER2 (Christianson *et al.*, 1998). The ectodomain shedding of HER2 is carried out by ADAM10 (Liu *et al.*, 2006), one of the proteases predicted to be responsible for the ectodomain shedding of ZIP10. It is possible that cancer cells treated with an anti-ZIP10 antibody could express truncated ZIP10 which still possesses zinc transport ability, in an effort to overcome anti-ZIP10 antibody binding.

A further mechanism of trastuzumab resistance is the expression of mucin 4, a membrane associated glycoprotein that interferes with trastuzumab binding to the HER2 receptor (Price-Schiavi *et al.*, 2002; Nagy *et al.*, 2005). However, this can be circumvented to a degree by a combination of trastuzumab and conventional chemotherapy, that can improve outcomes relative to those of patients on trastuzumab alone (Slamon *et al.*, 2001).

Antibodies are also used in cancer treatment for the delivery of radiotherapy or cytotoxic drugs. One such example is trastuzumab emtansine (T-DM1); a combination of trastuzumab and the cytotoxic agent, DM1. Following internalisation of the antibody-drug conjugate (ADC), proteolytic degradation releases DM1 which causes mitotic disruption and leads to apoptosis (Philips et al 2008). T-DM1 has now been recommended as first-line therapy for patients with HER2-positive breast cancer in whom taxane therapy is unsuitable (Perez *et al.*, 2019). SGN-LIV1 is an ADC, composed of an anti-ZIP6 antibody and anti-mitotic agent, monomethyl auristatin E (MMAE). Following binding to the N-terminus of ZIP6, the ADC is internalised and proteolysis releases MMAE which works by preventing microtubule polymerisation (Doronina et al. 2003; Sussman et al. 2014). SGN-LIV1 is currently being investigated in clinical trials (clinicaltrials.gov identifier: NCT01969643) for the treatment of metastatic breast cancer.

6.8. Anti-ZIP6 and -ZIP10 antibodies in cancer therapy

The evidence presented here highlights the growing potential for the use of monoclonal antibodies in the treatment of cancer. The finding that ZIP6 and ZIP10 are central to zinc-mediated mitotic entry in cancer cells, and that our anti-ZIP6 and -ZIP10 antibodies prevent cell division *in vitro* provides an opportunity for the development of novel agents to treat cancer. Further investigation is being carried out to understand the ability of these antibodies to slow tumour growth and the effect of antibody binding on the downstream signalling pathway.

One benefit of these antibodies is that since both ZIP6 and ZIP10 play a crucial role in epithelial to mesenchymal transition, the first stage of cancer cell metastasis (Roche, 2018), there is an opportunity to target not only dividing tumour cells but also those at risk of metastasizing. This could make this therapy more desirable than chemotherapy for example, which only targets dividing cells.

The finding that the melanoma cell line was more sensitive to the anti-ZIP10 antibody than the other cell lines was particularly interesting. ZIP10-mediated zinc entry is important for epidermal development (Bin *et al.*, 2017, 2019), and in melanocytes specifically, zinc is required for proliferation (Rudolf and Rudolf, 2017). ZIP10-mediated zinc import is perhaps a more crucial signalling pathway in melanocytes, causing their greater sensitivity to the anti-ZIP10 antibody compared with other cell lines. This may be relevant *in vivo* as well because the therapeutic dose of the antibody may be lower than that which causes toxicity by the non-specific binding to non-cancerous cells.

Treatment of MCF7 cells with either the anti-ZIP6 or -ZIP10 antibody did not reduce cell viability, at least in the first 18 hours of treatment (Ziliotto, 2018) which may indicate that treatment with the antibodies is cytostatic rather than cytotoxic. Cytostatic drugs work by inhibiting tumour growth as opposed to cytotoxic drugs that kill tumour cells (Kummar *et al.*, 2006). To improve the cytotoxic ability of the antibodies, one option could be the generation of a bispecific antibody (discussed in the previous chapter) which would have one binding region for ZIP6 or ZIP10, and a second binding region for an immune cell, to elicit an immune response against the tumour cell (figure 6.5A).

Furthermore, there is the option to produce antibodies with targets on two separate regions of the same protein (biparatropic bispecific antibodies) (figure 6.5B). ZW25, a biparatropic

bispecific monoclonal antibody, is targeted to HER2 and has been shown to be more potent than the monospecific antibody, trastuzumab (Weisser *et al.*, 2017) in pre-clinical models and is now being testing clinically in a range of HER2 expressing cancers (clinicaltrials.gov identifiers: NCT02892123, NCT0392966). If two functional regions in ZIP6 and/or ZIP10 were identified, biparatropic bispecific antibodies would enable the targeting of both and potentially increase efficacy by completely blocking transporter function.

6.9. Disadvantages of antibodies in cancer treatment

The evidence supporting the efficacy of antibodies in cancer therapy is continuing to grow, however antibodies do have some disadvantages over more conventional therapies. Peptide-based drugs are not orally bioavailable (Craik *et al.*, 2013); this means delivery must be by injection which is less favourable for the patient. In addition, the estimated cost of antibody production is twice that of conventional drugs due to the increased consumables required for culturing large volumes of hybridoma cells (Craik *et al.*, 2013). Furthermore, antibodies developed from animal serum must be humanised to reduce toxicity associated with non-human antibodies (Matthews, 2015). This involves alterations in the antibody's constant region (figure 6.6A) to prevent it provoking an inappropriate immune response upon delivery. However, the process of humanising antibodies can come with its own challenges including loss of affinity to its target protein (Pavlinkova *et al.*, 2001).

Antibodies are large molecules by nature (approximately 150 kDa) (figure 6.6A) that can make it difficult for them to reach inner cells in solid tumours which are typically tightly packed together (Jain, 1990; Yokota *et al.*, 1992). The failure of large molecules to reach every cell in a tumour can result in residual cancer cells following the end of treatment and the potential for the cancer to return and metastasize. To overcome the limitations of such a large molecule, antibodies are being produced with only the antigen binding fragment (Fab fragment) (figure 6.6B). Clinically, Fab fragment antibodies are used in the treatment of thrombosis (abciximab) (Hang Lee, Thye Ho and Cheem Tan, 2005) and macular degeneration (ranibizumab) (Dhoot and Kaiser, 2012) but the potential for their use in cancer to improve tumour penetration is still under investigation. A further advantage of Fab fragment antibodies is that there is reduced non-specific binding, which stems from binding of the constant region fragment (Fc) to off-target proteins (Nelson, 2010). Furthermore, zinc binds IgG in the Fc region of IgG antibodies, and not in the Fab region (Yamanaka *et al.*, 2016) so the use of a Fab fragment therapeutically might minimise off-target effects of binding free zinc and reducing its availability for other cellular processes.

The smaller size of Fab fragments however does decrease their plasma half-life (Nelson, 2010), and the loss of the Fc region abolishes antibody-dependent cellular cytotoxicity unless the Fab fragment is conjugated to an cytotoxic agent (Sanz *et al.*, 2005).

Despite the shortcomings of antibody use in cancer therapies, they have become some of the most standard agents used in many haematological and solid cancers (Coulson, Levy and Gossell-Williams, 2014). Furthermore, the success rate of antibodies in clinical trials is better than that for small molecules (Coulson, Levy and Gossell-Williams, 2014) so it is likely that the industry will see a shift towards this type of treatment in the future.

6.10. Anti-ZIP6 and -ZIP10 antibodies beyond cancer therapy

In addition to their use as cancer therapies, there is potential for the anti-ZIP6 and -ZIP10 antibodies to be used in treatments for hyperproliferative disease, a disease of abnormally high cell proliferation. Hyperproliferative cells differ from cancer cells because they maintain their identity; cancer cells acquire multiple mutations so that they are no longer recognisable as their original type (Roy and Hebrok, 2015). One example of hyperproliferative disease is psoriasis. The clinical manifestation of psoriasis includes red flaky patches of skin caused by the hyperproliferation of keratinocytes due to the inappropriate immune response to autoantigens (Krueger and Bowcock, 2005). While topical creams are used in the treatment of mild psoriasis, monoclonal antibodies are used for the treatment of more severe forms, and have proved to be highly effective in some patients (Hawkes *et al.*, 2018). Monoclonal antibodies mainly target aspects of the immune system that are inappropriately active, such as TNF-α (tumour necrosis factor alpha), interleukin 17 and interleukin 23 (Kim and Lebwohl, 2019). One approach being tested for the treatment of psoriasis is the inhibition of keratinocyte proliferation using cannabinoids (Wilkinson and Williamson, 2007) and KRT16 (keratin 16) inhibitors (Chen *et al.*, 2019) that highlights the potential for other anti-proliferative agents such as anti-ZIP6 or -ZIP10 antibodies to be used as treatment in this disease.

Figure 6.5. Bispecific and biparatropic antibodies

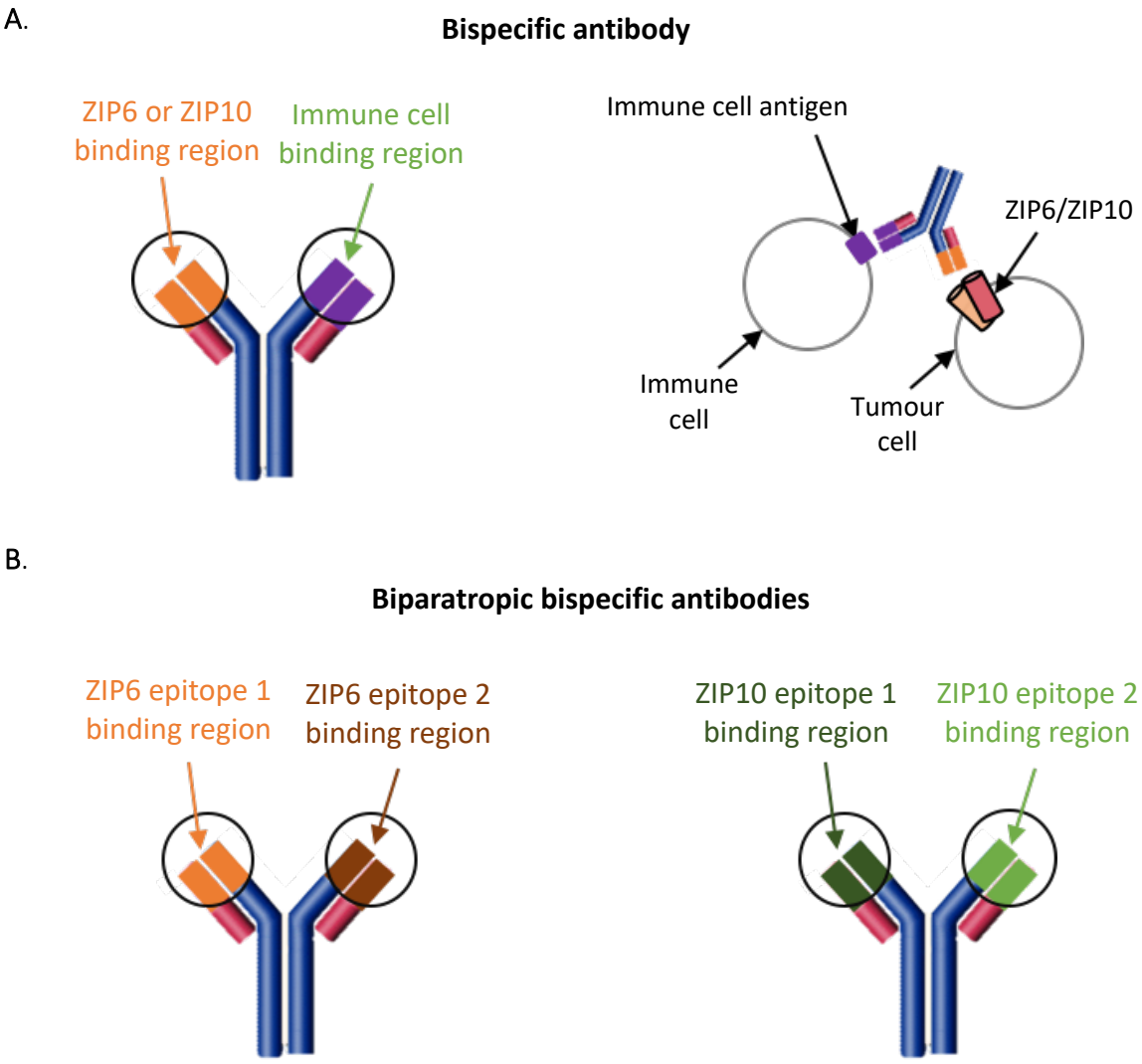

***A**. Bispecific antibodies have binding regions for two separate antigens. To target ZIP6/ZIP10-mediated zinc influx, one antibody could contain a ZIP6 and a ZIP10 binding region, allowing binding to one heteromer by two points of contact, or the cross-linking of two cells expressing the heteromer at the plasma membrane. Alternatively, one antigen-binding region may bind the epitope of an immune cell, to elicit an immune reaction to the tumour cell expressing ZIP6 or ZIP10. **B**. Biparatropic bispecific antibodies contain two different antigen binding regions which bind to the same protein. ZIP6/ZIP10 antibodies could be developed to bind both the N-terminus and one of the extracellular loops to target multiple regions of the protein which regulate its function.*

Figure 6.6. Fab fragment antibodies

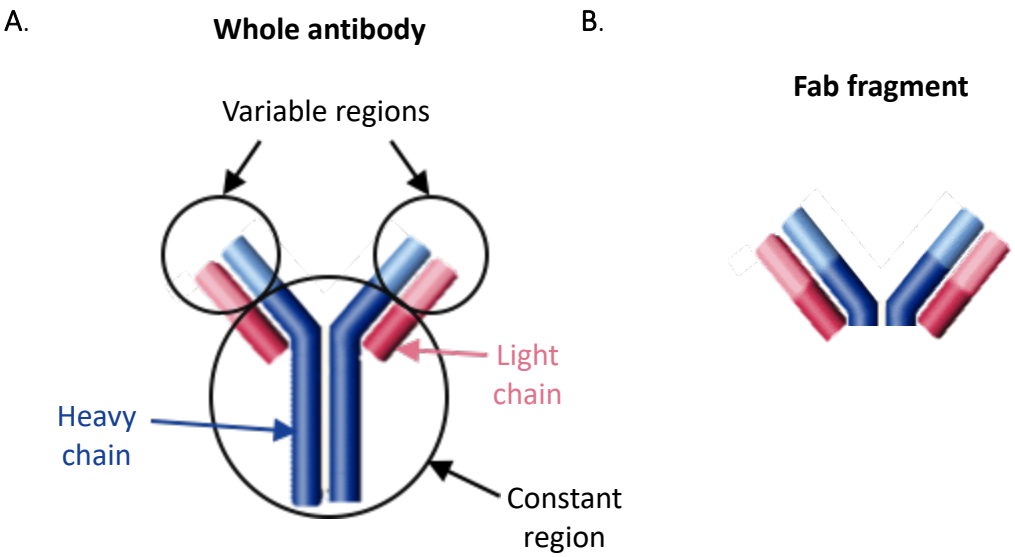

***A**. Antibodies are made of two heavy chains and two light chains* (Stanfield and Wilson, 2014) *each with a variable, antibody binding region, and a constant region. **B**. Fab fragments are composed of just the antigen binding regions of the antibody. Their smaller size enables them to penetrate compact tumours more readily.*

6.11. General limitations and future work

Although the data in this project have demonstrated the potential for targeting ZIP6 and ZIP10 in cancer, it is important to discuss the limitations of the work that was carried out, so that they can be taken into consideration for follow-up work.

The study of antibody inhibition used mainly cells in 2-dimensions and only one study *in vivo* with a small number of animals. Future work to characterise the antibodies should be conducted in bigger animal studies and the collection of PK (pharmacokinetic) and PD (pharmacodynamic) data should be prioritised. Tissue and RNA samples from the animals were collected at the end of the study and analysis of these could lead to insights about the general toxicity of the drug, and also the downstream signalling which affects gene expression. In addition, the potential for these antibodies to be used as anti-metastatic drugs could be tested by tail-vein injection of the drug(s) simultaneously with the cancer cells. The speed at which the cells form solid tumours in distal organs would be a measure of the antibody's ability to prevent metastasis.

In a population of cells treated with the antibody, non-mitotic cells are not an indication that the downstream signalling pathway has been disrupted, only that they have not entered mitosis. To find out more detail about the specific downstream effect of antibody binding, a useful study would be the conjugation of the anti-ZIP6 and -ZIP10 antibodies to a fluorophore and monitoring of cells treated with the new construct under a fluorescent microscope, in real-time. This would allow a much more thorough analysis of the specific response of cells upon antibody binding and at exactly which stage this occurs.

6.12. General conclusions

This project has used a variety of techniques to understand the role and regulation of ZIP10 in cell division and to prove that ZIP transporters could be useful targets in the treatment of diseases of uncontrolled cell division, including cancer. In addition, the upregulation of ZIP6 and ZIP10 in mitosis implicates their potential use as biomarkers for cancer diagnosis. The work has confirmed that ZIP10 undergoes proteolytic cleavage, glycosylation and phosphorylation, although the exact role of these modifications is yet to be determined. Furthermore, the data presented here show that ZIP10 responds to zinc in its environment to maintain homeostasis.

The undeniable evidence that zinc is an important metal to human life confirms the importance of understanding the role of ZIPs in maintaining human health. ZIPs have been implicated in many disease areas, for example, ZIP4 in acrodermatitis enteropathica (Weaver *et al.*, 2010), ZIP8 in inflammation (Pyle *et al.*, 2017), ZIP13 in the connective tissue disorder Ehlers-Danlos syndrome (EDS) (Bin *et al.*, 2014) and ZIP14 in asthma (Lang *et al.*, 2007). In addition, as proliferation is important in all aspects of biology, the work presented here is of general interest and should not be restricted to the field of zinc biology.

Currently, there are no licensed cancer therapies that target zinc transporters, but this project has highlighted the potential of ZIP transporters as completely novel therapeutic targets and is supported by recent data on the potential for targeting ZIP6 in metastatic breast cancer (Sussman *et al.,* 2014) and ZIP7 in lymphoblastic leukaemia (Nolin *et al.*, 2019).

References

Abdelmohsen, K. *et al.* (2009) 'Ubiquitin-mediated proteolysis of HuR by heat shock', *The EMBO journal*. 28(9), pp. 1271–1282.

Abe, S. *et al.* (2011) 'The initial phase of chromosome condensation requires Cdk1-mediated phosphorylation of the CAP-D3 subunit of condensin II', *Genes & Development*. 25(8), pp. 863–874.

Adam, K. *et al.* (2018) 'A PIM-CHK1 signaling pathway regulates PLK1 phosphorylation and function during mitosis', *Journal of Cell Science*, 131(15), p. jcs213116.

Ahmad, K. A. *et al.* (2008) 'Protein kinase CK2--a key suppressor of apoptosis', *Advances in enzyme regulation*. 48, pp. 179–187.

Ahonen, L. J. *et al.* (2005) 'Polo-like kinase 1 creates the tension-sensing 3F3/2 phosphoepitope and modulates the association of spindle-checkpoint proteins at kinetochores', *Current Biology*, 15(12), pp. 1078–1089.

Akopyan, K. *et al.* (2014) 'Assessing Kinetics from Fixed Cells Reveals Activation of the Mitotic Entry Network at the S/G2 Transition', *Molecular Cell*. 53(5), pp. 843–853.

Al-Ebraheem, A., Farquharson, MJ., and Ryan, E. (2009) 'The evaluation of biologically important trace metals in liver, kidney and breast tissue', *Applied Radiation and Isotopes*, 67(3), pp. 470–474.

Altmeppen, HC. *et al.* (2012) 'Proteolytic processing of the prion protein in health and disease', *American Journal of Neurodegenerative Disease*. e-Century Publishing Corporation, 1(1), pp. 15–31.

Andreini, C. *et al.* (2006) 'Counting the zinc-proteins encoded in the human genome', *Journal of Proteome Research*, 5(1), pp. 196–201.

Ardito, F. *et al.* (2017) 'The crucial role of protein phosphorylation in cell signaling and its use as targeted therapy', *International journal of molecular medicine*, 40(2), pp. 271–280.

Arinola, OG. and Charles-Davies, MA. (2008) 'Micronutrient levels in the plasma of Nigerian females with breast cancer', *African Journal of Biotechnology*, 7(11), pp. 1620–3.

Arnould, L. *et al.* (2006) 'Trastuzumab-based treatment of HER2-positive breast cancer: an antibody-dependent cellular cytotoxicity mechanism?', *British journal of cancer*, 94(2), pp. 259–267.

Arruebo, M. *et al.* (2011) 'Assessment of the evolution of cancer treatment therapies', *Cancers*, 3(3), pp. 3279–3330.

Ascoli, CA. and Aggeler, B. (2018) 'Overlooked benefits of using polyclonal antibodies', *BioTechniques*, 65(3), pp. 127–136.

Asghar, U. *et al.* (2015) 'The history and future of targeting cyclin-dependent kinases in cancer therapy', *Nature reviews. Drug discovery*, 14(2), pp. 130–146.

Attwood, P. V *et al.* (2007) 'Focus on phosphohistidine.', *Amino acids*. 32(1), pp. 145–156.

Avalle, L. *et al.* (2017) 'STAT3 in cancer: A double edged sword.', *Cytokine*. 98, pp. 42–50.

Bachmann, M. *et al.* (2006) 'The oncogenic serine/threonine kinase Pim-1 directly phosphorylates and activates the G2/M specific phosphatase Cdc25C', *The International Journal of Biochemistry & Cell Biology*, 38(3), pp. 430–443.

Baek, SH. *et al.* (2007) 'Zinc-induced downregulation of Notch signaling is associated with cytoplasmic retention of Notch1-IC and RBP-Jk via PI3k-Akt signaling pathway.', *Cancer letters*. 255(1), pp. 117–126.

Bafaro, EM. *et al.* (2015) 'The large intracellular loop of hZIP4 is an intrinsically disordered zinc binding domain', *Metallomics,* 7(9), pp. 1319–1330.

Bayer, KU. and Schulman, H. (2019) 'CaM Kinase: Still Inspiring at 40', *Neuron*, 103(3), pp. 380–394.

Beel, AJ. and Sanders, CR. (2008) 'Substrate Specificity of γ-Secretase and Other Intramembrane Proteases', *Cellular and molecular life sciences*, 65(9), pp. 1311–1334.

Bernhardt, ML. *et al.* (2011) 'Zinc requirement during meiosis I-meiosis II transition in mouse oocytes is independent of the MOS-MAPK pathway', *Biology of reproduction*. 84(3), pp. 526–536.

Bernhardt, M. L. *et al.* (2012) 'A zinc-dependent mechanism regulates meiotic progression in mammalian oocytes', *Biology of reproduction*. 86(4), pp. 114.

Bigenzahn, JW. *et al.* (2018) 'LZTR1 is a regulator of RAS ubiquitination and signaling', *Science*, 362(6419), pp. 1171 LP – 1177.

Bin, BH. *et al.* (2014) 'Spondylocheirodysplastic Ehlers-Danlos syndrome (SCD-EDS) and the mutant zinc transporter ZIP13', *Rare diseases,* 2(1), pp. e974982–e974982.

Bin, BH. *et al.* (2017) 'Requirement of zinc transporter ZIP10 for epidermal development: Implication of the ZIP10-p63 axis in epithelial homeostasis', *Proceedings of the National Academy of Sciences of the United States of America*, 114(46), pp. 12243–12248.

Bin, BH. *et al.* (2019) 'The epithelial zinc transporter ZIP10 epigenetically regulates human epidermal homeostasis by modulating histone acetyltransferase activity', *British Journal of Dermatology*, 180(4), pp. 869–880.

Bjellqvist, B. *et al.* (1993) 'The focusing positions of polypeptides in immobilized pH gradients can be predicted from their amino acid sequences', *Electrophoresis*, 14(1), pp. 1023–1031.

Blom, N. *et al.* (2004) 'Prediction of post-translational glycosylation and phosphorylation of proteins from the amino acid sequence.', *Proteomics*, 4(6), pp. 1633–49.

Blum, W. *et al.* (2010) 'Phase I clinical and pharmacokinetic study of a novel schedule of flavopiridol in relapsed or refractory acute leukemias', *Haematologica*, 95(7), pp. 1098–1105.

Bodiga, VL. *et al.* (2017) 'Zinc Dyshomeostasis in Cardiomyocytes after Acute Hypoxia/Reoxygenation', *Biological Trace Element Research*, 179(1), pp. 117–129.

Boeras, DI. *et al.* (2008) 'Alzheimer's presenilin 1 causes chromosome missegregation and aneuploidy', *Neurobiology of aging*, 29(3), pp. 319–328.

Bracken, AP. *et al.* (2004) 'E2F target genes: unraveling the biology', 29(8), pp.409–417.

Le Bras, GF., Taubenslag, KJ. and Andl, CD. (2012) 'The regulation of cell-cell adhesion during epithelial-mesenchymal transition, motility and tumor progression', *Cell adhesion & migration*, 6(4), pp. 365–373.

Bremner, I., Young, BW. and Mills, CF. (1976) 'Protective effect of zinc supplementation against copper toxicosis in sheep', *British Journal of Nutrition*, 36(3), pp. 551–561.

Brethour, D. *et al.* (2017) 'A ZIP6-ZIP10 heteromer controls NCAM1 phosphorylation and integration into focal adhesion complexes during epithelial-to-mesenchymal transition', *Scientific Reports*, 7, p.

40313.

Brewer, GJ. *et al.* (1979) 'Zinc inhibition of calmodulin: A proposed molecular mechanism of zinc action on cellular functions', *American Journal of Hematology*, 7(1), pp. 53–60.

Brito, DA. and Rieder, CL. (2006) 'Mitotic checkpoint slippage in humans occurs via cyclin B destruction in the presence of an active checkpoint', *Current biology*, 16(12), pp. 1194–1200.

Brown, DC. and Gatter, KC. (1990) 'Monoclonal antibody Ki-67: its use in histopathology', *Histopathology*, pp. 489–503.

Brown, KH. *et al.* (2002) 'Effect of supplemental zinc on the growth and serum zinc concentrations of prepubertal children: a meta-analysis of randomized controlled trials', *Am J Clin Nutr*, 75(6), pp. 1062–1071.

Brown, MS. *et al.* (2000) 'Regulated Intramembrane Proteolysis: A Control Mechanism Conserved from Bacteria to Humans', *Cell*, 100(4), pp. 391–398.

Capasso, JM. *et al.* (1989) 'Mechanism of phosphorylation in the lumen of the Golgi apparatus. Translocation of adenosine 5'-triphosphate into Golgi vesicles from rat liver and mammary gland', *Journal of Biological Chemistry*, 264(9), pp. 5233–5240.

Chambard, JC. *et al.* (2007) 'ERK implication in cell cycle regulation', *Biochimica et Biophysica Act*, 1773(8), pp. 1299–1310.

Chandler, P. *et al.* (2016) 'Subtype-specific accumulation of intracellular zinc pools is associated with the malignant phenotype in breast cancer', *Molecular Cancer*, 15, p. 2.

Chang, DC., Xu, N. and Luo, KQ. (2003) 'Degradation of Cyclin B Is Required for the Onset of Anaphase in Mammalian Cells', *Journal of Biological Chemistry* , 278(39), pp. 37865–37873.

Chang, ET. *et al.* (2004) 'Re: Zinc Supplement Use and Risk of Prostate Cancer', *Journal of the National Cancer Institute*, 96(14), p. 1108.

Chen, HZ., Tsai, SY. and Leone, G. (2009) 'Emerging roles of E2Fs in cancer: an exit from cell cycle control', *Nature reviews. Cancer*, 9(11), pp. 785–797.

Chen, JG. *et al.* (2019) 'Silencing KRT16 inhibits keratinocyte proliferation and VEGF secretion in psoriasis via inhibition of ERK signaling pathway', *The Kaohsiung Journal of Medical Sciences*, 35(5), pp. 284–296.

Chen, Q. *et al.* (2012) 'The role of zinc transporter ZIP4 in prostate carcinoma', *Urologic Oncology: Seminars and Original Investigations*, 30(6), pp. 906–911.

Cheng, B. and Crasta, K. (2017) 'Consequences of mitotic slippage for antimicrotubule drug therapy', *Endocrine-Related Cancer*, 24(9), pp. T97–T106.

Chesters, JK. and Petrie, L. (1999) 'A possible role for cyclins in the zinc requirements during G1 and G2 phases of the cell cycle', *Journal of Nutritional Biochemistry*, 10(5), pp. 279–290.

Chesters, JK., Petrie, L. and Vint, H. (1989) 'Specificity and timing of the Zn2+ requirement for DNA synthesis by 3T3 cells', *Experimental Cell Research*, 184(2), pp. 499–508.

Cho, IJ. *et al.* (2019) 'Mechanisms, Hallmarks, and Implications of Stem Cell Quiescence.', *Stem cell reports*, 12(6), pp. 1190–1200.

Choudhury, NR. *et al.* (2017) 'RNA-binding activity of TRIM25 is mediated by its PRY/SPRY domain and is required for ubiquitination', *BMC biology*, 15(1), p. 105.

Christianson, TA. *et al.* (1998) 'NH2-terminally Truncated HER-2/neu Protein: Relationship with Shedding of the Extracellular Domain and with Prognostic Factors in Breast Cancer1', Cancer Research, 58(22), pp. 5123–5129.

Clynes, RA. *et al.* (2000) 'Inhibitory Fc receptors modulate in vivo cytoxicity against tumor targets', *Nature Medicine*, 6(4), pp. 443–446.

Codony-Servat, J. *et al.* (1999) 'Cleavage of the HER2 ectodomain is a pervanadate-activable process that is inhibited by the tissue inhibitor of metalloproteases-1 in breast cancer cells', *Cancer Research*, 59(6), pp. 1196–1201.

Cohen, C., Garvin, D. and Kochian, L. (2004) 'Kinetic properties of a micronutrient transporter from Pisum sativum indicate a primary function in Fe uptake from the soil', *Planta*, 218(5), pp. 748–792.

Coiffier, B. *et al.* (2002) 'CHOP Chemotherapy plus Rituximab Compared with CHOP Alone in Elderly Patients with Diffuse Large-B-Cell Lymphoma', *New England Journal of Medicine*, 346(4), pp. 235–242.

Coleman, SJ. *et al.* (2014) 'Nuclear translocation of FGFR1 and FGF2 in pancreatic stellate cells facilitates pancreatic cancer cell invasion', *EMBO Molecular Medicine*, 6(4), pp. 467–481.

Colvin, RA. *et al.* (2008) 'Insights into Zn homeostasis in neurons from experimental and modeling studies', *American Journal of Physiology,* 294(3), pp. C726 LP-C742.

Colvin, RA *et al.* (2010) 'Cytosolic zinc buffering and muffling: their role in intracellular zinc homeostasis.', *Metallomics*, 2(5), pp. 306–317.

Consortium, TU. (2018) 'UniProt: a worldwide hub of protein knowledge', *Nucleic Acids Research*, 47(D1), pp. D506–D515.

Costello, LC. *et al.* (2004) 'Role of zinc in the pathogenesis and treatment of prostate cancer: critical issues to resolve', *Prostate Cancer And Prostatic Diseases*, 7, p. 111.

Costello, LC. *et al.* (2005) 'Zinc and Prostate Cancer: A Critical Scientific, Medical, and Public Interest Issue (United States)', *Cancer Causes & Control*, 16(8), pp. 901–915.

Costello, LC., Liu, Y. and Franklin, RB. (1995) 'Testosterone stimulates the biosynthesis of m-aconitase and citrate oxidation in prostate epithelial cells', *Molecular and Cellular Endocrinology*, 112(1), pp. 45–51.

Coulson, A., Levy, A. and Gossell-Williams, M. (2014) 'Monoclonal Antibodies in Cancer Therapy: Mechanisms, Successes and Limitations', *The West Indian medical journal*, 63(6), pp. 650–654.

Craik, DJ. *et al.* (2013) 'The Future of Peptide-based Drugs', *Chemical Biology & Drug Design*, 81(1), pp. 136–147.

Cretella, D. *et al.* (2019) 'Pre-treatment with the CDK4/6 inhibitor palbociclib improves the efficacy of paclitaxel in TNBC cells', *Scientific reports*, 9(1), p. 13014.

Croxford, T. P., McCormick, N. H. and Kelleher, S. L. (2011) 'Moderate zinc deficiency reduces testicular Zip6 and Zip10 abundance and impairs spermatogenesis in mice', *The Journal of nutrition*, 141(3), pp. 359–365.

Cui, Y. *et al.* (2007) 'Levels of zinc, selenium, calcium, and iron in benign breast tissue and risk of subsequent breast cancer.', *Cancer epidemiology, biomarkers & prevention,* 16(8), pp. 1682–1685.

Dalton, TP. *et al.* (2005) 'Identification of mouse SLC39A8 as the transporter responsible for

cadmium-induced toxicity in the testis', *Proceedings of the National Academy of Sciences of the United States of America*, 102(9), pp. 3401–3406.

Danscher G, Obel J *et al*. (1980) 'Electron microscopic demonstration of metals in rat mast cells', *Histochemistry*, 66(3), pp. 293–300.

Dardel, F. *et al.* (1998) 'Solution structure of nickel-peptide deformylase', *Journal of Molecular Biology*, 280(3), pp. 501–513.

Davis, ZH. *et al.* (2015) 'Global mapping of herpesvirus-host protein complexes reveals a transcription strategy for late genes', *Molecular cell*, 57(2), pp. 349–360.

Daya-Makin, M. *et al.* (1994) 'Activation of a Tumor-associated Protein Kinase and Casein Kinase 2 in Human Squamous Cell Carcinomas and Adenocarcinomas of the Lung', *Cancer Research*, 54(8), pp. 2262 LP – 2268.

Decker, T. and Kovarik, P. (2000) 'Serine phosphorylation of STATs', *Oncogene*, 19(21), pp. 2628–2637.

Dhar, N. K. *et al.* (1973) 'Distribution and concentration of zinc in the subcellular fractions of benign hyperplastic and malignant neoplastic human prostate', *Experimental and Molecular Pathology*, 19(2), pp. 139–142.

Dhoot, DS. and Kaiser, P. K. (2012) 'Ranibizumab for age-related macular degeneration.', *Expert opinion on biological therapy*. England, 12(3), pp. 371–381.

Dickson, MA. (2014) 'Molecular Pathways: CDK4 Inhibitors for Cancer Therapy', *Clinical Cancer Research*, 20(13), pp. 3379 LP – 3383.

Dinkel, H. *et al.* (2016) 'ELM 2016—data update and new functionality of the eukaryotic linear motif resource', *Nucleic Acids Research*, pp. D294–D300.

Dodig, S., Cepelak, I. and Pavic, I. (2019) 'Hallmarks of senescence and aging.', *Biochemia medica*. Croatia, 29(3), p. 30501.

Donaldson, MM. *et al.* (2001) 'Metaphase Arrest with Centromere Separation in polo Mutants of Drosophila', *The Journal of Cell Biology*, 153(4), pp. 663 LP – 676.

Doronina, SO. *et al.* (2003) 'Development of potent monoclonal antibody auristatin conjugates for cancer therapy', *Nature Biotechnology*, 21(7), pp. 778–784.

Dressman, MA *et al.* (2001) 'Genes that co-cluster with estrogen receptor alpha in microarray analysis of breast biopsies.', *The pharmacogenomics journal*, 1(2), pp. 135–41.

Du, W. and Searle, JS. (2009) 'The rb pathway and cancer therapeutics', *Current drug targets*, 10(7), pp. 581–589.

Dubská, L., Anděra, L. and Sheard, MA. (2005) 'HER2 signaling downregulation by trastuzumab and suppression of the PI3K/Akt pathway: An unexpected effect on TRAIL-induced apoptosis', *FEBS Letters*, 579(19), pp. 4149–4158.

Dufner-Beattie, J. *et al.* (2004) 'The Adaptive Response to Dietary Zinc in Mice Involves the Differential Cellular Localization and Zinc Regulation of the Zinc Transporters ZIP4 and ZIP5', *Journal of Biological Chemistry* , 279(47), pp. 49082–49090..

Dunn, MW. (2011) 'Prostate Cancer Overview', *Seminars in Oncology Nursing*, 27(4), pp. 241–250.

Ehsani, S. *et al.* (2012) 'LIV-1 ZIP Ectodomain Shedding in Prion-Infected Mice Resembles Cellular

Response to Transition Metal Starvation', *Journal of molecular biology*, 422(4), pp. 556–574.

Eide, D. *et al.* (1996) 'A novel iron-regulated metal transporter from plants identified by functional expression in yeast', *Proceedings of the National Academy of Sciences of the United States of America*, 93(11), pp. 5624–5628.

Elsayed, I. and Wang, X. (2019) 'PLK1 inhibition in cancer therapy : potentials and challenges', 11, pp. 1383–1386.

Emri, E. *et al.* (2013) 'Correlation among metallothionein expression, intratumoural macrophage infiltration and the risk of metastasis in human cutaneous malignant melanoma', *Journal of the European Academy of Dermatology and Venereology*, 27(3), pp. e320–e327.

Endo, M. (2009) 'Calcium-Induced Calcium Release in Skeletal Muscle', *Physiological Reviews*. American Physiological Society, 89(4), pp. 1153–1176.

Ertych, N. *et al.* (2016) 'CHK2-BRCA1 tumor-suppressor axis restrains oncogenic Aurora-A kinase to ensure proper mitotic microtubule assembly', *Proceedings of the National Academy of Sciences of the United States of America*, 113(7), pp. 1817–1822.

Falchuk, KH., Krishan, A. and Sullivan, J. (1977) '1,10-Phenanthroline Inhibition of Lymphoblast Cell Cycle', *Cancer Research*, 37(7 Part 1), pp. 2050 LP – 2056.

Farquharson, MJ. *et al.* (2009) 'Zinc presence in invasive ductal carcinoma of the breast and its correlation with oestrogen receptor status.', *Physics in medicine and biology*, 54(13), pp. 4213–23.

Feeney, GP. *et al.* (2005) 'The phylogeny of teleost ZIP and ZnT zinc transporters and their tissue specific expression and response to zinc in zebrafish', *Biochimica et Biophysica Acta*, 1732(1), pp. 88–95.

Feitelson, MA. *et al.* (2015) 'Sustained proliferation in cancer: Mechanisms and novel therapeutic targets', *Seminars in cancer biology*, pp. S25–S54.

Feng, P. *et al.* (2002) 'Direct Effect of Zinc on Mitochondrial Apoptogenesis in Prostate Cells', *The Prostate*, 52(4), pp. 311–318.

Figueroa-Magalhães, MC. *et al.* (2014) 'Treatment of HER2-positive breast cancer', *Breast*, 23(2), pp. 128–136.

Finn, RS. *et al.* (2015) 'The cyclin-dependent kinase 4/6 inhibitor palbociclib in combination with letrozole versus letrozole alone as first-line treatment of oestrogen receptor-positive, HER2-negative, advanced breast cancer (PALOMA-1/TRIO-18): a randomised phase 2 study', *The Lancet Oncology*, 16(1), pp. 25–35.

Fisher, B. and Wolmark, N. (1981) 'The current status of systemic adjuvant therapy in the management of primary breast cancer.', *The Surgical clinics of North America*, 61(6), pp. 1347–1360.

Foley, EA. and Kapoor, TM. (2013) 'Microtubule attachment and spindle assembly checkpoint signaling at the kinetochore', *Nature reviews. Molecular cell biology*, 14(1), pp. 25–37.

Fong, LY. *et al.* (2018) 'Human-like hyperplastic prostate with low ZIP1 induced solely by Zn deficiency in rats', *Proceedings of the National Academy of Sciences of the United States of America.*, 115(47), pp. E11091–E11100.

Fosgerau, K. and Hoffmann, T. (2015) 'Peptide therapeutics: current status and future directions', *Drug Discovery Today*, 20(1), pp. 122–128.

Frame, MC. and Roskoski, RB. (2017) 'Src Family Tyrosine Kinases', in. Elsevier.

Francis, SH. *et al.* (2010) 'cGMP-dependent protein kinases and cGMP phosphodiesterases in nitric oxide and cGMP action', *Pharmacological reviews*, 62(3), pp. 525–563.

Franklin, RB. *et al.* (2005) 'hZIP1 zinc uptake transporter down regulation and zinc depletion in prostate cancer', *Molecular Cancer*. London: BioMed Central, 4, p. 32.

Franz-Wachtel, M. *et al.* (2012) 'Global detection of protein kinase D-dependent phosphorylation events in nocodazole-treated human cells', *Molecular & cellular proteomics*, 11(5), pp. 160–170.

Fry, DW. *et al.* (2004) 'Specific inhibition of cyclin-dependent kinase 4/6 by PD 0332991 and associated antitumor activity in human tumor xenografts', *Molecular Cancer Therapeutics*, 3(11), pp. 1427 LP – 1438.

Fu, Y. *et al.* (2007) 'Weakened spindle checkpoint with reduced BubR1 expression in paclitaxel-resistant ovarian carcinoma cell line SKOV3-TR30', *Gynecologic Oncology*, 105(1), pp. 66–73.

Fuhs, SR. and Hunter, T. (2017) 'pHisphorylation: the emergence of histidine phosphorylation as a reversible regulatory modification', *Current opinion in cell biology*, 45, pp. 8–16.

Fujii, C. *et al.* (2005) 'Aberrant expression of serine/threonine kinase Pim-3 in hepatocellular carcinoma development and its role in the proliferation of human hepatoma cell lines', *International Journal of Cancer*, 114(2), pp. 209–218.

Fung, TK. and Poon, RYC. (2005) 'A roller coaster ride with the mitotic cyclins', *Seminars in Cell & Developmental Biology*, 16(3), pp. 335–342.

Gaither, LA. and Eide, DJ. (2000) 'Functional Expression of the Human hZIP2 Zinc Transporter', *Journal of Biological Chemistry* , 275(8), pp. 5560–5564.

Gao, B. *et al.* (2001) 'Constitutive activation of JAK-STAT3 signaling by BRCA1 in human prostate cancer cells', *FEBS Letters*, 488(3), pp. 179–184.

Garcia, R *et al.* (1997) 'Constitutive activation of Stat3 in fibroblasts transformed by diverse oncoproteins and in breast carcinoma cells.', *Cell growth & differentiation*, 8(12), pp. 1267–76.

Garcia, R *et al.* (1997) 'Constitutive activation of Stat3 in fibroblasts transformed by diverse oncoproteins and in breast carcinoma cells', *Cell Growth Differ*, 8, pp. 1267–1276.

Garland, M. *et al.* (1996) 'Toenail Trace Element Levels and Breast Cancer: A Prospective Study', *American Journal of Epidemiology*, 144(7), pp. 653–660.

Gee, KR. *et al.* (2002) 'Detection and Imaging of Zinc Secretion from Pancreatic β-Cells Using a New Fluorescent Zinc Indicator', *Journal of the American Chemical Society*, 124(5), pp. 776–778.

Gerlich, D. *et al.* (2006) 'Condensin I Stabilizes Chromosomes Mechanically through a Dynamic Interaction in Live Cells', *Current Biology*, 16(4), pp. 333–344.

Gkouveris, I. *et al.* (2014) 'Erk1/2 activation and modulation of STAT3 signaling in oral cancer', *Oncology Reports*, 32(5), pp. 2175–2182.

Gnad, F. *et al.* (2007) 'PHOSIDA (phosphorylation site database): management, structural and evolutionary investigation, and prediction of phosphosites.', *Genome biology*, 8(11), p. R250.

Goel TS. (2006) 'Comparative study of zinc levels in benign and malignant lesions of the prostate', *Scandanavian Journal of Urology and Nephrology.* , 40(2), pp. 108–12.

Gökbuget, N. *et al.* (2018) 'Blinatumomab for minimal residual disease in adults with B-cell precursor acute lymphoblastic leukemia', *Blood*, 131(14), pp. 1522–1531.

Gonzalez, A. *et al.* (2009) 'Zinc intake from supplements and diet and prostate cancer.', *Nutrition and cancer*, 61(2), pp. 206–215.

Goujon, M. *et al.* (2010) 'A new bioinformatics analysis tools framework at EMBL–EBI', *Nucleic Acids Research*, pp. W695–W699.

Goulding, H. *et al.* (1995) 'Metallothionein expression in human breast cancer.', *British Journal of Cancer*, 72(4), pp. 968–972.

Gouw, M. *et al.* (2017) 'The eukaryotic linear motif resource – 2018 update', *Nucleic Acids Research*, 46(D1), pp. D428–D434.

Gradishar, WJ. (2012) 'Taxanes for the treatment of metastatic breast cancer', *Breast cancer : basic and clinical research*, 6, pp. 159–171.

Grattan, BJ. and Freake, HC. (2012) 'Zinc and cancer: implications for LIV-1 in breast cancer', *Nutrients*, 4(7), pp. 648–675.

Grimes, CA. and Jope, RS. (2001) 'The multifaceted roles of glycogen synthase kinase 3β in cellular signaling', *Progress in Neurobiology*, 65(4), pp. 391–426.

Grotz, N. *et al.* (1998) 'Identification of a family of zinc transporter genes from Arabidopsis that respond to zinc deficiency', *Proceedings of the National Academy of Sciences of the United States of America*, 95(12), pp. 7220–7224.

de Gruijl, FR. (2017) 'UV adaptation: Pigmentation and protection against overexposure.', *Experimental dermatology*. Denmark, 26(7), pp. 557–562.

Guanizo, AC. *et al.* (2018) 'STAT3: a multifaceted oncoprotein', *Growth Factors*, 36(1–2), pp. 1–14.

Guerinot, M (2000) 'The ZIP family of metal transporters', *Biochimica et Biophysica Acta (BBA) - Biomembranes*, 1465(1), pp. 190–198.

Gumulec, J. *et al.* (2014) 'Serum and Tissue Zinc in Epithelial Malignancies: A Meta-Analysis', *PLoS ONE*, 9(6), p. e99790.

Gupta, GD. *et al.* (2015) 'A Dynamic Protein Interaction Landscape of the Human Centrosome-Cilium Interface', *Cell*, 163(6), pp. 1484–1499.

Gupta, R., Jung, E. and Brunak, S. (2004) *Prediction of N-glycosylation sites in human proteins*. Pacific Symposium on Biocomputing, 7, pp. 310–322.

Gupta, SK. *et al.* (1991) 'Serum trace elements and Cu/Zn ratio in breast cancer patients', *Journal of Surgical Oncology*, 46(3), pp. 178–181.

Gutteridge, REA. *et al.* (2016) 'Plk1 Inhibitors in Cancer Therapy: From Laboratory to Clinics', *Molecular cancer therapeutics*, 15(7), pp. 1427–1435.

Györkey, F. *et al.* (1967) 'Zinc and Magnesium in Human Prostate Gland: Normal, Hyperplastic, and Neoplastic', *Cancer Research*, 27(8 Part 1), pp. 1348 LP – 1353.

Haapasalo, A. and Kovacs, D. M. (2011) 'The many substrates of presenilin/γ-secretase', *Journal of Alzheimer's disease*, 25(1), pp. 3–28.

Haase, H. and Maret, W. (2003) 'Intracellular zinc fluctuations modulate protein tyrosine

phosphatase activity in insulin/insulin-like growth factor-1 signaling', *Experimental Cell Research*, 291(2), pp. 289–298.

Haase, H. and Rink, L. (2009) 'The immune system and the impact of zinc during aging', *Immunity & Ageing*, 6(1), p. 9.

Habib, FK. *et al.* (1979) 'Cancer of the prostate: early diagnosis by zinc and hormone analysis?', *British Journal of Cancer*, 39(6), pp. 700–704.

Habu, T. and Matsumoto, T. (2013) 'p31(comet) inactivates the chemically induced Mad2-dependent spindle assembly checkpoint and leads to resistance to anti-mitotic drugs', *SpringerPlus*, 2, p. 562.

Haensel, D. and Dai, X. (2018) 'Epithelial-to-mesenchymal transition in cutaneous wound healing: Where we are and where we are heading', *Developmental dynamics*, 247(3), pp. 473–480.

Hainsworth, JD. *et al.* (2003) 'Single-Agent Rituximab as First-Line and Maintenance Treatment for Patients With Chronic Lymphocytic Leukemia or Small Lymphocytic Lymphoma: A Phase II Trial of the Minnie Pearl Cancer Research Network', *Journal of Clinical Oncology*, 21(9), pp. 1746–1751.

Halsted, JA. and Prasad, AS. (1961) 'Syndrome of Iron Deficiency Anemia, Hepatosplenomegaly, Hypogonadism, Dwarfism and Geophagia', *Transactions of the American Clinical and Climatological Association*, 72, pp. 130–149.

Hanahan, D. and Weinberg, RA. (2011) 'Hallmarks of Cancer: The Next Generation', *Cell*. Elsevier, 144(5), pp. 646–674.

Hang Lee, C., Thye Ho, K. and Cheem Tan, H. (2005) 'Instant dissolution of intracoronary thrombus by abciximab', *International Journal of Cardiology*, 104(1), pp. 102–103.

Hansson, EM. *et al.* (2010) 'Control of Notch-ligand endocytosis by ligand-receptor interaction', *Journal of Cell Science*, 123(17), pp. 2931 LP – 2942.

Haque, MM. and Desai, KV (2019) 'Pathways to Endocrine Therapy Resistance in Breast Cancer.', *Frontiers in endocrinology*, 10, p. 573.

Harbour, JW. and Dean, DC. (2000) 'The Rb / E2F pathway : expanding roles and emerging paradigms', (314), pp. 2393–2409.

Hartmann, M., Herrlich, A. and Herrlich, P. (2013) 'Who decides when to cleave an ectodomain?', *Trends in Biochemical Sciences*, 38(3), pp. 111–120.

Hawkes, JE. *et al.* (2018) 'Discovery of the IL-23/IL-17 Signaling Pathway and the Treatment of Psoriasis', *Journal of immunology (Baltimore, Md. : 1950)*, 201(6), pp. 1605–1613.

Hay, ED. (1995) 'An overview of epithelio-mesenchymal transformation.', *Acta anatomica*, 154(1), pp. 8–20.

He, Y. *et al.* (2016) 'Cell Division Cycle 6 Promotes Mitotic Slippage and Contributes to Drug Resistance in Paclitaxel-Treated Cancer Cells', *PloS one*., 11(9), pp. e0162633–e0162633.

Hein, MY. *et al.* (2015) 'A Human Interactome in Three Quantitative Dimensions Organized by Stoichiometries and Abundances', *Cell*, 163(3), pp. 712–723.

Hendzel, MJ. *et al.* (1997) 'Mitosis-specific phosphorylation of histone H3 initiates primarily within pericentromeric heterochromatin during G2 and spreads in an ordered fashion coincident with mitotic chromosome condensation.', *Chromosoma*, 106(6), pp. 348–360.

Hershko, A. (1999) 'Mechanisms and regulation of the degradation of cyclin B', *Philosophical*

Transactions of the Royal Society B, 354(1389), pp. 1571–1576.

Hiddemann, W. *et al.* (2005) 'Frontline therapy with rituximab added to the combination of cyclophosphamide, doxorubicin, vincristine, and prednisone (CHOP) significantly improves the outcome for patients with advanced-stage follicular lymphoma compared with therapy with CHOP alone: results of a prospective randomized study of the German Low-Grade Lymphoma Study Group', *Blood*, 106(12), pp. 3725–3732.

Hogstrand, C. *et al.* (2013) 'A mechanism for epithelial–mesenchymal transition and anoikis resistance in breast cancer triggered by zinc channel ZIP6 and STAT3 (signal transducer and activator of transcription 3)', *Biochemical Journal*, 455(Pt 2), pp. 229–237.

Hooper, NM. (1994) 'Families of zinc metalloproteases', *FEBS Letters*, 354(1), pp. 1–6.

Hori, K., Sen, A. and Artavanis-Tsakonas, S. (2013) 'Notch signaling at a glance.', *Journal of cell science*. England, 126(Pt 10), pp. 2135–2140.

Hornbeck, PV *et al.* (2004) 'PhosphoSite: A bioinformatics resource dedicated to physiological protein phosphorylation.', *Proteomics*, 4(6), pp. 1551–61.

Hosseini, K. *et al.* (2019) 'EMT-induced cell mechanical changes enhance mitotic rounding strength', *bioRxiv*, p. 598052.

Huang, CY. *et al.* (2017) 'A review on the effects of current chemotherapy drugs and natural agents in treating non-small cell lung cancer', *BioMedicine*, 7(4), p. 23.

Huang, G. *et al.* (2014) 'STAT3 phosphorylation at tyrosine 705 and serine 727 differentially regulates mouse ESC fates', *Stem cells*, 32(5), pp. 1149–1160.

Hubbard, SR. (2013) 'The insulin receptor: both a prototypical and atypical receptor tyrosine kinase', *Cold Spring Harbor perspectives in biology*, 5(3), pp. a008946–a008946.

Hunter, T. (2012) 'Why nature chose phosphate to modify proteins', *Philosophical Transactions of the Royal Society B: Biological Sciences*, 367(1602), pp. 2513–2516.

Huppert, SS. *et al.* (2000) 'Embryonic lethality in mice homozygous for a processing-deficient allele of Notch1', *Nature*, 405(6789), pp. 966–970.

Huttlin, EL. *et al.* (2017) 'Architecture of the human interactome defines protein communities and disease networks', *Nature*, 545(7655), pp. 505–509.

Iancu, C. *et al.* (2001) 'Effects of stathmin inhibition on the mitotic spindle', *Journal of Cell Science*, 114(5), pp. 909 LP – 916.

Ibrahim, B. (2015) 'Spindle assembly checkpoint is sufficient for complete Cdc20 sequestering in mitotic control', *Computational and Structural Biotechnology Journal*, 13, pp. 320–328.

Ishida, S. *et al.* (2001) 'Role for E2F in control of both DNA replication and mitotic functions as revealed from DNA microarray analysis', *Molecular and cellular biology*. American Society for Microbiology, 21(14), pp. 4684–4699.

Jain, RK. (1990) 'Physiological Barriers to Delivery of Monoclonal Antibodies and Other Macromolecules in Tumors', *Cancer Research*, 50(3 Supplement), pp. 814s LP-819s.

Jenkitkasemwong, S. *et al.* (2012) 'Physiologic implications of metal-ion transport by ZIP14 and ZIP8', *Biometals : an international journal on the role of metal ions in biology, biochemistry, and medicine*, 25(4), pp. 643–655.

Jin, J. *et al.* (2015) 'Knockdown of zinc transporter ZIP5 (SLC39A5) expression significantly inhibits human esophageal cancer progression', *Oncology reports*, 34.

Jin, R. *et al.* (1999) 'Metallothionein expression and zinc levels in invasive ductal breast carcinoma.', *Oncology Reports*. Spandidos Publications, 6(4), pp. 871–876.

Josep, J. and Serra, B. (2006) 'Alternative initiation of HER2 translation produces active HER2 C-terminal fragments', Cellular and Molecular Biology, 65(9), p 867.

Junttila, TT. *et al.* (2009) 'Ligand-Independent HER2/HER3/PI3K Complex Is Disrupted by Trastuzumab and Is Effectively Inhibited by the PI3K Inhibitor GDC-0941', *Cancer Cell*, 15(5), pp. 429–440.

Kagara, N. *et al.* (2007) 'Zinc and its transporter ZIP10 are involved in invasive behavior of breast cancer cells', *Cancer Science*, 98(5), pp. 692–697.

Kaler, P. and Prasad, R. (2007) 'Molecular cloning and functional characterization of novel zinc transporter rZip10 (Slc39a10) involved in zinc uptake across rat renal brush-border membrane', *American Journal of Physiology-Renal Physiology*, 292(1), pp. F217–F229.

Kalluri, R. and Weinberg, RA. (2009) 'The basics of epithelial-mesenchymal transition', *The Journal of clinical investigation*, 119(6), pp. 1420–1428.

Kambe, T. and Andrews, GK. (2009) 'Novel Proteolytic Processing of the Ectodomain of the Zinc Transporter ZIP4 (SLC39A4) during Zinc Deficiency Is Inhibited by Acrodermatitis Enteropathica Mutations', *Molecular and Cellular Biology*, 29(1), pp. 129–139.

Kantarjian, H. *et al.* (2017) 'Blinatumomab versus Chemotherapy for Advanced Acute Lymphoblastic Leukemia', *The New England journal of medicine*, 376(9), pp. 836–847.

Kato, JY. and Sherr, CJ. (1993) 'Inhibition of granulocyte differentiation by G1 cyclins D2 and D3 but not D1', *Proceedings of the National Academy of Sciences of the United States of America*, 90(24), pp. 11513–11517.

Kelwick, R. *et al.* (2015) 'The ADAMTS (A Disintegrin and Metalloproteinase with Thrombospondin motifs) family.', *Genome biology*, 16, p. 113.

Kettenbach, AN. *et al.* (2011) 'Quantitative phosphoproteomics identifies substrates and functional modules of Aurora and Polo-like kinase activities in mitotic cells', *Science signaling*, 4(179), pp. rs5–rs5.

Kew, MC. and Mallett, RC. (1974) 'Hepatic zinc concentrations in primary cancer of the liver.', *British Journal of Cancer*, 29(1), pp. 80–83.

Kim, A. M. *et al.* (2010) 'Zinc Availability Regulates Exit from Meiosis in Maturing Mammalian Oocytes', *Nature chemical biology*, 6(9), pp. 674–681.

Kim, BE. *et al.* (2004) 'Zn2+-stimulated Endocytosis of the mZIP4 Zinc Transporter Regulates Its Location at the Plasma Membrane', *Journal of Biological Chemistry* , 279(6), pp. 4523–4530.

Kim, HG. *et al.* (2011) 'Metallothionein-2A overexpression increases the expression of matrix metalloproteinase-9 and invasion of breast cancer cells', *FEBS Letters*, 585(2), pp. 421–428.

Kim, HJ. and Lebwohl, M. G. (2019) 'Biologics and Psoriasis: The Beat Goes On', *Dermatologic Clinics*, 37(1), pp. 29–36.

Kim, JH. *et al.* (2019) 'Non-SMC condensin I complex subunit H mediates mature chromosome

condensation and DNA damage in pancreatic cancer cells.', *Scientific reports*, 9(1), p. 17889.

Kimura, K. *et al.* (1998) 'Phosphorylation and Activation of 13S Condensin by Cdc2 in Vitro', *Science*, 282(5388), pp. 487 LP – 490.

Kitabayashi, C. *et al.* (2010) 'Zinc suppresses Th17 development via inhibition of STAT3 activation', *International Immunology*, 22(5), pp. 375–386.

Klapper, LN. *et al.* (2000) 'Tumor-inhibitory Antibodies to HER-2/ErbB-2 May Act by Recruiting c-Cbl and Enhancing Ubiquitination of HER-2', *Cancer Research*, 60(13), pp. 3384 LP – 3388.

Klement, E. and Medzihradszky, K. F. (2017) 'Extracellular Protein Phosphorylation, the Neglected Side of the Modification', *Molecular & cellular proteomics*, 16(1), pp. 1–7.

Kolarsick, PAJ., Kolarsick, MA. and Goodwin, C. (2006) 'Anatomy and Physiology of the Skin'.

Kolonel, L., Yoshizawa, C. and Hankin, J. (1988) 'Diet and prostatic cancer: a case-control study in Hawaii', *Am J Epidemiol*, 127(5), pp. 999–1012.

Kong, BY. *et al.* (2014) 'Maternally-derived zinc transporters ZIP6 and ZIP10 drive the mammalian oocyte-to-egg transition', *Molecular Human Reproduction*, 20(11), pp. 1077–1089.

Koseoglu, MM., Graves, LM. and Marzluff, WF. (2008) 'Phosphorylation of threonine 61 by cyclin a/Cdk1 triggers degradation of stem-loop binding protein at the end of S phase', *Molecular and cellular biology*, 28(14), pp. 4469–4479.

Kosugi, S. *et al.* (2009) 'Systematic identification of cell cycle-dependent yeast nucleocytoplasmic shuttling proteins by prediction of composite motifs', *Proceedings of the National Academy of Sciences of the United States of America*, 106(25), pp. 10171–10176.

Kovacs, GG. and Budka, H. (2008) 'Prion diseases: from protein to cell pathology', *The American journal of pathology*, 172(3), pp. 555–565.

Kovalski, JR. *et al.* (2019) 'The Functional Proximal Proteome of Oncogenic Ras Includes mTORC2', *Molecular Cell*, 73(4), pp. 830-844.e12.

Krężel, A., Hao, Q. and Maret, W. (2007) 'The zinc/thiolate redox biochemistry of metallothionein and the control of zinc ion fluctuations in cell signaling', *Archives of Biochemistry and Biophysics*, 463(2), pp. 188–200.

Krueger, JG. and Bowcock, A. (2005) 'Psoriasis pathophysiology: current concepts of pathogenesis', *Annals of the Rheumatic Diseases*, 64(suppl 2), p. ii30 LP-ii36.

Kucharzewski, M. *et al.* (2003) 'Selenium, copper, and zinc concentrations in intestinal cancer tissue and in colon and rectum polyps', *Biological Trace Element Research*, 92(1), pp. 1–10.

Kumar, R. *et al.* (2017) 'The STUbL RNF4 regulates protein group SUMOylation by targeting the SUMO conjugation machinery', *Nature communications*, 8(1), p. 1809.

Kummar, S. *et al.* (2006) 'Drug development in oncology: classical cytotoxics and molecularly targeted agents', *British journal of clinical pharmacology*, 62(1), pp. 15–26.

Kusaba, T. *et al.* (2006) 'Activation of STAT3 is a marker of poor prognosis in human colorectal cancer', *Oncology Reports*, 15(6), pp. 1445–1451.

Labrijn, AF. *et al.* (2019) 'Bispecific antibodies: a mechanistic review of the pipeline', *Nature Reviews Drug Discovery*. Springer US, 18(8), pp. 585–608.

Landesman-Bollag, E. *et al.* (2001) 'Protein kinase CK2 in mammary gland tumorigenesis', *Oncogene*, 20(25), pp. 3247–3257.

Lang, C. *et al.* (2007) 'Anti-inflammatory effects of zinc and alterations in zinc transporter mRNA in mouse models of allergic inflammation', *American Journal of Physiology-Lung Cellular and Molecular Physiology*, 292(2), pp. L577–L584.

Lavanya, V. *et al.* (2014) 'Small molecule inhibitors as emerging cancer therapeutics', 1(3), pp. 39–46.

Lee, SY., Jang, C. and Lee, KA. (2014) 'Polo-Like Kinases (Plks), a Key Regulator of Cell Cycle and New Potential Target for Cancer Therapy', *Development & reproduction*, 18(1), pp. 65–71.

Leitzmann, M. *et al.* (2003) 'Zinc supplement use and risk of prostate cancer.', *J Natl Cancer Inst*, 95(13), pp. 1004–7.

Lew, DJ., Dulić, V. and Reed, SI. (1991) 'Isolation of three novel human cyclins by rescue of G1 cyclin (cln) function in yeast', *Cell*, 66(6), pp. 1197–1206.

Lewis, V. *et al.* (2016) 'Prion protein ``gamma-cleavage'': characterizing a novel endoproteolytic processing event', *Cellular and Molecular Life Sciences*, 73(3), pp. 667–683.

Li, M. *et al.* (2009) 'Downregulation of ZIP4 by RNA Interference Inhibits Pancreatic Cancer Growth and Increases the Survival of Nude Mice with Pancreatic Cancer Xenografts', *Clinical cancer research : an official journal of the American Association for Cancer Research*, 15(19), pp. 5993–6001.

Li, W. *et al.* (2015) 'The EMBL-EBI bioinformatics web and programmatic tools framework', *Nucleic acids research*, 43(W1), pp. W580-4.

Li, X. *et al.* (2013) 'Structure of a presenilin family intramembrane aspartate protease', *Nature*. Nature Publishing Group, 493(7430), pp. 56–61.

Li, YY. *et al.* (2006) 'Pim-3, a Proto-Oncogene with Serine/Threonine Kinase Activity, Is Aberrantly Expressed in Human Pancreatic Cancer and Phosphorylates Bad to Block Bad-Mediated Apoptosis in Human Pancreatic Cancer Cell Lines', *Cancer Research*, 66(13), pp. 6741 LP – 6747.

Li, Y. and Maret, W. (2009) 'Transient fluctuations of intracellular zinc ions in cell proliferation', *Experimental Cell Research*, 315(14), pp. 2463–2470.

Liang, JY. *et al.* (1999) 'Inhibitory effect of zinc on human prostatic carcinoma cell growth', *The Prostate*, 40(3), pp. 200–207.

Lichten, LA. *et al.* (2011) 'MTF-1-mediated repression of the zinc transporter Zip10 is alleviated by zinc restriction', *PloS one*, 6(6), pp. e21526–e21526.

Lichten, LA., Liuzzi, JP. and Cousins, RJ. (2007) 'Zinc suppresses hepatic Zip10 expression through activation of MTF-1', *The FASEB Journal*, 21(5), pp. A170–A170.

Lim, S. and Kaldis, P. (2013) 'Cdks, cyclins and CKIs: roles beyond cell cycle regulation', *Development*, 140(15), pp. 3079 LP – 3093.

Lin, Y.-F. *et al.* (2009) 'Arabidopsis IRT3 is a zinc-regulated and plasma membrane localized zinc/iron transporter', *New Phytologist*, 182(2), pp. 392–404.

Liu, PC. *et al.* (2006) 'Identification of ADAM10 as a Major Source of HER2 Ectodomain Sheddase Actvity in HER2 Overexpressing Breast Cancer Cells', *Cancer Biology and Therapeutics*, 5(6), pp. 657–664.

Liu, X. *et al.* (2018) 'An AP-MS- and BioID-compatible MAC-tag enables comprehensive mapping of protein interactions and subcellular localizations', *Nature communications*, 9(1), p. 1188.

Liu, Y. *et al.* (2007) 'Identification of differential expression of genes in hepatocellular carcinoma by suppression subtractive hybridization combined cDNA microarray', *Oncology Reports*, 18(4), pp. 943–951.

Liuzzi, JP. *et al.* (2006) 'Zip14 (Slc39a14) mediates non-transferrin-bound iron uptake into cells', *Proceedings of the National Academy of Sciences of the United States of America*, 103(37), pp. 13612–13617.

Loizou, JI. *et al.* (2004) 'The Protein Kinase CK2 Facilitates Repair of Chromosomal DNA Single-Strand Breaks', *Cell*. Elsevier, 117(1), pp. 17–28.

Lu, J. *et al.* (2008) 'Albumin as a zinc carrier: properties of its high-affinity zinc-binding site', *Biochemical Society Transactions*, 36(6), pp. 1317 LP – 1321.

Lue, H.-W. *et al.* (2011) 'LIV-1 promotes prostate cancer epithelial-to-mesenchymal transition and metastasis through HB-EGF shedding and EGFR-mediated ERK signaling.', *PloS one*, 6(11), p. e27720.

Luque-Cabal, M. *et al.* (2016) 'Mechanisms Behind the Resistance to Trastuzumab in HER2-Amplified Breast Cancer and Strategies to Overcome It', *Clinical Medicine Insights. Oncology*, 10(Suppl 1), pp. 21–30.

Ma, HT. *et al.* (2012) 'Depletion of p31comet protein promotes sensitivity to antimitotic drugs', *The Journal of biological chemistry*, 287(25), pp. 21561–21569.

Mackay, HJ. *et al.* (2012) 'A phase II trial of the Src kinase inhibitor saracatinib (AZD0530) in patients with metastatic or locally advanced gastric or gastro esophageal junction (GEJ) adenocarcinoma: a trial of the PMH phase II consortium.', *Investigational new drugs*, 30(3), pp. 1158–1163.

Malumbres, M. *et al.* (2004) 'Mammalian Cells Cycle without the D-Type Cyclin-Dependent Kinases Cdk4 and Cdk6', *Cell*, 118(4), pp. 493–504.

Malumbres, M. and Barbacid, M. (2009) 'Cell cycle, CDKs and cancer: a changing paradigm', *Nat Rev Cancer*, 9(3), pp. 153–166.

Manni, S. *et al.* (2008) 'Phosphorylation of the cAMP-dependent protein kinase (PKA) regulatory subunit modulates PKA-AKAP interaction, substrate phosphorylation, and calcium signaling in cardiac cells', *Journal of Biological Chemistry*, 283(35), pp. 24145–24154.

Manning, DL. *et al.* (1988) 'Effects of oestrogen on the expression of a 4.4 kb mRNA in the ZR-75-1 human breast cancer cell line.', *Molecular and cellular endocrinology*, 59(3), pp. 205–212.

Manning, DL. *et al.* (1993) 'The role of four oestrogen-responsive genes, pLIV1, pS2, pSYD3 and pSYD8, in predicting responsiveness to endocrine therapy in primary breast cancer', *European Journal of Cancer*, 29(10), pp. 1462–1468.

Manning, DL. *et al.* (1994) 'Oestrogen-regulated genes in breast cancer: association of pLIV1 with lymph node involvement.', *European journal of cancer*, 30A(5), pp. 675–8.

Mao, X. *et al.* (2007) 'A Histidine-rich Cluster Mediates the Ubiquitination and Degradation of the Human Zinc Transporter, hZIP4, and Protects against Zinc Cytotoxicity', *Journal of Biological Chemistry* , 282(10), pp. 6992–7000.

Maret, W. and Vallee, BL. (1998) 'Thiolate ligands in metallothionein confer redox activity on zinc clusters', *Proceedings of the National Academy of Sciences of the United States of America*., 95(7),

pp. 3478–3482.

Margalioth, Ehud J *et al.* (1983) 'Copper and Zinc Levels in Normal and Malignant Tissues', *Cancer*, 52, pp. 868–872.

Martins, LR. *et al.* (2014) 'Activity of the clinical-stage CK2-specific inhibitor CX-4945 against chronic lymphocytic leukemia', *Leukemia*. Macmillan Publishers Limited, 28(1), pp. 179–182.

Matson, DR. and Stukenberg, P. T. (2011) 'Spindle poisons and cell fate: a tale of two pathways', *Molecular interventions*, 11(2), pp. 141–150.

Matsushime, H. *et al.* (1994) 'D-type cyclin-dependent kinase activity in mammalian cells', *Molecular and cellular biology*, 14(3), pp. 2066–2076.

Matthews, D. (2015) *Developing antibody therapeutics*. Available at: https://www.drugtargetreview.com/article/4540/developing-antibody-therapeutics/ (Accessed: 6 February 2020).

McCall, KA., Huang, C. and Fierke, CA. (2000) 'Function and mechanism of zinc metalloenzymes.', *The Journal of nutrition*, 130(5S Suppl), pp. 1437S–46S.

McDonald, K. *et al.* (1992) 'Kinetochore microtubules in PTK cells', *The Journal of Cell Biology*, 118(2), pp. 369–383.

McIlwain, DR., Berger, T. and Mak, TW. (2013) 'Caspase Functions in Cell Death and Disease', *Cold Spring Harbor Perspectives in Biology* , 5(4).

McMahon, HEM. *et al.* (2001) 'Cleavage of the Amino Terminus of the Prion Protein by Reactive Oxygen Species', *Journal of Biological Chemistry* , 276(3), pp. 2286–2291.

Miao, X. *et al.* (2013) 'Zinc homeostasis in the metabolic syndrome and diabetes', *Frontiers of Medicine*, 7(1), pp. 31–52.

Michaelsson G, Ljunghall KDB. (1980) 'Zinc in epidermis and dermis in healthy subjects', *Acta Derm Venereol*, 60(4), pp. 295–299.

Miller, EM. and Schwartzberg, LS. (2019) 'Biosimilars for breast cancer: a review of HER2-targeted antibodies in the United States', *Therapeutic advances in medical oncology*, 11, pp. 1758835919887044–1758835919887044.

Miller, ML. *et al.* (2008) 'Linear motif atlas for phosphorylation-dependent signaling', *Science signaling*, 1(35), pp. ra2–ra2.

Miyai, T. *et al.* (2014) 'Zinc transporter SLC39A10/ZIP10 facilitates antiapoptotic signaling during early B-cell development', *Proceedings of the National Academy of Sciences*, 111(32), pp. 11780–11785.

Mócsai, A., Ruland, J. and Tybulewicz, V. L. J. (2010) 'The SYK tyrosine kinase: a crucial player in diverse biological functions', *Nature reviews. Immunology*, 10(6), pp. 387–402.

Molina, M. *et al.* (2001) 'Trastuzumab (Herceptin), a Humanized Anti-HER2 Receptor Monoclonal Antibody, Inhibits Basal and Activated HER2 Ectodomain Cleavage in Breast Cancer Cells', *Cancer Research*, 61(12), pp. 4744 LP – 4749.

Morris, EJ. *et al.* (2017) 'Stat3 regulates centrosome clustering in cancer cells via Stathmin/PLK1', *Nature communications*, 8, p. 15289.

Motiwala, T. and Jacob, ST. (2006) 'Role of Protein Tyrosine Phosphatases in Cancer', *Progress in*

nucleic acid research and molecular biology, 81, pp. 297–329.

Moynahan, EJ. (1974) 'Acrodermatitis enteropathica: A lethal inherited human zinc-deficiency disorder', *The Lancet*, 304(7877), pp. 399–400.

Mueller, PR. *et al.* (1995) 'Myt1: A Membrane-Associated Inhibitory Kinase That Phosphorylates Cdc2 on Both Threonine-14 and Tyrosine-15', *Science*, 270(5233), pp. 86 LP – 90.

Mulay, IL. *et al.* (1971) 'Trace-Metal Analysis of Cancerous and Non- cancerous Human Tissues', *Journal of the national cancer institute*, 47(1), pp. 1–13.

Muller, L. and Lindberg, I. (1999) 'The cell biology of the prohormone convertases PC1 and PC2', *Progress in nucleic acid research and molecular biology*, 63, pp. 69–108.

Musolino, A. *et al.* (2008) 'Immunoglobulin G Fragment C Receptor Polymorphisms and Clinical Efficacy of Trastuzumab-Based Therapy in Patients With HER-2/neu–Positive Metastatic Breast Cancer', *Journal of Clinical Oncology*, 26(11), pp. 1789–1796.

Nagase, H. and Woessner, JF. (1999) 'Matrix Metalloproteinases', *Journal of Biological Chemistry* , 274(31), pp. 21491–21494.

Nagata, Y. *et al.* (2004) 'PTEN activation contributes to tumor inhibition by trastuzumab, and loss of PTEN predicts trastuzumab resistance in patients', *Cancer Cell*. Elsevier, 6(2), pp. 117–127.

Nagy, P. *et al.* (2005) 'Decreased Accessibility and Lack of Activation of ErbB2 in JIMT-1, a Herceptin-Resistant, MUC4-Expressing Breast Cancer Cell Line', *Cancer Research*, 65(2), pp. 473 LP – 482.

Nasrazadani, A. *et al.* (2018) 'Precision Medicine in Hormone Receptor-Positive Breast Cancer', *Frontiers in oncology*. Frontiers Media S.A., 8, p. 144.

Nelson, A. L. (2010) 'Antibody fragments: hope and hype', *mAbs*, 2(1), pp. 77–83.

Ng, DCH. *et al.* (2006) 'Stat3 regulates microtubules by antagonizing the depolymerization activity of stathmin', *The Journal of Cell Biology*, 172(2), pp. 245 LP – 257.

Nicholson, DW. *et al.* (1995) 'Identification and inhibition of the ICE/CED-3 protease necessary for mammalian apoptosis', *Nature*, 376(6535), pp. 37–43.

Nimmanon, T. (2016) 'Post – translational mechanisms of the ZIP family of zinc channels' (Doctoral dissertation), Cardiff University, Cardiff, UK.

Nimmanon, T. *et al.* (2017) 'Phosphorylation of zinc channel ZIP7 drives MAPK, PI3K and mTOR growth and proliferation signalling', *Metallomics*. Royal Society of Chemistry.

Nimmanon, T et al. 'Inhibiiton of zinc transporter ZIP6/ZIP10 heteromer prevents the zinc influx required to trigger mitosis. Manuscript submitted.

Nimmanon, T and Taylor KM (2019). Post translational mechanisms of zinc signalling in cancer *in Zinc Signalin.* Sinapore: Springer Nature, pp 319–345.

Nolin, E. *et al.* (2019) 'Discovery of a ZIP7 inhibitor from a Notch pathway screen', *Nature Chemical Biology*, 15(2), pp. 179–188.

Nurgali, K., Jagoe, RT. and Abalo, R. (2018) 'Editorial: Adverse Effects of Cancer Chemotherapy: Anything New to Improve Tolerance and Reduce Sequelae?', *Frontiers in pharmacology*, 9, p. 245.

Offner, S. *et al.* (2006) 'Induction of regular cytolytic T cell synapses by bispecific single-chain antibody constructs on MHC class I-negative tumor cells', *Molecular Immunology*, 43(6), pp. 763–

771.

Ogunlewe, JO. and Osegbe, DN. (1989) 'Zinc and cadmium concentrations in indigenous blacks with normal, hypertrophic, and malignant prostate.', *Cancer*, 63(7), pp. 1388–92.

Ohana, E. *et al.* (2009) 'Identification of the Zn2+ binding site and mode of operation of a mammalian Zn2+ transporter', *The Journal of biological chemistry*, 284(26), pp. 17677–17686.

Oka, M. *et al.* (2004) 'Phosphatidylinositol 3-Kinase/Akt-Dependent and -Independent Protection Against Apoptosis in Normal Human Melanocytes', *Journal of Investigative Dermatology*, 123(5), pp. 930–936.

Oldenburg, J. *et al.* (2017) 'Emicizumab Prophylaxis in Hemophilia A with Inhibitors', *The New England journal of medicine*, 2017, pp. 809–818.

Olsen, JV *et al.* (2006) 'Global, In Vivo, and Site-Specific Phosphorylation Dynamics in Signaling Networks', *Cell*, 127(3), pp. 635–648.

Olsen, JV *et al.* (2010) 'Quantitative Phosphoproteomics Reveals Widespread Full Phosphorylation Site Occupancy During Mitosis', *Science Signaling*, 3(104), p. ra3 LP-ra3.

Olsen, JV, Ong, SE. and Mann, M. (2004) 'Trypsin Cleaves Exclusively C-terminal to Arginine and Lysine Residues', *Molecular and Cellular Proteomics*, 3(6), pp. 608 LP – 614.

Oughtred, R. *et al.* (2019) 'The BioGRID interaction database: 2019 update', *Nucleic acids research*., 47(D1), pp. D529–D541.

Pagano, M. *et al.* (1992) 'Cyclin A is required at two points in the human cell cycle', *The EMBO journal*, 11(3), pp. 961–971.

Pal, D. *et al.* (2014) *Association between ZIP10 gene expression and tumor aggressiveness in renal cell carcinoma*, *Gene*, 552(1), pp.195–198.

Palmiter, RD. and Findley, SD. (1995) 'Cloning and functional characterization of a mammalian zinc transporter that confers resistance to zinc', *The EMBO journal*, 14(4), pp. 639–649.

Pan, Z. *et al.* (2017) 'Zinc transporters and dysregulated channels in cancers', *Frontiers in bioscience*, 22, pp. 623–643.

Parker, LL. and Piwnica-Worms, H. (1992) 'Inactivation of the p34cdc2-cyclin B complex by the human WEE1 tyrosine kinase', *Science*, 257(5078), pp. 1955 LP – 1957.

Passerini, A. *et al.* (2007) 'Predicting zinc binding at the proteome level', *BMC Bioinformatics*., 8, p. 39.

Pavanello, F., Zucca, E. and Ghielmini, M. (2017) 'Rituximab: 13 open questions after 25 years of clinical use', *Cancer Treatment Reviews*, 53, pp. 38–46.

Pavlinkova, G. *et al.* (2001) 'Effects of humanization and gene shuffling on immunogenicity and antigen binding of anti-tag-72 single-chain Fvs', *International Journal of Cancer*, 94(5), pp. 717–726.

Peairs, KS. *et al.* (2011) 'Diabetes mellitus and breast cancer outcomes: a systematic review and meta-analysis', *Journal of clinical oncology : official journal of the American Society of Clinical Oncology*, 29(1), pp. 40–46.

Pedas, P. *et al.* (2008) 'Manganese efficiency in barley: identification and characterization of the metal ion transporter HvIRT1', *Plant physiology*, 148(1), pp. 455–466.

Penela, P. *et al.* (2019) 'G protein-coupled receptor kinase 2 (GRK2) as a multifunctional signaling hub', *Cellular and Molecular Life Sciences*.

Perez, E. A. *et al.* (2019) 'Trastuzumab emtansine with or without pertuzumab versus trastuzumab with taxane for human epidermal growth factor receptor 2–positive advanced breast cancer: Final results from MARIANNE', *Cancer*, Ltd, 125(22), pp. 3974–3984.

Perou, CM. *et al.* (2000) 'Molecular portraits of human breast tumours', *Nature*, 406(6797), pp. 747–752.

Piazza, F. *et al.* (2012) 'Protein kinase CK2 in hematologic malignancies: reliance on a pivotal cell survival regulator by oncogenic signaling pathways', *Leukemia*, 26, p. 1174.

Pickup, M., Novitskiy, S. and Moses, HL. (2013) 'The roles of TGFβ in the tumour microenvironment', *Nature reviews. Cancer*, 13(11), pp. 788–799.

Picton, C. *et al.* (1982) 'Multisite phosphorylation of glycogen synthase from rabbit skeletal muscle: Phosphorylation of site 5 by glycogen synthase kinase-5 (casein kinase-II) is a prerequisite for phosphorylation of sites 3 by glycogen synthase kinase-3', *FEBS Letters*, 150(1), pp. 191–196.

Pierotti, AR. *et al.* (1994) 'N-Arginine dibasic convertase , a metalloendopeptidase as a prototype of a class of processing enzymes Isolatin and Cherizatin of cDNA Cones E d', 91(June), pp. 6078–6082.

Pierre, F. *et al.* (2011) 'Pre-clinical characterization of CX-4945, a potent and selective small molecule inhibitor of CK2 for the treatment of cancer', *Molecular and Cellular Biochemistry*, 356(1), p. 37.

Pitt, SJ. and Stewart, AJ. (2015) 'Examining a new role for zinc in regulating calcium release in cardiac muscle', *Biochemical Society Transactions*, 43(3), pp. 359–363.

Popivanova, BK. *et al.* (2007) 'Proto-oncogene, Pim-3 with serine/threonine kinase activity, is aberrantly expressed in human colon cancer cells and can prevent Bad-mediated apoptosis', *Cancer Science*, 98(3), pp. 321–328.

Prasad, AS. *et al.* (2010) 'Dietary zinc and prostate cancer in the TRAMP mouse model', *Journal of medicinal food*, 13(1), pp. 70–76.

Price-Schiavi, SA. *et al.* (2002) 'Rat Muc4 (sialomucin complex) reduces binding of anti-ErbB2 antibodies to tumor cell surfaces, a potential mechanism for herceptin resistance', *International Journal of Cancer*, 99(6), pp. 783–791.

Pugacheva, EN., Roegiers, F. and Golemis, E. A. (2006) 'Interdependence of cell attachment and cell cycle signaling', *Current opinion in cell biology*, 18(5), pp. 507–515.

Pyle, CJ. *et al.* (2017) 'Zinc Modulates Endotoxin-Induced Human Macrophage Inflammation through ZIP8 Induction and C/EBPβ Inhibition', *PloS one*, 12(1), pp. e0169531–e0169531.

Radtke, F. *et al.* (1993) 'Cloned transcription factor MTF-1 activates the mouse metallothionein I promoter', *The EMBO journal*, 12(4), pp. 1355–1362.

Redegeld, FA., Caldwell, CC. and Sitkovsky, MV (1999) 'Ecto-protein kinases: ecto-domain phosphorylation as a novel target for pharmacological manipulation?', *Trends in Pharmacological Sciences*, 20(11), pp. 453–459.

Reff, M. *et al.* (1994) 'Depletion of B cells in vivo by a chimeric mouse human monoclonal antibody to CD20', *Blood*, 83(2), pp. 435–445.

Rieder, C. L. and Maiato, H. (2004) 'Stuck in Division or Passing through: What Happens When Cells

Cannot Satisfy the Spindle Assembly Checkpoint', *Developmental Cell*. Elsevier, 7(5), pp. 637–651.

Riesop, D. *et al.* (2015) 'Zinc distribution within breast cancer tissue: A possible marker for histological grading?', *Journal of Cancer Research and Clinical Oncology*, 141(7), pp. 1321–1331.

Rivera, E. and Gomez, H. (2010) 'Chemotherapy resistance in metastatic breast cancer: the evolving role of ixabepilone', *Breast cancer research*, Suppl 2(Suppl 2), pp. S2–S2.

Roche, J. (2018) 'The Epithelial-to-Mesenchymal Transition in Cancer', *Cancers*. MDPI, 10(2), p. 52.

Rodriguez, J. *et al.* (2016) 'Substrate-Trapped Interactors of PHD3 and FIH Cluster in Distinct Signaling Pathways', *Cell reports*. Cell Press, 14(11), pp. 2745–2760.

Roshak, AK. *et al.* (2000) 'The human polo-like kinase, PLK, regulates cdc2/cyclin B through phosphorylation and activation of the cdc25C phosphatase', *Cellular Signalling*, 12(6), pp. 405–411.

Roux, PP. and Blenis, J. (2004) 'ERK and p38 MAPK-activated protein kinases: a family of protein kinases with diverse biological functions', *Microbiology and molecular biology reviews : MMBR*. American Society for Microbiology, 68(2), pp. 320–344.

Roy, N. and Hebrok, M. (2015) 'Regulation of Cellular Identity in Cancer', *Developmental cell*, 35(6), pp. 674–684.

Rozeboom, B., Dey, N. and De, P. (2019) 'ER+ metastatic breast cancer: past, present, and a prescription for an apoptosis-targeted future', *American journal of cancer research*, 9(12), pp. 2821–2831.

Rudolf, E. and Rudolf, K. (2017) 'Increases in Intracellular Zinc Enhance Proliferative Signaling as well as Mitochondrial and Endolysosomal Activity in Human Melanocytes', *Cellular Physiology and Biochemistry*, 43(1), pp. 1–16.

Rusan, NM. *et al.* (2001) 'Cell Cycle-Dependent Changes in Microtubule Dynamics in Living Cells Expressing Green Fluorescent Protein-α Tubulin', *Molecular Biology of the Cell*, 12(4), pp. 971–980.

Ryu, MS. *et al.* (2008) 'Zinc Transporters ZnT1 (Slc30a1), Zip8 (Slc39a8), and Zip10 (Slc39a10) in Mouse Red Blood Cells Are Differentially Regulated during Erythroid Development and by Dietary Zinc Deficiency', *The Journal of Nutrition*, 138(11), pp. 2076–2083.

Sakaguchi, M. *et al.* (2012) 'Role and Regulation of STAT3 Phosphorylation at Ser727 in Melanocytes and Melanoma Cells', *Journal of Investigative Dermatology*, 132(7), pp. 1877–1885.

Sánchez-Pedreño P. (1998) 'Serum zinc levels are increased in melanoma patients', *Melanoma Res*, 8(3), pp. 273–7.

Santoliquido PM, Southwick HW (1976) 'Trace metal levels in cancer of the breast', *Surgery, Gynecology & Obstetrics*, 142(2), pp. 65–70.

Sanz, L. *et al.* (2005) 'Antibody engineering: facing new challenges in cancer therapy.', *Acta pharmacologica Sinica*, 26(6), pp. 641–648.

Schirrmacher, V. (2019) 'From chemotherapy to biological therapy: A review of novel concepts to reduce the side effects of systemic cancer treatment (Review)', *International journal of oncology*, 54(2), pp. 407–419.

Schmitt-Ulms, G. *et al.* (2009) 'Evolutionary Descent of Prion Genes from the ZIP Family of Metal Ion Transporters', *PLoS ONE*, 4(9), p. e7208.

Seidah, NG. *et al.* (2013) 'The multifaceted proprotein convertases: their unique, redundant,

complementary, and opposite functions', *The Journal of biological chemistry*. 2013/06/17. American Society for Biochemistry and Molecular Biology, 288(30), pp. 21473–21481.

Seidah, NG. and Chrétien, M. (1999) 'Proprotein and prohormone convertases: a family of subtilases generating diverse bioactive polypeptides, *Brain Research*, 848(1), pp. 45–62.

Sensi, SL. *et al.* (2009) 'Zinc in the physiology and pathology of the CNS', *Nat Rev Neurosci*, 10(11), pp. 780–791.

Shao, H. *et al.* (2004) 'Structural requirements for signal transducer and activator of transcription 3 binding to phosphotyrosine ligands containing the YXXQ motif.', *The Journal of biological chemistry*. United States, 279(18), pp. 18967–18973.

Sheaff, RJ., Groudine, M. and Roberts, JM. (1997) 'Cyclin E-CDK2 is a regulator of p27 Kip1', pp. 1464–1478.

Shi, X. *et al.* (2006) 'Phosphorylation of STAT3 Serine-727 by Cyclin-Dependent Kinase 1 Is Critical for Nocodazole-Induced Mitotic Arrest', *Biochemistry*, 45(18), pp. 5857–5867.

Shupp, A., Casimiro, M. C. and Pestell, R. G. (2017) 'Biological functions of CDK5 and potential CDK5 targeted clinical treatments', *Oncotarget*, 8(10), pp. 17373–17382.

Siddiqui-Jain, A. *et al.* (2010) 'CX-4945, an Orally Bioavailable Selective Inhibitor of Protein Kinase CK2, Inhibits Prosurvival and Angiogenic Signaling and Exhibits Antitumor Efficacy', *Cancer Research*, 70(24), pp. 10288 LP – 10298.

Silva, VC. and Cassimeris, L. (2013) 'Stathmin and microtubules regulate mitotic entry in HeLa cells by controlling activation of both Aurora kinase A and Plk1', *Molecular biology of the cell*, 24(24), pp. 3819–3831.

Slamon, DJ. *et al.* (2001) 'Use of Chemotherapy plus a Monoclonal Antibody against HER2 for Metastatic Breast Cancer That Overexpresses HER2', *New England Journal of Medicine*, 344(11), pp. 783–792.

Srivastava, S. *et al.* (2016) 'Histidine phosphorylation relieves copper inhibition in the mammalian potassium channel KCa3.1.', *eLife*, 5.

St-Denis, N. *et al.* (2015) 'Systematic investigation of hierarchical phosphorylation by protein kinase CK2', *Journal of Proteomics*, 118, pp. 49–62.

St-Denis, N. *et al.* (2016) 'Phenotypic and Interaction Profiling of the Human Phosphatases Identifies Diverse Mitotic Regulators', *Cell Reports*, 17(9), pp. 2488–2501.

Stanfield, R. L. and Wilson, I. (2014) 'Antibody Structure', *Microbiology Spectrum*, 2(2), pp. 1–11.

Steinman, R. A. *et al.* (2003) 'Activation of Stat3 by cell confluence reveals negative regulation of Stat3 by cdk2', *Oncogene*, 22(23), pp. 3608–3615.

Stewart, A. J. *et al.* (2003) 'Interdomain zinc site on human albumin', *Proceedings of the National Academy of Sciences* , 100(7), pp. 3701–3706.

Strohl, W. (2017) 'Chimeric Genes, Proteins', in. Elsevier.

Sussman, D. *et al.* (2014) 'SGN–LIV1A: A Novel Antibody–Drug Conjugate Targeting LIV-1 for the Treatment of Metastatic Breast Cancer', *Molecular Cancer Therapeutics*, 13(12), pp. 2991 LP – 3000.

Tagliabracci, V. S. *et al.* (2014) 'Dynamic regulation of FGF23 by Fam20C phosphorylation, GalNAc-T3 glycosylation, and furin proteolysis', *Proceedings of the National Academy of Sciences*, p.

201402218..

Takagishi, T., Hara, T. and Fukada, T. (2017) 'Recent Advances in the Role of SLC39A/ZIP Zinc Transporters In Vivo', *International journal of molecular sciences*, 18(12), p. 2708.

Takatani-Nakase, T. (2013) 'Migration Behavior of Breast Cancer Cells in the Environment of High Glucose Level and the Role of Zinc and Its Transporter', *Yakugaku zasshi : Journal of the Pharmaceutical Society of Japan*, 133, pp. 1195–1199.

Takatani-Nakase, T. *et al.* (2014) 'High glucose level promotes migration behavior of breast cancer cells through zinc and its transporters', *PLoS ONE*, 9(2).

Tavernier, N., Noatynska, A., *et al.* (2015) 'Cdk1 phosphorylates SPAT-1/Bora to trigger PLK-1 activation and drive mitotic entry in C. elegans embryos', *The Journal of Cell Biology*, 208(6), pp. 661 LP – 669.

Tavernier, N., Panbianco, C., *et al.* (2015) 'Cdk1 plays matchmaker for the Polo-like kinase and its activator SPAT-1/Bora', *Cell cycle (Georgetown, Tex.)*. 2015/06/03. Taylor & Francis, 14(15), pp. 2394–2398.

Taylor, KM. *et al.* (2007) 'The Emerging Role of the LIV-1 Subfamily of Zinc Transporters in Breast Cancer', *Molecular Medicine*, 13(7–8), pp. 396–406.

Taylor, KM. *et al.* (2008) 'ZIP7-mediated intracellular zinc transport contributes to aberrant growth factor signaling in antihormone-resistant breast cancer cells', *Endocrinology*, 149(10), pp. 4912–4920.

Taylor, KM *et al.* (2008) 'ZIP7-mediated intracellular zinc transport contributes to aberrant growth factor signaling in antihormone-resistant breast cancer Cells', *Endocrinology*, 149.

Taylor, K.M. *et al.* (2012) 'Protein kinase CK2 triggers cytosolic zinc signaling pathways by phosphorylation of zinc channel ZIP7', *Science signaling*, 5(210), pp. ra11–ra11.

Taylor, KM. *et al.* (2016) 'Zinc transporter ZIP10 forms a heteromer with ZIP6 which regulates embryonic development and cell migration', *Biochemical Journal*, 473(16), pp. 2531–2544.

Taylor, KM. and Nicholson, RI. (2003) 'The LZT proteins; the LIV-1 subfamily of zinc transporters', *Biochimica et Biophysica Acta (BBA) - Biomembranes*, 1611(1–2), pp. 16–30.

Thokala, S. *et al.* (2019) 'Comparative Response of Cardiomyocyte ZIPs and ZnTs to Extracellular Zinc and TPEN', *Biological Trace Element Research*, 192(19).

Tichý, V. *et al.* (2013) 'Redox state of p63 and p73 core domains regulates sequence-specific DNA binding', *Biochemical and Biophysical Research Communications*, 433(4), pp. 445–449.

Le Tourneau, C. *et al.* (2010) 'Phase I evaluation of seliciclib, a novel oral cyclin-dependent kinase inhibitor, in patients with advanced malignancies', *European Journal of Cancer*, 46(18), pp. 3243–3250.

Toyoshima-Morimoto, F., Taniguchi, E. and Nishida, E. (2002) 'Plk1 promotes nuclear translocation of human Cdc25C during prophase', *EMBO reports*, 3(4), pp. 341–348.

Tozlu, S. *et al.* (2006) 'Identification of novel genes that co-cluster with estrogen receptor alpha in breast tumor biopsy specimens, using a large-scale real-time reverse transcription-PCR approach', *Endocrine-Related Cancer*, 13(4), pp. 1109–1120.

Trisciuoglio, D., Di Martile, M. and Del Bufalo, D. (2018) 'Emerging Role of Histone Acetyltransferase

in Stem Cells and Cancer', *Stem cells international*, 2018, p. 8908751.

Tupper, R., Watts, RWE. and Wormall, A. (1955) 'The incorporation of (65)Zn in mammary tumours and some other tissues of mice after injection of the isotope', *Biochemical Journal*, 59(2), pp. 264–268.

Unno, J. *et al.* (2009) 'LIV-1 enhances the aggressive phenotype through the induction of epithelial to mesenchymal transition in human pancreatic carcinoma cells.', *Int J Oncol.*, 35(4), pp. 813–21.

Vallee, BL. and Galdes, A. (1984) 'The Metallobiochemistry of Zinc Enzymes', *Advances in Enzymology and Related Areas of Molecular Biology*, pp. 283–430.

VanArsdale, T. *et al.* (2015) 'Molecular Pathways: Targeting the Cyclin D–CDK4/6 Axis for Cancer Treatment', *Clinical Cancer Research*, 21(13), pp. 2905 LP – 2910.

Vidal, GA. *et al.* (2005) 'Presenilin-dependent γ-secretase processing regulates multiple ERBB4/HER4 activities', *Journal of Biological Chemistry*, 280(20), pp. 19777–19783.

Vincent, B. *et al.* (2001) 'The disintegrins ADAM10 and TACE contribute to the constitutive and phorbol-esters-regulated normal cleavage of the cellular prion protein', *Journal of Biological Chemistry* .

Vultur, A. *et al.* (2004) 'Cell-to-cell adhesion modulates Stat3 activity in normal and breast carcinoma cells', *Oncogene*. Nature Publishing Group, 23(15), pp. 2600–2616.

Litchfield, D. *et al.* (1990) 'Synthetic phosphopeptides are substrates for casein kinase II', *FEBS Letters*, 261(1), pp. 117–120.

Walther, I., Schulze, J. and Forth, W. (1998) 'Inhibition of protein synthesis by zinc: comparison between protein synthesis and RNA synthesis', *Human & Experimental Toxicology*., 17(12), pp. 661–667.

Weaver, BP. *et al.* (2007) 'Novel zinc-responsive post-transcriptional mechanisms reciprocally regulate expression of the mouse Slc39a4 and Slc39a5 zinc transporters (Zip4 and Zip5)', *Biological chemistry*, 388(12), pp. 1301–1312.

Weaver, BP. *et al.* (2010) 'Zip4 (Slc39a4) expression is activated in hepatocellular carcinomas and functions to repress apoptosis, enhance cell cycle and increase migration', *PloS one*, 5(10), p. e13158.

Weinlich, G. *et al.* (2003) 'Metallothionein-overexpression as a prognostic factor for progression and survival in melanoma. A prospective study on 520 patients', *British Journal of Dermatology*, 149(3), pp. 535–541.

Weisser, N. *et al.* (2017) 'Abstract 31: Preclinical development of a novel biparatopic HER2 antibody with activity in low to high HER2 expressing cancers', *Cancer Research*, 77(13 Supplement), pp. 31 LP – 31.

Welch, DR. and Hurst, DR. (2019) 'Defining the Hallmarks of Metastasis.', *Cancer research*. United States, 79(12), pp. 3011–3027.

Wells, A. *et al.* (2013) 'The dormancy dilemma: quiescence versus balanced proliferation.', *Cancer research*. United States, 73(13), pp. 3811–3816.

Wilkinson, JD. and Williamson, EM. (2007) 'Cannabinoids inhibit human keratinocyte proliferation through a non-CB1/CB2 mechanism and have a potential therapeutic value in the treatment of psoriasis', *Journal of Dermatological Science*, 45(2), pp. 87–92.

Wimmer, U. *et al.* (2005) 'Two major branches of anti-cadmium defense in the mouse: MTF-1/metallothioneins and glutathione', *Nucleic acids research*, 33(18), pp. 5715–5727.

Wintz, H. *et al.* (2003) 'Expression Profiles of Arabidopsis thaliana in Mineral Deficiencies Reveal Novel Transporters Involved in Metal Homeostasis', *Journal of Biological Chemistry* , 278(48), pp. 47644–47653.

Wolfe, M. S. (2009) 'Intramembrane Proteolysis', *Chemical reviews*, 109(4), pp. 1599–1612.

Wormald, M. R. *et al.* (2002) 'Conformational studies of oligosaccharides and glycopeptides: Complementarity of NMR, X-ray crystallography, and molecular modelling', *Chemical Reviews*, 102(2), pp. 371–386.

Wu, F. *et al.* (2010) 'Studies of phosphoproteomic changes induced by nucleophosmin-anaplastic lymphoma kinase (ALK) highlight deregulation of tumor necrosis factor (TNF)/Fas/TNF-related apoptosis-induced ligand signaling pathway in ALK-positive anaplastic large cell lymphoma', *Molecular & cellular proteomics*, 9(7), pp. 1616–1632.

Wu, X., Tang, J. and Xie, M. (2015) 'Serum and hair zinc levels in breast cancer: a meta-analysis', *Scientific Reports*, 5, p. 12249.

Xu, X.-M. *et al.* (2016) 'Decreased expression of SLC 39A14 is associated with tumor aggressiveness and biochemical recurrence of human prostate cancer', *OncoTargets and therapy*, 9, pp. 4197–4205.

Yamaguchi, S. *et al.* (2009) 'Zinc is an essential trace element for spermatogenesis', *Proceedings of the National Academy of Sciences of the United States of America*, 106(26), pp. 10859–10864.

Yamaguchi, T. *et al.* (2005) 'Phosphorylation by Cdk1 induces Plk1-mediated vimentin phosphorylation during mitosis', *The Journal of cell biology*, 171(3), pp. 431–436.

Yamanaka, Y. *et al.* (2016) 'Binding Analysis of Human Immunoglobulin G as a Zinc-Binding Protein', *Antibodies*, 5(2), p. 13.

Yamasaki, S. *et al.* (2007) 'Zinc is a novel intracellular second messenger', *The Journal of Cell Biology*. The Rockefeller University Press, 177(4), pp. 637–645.

Yamashita, S. *et al.* (2004) 'Zinc transporter LIVI controls epithelial-mesenchymal transition in zebrafish gastrula organizer', *Nature*, 429(6989), pp. 298–302.

Yamazaki, H., Kosako, H. and Yoshimura, S. H. (2020) 'Quantitative proteomics indicate a strong correlation of mitotic phospho-/dephosphorylation with non-structured regions of substrates', *Biochimica et Biophysica Acta*, 1868(1), p. 140295.

Yan, M. *et al.* (2008) 'Zinc Deficiency Alters DNA Damage Response Genes in Normal Human Prostate Epithelial Cells()', *The Journal of nutrition*, 138(4), pp. 667–673.

Yap, X. *et al.* (2009) 'Over-expression of metallothionein predicts chemoresistance in breast cancer', *The Journal of Pathology*, 217(4), pp. 563–570.

Yata, K. *et al.* (2012) 'Plk1 and CK2 Act in Concert to Regulate Rad51 during DNA Double Strand Break Repair', *Molecular Cell*, 45(3), pp. 371–383.

Yde, C. W. *et al.* (2007) 'Induction of cell death in antiestrogen resistant human breast cancer cells by the protein kinase CK2 inhibitor DMAT', *Cancer Letters*, 256(2), pp. 229–237.

Yde, C. W. *et al.* (2008) 'The regulatory [beta]-subunit of protein kinase CK2 regulates cell-cycle progression at the onset of mitosis', *Oncogene*, 27(37), pp. 4986–4997.

Yenice, S. *et al.* (1994) 'Nuclear casein kinase 2 (CK-2) activity in human normal, benign hyperplastic, and cancerous prostate', *The prostate*, pp. 11–16.

Yokota, T. *et al.* (1992) 'Rapid Tumor Penetration of a Single-Chain Fv and Comparison with Other Immunoglobulin Forms', *Cancer Research*, 52(12), pp. 3402 LP – 3408.

Yoshida, K. *et al.* (2008) 'Physiological roles of semenogelin I and zinc in sperm motility and semen coagulation on ejaculation in humans', *MHR: Basic science of reproductive medicine*, 14(3), pp. 151–156.

Zach, S., Felk, S. and Gillardon, F. (2010) 'Signal Transduction Protein Array Analysis Links LRRK2 to Ste20 Kinases and PKC Zeta That Modulate Neuronal Plasticity', *PLOS ONE*, 5(10), p. e13191.

Zafir-Lavie, I., Michaeli, Y. and Reiter, Y. (2007) 'Novel antibodies as anticancer agents', *Oncogene*, 26(25), pp. 3714–3733.

Zaichick, V. Y., Sviridova, T. V and Zaichick, S. V (1997) 'Zinc in the human prostate gland: Normal, hyperplastic and cancerous', *International Urology and Nephrology*, 29(5), pp. 565–574.

Zamirska, A. *et al.* (2012) 'Expression of metallothioneins in cutaneous squamous cell carcinoma and actinic keratosis', *Pathology oncology research*, 18(4), pp. 849–855.

Zaret, KS. (2014) 'Genome reactivation after the silence in mitosis: recapitulating mechanisms of development?', *Developmental cell*, 29(2), pp. 132–134.

Zhang, S. *et al.* (2011) 'Combating trastuzumab resistance by targeting SRC, a common node downstream of multiple resistance pathways', *Nature medicine*, 17(4), pp. 461–469.

Zhang, T., Sui, D. and Hu, J. (2016) 'Structural insights of ZIP4 extracellular domain critical for optimal zinc transport', *Nature Communications*, 7, p. 11979.

Zhang, Y. *et al.* (2009) 'Vitamin and mineral use and risk of prostate cancer: the case-control surveillance study', *Cancer causes & control*, 20(5), pp. 691–698.

Zhao, J. *et al.* (2016) 'Comparative study of serum zinc concentrations in benign and malignant prostate disease: A Systematic Review and Meta-Analysis', *Scientific Reports*, 6, p. 25778.

Zheng, D. *et al.* (2008) 'Regulation of ZIP and ZnT zinc transporters in zebrafish gill: zinc repression of ZIP10 transcription by an intronic MRE cluster', *Physiological genomics*, 34(2), pp. 205–214.

Zheng, Y. *et al.* (2013) 'Targeting Protein Kinase CK2 Suppresses Pro-survival Signaling Pathways and Growth of Glioblastoma', *Clinical cancer research : an official journal of the American Association for Cancer Research*, 19(23), pp. 6484–6494.

Zhuang, X., Northup, J. K. and Ray, K. (2012) 'Large putative PEST-like sequence motif at the carboxyl tail of human calcium receptor directs lysosomal degradation and regulates cell surface receptor level', *The Journal of biological chemistry*, 287(6), pp. 4165–4176.

Ziliotto, S. (2018) *Understanding how targeting zinc transporters prevents the development of aggressive cancer* (Doctoral dissertation), Cardiff University, Cardiff, UK.

Ziliotto, S. *et al.* (2019) 'Activated zinc transporter ZIP7 as an indicatory of anti-hormone resistance in breast cancer'. Metallomics, 11(9), pp. 1579–1592.

Appendices

1. Buffers used for the ELISA

Buffer	Composition
Coating buffer	PBS concentrate (10 x)
Wash buffer	1 x PBS, 0.05% Tween-20
Blocking buffer	10% Assay buffer A, deionised water
Assay buffer A	1 x PBS, 1% Tween-20, 10 % BSA

2. TBS-T

12.1 g Tris base

58 g NaCl

5 mL Tween-20 (Sigma; P2287)

Reagents were dissolved in 900 mL deionised H_2O and the pH adjusted to 7.6 with 5 M HCl. The final volume was adjusted to 1 L with deionised H_2O. The stock solution was diluted 1:10 for use.

3. Buffers used for the preparation of recombinant ZIP10 plasmids

Buffer	Composition
Buffer P1 (resuspension buffer)	50 mM Tris-Cl pH 8.0, 10 mM EDTA, 100 μg/mL RNase A
Buffer P2 (lysis buffer)	200 mM NaOH, 1% SDS (w/v)
Buffer P3 (neutralisation buffer)	3.0 M potassium acetate pH 5.5
Buffer ER	Proprietary formulation
Buffer QC (wash buffer)	1.0 M NaCl, 50 mM MOPS pH 7.0, 15% isopropanol (v/v)
Buffer QN (elution buffer)	1.25 M NaCl, 50 mM MOPS pH 7.0, 15% isopropanol (v/v)
Buffer TE	10 mM TRIS-Cl pH 8.0, 1 mM EDTA

4. Lysis buffer

50 mM Tris base (Fisher; BP152-1)

150 mM NaCl (Fisher; S/3160/65)

5 mM EGTA (Sigma; 3889)

1% Triton X-100 (v/v) (Sigma; T8532)

The pH was made up to 7.6 with 5 M HCl.

5. Laemmli buffer (4 x concentrated)

800 mg SDS (Sigma; L4390)

4 mL glycerol (Sigma; G5516)

4.8 mL 0.5M Stacking gel buffer (pH 6.8) (Bio-Rad; 161-0799)

1.2 mL deionised H_2O

2 x and 1 x laemmli buffers were made up from the 4 x concentrated stock in deionised H_2O.

6. Composition of resolving gel for SDS-PAGE

% Gel	Composition
7.5 %	9.6 mL deionised H_2O, 5 mL TRIS-HCl buffer pH 8.8, 5 mL 30% acrylamide (v/v), 200 μL 10% SDS (w/v), 200 μL 10% APS (w/v), 12 μL TEMED
10 %	8 mL deionised H_2O, 5 mL TRIS-HCl buffer pH 8.8, 6.8 mL 30% acrylamide (v/v), 200 μL 10% SDS (w/v), 200 μL 10% APS (w/v), 12 μL TEMED
14 %	5 mL deionised H_2O, 5 mL TRIS-HCl buffer pH 8.8, 9.52 mL 30% acrylamide (v/v), 200 μL 10% SDS (w/v), 200 μL 10% APS (w/v), 12 μL TEMED

Composition of stacking gel for SDS-PAGE

6.1 mL deionised H_2O

2.5 mL TRIS-HCl buffer, pH 6.8

1.3 mL 30% acrylamide (v/v)

100 μL 10% SDS (w/v)

50 μL 10% APS (w/v)

10 μL TEMED

7. Running buffer

30 g Tris base

144 g glycine (Fisher; G/P460/53)

10 g SDS

Reagents were dissolved in 800 mL deionised H_2O and the pH adjusted to 8.3 with 5 M HCl. The final volume was adjusted to 1 L with deionised H_2O. The stock solution was diluted 1:10 for use.

8. Transfer buffer

3.03 g Tris base

14.4 g glycine

800 mL deionised H_2O

200 mL methanol (Fisher; 10284580)

9. KRH buffer

Solution A	Solution B	Solution C
120 mM NaCl, 25 mM HEPES, 4.8 mL KCl, 1.2 mM KH_2PO_4	1.2 mM $MgSO_4$	1.3 mM $CaCl_2$

To make the final KRH buffer, 20 mL solution A was added to 80 mL water, then 1 mL solution B and C were added. The pH was adjusted to 7.4 with 2 M NaOH.

10. Site-directed mutagenesis of ZIP10 S549 and T540

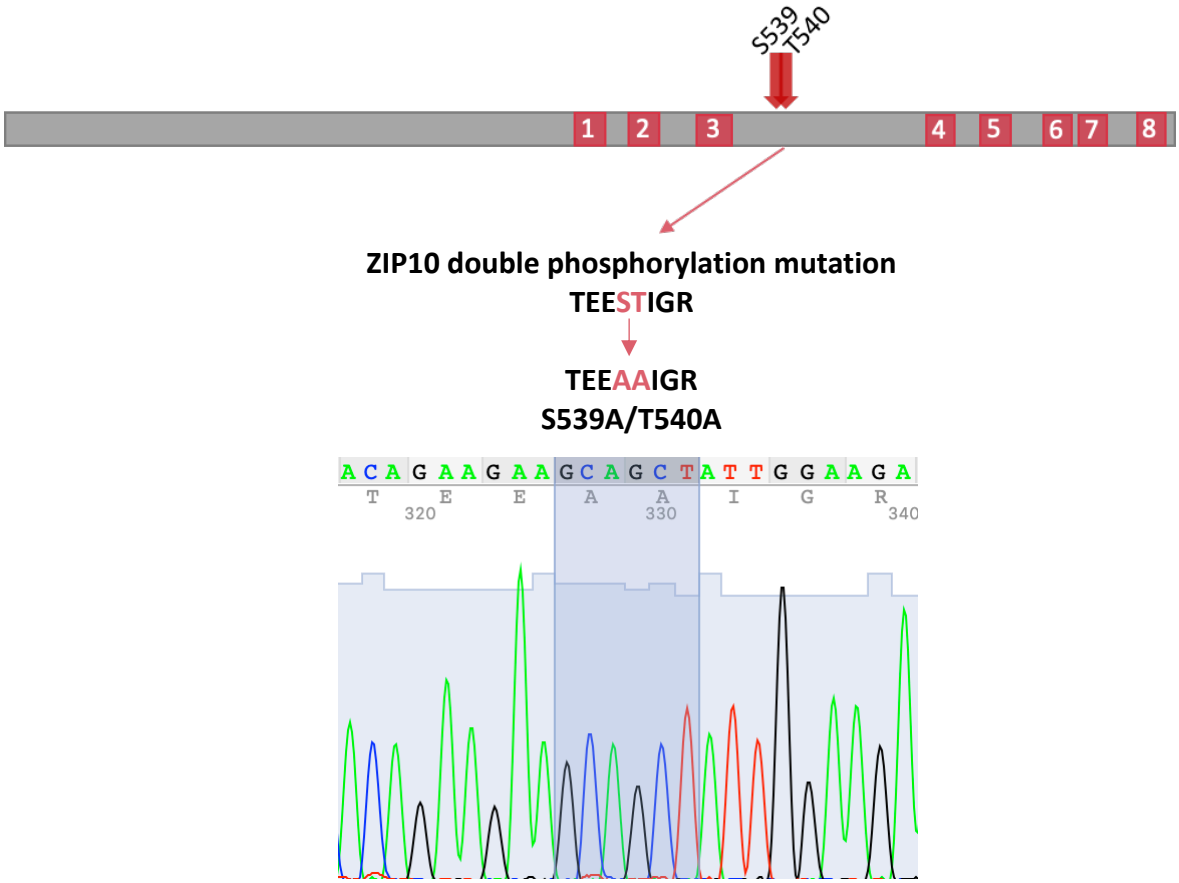

Serine 539 and threonine 540 were mutated to alanine by site-directed mutagenesis. The human WT amino acid sequence and the mutant sequence are shown. The chromatogram highlights the successful mutation of serine 539 and threonine 540 to alanine residues. S, serine; T, threonine; A, alanine.